This electronic thesis or dissertation has been downloaded from the King's Research Portal at https://kclpure.kcl.ac.uk/portal/

Investigations into the molecular regulation of gene expression in airway smooth muscle cells

Pagdin, Thomas William

Awarding institution:
King's College London

The copyright of this thesis rests with the author and no quotation from it or information derived from it may be published without proper acknowledgement.

END USER LICENCE AGREEMENT

This work is licensed under a Creative Commons Attribution-NonCommercial-NoDerivatives 4.0 International licence. https://creativecommons.org/licenses/by-nc-nd/4.0/

You are free to:

- Share: to copy, distribute and transmit the work

Under the following conditions:

- Attribution: You must attribute the work in the manner specified by the author (but not in any way that suggests that they endorse you or your use of the work).
- Non Commercial: You may not use this work for commercial purposes.
- No Derivative Works - You may not alter, transform, or build upon this work.

Any of these conditions can be waived if you receive permission from the author. Your fair dealings and other rights are in no way affected by the above.

Take down policy

If you believe that this document breaches copyright please contact librarypure@kcl.ac.uk providing details, and we will remove access to the work immediately and investigate your claim.

Download date: 06. Nov. 2017

This electronic theses or dissertation has been downloaded from the King's Research Portal at https://kclpure.kcl.ac.uk/portal/

KING'S College LONDON

Title: Investigations into the molecular regulation of gene expression in airway smooth muscle cells

Author: Tom Pagdin

The copyright of this thesis rests with the author and no quotation from it or information derived from it may be published without proper acknowledgement.

END USER LICENSE AGREEMENT

This work is licensed under a Creative Commons Attribution-NonCommercial-NoDerivs 3.0 Unported License. http://creativecommons.org/licenses/by-nc-nd/3.0/

You are free to:

- Share: to copy, distribute and transmit the work

Under the following conditions:

- Attribution: You must attribute the work in the manner specified by the author (but not in any way that suggests that they endorse you or your use of the work).
- Non Commercial: You may not use this work for commercial purposes.
- No Derivative Works - You may not alter, transform, or build upon this work.

Any of these conditions can be waived if you receive permission from the author. Your fair dealings and other rights are in no way affected by the above.

Take down policy

If you believe that this document breaches copyright please contact librarypure@kcl.ac.uk providing details, and we will remove access to the work immediately and investigate your claim.

Investigations into the molecular regulation of gene expression in human airway smooth muscle cells

Tom Pagdin

Submitted to King's College London for the degree of Doctor of Philosophy

MRC and Asthma UK Centre in Allergic Mechanisms of Asthma,
Department of Asthma, Allergy and Respiratory Science,
5th Floor, Tower Wing, Guy's Hospital, London, SE1 9RT

The work submitted in this thesis is my own

Tom Pagdin

Abstract

The phenotype of airway smooth muscle (ASM) differs in asthmatic patients compared to healthy individuals. Hyperplasia, hypertrophy, increased contraction and altered synthetic capabilities of asthmatic airway smooth muscle cells (ASMCs) have all been reported, however, the molecular mechanisms underlying a number of these changes remain unclear. This project utilizes molecular techniques to investigate the regulation of gene expression in cultured ASMCs isolated from both healthy and asthmatic individuals.

microRNAs (miRNAs) are short, non-coding RNAs that exert a post-transcriptional regulation on gene expression by targeting specific mRNAs for down regulation through either mRNA degradation or translational repression. During this project microarray studies have been performed to determine differences in the miRNA expression profile of cultured ASMCs isolated from healthy or moderate asthmatic volunteers. These studies have identified a number miRNAs with differential expression in asthmatic ASMCs compared to healthy controls. Of particular note, it is demonstrated that the abundance of both mature miR-155 and its host transcript, BIC, are approximately three-fold lower in cultured asthmatic ASMCs compared to healthy controls. Various experimental approaches to identify endogenous targets for miR-155 in cultured ASMCs are described.

The advent of next-generation sequencing technology has had a great influence on the field of chromatin and transcriptional regulation. In particular it has been shown that specific histone modifications demarcate functional and architectural regions within the genome. Investigations using chromatin-immunoprecipitation followed by next-generation sequencing (ChIP-seq) to generate a profile of histone methylation enrichments across the genome of cultured healthy ASMCs are described. It is envisaged that this data set will provide a resource for researchers interested in the transcriptional regulation of gene expression in ASM, in particular it will facilitate the identification of novel distal elements involved in the regulation of specific loci.

Acknowledgments

I would like to express special thanks to my supervisors Paul and Dave. Paul has offered great support and encouragement throughout this entire process and the thesis would not have been possible without his guidance, support and insight regarding the planning and implementation of experimental work and the writing of this thesis. I thank Dave for the technical advice and help he has provided, particularly concerning the analysis of microarray experiments that has been performed. I would also like to thank him for teaching me to continually appraise work with a critical mind. Most of all I would like to thank both Paul and Dave for the time and patience they have given me and for making my studies an enjoyable and rewarding experience. I also express my gratitude to Stuart Hirst, who was one of the original principal investigators of this project and without whom this work would not have been possible.

Many other people have provided great help and assistance during my time in the Asthma, Allergy and Respiratory Science Department and I would therefore like to thank; Venu Pullabhatla for his help with ChIP-seq analysis, Varsha Kanabar and Lotta Karner for their advice on smooth muscle biology and the preliminary data they provided, Dave Fear for his character building encouragement and members of the lab including Holly Bowen, Audrey Kelly, Batika Rana, Celine Parmentier, Holly Foster and Lisi Fürst.

Finally I would like to thank Emma, Mum, Dad and Jennie for all of their help, encouragement and support.

Abbreviations

AGO	Argonaute
AHR	Airway hyperresponsiveness
ANOVA	Analysis of variance
anti-miR	Antagomir
AoSM(C)	Aortic smooth muscle (cell)
ASM(C)	Airway smooth muscle (cell)
BAL	Bronchoalveolar lavage
CCLx	Chemokine ligand x
CCRx	Chemokine receptor x
cDNA	Complementary DNA
CEAS	Cis-regulatory element annotation system
ChIP	Chromatin immunoprecipitation
ChIP-seq	Chromatin immunoprecipitation followed by next-generation sequencing
Ct	Threshold cycle
CXCLx	Chemokine (C-X-C motif) ligand x
CXCRx	Chemokine (C-X-C motif) receptor x
DNA	Deoxyribonucleic acid
dNTP	Deoxyribonucleotide
dsRNA	Double-stranded RNA
ELISA	Enzyme-linked immunosorbent assay
ENCODE	Encyclopedia of DNA elements
FAM	Fluorescein amidite
FEV_1	Forced expiratory volume in 1 second
HAT	Histone acetyl transferase
HDAC	Histone deacetylase
HKDM	Histone lysine demethylase
HKMT	Histone lysine transferase
Igx	Immunoglobulin - x
IL-x	Interleukin - x

IL-xR	Interleukin - x receptor
miRNA	microRNA
MMPx	Matrix metalloproteinase x
mRNA	Messenger RNA
nt	Nucleotide
ORF	Open reading frame
PCA	Principal component analysis
PCR	Polymerase chain reaction
RISC	RNA-induced silencing complex
RNA	Ribonucleic acid
RT-PCR	Reverse transcription-polymerase chain reaction
RT-qPCR	Reverse transcription-quantitative polymerase chain reaction
SABA	Short acting β_2-agonist
SICER	Spatial clustering approach for the identification of ChIP-enriched regions
siRNA	Small interfering RNA
SNP	Single nucleotide polymorphism
ssRNA	Single-stranded RNA
Th1/2	T-helper 1/2 cell
TSS	Transcriptional start site
UTR	Untranslated region

Table of contents

List of figures

List of tables

Chapter 1 - General Introduction

1.1. Asthma

Asthma is a complex disease with varying symptoms and presentations that range from being mild and easily controllable through to potentially life threatening. It is frequently described as being characterised by reversible and reoccurring symptoms that include airflow obstruction, bronchial hyperresponsiveness and underlying inflammation. Studies on large patient populations, however, show that asthma can be classified into distinct subgroups by unsupervised hierarchical clustering methods (Lötvall et al. 2011). These reports have lead to asthma being increasingly viewed as a syndrome with a variety of underlying causes and clinical presentations.

The Asthma UK charity estimates that over five million people in the UK receive treatment for asthma, resulting in at least 12.7 million lost working days a year and an annual cost of approximately £889 million to the NHS and £2.3 billion to the UK economy as a whole (Asthma 2011). It is clear that further understanding of asthma etiology is required to develop our understanding of the condition and ultimately lead to patient benefits.

1.2 Inflammation in asthma

1.2.1 Classical allergic asthma

Evidence that inflammation is an important factor in asthma etiology was initially derived from autopsies on patients with fatal asthma. These showed infiltration of eosinophils and basophils into the airways, mast cell degranulation, sub-basement membrane thickening, loss of epithelial cell integrity, increased mucus production and hypertrophy and hyperplasia of the airway smooth muscle (ASM) (Huber 1922). Although it was initially believed that these features were specific for fatal asthma, studies of bronchoalveolar lavage (BAL) fluid and endobronchial biopsies have subsequently demonstrated these features in patients with varying disease severity (Wills-Karp 1999).

The genetic factor correlated most strongly to asthma is atopy, a state whereby an individual produces increased amounts of immunoglobulin-E (IgE) (Ono 2000), suggesting that allergy and atopy are central to asthma etiology. Allergy is characterised by an increased T helper 2 (Th2) immune response to environmental allergens that do not generate an immune response in the majority of individuals. The Type 2 immune response is responsible for host defense against large parasitic

infections, such as helminths (Harris & Gause 2011), and is dependent upon Th2 cells, B cells, mast cells and eosinophils.

The classical allergic asthmatic response typically comprises two phases. The initial phase, usually resolved within 2-3 hours, involves bronchoconstriction, airway oedema and increased mucus secretion. This is generally followed by a secondary, or late phase, of bronchoconstriction caused by infiltrating eosinophils and lymphocytes. The production of IgE is central to the establishment of any allergic reaction. In order for IgE to be produced, an inhaled allergen must first be taken up and processed by an antigen-presenting cell, which is classically a dendritic cell resident below the epithelial layer of the airways. This dendritic cell then migrates to the draining lymph node whereupon it presents antigen to resident T and B cells via a major histocompatibility complex (MHC) class II molecule. Dependent upon the presence of appropriate signaling, specifically interleukin (IL)-4 and IL-13 and the binding of CD40 on the B cell to its ligand on T cells, B cells then undergo a process of isotype switching whereby naïve B cells expressing membrane bound IgM switch to producing IgE through genomic rearrangement of the immunoglobulin heavy chain locus (Gould et al. 2003).

1.2.1.1 Th2 Cells

The establishment of an adaptive immune response is regulated by the action of T helper cells. T helper cells were classically described by Th1/Th2 paradigm first elucidated in mice and based upon the expression of distinct sets of effector cytokines by lymphocytes expressing the CD4 cell surface marker (Mosmann et al. 1986). Evidence from human studies has subsequently shown that human Th1 cells derived from the *in vitro* differentiation of naïve $CD4^+$ cells are characterised by the expression of the signature cytokine, Interferon-γ (IFNγ), whilst *in vitro* differentiated Th2 cells are characterised by the expression of IL-4, IL-5 and IL-13 (Cousins et al. 2002).

Th1 and Th2 effector cells are derived from a common naïve $CD4^+$ T cell precursor. The decision as to whether a naïve $CD4^+$ T cell differentiates to a Th1 or a Th2 phenotype is controlled by cytokines, which initiate self-reinforcing transcriptional circuits and drive differentiation to a distinct phenotype. Th2 cells are derived from naïve $CD4^+$ T cells under conditions of direct T-cell receptor (TCR) stimulation, co-stimulation through CD28 and IL-4 signaling. Th2 lineage commitment is initiated

by signaling through the IL-4 receptor (IL-4R), which signals through Signal Transducers and Activators of Transcription 6 (STAT6) and results in the enhanced expression of GATA3. GATA3 induces the expression of the Th2 cytokines IL-4, IL-5 and IL-13 and is also able to upregulate its own expression through a positive feedback loop in a STAT6 independent manner (Ouyang et al. 2000). c-maf is also upregulated by the IL-4R/STAT6 signaling pathway and has been shown to have an active role in stimulating IL-4 expression (Kim et al. 1999).

Each of the signature Th2 cytokines has been shown to promote features of the allergic asthmatic phenotype; IL-4 and IL-13 induce B-cell isotype switching to IgE (Finkelman et al. 1988) (Punnonen et al. 1993) and mast cell activation (Madden et al. 1991), IL-4 alone upregulates CD106, leading to the preferential migration of eosinophils into tissues (Schleimer et al. 1992) and IL-5 is a primary stimulator of eosinophil and basophil differentiation, maturation and activation (Campbell et al. 1988). Correlative evidence for an increased Th2 inflammatory response in asthma includes reports of increased GATA3 protein, IL-4 and IL-5 mRNA and IL-4, IL-5 and IL-13 protein in the lungs of asthmatic individuals compared to healthy controls (Robinson et al. 1992) (Humbert et al. 1996).

1.2.1.2 Mast Cells

Following initial allergen exposure and production of allergen-specific IgE molecules by B cells, IgE circulates briefly in the blood before binding to high-affinity IgE receptors (FcεRI) on mast cells present in the lung. Upon subsequent exposure to allergen, the IgE bound to FcεRI on the surface of mast cells is cross-linked by the allergen, leading to activation and degranulation of the mast cell. Degranulation results in the release of numerous preformed mediators, including histamine, leukotrienes and prostaglandin-D_2 (PGD_2). These effector molecules can stimulate many features of the asthmatic response including increased mucus secretion from goblet cells and contraction of ASM, leading to bronchoconstriction of the airways. It is generally accepted that degranulation of mast cells is the primary cause of the initial phase of the allergic asthmatic response. In addition, mast cells secrete various cytokines and chemokines, including tumour necrosis factor-α (TNFα), IL-4, IL-5, chemokine (C-C motif) ligand 2 (CCL2) and CCL5 and in doing so may also contribute to the late phase response (Stone et al. 2010).

1.2.1.3 Eosinophils

Eosinophils are believed to be the major effector cell involved in the late phase asthmatic response. There are increased numbers of eosinophils in both the serum and BAL fluid of asthmatic individuals (Bousquet et al. 1990), whilst the number of eosinophils in induced sputum correlates to disease severity (Louis et al. 2002) and increased eosinophilia is associated with increased sub-basement thickening and a decrease in steroid responsiveness (Berry et al. 2007). Eosinophils mature and develop in the bone marrow in response to cytokines such as IL-3 (Metcalf et al. 1987), IL-5 and Granulocyte macrophage colony-stimulating factor (GM-CSF) (Begley et al. 1986) and following maturation they migrate to sites of tissue inflammation in response to chemokines such as CCL11 and CCL5. Once activated eosinophils secrete a number of effector molecules including eosinophil specific proteins such as eosinophilic cationic protein (ECP) and major basic protein (MBP), a number of cytokines including IL-2, IL-4, IL-5 and transforming growth factor β (TGFβ) and lipid mediators such as leukotrienes (Weller et al. 1996). It has been shown that MBP stimulates hyperreactivity of ASM *in vitro* (Flavahan et al. 1988) and administration of MBP to primates results in AHR (Gundel et al. 1991). Eosinophils and their mediators are capable of causing epithelial detachment and lysis, thus contributing to the remodeling of the airways (Hisamatsu et al. 1990).

1.2.2 Non-allergic severe asthma

Increasing evidence indicates that in addition to the allergic asthmatic response there are a variety of underlying molecular and cellular phenotypes that result in the presentation of asthmatic symptoms. One subgroup of patients that are increasingly noted are those with severe asthma in which the underlying inflammation appears to be neutrophilic rather than eosinphilic in nature.

1.2.2.1 Neutrophils

Neutrophils are the most abundant cell type in the induced sputum of both healthy and asthmatic individuals (Woodruff et al. 2001). It is suggested that although there is no difference in the levels of neutrophilia between healthy, mild and moderate asthmatic individuals there are a subgroup of severe asthmatics who display increased levels of neutrophilia (Fahy 2009) (Wenzel et al. 1997). One potential caveat to this data is that severe asthmatics are usually treated with high dose corticosteroids and this treatment is known to increase neutrophil survival. Investigations attempting to correct for this factor have, however, corroborated the

initial findings (Woodruff et al. 2001), suggesting that neutrophils may indeed play an important role in a subgroup of severe asthmatic patients. In addition, a study examining neutrophil counts in patients intubated for asthma treatment compared to patients intubated for non-pulmonary conditions found a statistically significant higher number of neutrophils in the asthmatic patients, despite the fact that only five out of the ten patients studied were treated with corticosteroids (Ordoñez et al. 2000). This provides further evidence that, in some cases, neutrophilia may be an intrinsic feature of the severe asthmatic phenotype.

Mechanistically neutrophils may contribute to the asthmatic phenotype in a number of ways, for example they can secrete neutrophil elastase, which has been shown to stimulate increased mucus production by goblet cells (Foley & Hamid 2007). Severe asthmatics have increased levels of a neutrophil-specific form of matrix metalloproteinase (MMP)-9 in their BAL fluid (Cundall et al. 2003) and increased levels of the neutrophil-specific MMP9 have been shown to inversely correlate with forced expiratory volume in 1 second (FEV_1) (Vignola et al. 1998).

1.2.2.2 Th17 cells

In addition to neutrophils, there is increasing evidence that Th17 cells contribute to severe asthma. Th17 cells are characterised by the expression of the transcription factor RAR-related orphan receptor γt (RORγt) and the production of the signature cytokines, IL-17A and IL-17F. In humans their differentiation from naïve CD4+ precursors is believed to be driven by IL-1β and IL-23 (Wilson et al. 2007) (Chen et al. 2007) and enhanced by IL-6 (Acosta-Rodriguez et al. 2007). Analysis of bronchial biopsies has suggested increased levels of IL-17A mRNA and protein in asthmatic patients compared to healthy controls (Molet et al. 2001) and it has been demonstrated the level of IL-17A and IL-17F protein correlates with disease severity (Chakir et al. 2003). Functionally, expression of the IL-17 receptor, IL-17RA, has been described on airway epithelial cells, suggesting these cells may be targets of IL-17 actions (Huang et al. 2007). IL-17RA signaling results in the expression of a number of chemokines that are chemoattractive for neutrophils, including chemokine (C-X-C motif) ligand 1 (CXCL1), CXCL2 and CXCL8 (Fossiez et al. 1996) (Ruddy et al. 2004) (Laan et al. 1999).

1.3 Asthma therapy

Anti-inflammatory and bronchodilator treatment strategies are the mainstays of asthma therapy. Patients with only mild asthma are initially treated with β2 agonists, such as salbutamol or formotorol, which act to promote ASM relaxation. Patients that do not respond to simple β2 agonists treatment, however, are progressed to anti-inflammatory treatment regimes.

1.3.1 Gluococorticoids

Glucocorticoids are commonly used in asthma therapy as general immunomodulators**.** The actions of glucocorticoids are mediated the glucocorticoid nuclear receptor (GR). Glucocorticoids are highly lipophilic and diffuse freely through the plasma membrane into the cytoplasm of target cells where they bind GR, facilitating its release from a complex containing factors such as heat shock protein (hsp)-90, which serve to retain unliganded GR in the cytoplasm (Srinivasan et al. 1994). Activated GR then translocates to the nucleus, where it regulates the expression of many target genes involved in inflammation.

GR is able to modulate the inflammatory response by inducing the expression of anti-inflammatory genes, such as IL-10 and inhibitor of NF-κBα (I-κBα) (John et al. 1998) (Auphan et al. 1995). The major mechanism by which GR decreases inflammation, however, is thought to be through the repression of pro-inflammatory genes. GR is able to directly repress the expression of specific target genes through binding to glucocorticoid response elements (GREs) in gene promoters and recruiting histone deacetylase complexes (HDACs) or influencing the phosphorylation state of RNA polymerase II (Ito et al. 2000) (Nissen & Yamamoto 2000), resulting in the repression of gene expression. GR also interacts with and inhibits transcription factors such as AP-1 (Jonat et al. 1990) and NFκB (Ray & Prefontaine 1994), thus preventing them from activating the expression of their target genes.

The molecular complexity of glucocorticoids function is increased by the variety of GR isoforms that can be expressed. In humans, a single gene at 5q31-32 is responsible for the expression of the GR, however, numerous alternative isoforms can be generated from this locus through the use of alternative promoters and differential splice sites. These alternative isoforms contain different functional domains and can hence act to mediate differing downstream actions following their

activation. The cell type and developmental stage specific expression of differing GR isoforms may therefore explain the widely varying results of glucocorticoids treatment in different cell types (Lu & Cidlowski 2004). It has been shown that various N-terminal isoforms of the GR are expressed following the transfection of a single exogenous DNA sequence into cell lines not expressing endogenous GR (Lu & Cidlowski 2005). These N-terminal variants caused differential activation of reporter genes and regulated differing subsets of endogenous GR responsive genes, suggesting that different GR isoforms may be responsible for specific glucocorticoids responses. The best studied GR variant is GRβ, which acts as a ligand-independent dominant negative regulator of GRα (Oakley et al. 1996) (Bamberger 1995). Interestingly, increased GRβ expression has been correlated with several diseases associated with glucocorticoids resistance, including asthma (Sousa et al. 2000). Glucocorticoids resistance in a sub-population of asthmatics currently poses a great therapeutic challenge (Durham et al. 2011) and, along with the undesirable side-effects of long-term glucocorticoids usage, has lead to increased investigations into biological therapies for asthma.

1.3.2 Anti-cytokine therapies

Increasing emphasis has been placed on finding targeted and rationale therapies to improve upon the efficacy offered by general glucocorticoids and β2 agonists treatment and to provide treatment options for cases where glucocorticoids are ineffective.

The anti-IgE antibody, omalizumab, has been shown to have beneficial effects in a number of trials targeted at treating patients with severe, poorly controlled allergic asthma. A number of early omalizumab trials reported a significant decrease in the number of exacerbations and glucocorticoid use in chronic asthmatics (Milgrom et al. 2001) (Busse 2001). More recently, a Cochrane Systematic Review investigating the efficacy of omalizumab in treating chronic asthmatics with elevated serum IgE concluded that there was a significant decrease in the number of exacerbations and glucocorticoid use. It was, however, noted that the size of these effects was small, especially considering the financial cost of treatment (Cochrane Collaboration 2011).

In addition to anti-IgE therapy, a number of approaches targeting the Th2 cytokines, IL-4, IL-5 and IL-13 are currently under investigation to determine their efficacy as

asthma treatments. Mepolizumab, a neutralizing antibody against IL-5, has been shown to cause a decrease in inflammation with no affect on airway hyperresponsiveness in mild to moderate asthmatics. Leckie *et al.* showed decreased levels of eosinophilia but no decrease in the level of airway hyperresponsiveness to histamine (Leckie et al. 2000); whilst Flood-Page *et al.* demonstrated a reduction in tissue eosinophilia but no alteration in clinical exacerbations as measured by a variety of end-points (Flood-Page et al. 2007). More recent data, however, has suggested efficacy of mepolizumab in reducing the number of exacerbations suffered by severe asthmatics with high levels of neutrophilia (Haldar et al. 2009) (Mehr et al. 2009). These data highlight the importance of sub-grouping and stratifying the cellular and molecular etiology of asthmatic symptom presentation to increase the efficacy of treatment strategies.

Early attempts to target IL-4 specifically have proved unsuccessful, leading to the hypothesis that joint targeting of IL-4 and IL-13 may be more beneficial (Wenzel et al. 2007). Two separate studies investigating antibodies that block IL-4Rα and thus prevent both IL-4 and IL-13 signaling have produced similar results, with a decrease in the number of induced exacerbations but no affect on stable symptoms such as lung function (Wenzel et al. 2007) (Corren et al. 2010). A recent study investigating the efficacy of the anti-IL-13 antibody, Lebrikizumab, has reported very promising outcomes in patients with a high Th2 status, as defined by total IgE levels, blood eosinophil counts and serum periostin levels (Corren et al. 2011). This is further evidence as to the importance of the underlying molecular phenotype in influencing treatment outcomes.

Despite the large amount of data describing the role of inflammation in the etiology of asthma, the results of several clinical trials targeting the inflammatory cascade, some of which have been described above, have proved less encouraging than expected. There are a number of potential reasons for this, including issues involving initial patient selection and the measurement of relevant endpoints. In addition it may be that specific treatments are effective in only a subgroup of patients, for example mepolizumab in patients with high levels of neutrophilia, or that targeting individual molecules is too simplistic and the targeting of multiple inflammatory mediators simultaneously would be more successful. An alternative hypothesis is that following the establishment of asthmatic features by an initial inflammatory response, caused for example by an inappropriate allergic response or

epithelial damage, the subsequent airway remodeling is sufficient to produce symptoms even when the initial inflammation is resolved. This apparent uncoupling between inflammation and airway hyperresponsiveness has lead to a renewed interest in the study of the structural cells of the airways, particularly airway smooth muscle (ASM).

1.4 Structural changes of the asthmatic lung

The establishment of an inflammatory response has profound influences on the resident structural cells of the lung and it is these affects on structural cells that cause asthmatic symptoms. In addition, a large body of evidence has demonstrated that many structural cells secrete various immunomodulatory factors, such as cytokines and chemokines, and are thus able to contribute to the inflammation of the asthmatic lung.

1.4.1 Epithelial layer degradation

A proposed major feature of asthmatic airways is epithelial cell shedding. This was first noted in biopsies from patients with fatal asthma (Huber 1922) and has since been observed in patients with mild and moderate disease (Laitinen et al. 1985). Further evidence for epithelial shedding is borne from studies demonstrating increased numbers of epithelial cells in the BAL fluid of asthmatic patients compared to healthy controls (Wardlaw et al. 1988) and indications that the level of epithelial loss correlates with the severity of airway hyperresponsiveness (Jeffery et al. 1989). Despite these findings, there are reports detailing no differences in the damage to the epithelial layer of asthmatic and healthy subjects (Woltmann et al. 1999). This had lead to speculation that the observed damage to the epithelial layer may be an artifact of the biopsy procedure. Evidence to counter this speculation is primarily derived from data showing increased expression of molecules involved in wound repair processes in asthmatic patients compared to healthy individuals. Lackie *et al.* have demonstrated increased expression of the cell adhesion molecule, CD44, in asthmatic epithelial cells (Lackie et al. 1997), whilst there is also evidence for increased expression of epidermal growth factor receptor on the epithelial cells of children (Fedorov et al. 2005) and adults (Puddicombe et al. 2000) with asthma. These data imply that damage to the epithelium occurred *in vivo* rather than during the biopsy process.

It is speculated that damage to the epithelial layer followed by aberrant repair processes may be a mechanism for the initiation of the asthmatic response (Davies 2009). There is evidence that asthmatic epithelial cells are intrinsically more susceptible to damage in comparison to healthy cells, possibly due to decreased epithelial contacts with the basal lamina (Shebani et al. 2005) and a decreased number of desomosomes (Shahana et al. 2005). This may lead to damage to the epithelial layer, as it is unable to cope with the mechanical strain imparted by the contracting ASM during hyperresponsive reactions. Additionally, the inflammation present in the asthmatic lung, in particular the production of MBP by eosinophils, may result in damage to the epithelial layer (Hastie et al. 1987). Interestingly, there are reports of airway remodeling in the absence of inflammation, as defined by the absence of eosinophilia, in some peadiatric asthmatic patients (Fedorov et al. 2005). This has lead to speculation that in certain circumstances epithelial damage alone may be sufficient to initiate and perpetuate airway remodeling. Clearly, it may be that the inflammation is non-eosinophilic in nature (see Chapter 1.2.2) and further studies are therefore required in this area.

There is evidence that epithelial cells could directly contribute to the establishment of asthmatic symptoms. *In vitro* studies have demonstrated that epithelial cells can express a variety of growth factors following injury, including fibroblast growth factor (FGF), insulin-like growth factor (IGF), platelet-derived growth factor (PDGF) and TGFβ and that epithelial cells are able to stimulate myofibroblast proliferation and collagen expression in co-culture models (Zhang et al. 1999).

1.4.2 Goblet cell hyperplasia

Goblet cell hyperplasia and increased mucus production were first described in the early observations of patients with fatal asthma (Huber 1922) and have since been observed in mild asthmatic patients (Ordoñez et al. 2001). The increase in mucus secretion is a pivotal feature in the development of asthmatic symptoms and levels of mucus hypersecretion directly correlate with decreases in FEV_1 (Lange et al. 1990). It is unclear whether goblet cells in the epithelial layer or submucosal glands are the main source of the increased mucus in asthma, however, there is evidence for an increase in the submucosal gland area in both fatal asthma (Chen et al. 2004) and mild disease (Benayoun et al. 2003). The main constituents of mucus are proteins known as mucins. Ordonez *et al.* have performed reverse transcription-quantitative PCR (RT-qPCR) analysis of asthmatic mucus and report an increase in

the levels of mucin-5AC (MUC5AC) in comparison to healthy controls (Ordoñez et al. 2001). This suggests that, in addition to secreting increased levels of mucus, asthmatics may produce mucus with different properties.

1.4.3 Basement membrane thickening and fibrosis

Fibrosis predominantly occurs below the basement membrane of the asthmatic airways (Roche 1998), although there are reports of fibrosis deeper within the airway walls, especially around the ASM bundles (Wilson 1997). The consequences of increased fibrosis are controversial, with some studies showing a correlation with airflow limitation and airway hyperresponsiveness (Shiba et al. 2002) and others demonstrating no association (Chu et al. 1998). Irrespective of whether fibrosis affects the mechanics of breathing, there is strong evidence that it influences the phenotype of surrounding cells and that the composition of the asthmatic extracellular matrix (ECM) differs from that of healthy controls. In particular, asthmatic ECM has increased levels of Collagen Type I and Type III, tenascin and fibronectin (Roche 1998). As an example of how this altered composition may affect the surrounding cells, fibronectin has been shown to be chemotactic for epithelial cells and fibroblasts *in vitro* and induce fibroblast proliferation (Shoji et al. 1989).

1.5 Airway smooth muscle

1.5.1 Embryological origin and development of ASM

The presence of ASM is reported very early in fetal development as thin sheaths surrounding the lung buds that will subsequently develop into the trachea and primary bronchi of the mature lung (Tollet et al. 2001) (Sparrow et al. 1995). ASM is known to differentiate from the mesenchyme as a ring of cells around the epithelial bud that are able to express muscle proteins (Tollet et al. 2001). The differentiation of ASM and the formation of bundles is believed to be stimulated by a mesenchyme-epithelial interaction through a laminin polymer. Disruption of this laminin polymer formation or prevention of mesenchyme cell elongation inhibits the differentiation of bronchial smooth muscle (Schuger et al. 1997) (Yang et al. 1999). Yang *et al.* have proposed that the mechanical stretching of mesenchyme cells induces expression of the active splice variant of serum response factor (SRF). In the proposed model SRF then stimulates the expression of various genes involved in the formation or regulation of the smooth muscle contractile apparatus, for example α-*smooth muscle actin (*α*-SMA*), *smooth-muscle 22* α (*sm22*α) and *calponin*

(Yang et al. 2000), thus leading to the differentiation of functional smooth muscle cells.

The physiological role of ASM is controversial and a variety of hypotheses have been proposed for its function. It has been speculated that ASM may assist exhalation and mucus clearance by peristalsis (Mitzner 2004), facilitate optimisation of anatomical dead space volume and thus reduce the work of breathing (Widdicombe 1963) and produce phasic contractions within the pre-natal lung to stimulate fetal lung growth, in particular airway differentiation and branching (Nakamura & McCray 2000). Whilst all of these possibilities are plausible, none have yet been adequately confirmed experimentally.

Although a normal, physiological role for ASM remains controversial, it is clear that it has a major influence in the underlying pathology and presentation of asthmatic symptoms. As such, there are now a wide range of reports detailing the features of ASM and potential differences that may exist between the ASM of healthy and asthmatic individuals. The importance of ASM in the asthmatic response is demonstrated by the efficacy of ASM relaxants, such as β_2 agonists in relieving asthmatic symptoms for the majority of patients (British Thoracic Society Scottish Intercollegiate Guidelines Network 2008). In addition, the novel treatment of bronchial thermoplasty, which involves the use of targeted radiofrequency waves to destroy ASMCs and thus reduce the ASM mass, has produced encouraging benefits in early clinical trials (Pavord et al. 2007) (Cox et al. 2007) (Castro et al. 2010). These data suggest that ASM is a highly important cell type in the asthmatic response.

1.5.2 ASM in asthma

1.5.2.1 Increased ASM mass

Huber first reported an increase in the mass of ASM in autopsies of patients with fatal asthma (Huber 1922). There have since been a number of studies corroborating this finding (Dunnill et al. 1969) (Saetta et al. 1991) and it is now widely accepted that an increase in the mass of ASM is a common feature of fatal asthma. The majority of studies published also report an increase in the ASM mass of patients with non-fatal asthma compared to healthy controls. There are reports that the mass of ASM differs between fatal asthma, non-fatal asthma and controls (Kuwano et al. 1993) and that the amount of ASM mass correlates with disease

severity in both human patients (Pepe et al. 2005) and animal models (Sapienza et al. 1991). Despite this, there are also reports that describe no difference in ASM mass, either between severities of disease or between asthmatics and controls (Thomson et al. 1996).

There is varying evidence as to the underlying cause of increased ASM mass in asthma. Benayoun *et al.* have reported hypertrophy of ASMCs, as measured by an increase in the average cell diameter, which correlated with disease severity (Benayoun et al. 2003). In addition, Begueret *et al.* have used an ultrastructural technique to show an increase in the average size of ASMCs in atopic asthmatics compared to healthy controls (Begueret et al. 2007). In contrast to these reports, Woodruff *et al.* reported no difference in the average ASMC size, but a close to two-fold increase in the number of ASMCs in an equivalent area, between mild and moderate asthmatics and healthy controls (Woodruff et al. 2004). Although it could be speculated that these differences are due to the different severities of asthma studied, it is clear that this remains a controversial area. An interesting study by Ebina *et al.* has reported subgroups of asthmatic patients with differing evidence of hyperplasia and hypertrophy. Within this study one group of asthmatics displayed an increase in ASM mass in the central bronchial only, which was a result of hyperplasia of the ASMCs. In a second group of asthmatics, increased ASM mass was found throughout the airway and it appeared that both hyperplasia and hypertrophy of the cells were contributing factors (Ebina et al. 1993). This is again further evidence of the variation in presentation and underlying pathology of asthma.

Despite the lack of definitive *in vivo* evidence detailing the exact cause of increased ASM mass in asthma there is a large body of literature examining the potential causative mechanisms.

1.5.2.1.1 ASMC proliferation and apoptosis

It has been reported that asthmatic ASM has an increased rate of proliferation compared to ASM from healthy individuals in direct *ex vivo* cultures (Johnson et al. 2001). This suggests that increased proliferation may be causative of the increase in ASM mass in asthmatic patients. There are, however, a lack of data to support the proliferation of asthmatic ASMCs *in vivo,* as a number of studies have been unable to detect markers of active proliferation within the ASM bundles of endobronchial

biopsies (Ward et al. 2008) (Benayoun et al. 2003). These data do not discount the possibility of ASMC proliferation within bundles, as sampling by endobronchial biopsy inevitably means that only sections of the ASM bundles are analyzed and it may be that the active proliferation of ASMCs is compartmentalized within the bundles.

There are a variety of *in vitro* studies investigating potential factors that may stimulate the proliferation of ASMCs and a number of these mitogenic factors are increased in the asthmatic lung. A study of particular interest from Naureckas *et al.* demonstrated that BAL fluid from atopic asthmatic patients caused a greater proliferation of co-cultured ASMCs than BAL fluid from healthy individuals. The induced proliferation was even greater when BAL fluid collected 48 hours after allergen challenge of atopic individuals was used (Naureckas et al. 1999). A number of individual mediators have been shown to influence the proliferative rate of cultured ASMCs. Polypeptide growth factors such as PDGF (Hirst et al. 1996) and EGF (Krymskaya et al. 1999) stimulate the proliferation of ASMCs *in vitro* whilst leukotriene D_4 (LTD_4), a well-established contractile mediator has been shown to potentiate the proliferative effects of EGF (Panettieri et al. 1998). In addition, it has been suggested the cytokines may be able to influence the proliferation of ASM as IL-13 was shown to potentiate the proliferation of human ASMCs *in vitro* (Espinosa et al. 2003).

Although there is little literature in the area, it should be noted that any potential increase in the number of ASMCs in asthmatic bronchioles may be caused by a decrease in the level of apoptosis. This mechanism for increased ASM mass has been shown to occur in the Brown Norway rat model of chronic airway inflammation and remodeling (Martin & Ramos-Barbón 2003), however, there is as yet no evidence for it occurring in biopsies containing human ASMCs (Druilhe et al. 1998). Human ASMCs express Fas receptor, both *in vivo* and *in vitro*, and cross-linking of the receptor does result in apoptosis (Hamann et al. 2000), whilst *in vitro* studies have identified mediators, such as neutrophil elastase (Oltmanns et al. 2005) and endothelin-1 (McWhinnie et al. 2007), that are capable of inducing or inhibiting ASM apoptosis respectively.

1.5.2.1.2 ASMC migration

An additional mechanism that may be causative of the increase in ASM mass in asthmatic patients is an increase in the level of migration of progenitor cells into the ASM bundles.

ASMCs have been shown to migrate in response to a variety of stimuli *in vitro*, including CCL11, PDGF, TGFβ and IL-1β (Joubert et al. 2005) (Hedges et al. 1999). In addition, the common asthma treatments glucocorticoids and β_2-agonists have been shown to inhibit ASMC migration (Goncharova et al. 2003). The functional *in vivo* consequences of this observed *in vitro* migration is uncertain. It may be that ASMCs migrating out of bundles contribute to the myofibroblasts observed in the submucosal space, possibly in response to epithelial derived mediators such as IL-8 and CCL5. A second explanation for the appearance of myofibroblasts in the submucosal space is that they are myofibroblasts migrating towards ASM bundles and that they will eventually join the bundles and contribute to the increase in ASM mass. In support of this hypothesis, there is evidence for the presence of myofibroblasts between ASM bundles in asthmatics (Begueret et al. 2007) and TGFβ treatment of myofibroblasts *in vitro* drives their differentiation to an ASM phenotype, as determined by measuring the mRNA levels of ASM associated transcripts such as α-smooth muscle actin and calponin (Wicks et al. 2006). The origin of the myofibroblasts is uncertain; they may originate from resident lung fibroblasts (Powell et al. 1999), circulating fibrocytes (Schmidt et al. 2003) or epithelial cells that have undergone transition into mesenchymal cells (Willis et al. 2006).

1.5.2.1.3 Functional consequence of increased ASM mass

An increased ASM mass in asthma may be functionally significant simply by causing a narrowing of the internal lumen of the airways and therefore amplifying the effect of ASM shortening. This effect may be exaggerated, however, if the increase in ASM is accompanied by an increase the contractile power of the ASM bundles. Computer modeling to predict how different factors will influence airway narrowing predicted that an increase in ASM mass would increase the maximal airway narrowing by two orders of magnitude (Lambert et al. 1993). This modeling, however, contained a number of assumptions within the calculations. In particular it was assumed that the contractile function of the ASM and the length-tension relationship would remain constant but that the contractile power would increase in proportion to the

mass. Evidence from *in vitro* studies, however, suggests that ASMCs become less contractile as they proliferate (Halayko et al. 1996). It is therefore controversial as to whether an increase in ASM mass does indeed lead to an increase in the contractile power of the bundles, with some studies reporting a difference in contractile power of asthmatic ASM and others reporting no difference.

1.5.2.2 Contraction of ASM

Understanding the mechanisms involved in ASM contraction is important in the context of asthma because ASM contraction is central to airway hyperresponsiveness, the phenomenon that causes airways to narrow in response to challenge with a non-specific contractile agonist. This is demonstrated by the success of β_2-agonists, such as salbutamol, which act as ASM relaxants and provide rapid relief from airway limitation in most asthmatic patients.

As with all contractile responses, ASM contraction is dependent upon an increase in the concentration of intracellular calcium (Ca^{2+}). Contraction of ASM occurs as a biphasic response, with an initial sharp increase in the Ca^{2+} concentration, known as tension development, followed by a plateau of increased Ca^{2+} concentration just above baseline levels, known as tension maintenance (Murray & Kotlikoff 1991), (Pelaia et al. 2008). Increases in intracellular Ca^{2+} concentration occur through two mechanisms, either an influx of extracellular Ca^{2+} through channels in the plasma membrane or a release of Ca^{2+} from intracellular stores in the sarcoplasmic reticulum. The dominant mechanism leading to ASM contraction is thought to be the release of Ca^{2+} from the intracellular stores (Pelaia et al. 2008).

ASM is predominantly innervated by vagal efferent nerves that release acetylcholine (Ach) when stimulated. Ach subsequently binds to and activates muscarinic cholinergic receptors present on ASMCs. Five human muscarinic cholinergic receptors have been cloned (Hulme et al. 1990), with M_3 thought to be the most important in stimulating the contraction of ASM (Roffel et al. 1990). M_3 receptors are G-protein coupled receptors that couple to heterotrimeric guanosine triphosphate (GTP) binding proteins, known as Gq. Following the binding of Ach to M_3 receptors, guanine exchange in the alpha subunit of Gq is stimulated, with GDP being exchanged for GTP, leading to activation and subsequent release of the α subunit from the $\alpha\beta\gamma$ holomer. Activated αGq then activates phospholipase C, which catalyses the breakdown of phosphatidylinositol 4,5-bisphosphate (PIP_2) to inositol

triphosphate (IP_3) and diacylglycerol (DAG). IP_3 then binds to its receptors on the sarcoplasmic reticulum, leading to the release of Ca^{2+} from the sarcoplasmic reticulum and an increase in the intracellular Ca^{2+} concentration (Mignery & Südhof 1990). This Ca^{2+} activates the calcium-dependent kinase Calmodulin, which phosphorylates serine 19 of myosin light chain kinase (MYLK), leading to its activation. MYLK then phosphorylates myosin light chain (MLC) 20, which triggers cross-bridging cycling and thus contraction of the ASM (Figure 1.1).

In addition to direct agonist stimulated Ca^{2+}-dependent phosphorylation of MLC, there is evidence that a Ca^{2+} independent mechanism, known as Ca^{2+}-sensitization, also contributes to ASM contraction. This phenomenon of Ca^{2+}-sensitization occurs when there is no alteration in intracellular Ca^{2+} levels, but there is an increase in contraction. It occurs though protein kinase C or RhoA, which phosphorylate and inhibit MLC-phosphatase leading to an increase in the level of phosphorylated MLC. Ca^{2+}-sensitization has been shown to occur in the ASM of canines (Bremerich et al. 1997), rabbits and humans (Yoshii et al. 1999). Pharmacological inhibitors of RhoA increase levels of ASM relaxation and there is evidence for increased RhoA expression in a rat model of asthma (Chiba et al. 1999). As yet, however, there is no strong evidence for a role of RhoA or Ca^{2+} sensitization in asthmatic patients.

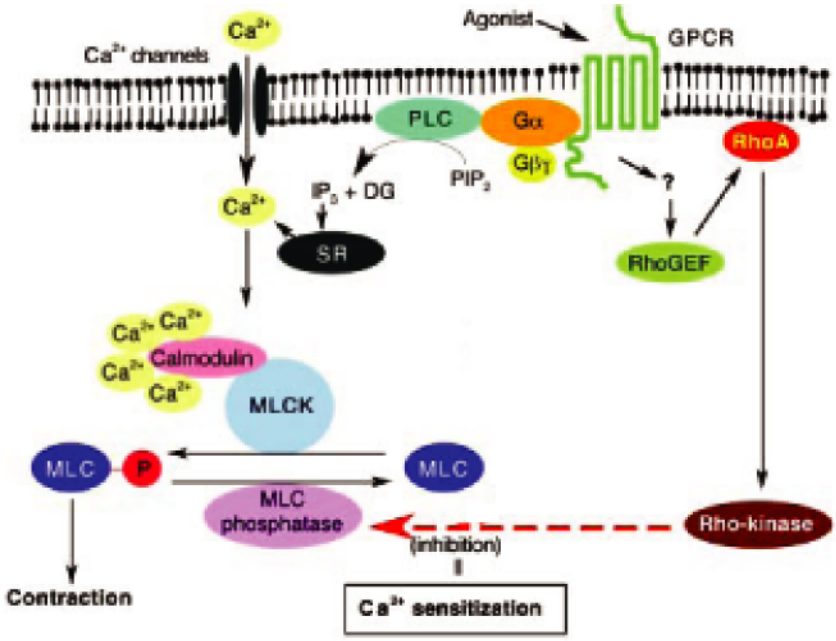

Figure 1.1 - ASM Contraction - ASM contraction is stimulated by the activation of signaling cascades downstream of G-protein coupled receptors that ultimately lead to the phosphorylation of myosin light chain. In addition, calcium independent signaling mechanisms that act via a RhoA mediated pathway are able to increase the contractility of ASM by inhibiting the function of myosin light chain phosphatase. [Figure adapted from (Chiba 2004)].

Due to obvious difficulties in obtaining intact ASM bundles there are relatively few studies comparing the intrinsic contractile properties of asthmatic and healthy ASM. There is some evidence that asthmatic ASM has an increase in maximal shortening (Thomson et al. 1996) (Bramley et al. 1994), however, these data are based on results from very few donors. There are reports of increased contraction of asthmatic ASM compared to healthy controls following stimulation with contractile stimuli (Bai 1990) along with evidence for asthmatic ASM specific responses (Joos et al. 2003). In contrast to this, however, there are also reports showing no differences in the contraction of asthmatic and healthy ASM (Roberts et al. 1987). Due to the difficulties in directly comparing the contractile responses of asthmatic and healthy ASM the majority of studies have inferred potential differences in contractility indirectly through assaying the expression of contractile mediators, in particular MYLK. Ammit *et al.* demonstrated that allergy and sensitization correlated with increased expression of MYLK (Ammit et al. 2000) and this model was progressed by Ma *et al.* who suggested that ASM from asthmatic patients showed increased

contractility when compared to healthy controls directly *ex vivo* and that this increased contractility correlated with an increased level of MYLK mRNA in asthmatics. It should be noted, however, that this data was collected from a small number of cells, raising questions as to the level of cell sampling per subject. The data is also not confirmed at the protein level (Ma et al. 2002). In contrast to this data, Woodruff *et al.* reported no difference the expression of MYLK mRNA between mild asthmatics and healthy individuals (Woodruff et al. 2004).

In addition to potential intrinsic differences in the contractility of asthmatic compared to healthy ASM, a variety of cytokines present in the inflammatory milieu of the asthmatic lung are known to stimulate ASM contraction. The pro-inflammatory cytokine TNFα potentiates the increase in free Ca^{2+} induced by bradykinin in a guinea-pig model system (Amrani 1993) and in human cells (Amrani et al. 1996). CD38 knock-out mice show decreased hyperresponsiveness following TNFα challenge, identifying a potential signaling pathway (Guedes et al. 2006). In addition, *in vitro* treatment of ASM with TNFα, IL-1β and IL-13 results in an increase in CD38 expression (Deshpande et al. 2003) (Deshpande et al. 2004). CD38 is a cell surface protein that catalyses the synthesis of ADP-ribose leading to an increase in calcium release and therefore increased contraction. IL-13 increases ASM contraction in response to stimuli such as bradykinin and histamine in both mouse and human cells (Tliba et al. 2003). Treatment of cultured human ASM with IL-13 increases RhoA expression, implying a potential mechanism for IL-13 mediated augmentation of contractile responses through Ca^{2+}-sensitization (Chiba et al. 2009).

1.5.2.3 Synthetic functions of ASM

The traditional view of ASM as a passive partner in the asthmatic phenotype is expanding through increasing evidence that ASMCs have synthetic capabilities. ASMCs have been shown, particularly *in vitro*, to express a number of factors, including chemokines, cytokines, cell adhesion molecules, co-stimulatory molecules and extracellular matrix (ECM) proteins, all of which could contribute to the asthmatic response. The relative contribution of this synthetic function of ASMCs compared to infiltrating inflammatory cells is unclear, however, the potential of ASMCs to influence their local inflammatory environment, either directly though cytokine release or indirectly through the recruitment of inflammatory cells by chemokines and cell adhesion molecules represents an exciting area of ASM research.

1.5.2.3.1 Immunomodulatory molecules

ASMCs can express immunomodulatory molecules such as cytokines, chemokines. cell adhesion molecules and co-stimulatory molecules. These features of ASMCs, which clearly influence inflammatory responses, may be exaggerated in asthma where the mass of ASM is increased.

1.5.2.3.1.1 Chemokine expression

The major mechanism by which ASMCs influence the inflammatory response appears to be through the secretion of various chemokines. The expression of CCL11 mRNA and protein has been detected in ASM bundles and it was suggested that this expression was increased in asthmatic patients compared to healthy controls (Ghaffar et al. 1999). Further, *in vitro* studies of cultured ASMCs have demonstrated that a variety of stimuli, including IL-1β, TNFα, IL-13 and TGFβ are able to increase the expression of CCL11 (Pang & Knox 2001) (Ghaffar et al. 1999) (Jarai et al. 2004). CCL5 expression has also been detected in the ASM bundles of bronchial biopsies from both healthy and mild asthmatic patients (Berkman et al. 1996). These immunohistochemistry findings were reproduced using ASMCs in culture, with TNFα shown to stimulate production of CCL5 (John et al. 1997). Brightling *et al.* have reported increased detection of CXCL10 in asthmatic ASM bundles and from asthmatic ASMCs in *ex vivo* culture (Brightling et al. 2005). This expression is associated with an increase in the detection of $CXCR3^+$ mast cells in asthmatic ASM bundles (discussed in Chapter 1.5.2.4). ASM also has the potential to express a range of other chemokines. IL-8 expression is induced following stimulation with either TNFα and IL-1β (Watson et al. 1998) or bradykinin (Pang & Knox 1998) whilst the Th2 specific chemokine CCL17 is expressed by ASM following a combination treatment containing IL-4, IL-13 and TNFα (Faffe et al. 2003).

1.5.2.3.1.2 Cytokine expression

ASMCs cultured *in vitro* produce detectable levels of IFNγ and IL-5 following passive sensitization with atopic sera (Hakonarson et al. 1999), whilst stimulation with a combination of IL-1β and TNFα induces GM-CSF expression (Oltmanns et al. 2003). The relevance of these levels of cytokines and a lack of corroborating *in vivo* data, either from animal models or detection of cytokine protein in biopsies, has lead to speculation as to the importance of this phenomenon. Further studies into the production of cytokines by ASM are therefore required, however, it could be hypothesized that the production of cytokines by ASMCs may have influence the

local inflammatory environment.

1.5.2.3.1.3 Cell-adhesion and co-stimulatory molecule expression

ASMCs are capable of expressing a number of molecules with roles in the recruitment and subsequent activation of inflammatory cells. Lazaar *et al.* showed that ASM constitutively expresses the cell-adhesion molecule CD44 and that TNFα stimulation increases the expression of CD54 and CD106 above minimal basal levels. This allows interaction between the ASM and activated, but not resting, T cells (Lazaar et al. 1994). ASM also expresses CD40 and cross-linking between this and CD40-ligand expressed on T cells and eosinophils modulates ASM function through NFκB signaling (Lazaar et al. 1998). Following co-treatment with TNFα and IFNγ, CD40 expression is significantly higher on cultured ASMCs from asthmatics compared to healthy controls (Krimmer et al. 2009).

1.5.2.3.2 Interaction of ASMCs and the extracellular matrix

Black *et al.* have shown that cultured ASMCs constitutively express the latent form of TGFβ (Black et al. 1996) whilst further studies have demonstrated that ASMCs also express plasmin, which is capable of activating latent TGFβ1 and TGFβ2 (Coutts et al. 2001). TGFβ is important in connective tissue synthesis and the ability of ASM to express and activate it therefore implies that ASM may have important roles in regulating ECM function. Following *in vitro* stimulation with 10% human serum, cultured human ASMCs secrete elastin, laminin β1, laminin β2, collagen I, III, IV and V. The component of serum stimulating the generation of these ECM factors is currently unknown. TGFβ has received much attention as its reported biological activities involve stimulating the synthesis of the above molecules. With relevance to asthma, *in vitro* stimulation with 10% human serum from asthmatics caused an increase in the synthesis of fibronectin, laminin γ, perlecan and chrondroitin sulphate by cultured ASMCs from healthy individuals when compared to stimulation with 10% serum from healthy individuals (Johnson et al. 2000).

The interaction between ASM and the ECM is bi-directional and there is evidence that the ECM is able to influence the function of ASM. Hirst *et al.* showed that changes in the ECM associated with asthma cause a more proliferative phenotype in ASM. *In vitro* culture of ASMCs on a matrix with high levels of collagen I and fibronectin, as is typical of the asthmatic lung, caused an increase in mitogen activated proliferation compared to cells grown on a matrix with high levels of

laminin, which is representative of the ECM found in healthy individuals (Hirst 2000). In addition, the same culture conditions also increased the levels of IL-1β induced CCL5 and CCL11 expression (Peng et al. 2005).

1.5.2.4 Localisation of mast cells in ASM bundles

The localisation of mast cells in ASM bundles was first reported by Brightling *et al*. (Brightling et al. 2002). It should be noted that there is speculation that a localisation of mast cells in the ASM bundles may be a feature of general obstructive pulmonary diseases, rather than being specific to asthma (Tunon-de-Lara et al. 2002). There is evidence for the possible mechanism of recruitment of mast cells to ASM bundles as human ASMCs treated *in vitro* with mast cell tryptase stimulate increased chemotaxis of mast cells (Berger et al. 2003). In addition it has been shown that asthmatic ASM expresses increased CXCL10, a mast cell chemokine, compared to healthy ASM both *in vivo* and during *ex vivo* cultures (Brightling et al. 2005).

The consequences of interactions between mast cells and ASM bundles are still unclear. A number of studies have suggested that mast cell mediators stimulate proliferation of ASMCs (Cho et al. 2003), however, there is also evidence that some mast cell mediators may suppress ASM proliferation (Lazaar et al. 2002). A recent study using co-culture models of mast cells and human ASMCs concluded that mast cells had no influence on either ASMC proliferation or survival (Kaur et al. 2010).

1.6 Aims of the thesis

As discussed during this introduction there are a wide range of reports suggesting intrinsic differences between the ASMCs of asthmatics compared to healthy individuals. In addition, there is strong evidence that a variety of molecules present in the inflammatory milieu of the asthmatic lung are able to influence the phenotype of ASM. In order to investigate these aspects of ASM biology further, microarray gene expression studies were performed in the Asthma, Allergy and Respiratory Disease Department prior to the initiation of this project. These microarray studies were aimed at investigating potential intrinsic differences in gene expression between ASMCs isolated from healthy individuals compared to mild and moderate asthmatic patients, along with identifying genes responsive to *in vitro* treatment of cultured ASMCs with IL-13 or TGFβ. Although these were only small pilot studies, interesting data was generated with a number of genes demonstrating differential

expression that correlated to the level of disease severity. In addition, a number of the identified genes had previous independent evidence that implicated them as potentially pro-asthmatic.

The aims of this project were therefore to build upon the data generated during these previous studies by investigating potential differences in the regulation of gene expression in healthy and asthmatic cultured ASMCs. The two main areas of investigation were the post-transcriptional regulation of gene expression by microRNAs (miRNAs) and the contribution of chromatin and histone modifications to the regulation of transcription in ASM. This thesis is therefore divided into three main areas of investigation.

i) Comparative microarray expression studies performed to determine if there is differential expression of miRNAs between healthy and asthmatic cultured ASMCs.

ii) Experiments performed to determine if an individual miRNA found to be differentially expressed between healthy and asthmatic cultured ASMCs has pro-asthmatic functions.

iii) Unbiased, genome-wide profiling of histone methylations in ASMC cultures derived from healthy individuals.

Chapter 2 - Methods

2.1 Cell culture

2.1.1 Human ASMC culture

Human ASMCs were obtained from deep endobronchial biopsies of healthy and moderate asthmatic volunteers. Moderate asthmatics were defined as demonstrating a history of typical symptoms over at least two years, with a minimum of 12% reversibility, a methacholine bronchial challenge response at <8mg/ml and a predicted forced expulsion volume (FEV_1) of between 70 and 90%. Healthy controls were defined by a life-long absence of symptoms and lung functions within normal limits. No subjects were current smokers and none were currently undergoing courses of steroid treatment. Ethical approval was granted by the Research Ethics Committee at King's College Hospital (KCL #11-03-209 and 10-H0804-066). All cell culture reagents, unless otherwise stated, were from Gibco Invitrogen.

Pure cultures of ASMCs were isolated as previously described (Hirst 2000), (Chan 2006). Briefly, ASM bundles were visualized using a dissecting microscope and dissected free of the surrounding tissues. The dissected ASM bundles were grown by explant culture in 12.5cm^2 cell culture flasks. Fluorescent immunocytochemistry routinely confirmed that near-confluent, fetal bovine serum (FBS)-deprived ASMCs (passage 2) stained (>95%) for α-smooth muscle actin, desmin, and calponin.

Cells were cultured at 37°c with an atmosphere of 5% CO_2 in Delbucco's Modified Medium (DMEM) containing 10% FBS, L-glutamine (2mM), sodium pyruvate (1mM), 1x non-essential amino acids, fungizone (2UG/ml) and gentamicin (50μg/ml). Media was changed every 72 hours and cells sub-cultured once they reached confluence by treatment with Trypsin-ethylenediaminetetraacetic acid (EDTA) (0.025%, Invitrogen). Cells were used for experiments at passages 3-7.

2.1.2 HEK293 cell culture

HEK293 cells were a gift from Dr Susan John (KCL, London, UK). Cells were cultured in DMEM (Invitrogen), supplemented with 10% FBS (Sigma), 100U/ml penicillin (Invitrogen), 100ug/ml streptomycin (Invitrogen) and 2mM L-glutamine (Invitrogen) and incubated at 37°c in humidified air containing 5% CO_2. Cells were routinely passaged (1:8 to 1:10 dilution) after reaching confluence.

2.2 Cell transfections

2.2.1 Transfection of human ASMCs with small RNAs

ASMCs were seeded at an initial density of $1.5x10^4$ cells/cm^2 and allowed to attach overnight at 37°c in DMEM + 10% FBS (as described in Chapter 2.1.1). The cells were growth arrested by a 72 hour incubation in serum free DMEM supplemented with L-glutamine (2mM), sodium pyruvate (1nM), 1x non-essential amino acids, fungizone (2UG/ml), ascorbate (0.1mM), bovine serum albumin (0.1%, Sigma), insulin (1uM, Sigma) and transferrin (5ug/ml, Sigma). Media was replaced with fresh serum-free media immediately prior to transfections, which were performed using Lipofectamine 2000 reagents (Invitrogen) according to the manufacturers instructions. Briefly, the appropriate amount of small RNA, either pre-miR-155, anti-miR-155 or the corresponding non-targeting control (All Ambion, see Table i), was diluted in OPTI-MEM (Invitrogen) such that the final concentration of RNA in the transfection solution was as desired. The Lipofectamine solution was diluted 1:50 in OPTI-MEM before being combined with the diluted oligonucleotide solution and incubated at room temperature for 20 minutes to allow the formation of liposomes. The lipofectamine/oligonucleotide mix was added dropwise to the ASMCs before incubation at 37°c with 5% CO_2 for 6 hours. After 6 hours a phosphate buffered saline (PBS) wash was performed and the media was replaced with fresh serum-free media. If required, a 6 hour timepoint was harvested for appropriate analysis, further timepoints were taken at the stated intervals.

2.2.2 Flow cytometry analysis of transfected ASMCs

ASMCs transfected with fluorescein amidite (FAM)-labeled non-targeting pre or anti-miR controls were assessed by flow cytometry to determine transfection efficiency. Transfected cells were harvested by Trypsin-EDTA treatment (0.025%, Invitrogen) and stained with Live/Dead Fixable Dead Cell Stain Kit (Invitrogen), according to the manufacturers instructions. Live cells were gated as those that were forward scatter high and dead cell stain low. 10,000 live events were counted for each sample and quadrant statistics were determined compared to mock transfected cells treated with Lipofectamine 2000 only.

2.2.3 Transfection of HEK293 cells

HEK293 cells were seeded at $2.8x10^4$ cells/cm^2 and allowed to attach overnight in DMEM with supplements (as described in Chapter 2.1.2). 50ng pGL4.13 and 5ng pRL-TK plasmids were combined with the appropriate amount of pre-miR-155 or

non-targeting control (Ambion, see Table i) to generate the required concentration of small RNA in the final transfection solution. The plasmid and oligonucleotide mix was added to 4x calcium chloride (Sigma) and the solution mixed. This solution was applied dropwise to 2x Hepes Buffered Saline (Sigma) whilst agitating and the mixture was incubated at room temperature for 30 minutes to allow a precipitate to form. The precipitate was added dropwise to the HEK293 monolayer and incubated overnight at 37°c in an atmosphere containing 5% CO_2 in humidified air. The media was replaced the following day, before a further overnight incubation and harvesting for analysis of luciferase activity the following day.

Small RNA	Catalogue Number
pre-miR-155	PM12601
Non-targeting pre-miR Control	AM17121
anti-miR-155	AM12601
Non-targeting anti-miR Control	AM17012

Table i – Small RNAs used in ASMC and HEK293 transfections- all small RNAs were from Ambion.

2.3 RNA isolation and reverse transcription-quantitative PCR (RT-qPCR)

2.3.1 RNA isolation and DNase treatment from cultured ASMCs

ASMCs were seeded at an initial density of $1.5x10^4$ cells/cm^2 and allowed to attach overnight at 37°c in DMEM + 10% FBS (media constituents as described in Chapter 2.1.1). The cells were growth arrested through a 72 hour incubation in serum-free DMEM (as described in Chapter 2.2.1). RNA was isolated from approximately $5x10^5$ cells per sample using TRIzol methodology (Invitrogen) as per the manufacturers instructions. DNase I digestion was performed using the TURBO DNase Kit (Ambion) according to the manufacturers instructions. RNA was quantitated using a Nanodrop 1000 (Thermo Scientific) and RNA quality was assessed using a Bioanalyser (Agilent). RNA samples used throughout the thesis routinely generated an RNA Integrity Number (Schroeder et al. 2006) of greater than 8 (Figure 2.1).

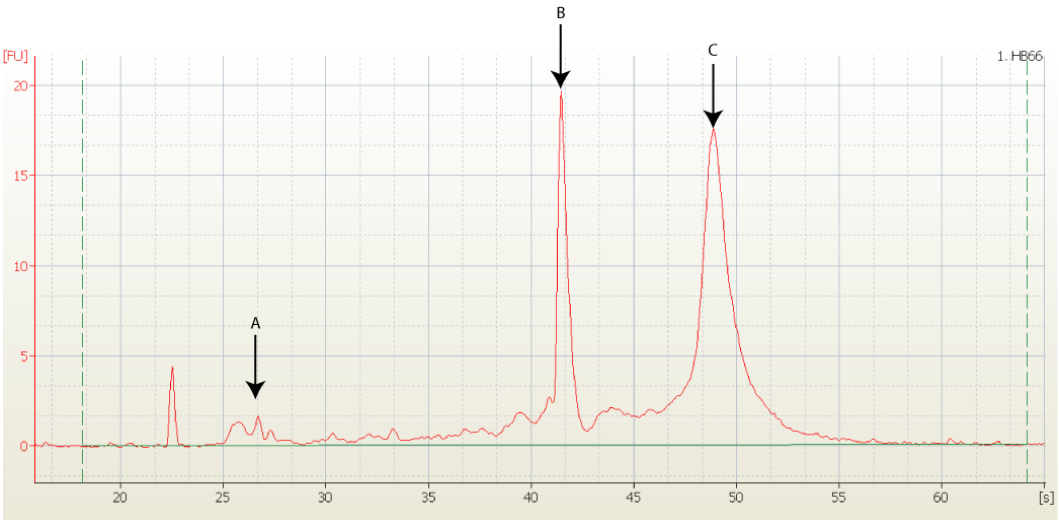

Figure 2.1 - Representative RNA sample - RNA was harvested using TRIzol methodology and DNase treated. The image is an electropherogram representation of an RNA sample as produced by the Agilent Bioanalyser Software. The arrows correspond to A) 5S RNA including miRNAs, B) 18S RNA and C) 28s RNA. The RNA Integrity Number of this sample, as determined by the Agilent software, was 8.0.

2.3.2 Hairpin primer specific RT-PCR for mature miRNAs

10ng total RNA (isolated as described in Chapter 2.3.1.) was incubated with a master mix containing final concentrations of 1mM dNTPs (Fermentas), RiboLock (8U, Fermentas), 1x reverse transcriptase buffer with 50U reverse transcriptase (High capacity cDNA archive kit, Applied Biosystems) and 1x miRNA specific primer (Applied Biosystems, Table ii). The reaction was incubated at 16°c for 30 minutes, 42°c for 30 minutes and 85°c for 5 minutes using a Mastercycler Gradient PCR machine (Eppendorf).

2.3.3 RT-PCR for total cDNA generation

RT-PCR was performed on 500ng RNA for all samples. First strand cDNA synthesis was performed by first incubating the RNA with 0.4μg $pd(N)_6$ random hexamers (Amersham) at 70°c for 5 minutes, before chilling on ice. A master mix containing 1x M-MuLV reaction buffer (Fermentas), 1mM dNTPs (Fermentas) and RiboLock (40U, Fermentas) was added and incubated at room temperature for 5 minutes. M-MuLV reverse transcriptase (400U/reaction, Fermentas) was added and the reaction incubated at 42°c for 1 hour before being stopped by a 10 minute incubation at 70°c. Reactions for all samples were also performed without the addition of M-MuLV reverse transcriptase as a control sample for potential genomic DNA contamination.

2.3.4 Quantitative PCR (qPCR) for mature miRNAs

Reactions were set up with a final concentration of 1x Taqman specific primer (see Table ii), 1x master mix (Applied Biosystems) and 2μl cDNA template generated from the corresponding reverse transcription reaction (see Chapter 2.3.2).

qPCR was performed using cycling parameters of an initial incubation at 50°c for 2 minutes and 95°c for 10 minutes, followed by 40 cycles of 95°c for 15 seconds and 60°c for 1 minute using an ABI Prism 7900HT Thermal Cycler (Applied Biosystems). For each primer set assayed a threshold cycle (Ct) was determined from the amplification plots generated using SDS 2.1 Software (Applied Biosystems). To prevent reaction components becoming a limiting factor, the threshold line was set within the middle of the exponential phase in the amplification curve. The Ct value corresponds to the cycle number at which the amplification curve crosses the threshold line. A low Ct value therefore reflects a higher concentration of primer target sequence in the sample and hence a higher expression level of the target miRNA. Expression levels of specific miRNAs are calculated relative to either RNU6B or let-7b as the endogenous control gene, stated in the results where appropriate. The expression level of specific miRNAs was calculated according to ΔΔCt methodology, expressed as $\Delta Ct = Ct^{target} - Ct^{control}$ and $\Delta\Delta Ct = 2^{-(\Delta^{CtTarget}/\Delta^{CtReference})}$.

miRNA	Primer ID Number
RNU6B	001093
miR-20a	000580
miR-93	000432
miR-146a	000468
miR-155	000479
miR-335	000546
Let-7b	002619

Table ii – miRNA RT and qPCR primer sets- All primers were from Applied Biosystems.

2.3.5 qPCR to determine mRNA expression

Primer sets to assess the expression of mRNAs by qPCR were either Taqman Gene Expression Assays (Applied Biosystems) or designed using the Universal Probe

Library (UPL, Roche) in combination with specific flanking primers (Eurofins MWG) (for details, see Table iii). 18S (Applied Biosystems) was used as the endogenous control for all mRNA qPCR experiments described and reactions were performed as multiplex or singleplex reactions for Taqman Gene Expression Assays and UPL assays respectively. Where reactions were performed as multiplex, primers were validated for their efficiency in this reaction set-up. ΔΔCt methodology was employed to analyse the data, with the sample used as the standard in individual experiments stated in the relevant results section.

Gene	Taqman / UPL	Primer Number	UPL	Flanking oligos (5'-3')
BIC	Taqman	hs01374570_m1	N/A	N/A
RhoA	UPL	N/A	9	ctcggattcgttgcctga
				ggaactggtccttgctgaag
MYLK	UPL	N/A	15	tgcttcagaatgaggacgtg
				acacctggcaactgcattc
CCL2	UPL	N/A	4	agtctctgccgcccttct
				gtgactggggcattgattg
CCL5	UPL	N/A	3	acaccagtggcaagtgctc
				acacacttggcggttctttc
CCL11	UPL	N/A	40	atgaaggtctccgcagca
				ggtggttgggacagaagc
CCL13	UPL	N/A	40	accttcaacatgaaagtctctgc
				ggacgttgagtgcatctgg
CCL26	UPL	N/A	38	cctgagtctccaccttggaa
				aaggggcttgtggctgta
CD38	Taqman	hs00277045_m1	N/A	N/A
CXCL10	Taqman	hs00171042_m1	N/A	N/A
CXCL11	Taqman	hs00171138_m1	N/A	N/A
IRF1	Taqman	hs00971960_m1	N/A	N/A
BRWD1	UPL	N/A	4	ccacccagtatttcaagagtca
				ctgtgtgcctgcagtctttt
COL21A1	UPL	N/A	7	ttaatgggtagtcccggtttc
				ctccccgtgttccatcct
MALAT1	UPL	N/A	10	gcaggtgctagttcttggagtt
				gctcctgacaaattatacatcaagg
ITGA8	UPL	N/A	3	tggctccagcttcctatgat
				tgctgagaatccccagtaaac
ZNF652	UPL	N/A	28	ttcgacgaacacatgaaaaca
				gtgagttctgcggtgtctctt

Table iii - Details of primers used for qPCR studies

2.3.6 Statistical analysis of qPCR

All statistical analysis of qPCR results was performed using Prism 5.0. Where paired or repeated measures analysis is performed, Friedman's Test with Dunn's multiple correction or 2-way ANOVA with Bonferroni multiple testing correction has been

used. In cases where non-repeated measures are analysed a Mann-Whitney U Test has been performed.

2.4 Protein analyses

2.4.1 Protein extraction

Following the transfection of ASMCs with pre or anti-miRNAs (described in Chapter 2.2.1), cytoplasmic and nuclear protein fractions were isolated from $1x10^6$ cells using a NE-PER kit (Thermo Scientific) according to the manufacturers instructions. Extracts were quantitated using a BCA assay (Pierce) to ensure that comparable amounts of total protein were used in subsequent analyses.

2.4.2 SDS-polyacrylamide gel electrophoresis and western blotting

Polyacrylamide gels were cast at 8% or 15% for interrogation of RhoA and MYLK protein expression respectively. 35µg of cytosolic protein extract, as determined by BCA assay, was denatured by the addition of sodium dodecyl sulfate (SDS) loading buffer (62.5mM Tris HCl [pH6.8], 2% SDS, 5% glycerol, 0.3M β2-mercaptoethanol and 0.01% bromophenol blue) and incubation at 95°c for 5 minutes. Proteins were separated by electrophoresis through the polyacrylamide gel in 1x running buffer (2.5mM Tris, 25mM Glycine [pH8.3] and 0.01% SDS) at 25mAmps/gel. Following the sufficient resolution of proteins at the required size, the proteins were transferred to a nitrocellulose membrane (Amersham) by electrophoretic transfer in 1x transfer buffer (25mM Tris HCl, 192mM glycine and 10% methanol) at 400mAmps for 90 minutes.

To probe for RhoA protein, membranes were initially blocked with 5% milk in TBS-Tween for 1 hour at room temperature. Membranes were probed with an anti-RhoA antibody (1:800, Abcam, ab54835) in 5% milk in TBS-Tween overnight at 4°c with rocking, before three washes with TBS-Tween. The membranes were then briefly re-blocked with 5% milk in TBS-Tween for 30 minutes at room temperature, before an anti-mouse-HRP secondary antibody was added (1:1000, Santa Cruz, sc-2055). The membranes were developed with ECL (Amersham) and the image exposed on High Sensitivity Hyperfilm (Amersham). The membranes were then stripped by a 1 hour incubation at 50°c with 1x stripping buffer (100mM β2-mercaptoethanol, 2% SDS and 62.5nM Tris HCL [pH6.8]) and re-probed with an anti-GAPDH antibody (1:25000, GeneTex, GTX28245) and anti-mouse-HRP secondary antibody (as before), as a loading control.

Probing for MYLK was carried out as for RhoA, except that blocking was performed in 5% bovine serum albumin in TBS-Tween. Antibodies used were anti-MYLK (1:4000, Abcam, EP1458Y) and anti-rabbit-HRP secondary (1:2500, Santa Cruz, sc-2004).

The quantification of western blots was performed by densitometry analysis using ImageQuant software. The intensity of each band was calculated and normalised to the background intensity of pixels immediately adjacent to the marked area containing a band. Intensities of RhoA bands were normalised to GAPDH and are expressed relative to the non-transfected mock sample.

2.4.3 CCL5 ELISA

Supernatants from transfected ASMCs (described in Chapter 2.2.1) were stored at -20°c. An ELISA to determine the levels of CCL5 in the supernatants of respective post-transfection cultures was performed using a Human CCL5/RANTES Quantkine ELISA kit (R&D Systems) according to the manufacturers instructions.

2.5 Cloning and testing potential miR-155 target sites

pGL4.13 and pRL-TK plasmids (Promega, see Figure 2.2) were a gift from Dr Susan John (KCL, London, UK).

Primers were designed to amplify regions of 300-500 base pairs centering on predicted miR-155 target sites. PCR reactions were performed for individual targets using the primers detailed in Table iv to amplify regions from template DNA of either cDNA isolated from healthy human ASMCs or total genomic DNA (Promega). PCR reactions were prepared as 5ng cDNA or 15ng genomic DNA template (as appropriate, see Table iv), 1x Taq Buffer (Fermentas), 2.5mM $MgCl_2$ (Fermentas), 2.5mM dNTPs (Fermentas), 0.4nM specific flanking primers (see Table iv) and 0.1U Recombinant Taq polymerase (Fermentas) and performed using the cycling parameters of 95°c for 10 minutes, followed by 25 cycles of 95°c, the specific annealing temperature for a primer pair and 72°c, for 1 minute each, followed by 10 minutes at 72°c. All PCRs were performed using a Mastercycler Gradient PCR machine (Eppendorf). The resultant PCR solutions were electrophorised, before the PCR product was excised and DNA purified from the agarose (Qiagen, Gel Extraction Kit). PCR products were sub-cloned directly 3' of the luciferase open-reading frame (ORF) in the pGL4.13 plasmid using Xba1 or Fse1 restriction sites (as indicated, see

Figure 2.2 and Table iv). PCR inserts were ligated into the pGL4.13 vector using T4 DNA ligase (Fermentas) before transformation of the ligation mix into TOP10 cells, according to the manufacturers instructions (Invitrogen). Plasmid DNA was prepared from individual colonies by Miniprep (Qiagen), Xba1 or Fse1 restriction digest performed to confirm the presence of a correctly sized insert and sequencing of the plasmid performed to ensure the integrity and orientation of the insert. Maxipreps were performed to generate sufficient quantities of individual plasmids (Qiagen).

Gene	Genomic / cDNA template	Primer Sequences (5'-3')
BACH1	Genomic	**CTAGTCTAGA**GAACCCTTGATTTCCTACCTCAGTG
		CTAGTCTAGAGCCCAGAACTCTTGTTTTG
H6PD	cDNA	**CTAGTCTAGA**ATTAGCGGGGAGAGAGATGGAG
		CTAGTCTAGAGGAGAAGCCAGACAGAAAAATCG
ETS	cDNA	**CTAGTCTAGA**CCCTACCATAGAGCCCTGCTTTTTG
		CTAGTCTAGAATAGACCCCAACAGAGTAAGCGG
FOS	cDNA	**CTAGTCTAGA**ACTCAAGTCCTTACCTCTTCC
		CTAGTCTAGAGTCAGAACATTCAGACCACC
JARID2	cDNA	**CTAGTCTAGA**ACCCACACCAAAAAGAGG
		CTAGTCTAGAGGCAGTTTCCAAAATCTG
MYLK	cDNA	**CTAGTCTAGA**TATCGGTTAGGTCATTTGTG
		CTAGTCTAGAGCCCAGAACTCTTGTTTTG
RhoA	cDNA	**CTAGGGCCGGCC**GCAAGCACAGCCCTTATG
		CTAGGGCCGGCCAAGCCCTGAAGTGGTGAC
Septin-11	cDNA	**CTAGTCTAGA**TGTATGCTTGTTCCAACCAC
		CTAGTCTAGAGGGTATCATTTATTCCGTGC

Table iv - Predicted miR-155 target site cloning – Shows the DNA source from which each predicted miR-155 target site was cloned along with the sequence of each primer used. The primer sequence in bold type indicates the restriction enzyme digest site added to each primer to enable efficient sub-cloning.

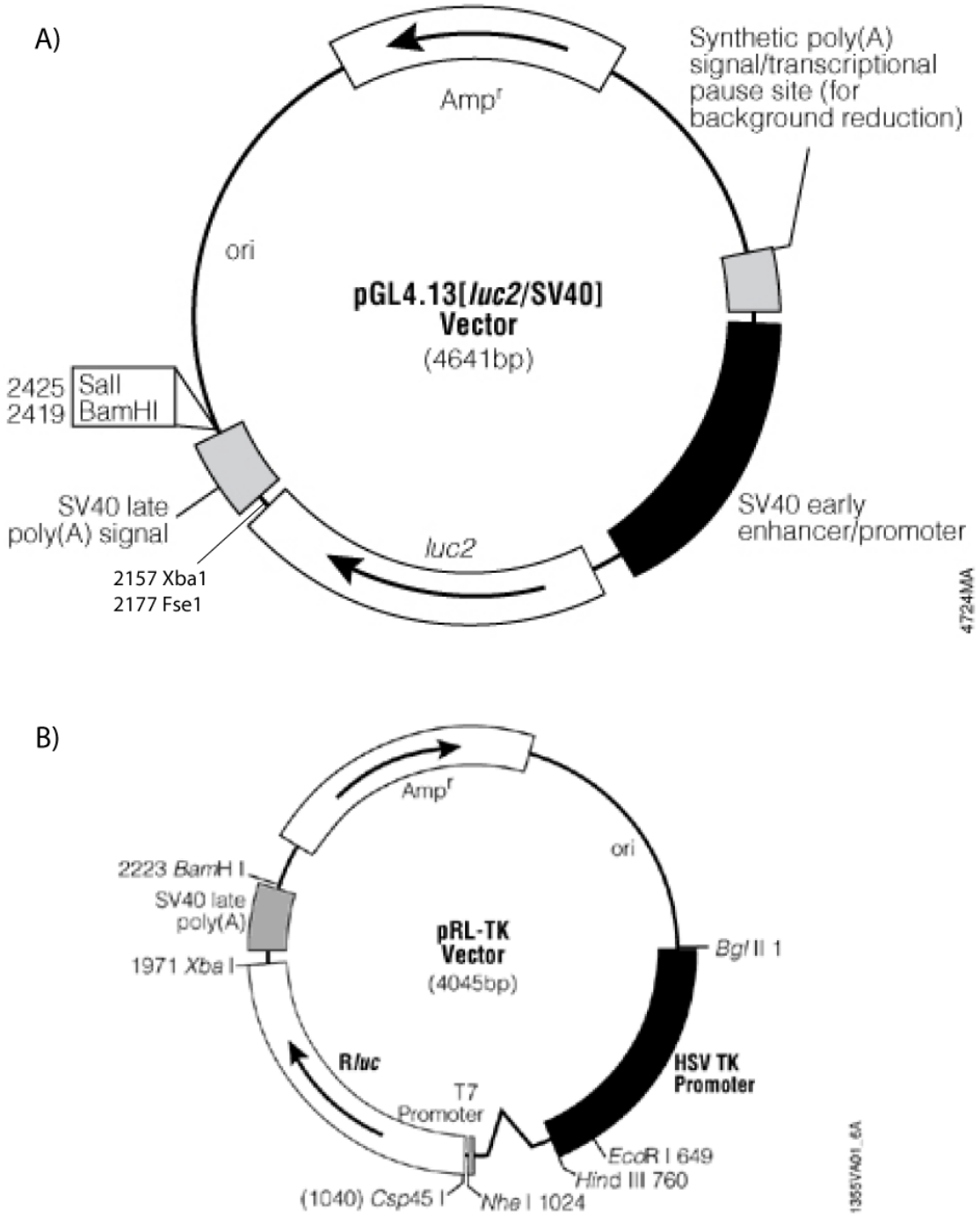

Figure 2.2 – Plasmid maps of pGL4.13 and pRL-TK vectors- pGL4.13 and pRL-TK vectors were used in Dual-luciferase assays. The location of the Xba1 and Fse1 restriction sites in pGL4.13 is shown.

2.5.2 Luciferase Assays

Luciferase assays were performed using the Dual Luciferase Reporter Assay System according to the manufacturers instructions (Promega) following the transfection of HEK293 cells as described in Chapter 2.2.3. Briefly, media was removed from the HEK293 cells and a PBS wash performed. Cells were then lysed in 'Passive Lysis Buffer' by a 15 minute incubation at room temperature with rocking. 10ul of lysate was taken and added to LARII buffer before luminescence was measured (Berthold Handheld Luminometer). Stop & Glo solution was added and Renilla luciferase measured as a transfection control. Triplicates of luminescence were recorded as technical replicates for each transfection and average luminescence calculated. Data are presented following correction for Renilla luciferase levels as a control for transfection efficiency and are expressed relative to cells transfected with pGL4.13 and pRL-TK but no small RNA.

2.6 Microarrays

2.6.1 Affymetrix GeneChip® miRNA microarray

2.6.1.1 FlashTag Biotin HSR RNA labeling

1μg of total RNA per sample was labeled using the Genisphere FlashTag™ Biotin labeling system (Genisphere, as per manufacturers instructions). All reagents used during the labeling protocol, unless otherwise stated, were those provided by Genisphere.

Initially, 1μg of total RNA was polyadenylated through a 15 minute incubation at 37°c of a final reaction mix containing 1x reaction buffer, 2.5mM $MnCl_2$, 1:750 stock ATP mix and 1:15 polyA polymerase enzyme and 1μg of total RNA. The polyadenylated RNA was biotin labeled through the addition of FlashTag Biotin HSR Ligation Mix and T4 DNA ligase, followed by a 30 minute incubation at 25°c. The reaction was stopped by addition of 2.5μl HSR stop solution. A 2μl aliquot of each sample was removed and used in an Enzyme Linked Oligosorbent Assay (ELOSA) assay to confirm successful biotin labeling of each sample.

2.6.1.2 Enzyme Linked Oligosorbent Assay (ELOSA) assay

To confirm successful labeling of each sample used in the microarray analysis, an ELOSA quality control assay was performed as per the manufacturers instructions (Genisphere). Briefly, 1x spotting oligonucletotides were added into the appropriate

number of wells in a 96-well plate, these were covered with an adhesive plate sealer and incubated overnight at 4°c. The spotting oligonucleotides were discarded before two washes with 0.02% Tween-20 in 1x PBS were performed. 5% bovine serum albumin in 1x PBS was added to the wells and incubated at room temperature for 1 hour. Hybridization mixes were prepared containing 2μl of labeled RNA and final concentrations of 1x SSC (0.75M sodium chloride, 0.075M sodium citrate), 0.05% SDS, 0.005% BSA and 1% Dextran sulfate. Positive and negative control samples were prepared by using Genisphere positive or negative control mixes respectively, rather than RNA samples. The bovine serum albumin blocking solution was discarded from the wells and replaced with the appropriate labeled sample, before incubation at room temperature for 1 hour. The wells were then washed 4 times with 0.02% Tween-20 in 1x PBS before 75μl of 1:4000 Streptavidin-horseradish peroxidase (SA-HRP) in 5% bovine serum albumin/1x PBS was added. The samples were incubated at room temperature for 30 minutes before the SA-HRP was discarded and the samples washed 4 times with 0.02% Tween-20 in 1x PBS. 100μl tetramethylbenzidine (TMB) substrate was added to each well and the samples were incubated for 30 minutes in the dark at room temperature. 100μl TMB Stop solution was added to each well and the absorbance was read at a wavelength of 450nm. Sample readings were corrected for background signal by subtraction of the negative control value and samples with an OD reading of greater than 0.1 following background corrections were taken to represent successfully labeled samples, as recommended by the manufacturer.

2.6.1.3 Affymetrix GeneChip® miRNA microarray hybridization

Following positive ELOSA assay results the labeled RNA samples were hybridized to GeneChip® miRNA arrays (Affymetrix). A hybridization cocktail containing final concentrations of 1x hybridization mix, 4% formamide, 10% DMSO, 1x eukaryotic hybridization controls (1.5pM bioB, 5pM bioC, 25pM bioD, 100pM cre, Affymetrix) and control oligonucleotide β2 (50pM, Affymetrix) was prepared. The hybridization cocktail was incubated with the labeled DNA at 99°c for 5 minutes followed by 45°c for 5 minutes. Samples were hybridized to the microarrays at 60rpm and 48°c for 16 hours using a GeneChip® Hybridization Oven 640 (Affymetrix).

2.6.1.4 Microarray washing, staining and scanning

Following the 16 hour incubation, the hybridization cocktail was removed from the microarrays, replaced with array holding buffer (Affymetrix) and the arrays were allowed to equilibrate to room temperature. The arrays were washed and stained on a Fluidics Station 450 (Affymetrix) using fluidics script FS450_0003 and the Hybridization, Wash and Stain Kit (Affymetrix). Fluorescent signals were detected using the GeneChip® Scanner 3000 (Affymetrix) and images were analysed using Gene Chip Operating Software (GCOS, Affymetrix) to generate raw data as .cel files and perform basic quality control on the data.

2.6.1.5 Quality control and data analysis performed in the Affymetrix QC Tool

Initial data analysis and quality control was performed using the miRNA QC Tool (Affymetrix) according to the manufacturers instructions.

Raw .cel files were imported into the software before the default workflow was run. This involved computing the intensity of signal from individual probes by comparison to GC matched 'anti-genomic controls'. The same GC matched 'anti-genomic' probes were subsequently used for background detection and correction. The intensities were normalised by quantile normalisation and a small constant addition was performed to correct for values that had dropped below zero following normalisation. Finally a threshold value was set to express all negative values as zero and median polish summarisation performed to smooth outliers. Various approaches were followed to visualize the data and assess the level of variation across samples (described in Chapter 3.2.2).

2.6.1.6 Data analysis performed in Partek Genomics Suite 2.0

Data was imported into Partek Genomics Suite Version 2.0 as .cel files before the default miRNA analysis workflow package was run, including normalisation of the data using the robust multi-array average (RMA) method developed by Irizarry *et al.* (Irizarry et al. 2003). Briefly this involved a GC-matched background correction of all probes, followed by quantile normalisation across all arrays, a Log_2 transformation and median polish summarization. Further details on analysis performed in Partek can be found in Chapter 3.2.3 and 3.2.4.

2.6.2 Affymetrix GeneChip® Genome U133.2 microarrays

2.6.2.1 Sample preparation and labeling

Affymetrix GeneChip® Genome U133.2 microarrays were performed using 100ng total RNA isolated from ASMCs transfected with either 20nM non-targeting pre-miR control, 20nM pre-miR-155, 100nM non-targeting anti-miR control or 100nM anti-miR-155 (described in Chapter 2.2.1). Mock transfected cells, treated with Lipofectamine 2000 only, were also analysed.

Total RNA was amplified and labeled using the MessageAmp™ Premier RNA Amplification Kit (Ambion), according to the manufacturers instructions. First strand cDNA synthesis was performed by preparing a master mix containing final concentrations of 1x First Strand Buffer Mix and 1x First Strand Enzyme Mix before combining this with 100ng of total RNA from transfected ASMCs. The reaction was incubated at 42°c for 2 hours then stopped by incubation on ice. The First Strand Mixes contain oligo(dT) primers which facilitate the generation of first strand cDNA specifically from polyadenylated RNA. Second strand cDNA synthesis was performed by preparing a master mix with final concentrations of 1x Second Strand Buffer Mix and 1x Second Strand Enzyme Mix, combining this with first strand synthesis reaction and incubating at 16°c for 1 hour. *In vitro* transcription (IVT) was performed by preparing a master mix with final concentrations of 1x T7 Biotin IVT Mix and 1x T7 Enzyme Mix and adding this to the second strand reaction before incubation at 40°c for 14 hours. The IVT reaction results in amplification of the cDNA and incorporation of biotin-labeled dUTP molecules and thus produces amplified RNA (aRNA). The resultant aRNA was purified using aRNA purification beads (Ambion).

The aRNA was quantified using a NanoDrop 1000 (Thermo Scientific) and 12.5μg of aRNA was fragmented. Fragmentation was performed by the addition of Fragmentation Buffer to the aRNA and incubation at 94°c for 35 minutes. The biotinylated aRNA and fragmented biotinylated aRNA were analysed on a Bioanalyser (Agilent).

2.6.2.2 Microarray hybridization, washing and scanning

Microarray hybridization, washing and scanning was performed according to the standard Affymetrix U133.2 workflow. A hybridization cocktail of 1x Hybridization Mix, 10% DMSO, 1x Eukaryotic Hybridization Controls (1.5pM bioB, 5pM bioC, 25pM

bioD, 100pM cre, Affymetrix) and control oligonucleotide β2 (50pM, Affymetrix) was prepared in a total volume of 225µl for each sample. The hybridization cocktail was added to each aRNA sample and incubated at 99°c for 5 minutes in a heat block followed by an incubation at 45°c for 5 minutes in a hybridization oven. These incubations were performed in order to denature then equilibrate the sample respectively. In addition each array was incubated with pre-hybridization buffer at 45°c for 10 minutes in a hybridization oven to allow the arrays to equilibrate. The aRNA and Hybridization Cocktail Mix was then applied to the microarray chips and incubated at 45°c at 60rpm for 18 hours in a hybridization oven.

The aRNA and Hybridization Cocktail mixture was removed from the microarray chips and replaced with Wash Buffer A (Non-stringent Wash Buffer A consisting of 20X SSPE (3M NaCl, 0.2M NaH_2PO_4, 0.02M EDTA and 10% Tween)). Arrays were washed and stained with streptavidin-PE according to the manufacturers instructions using a Gene Chip fluidics station 450 (Affymetrix). Fluorescent signals were detected using a Gene Chip scanner 3000 (Affymetrix) and images were analysed using the Gene Chip Operating Software (GCOS, Affymetrix) to generate raw data as .cel files. Initial quality control analysis was also performed in GCOS.

2.6.2.3 Data analysis performed in Partek Genomics Suite 2.0

Data were imported in Partek as .cel files before the default gene expression workflow was performed to allow normalisation of the data using the RMA method. Briefly this involved a background correction of all imported probe sets, including a model-fit transformation on all imported probes to remove the effects of GC content, quantile normalisation of intensities across all microarrays, a $\log_2$ transformation and a median polish summarisation. Further data analysis in Partek was performed as described in Chapter 4.2.3.

2.7 Chromatin harvest and chromatin immunoprecipitation

2.7.1 Nuclei harvest and chromatin preparation from formaldehyde cross-linked cultured ASMCs

All buffers used were pre-treated with protease inhibitors, phosphatase inhibitors (both Sigma, final concentration 1x) and 5mM sodium butyrate.

Approximately $15x10^6$ ASMCs were seeded at a density of $1.5x10^4$ cells/cm^2 for each chromatin preparation. Cells were allowed to attach overnight in DMEM +10% FBS

(as described in 2.1.1) before being growth arrested by a 72 hour incubation in serum-free DMEM (as detailed in 2.2.1). 37% Formaldehyde was added to the media to a final concentration of 1% and the cells were incubated at room temperature for 10 minutes with rocking. Cross-linking was neutralized by the addition of 1x glycine and cells were detached by Trypsin-EDTA (0.025%, Invitrogen) treatment and gentle scraping, before centrifugation (200g, 7min) to pellet the cells.

Cell pellets were resuspended in a swelling buffer (0.3M Sucrose, 60mM KCl, 15mM NaCl, 5mM $MgCl_2$, 0.1mM EDTA, 0.1mM Tris-HCl [pH7.5], 0.5mM DDT), gently mixed with a lysis buffer (as for swelling buffer with 0.4% IGEPAL-CA) and incubated on ice for 8 minutes. This detergent treatment allowed disruption of the cell membrane whilst retaining the integrity of the nuclear envelope. The sample was layered onto a sucrose cushion (as for swelling buffer but 1.2M sucrose) before centrifugation (Beckman J2-21M/E, rotor J13.1, 10000rpm, 20 mins, 4°c), to facilitate separation of the nuclei from cellular debris. The nuclei were then resuspended in a digest buffer (0.32M sucrose, 50mM Tris-Cl [pH7.5], 4mM $MgCl_2$, 1mM CaCl). An aliquot of nuclei was checked for integrity by 0.2% trypan blue staining (Sigma) and subjective microscope inspection to ensure nuclei had been successfully separated from cellular debris and that nuclear integrity had been retained. Nuclease T7 (20U, Roche) was added to the nuclei and incubated at 37°c for 10 minutes. Reactions were stopped with EDTA (780uM, pH8.0) before the sample was centrifuged (10,000g, 10mins, 4°c) and the supernatant (termed the S1 phase) retained.

The pellet was resuspended in sonication buffer (90mM Hepes pH7.9, 220mM NaCl, 10mM EDTA, 2% Triton X 100, 0.2% sodium Deoxycholate, 0.2% SDS, 0.5mM phenylmethylsulfonyl fluoride) and sonication performed (SONICS Vibra-cell, VCX 130PB, 2mm probe, 60%, 10 second bursts with 30 second ice breaks, for 10 bursts). The sample was centrifuged (10,000g, 10mins, 4°c) and the supernatant retained (termed Sonicated phase). The unreleased material (termed P) was also retained.

To analyse the success of chromatin preparations 10% of the S1 and sonicated fractions, along with the unreleased material, were reverse cross-linked by a 1 hour incubation at 37°c with RNase A (10ug, Fermentas) followed by incubation at 65°c for 3 hours with Proteinase K (20ug, Fermentas). DNA was then isolated from

protein components using a MINIElute Kit (Qiagen, as per manufacturers instructions). The isolated DNA was electrophorised and visualised on an agarose gel.

2.7.2 Chromatin Immunoprecipitation (ChIP)

ChIP reactions were set up by dividing isolated chromatin equally by volume between Input, ChIP and IgG control samples. 25µl Protein G magnetic beads (Active Motif) and 4ug of appropriate antibody (Table v) were added to the chromatin and reactions were diluted to 500µl with modified RIPA buffer (140mM NaCl, 10mM Tris-HCl [pH7.5], 1mM EDTA, 0.5mM EGTA, 1% TritonX-100, 0.01% SDS and 0.1% sodium deoxycholate) and incubated overnight at 4°C with rotation. Beads were washed with a sequence of wash buffer 1 (20mM Tris-Cl pH [8.1], 50mM NaCl, 2mM EDTA, 1% TritonX-100, 0.1% SDS), wash buffer 2 (10mM Tris-Cl [pH8.1], 150mM NaCl, 1mM EDTA, 1% NP40, 1% sodium deoxycholate, 250mM LiCl) and Tris-EDTA to reduce non-specific binding. Following removal of the final wash, elution buffer (0.1M $NaHCO_3$ and 1% SDS) was added before reverse cross-linking by incubation at 37°c with RNase A (10ug, Fermentas) for 1 hour followed by an incubation at 65°c for 3 hours with Proteinase K (20ug, Fermentas). DNA was then isolated from protein components by phenol:chloroform separation (25:24:1, Sigma) and recovered by isopropanol/sodium chloride precipitation using a glycogen carrier.

Input control samples were prepared by reverse-crosslinking and isolating DNA from an equal amount of chromatin as was added to the initial ChIP.

Antibody	Source	Code
H3K4me1	Abcam	ab8895
H3K4me3	Millipore	CS 200 580
H3K27me3	Upstate	07-449
Normal Rabbit IgG	Millipore	CS 200 581

Table v – Antibodies used in ChIP experiments.

2.7.3 ChIP-qPCR

ChIP-qPCR was performed using an ABI Prism 7900HT Thermal Cycler (Applied Biosystems) with cycle parameters of 2 minutes at 50°c and 10 minutes at 95°c for 1 cycle; followed by 40 cycles of 95°c for 15 seconds and 60°c for 1 minute. Reactions were set-up with 1:250 ChIP enriched DNA, 1x MasterMix (Applied Biosystems), 20nM specific forward and reverse flanking primers (Eurofins MWG) and 20nM specific UPL probe (Roche). DNA recovered from ChIPs was assayed in triplicate for technical replicates and quantified by absolute quantification for each primer set assayed.

Primer sets were designed using the Universal Probe Library (UPL, Roche) system. The sequence of the flanking oligos (Eurofins MWG) and the fluorescent UPL probe (Roche) are detailed in Table vi.

The amount of specific DNA in ChIP samples is expressed relative to Input DNA, which represents total genomic DNA from the amount of chromatin added to the initial ChIPs. To calculate the relative amount of target DNA, threshold cycles (Ct) were determined from the amplification plots generated using SDS software version 2.1 (Applied Biosystems) and a standard curve was constructed for each specific primer set using known dilutions of the input material. The relative amount of specific DNA recovered from the ChIP of interest is then expressed relative to the appropriate input sample.

Gene	UPL	Flanking oligos (5'-3')
β-Actin	77	ccgaaagttgccttttatgg
		caaaggcgaggctctgtg
GAPDH	44	cccgtccttgactccctagt
		gtgatcggtgctggttcc
sm-22α	44	agcgtcctggatctctctca
		tctgcactagccaagtcatcc
ARX	63	ccagccatgagcaatcagt
		tggagatttacttttgcactcg
NKX2.3	52	tgaggggacgcaattttct
		aatttctcgccctcgtcttc

Table vi - Details of the flanking primers and UPL probes used in ChIP-qPCR experiments.

2.7.4 ChIP followed by next-generation sequencing (ChIP-seq)

Due to the fact that ChIP-seq and the technologies that facilitate its implementation are very novel, a number of the specific details involved in the required protocols and procedures are proprietary. The principles and relevant details are, however, outlined below.

2.7.4.1 Illumina ChIP-seq library preparation

DNA samples enriched through ChIP, along with the respective Input control samples, were prepared as ChIP-seq libraries using standard protocols and reagents (Illumina, ChIP-seq Library Generation Kit). Briefly, this involved performing an end repair reaction on purified ChIP samples before the addition of adenosine bases to the blunt-ended DNA fragments and ligation of proprietary Illumina Linker Adaptors. To ensure that only DNA corresponding to mononucleosomes with ligated Linker Adaptors was analysed the samples were size separated by electrophoresis through an agarose gel and a band excised between 100 and 250bp. DNA was recovered using a gel extraction kit (Qiagen) according to standard protocols. The recovered DNA was amplified by 17 cycles of PCR with the cycle parameters of 95˚c for 30 seconds followed by 17 cycles of 95˚c for 10 seconds, 65˚c for 10 seconds and 72˚c for 30 seconds, before a final incubation of 72˚c for 5 minutes (using an Eppendorf Mastercycler Gradient). Following amplification samples were separated by electrophoresis through an agarose gel and size selected between 125 and 300 base pairs in order to remove primer artifacts that form during the amplification. To ensure that the DNA samples were appropriately sized and to enable quantification, the samples were analysed using a High Sensitivity DNA Bioanlayser Kit on the Agilent Bioanalyser (Agilent).

2.7.4.2 Cluster generation and Illumina next-generation sequencing

Cluster generation and high-throughput sequencing for the ChIP-seq experiment were performed by Dr Efterpi Papouli at the BRC Genomics Facility housed in the Medical and Molecular Genetics Department of King's College London. Sequencing was performed as 72 base, single-end reads on an Illumina GAIIx instrument and all processes were carried out according to the manufacturers instructions (Illumina).

Each respective ChIP-seq library was diluted to a concentration of 14pM in a NaOH denaturation reaction before being combined with Hybridization Buffer. Illumina sequencing occurs on the surface of a glass slide containing eight channels, known

as a flow cell. The flow cell lanes have oligonucleotides upon their surface that are complimentary to the Linker Adaptors ligated to the ChIP DNA during the library preparation procedure (see Chapter 2.6.4.1). The DNA fragments were added to the flow cell in buffer conditions that result in the adaptor at a single end of the fragments hybridising to its complimentary oligonucleotide on the flow cell. A 3' extension is performed from the double stranded DNA formed between the linker and the immobilized capture oligonucleotide. The original templates are then denatured, resulting in copies that are immobilized on the flow cell. Immobilized DNA template copies are amplified by isothermal bridge amplification, a process that involves the template looping over and hybridizing to adjacent immobilized oligonucleotides. DNA polymerase copies the templates from the hybridized oligonucleotides to form double stranded DNA 'bridges'. These bridges are denatured to form two new single stranded templates. This process is repeating on each template by eleven cycles of isothermal denaturation and amplification to produce millions of individual, dense clonal clusters containing approximately 2000 identical fragments.

Following cluster generation, Illumina next-generation sequencing uses sequencing by synthesis (SBS) technology to sequence all the clusters in parallel. In principle this involves rounds of sequencing cycles and during each cycle a single fluorescently-labeled deoxynucleotide triphosphate molecule is added to each nucleic acid chain through Watson-Crick base pairing to the provided template. The fluorescent label acts as a terminator and an image of the clusters can therefore be collected following the addition of each individual base, with the wavelength of light detected in each cluster allowing the nucleotide incorporated at that position to be determined. The fluorescent dye is then enzymatically cleaved and the process continues for the required number of cycles.

2.7.4.3 Sequence determination and alignment

The sequence of each oligonucleotide cluster was determined from the image files by the Illumina Pipeline (Illumina). Sequence alignment of Input and respective ChIP samples to the reference human genome (Build hg18, 2006) was performed by Dr Venu Pullabhatla using Novoalign v2.07.07 [www.novocraft.com]. Briefly, this process involves Basic Local Alignment Search Tool (BLAST) comparisons of sequences generated from the Illumina GAIIx and identifying those sequences that align uniquely to a single position within the genome.

2.7.4.4 Bioinformatics analysis of H3K4me1, H3K4me3 and H3K27me3 ChIP-seq datasets

The identification of regions of DNA associated with histones demarcated with H3K4me1, H3K4me3 or H3K27me3 was performed by Dr. Venu Pullabhatla using the spatial clustering approach for the identification of ChIP-enriched regions (SICER) algorithm (Zang et al. 2009). Algorithm parameters for each modification are described in the relevant results section. Further analysis of the datasets described in Chapter 5.2 was performed using tools available in ChIPseeqer-2.0 (Giannopoulou & Elemento 2011) or in collaboration with Dr. Venu Pullabhatla.

2.7.5 ChIP following by tiling array analysis (ChIP-chip)

2.7.5.1 Linker-mediated PCR (LM-PCR)

Linkers were produced by annealing equimolar amounts of asymmetric primers (sequences 5'-3': OL1- ATCCCTCGGATA, OL2 - AGGCAACTGTGCTATCCGAGGGAT) via an annealing reaction consisting of 98°c for 10 minutes, following by reductions in temperature by 5°c at 10 minutes intervals until 65°c, and then from 65°c to 25°c the temperature was reduced by 5°c at 20 minute intervals (performed in an Eppendorf Mastercycler gradient). Successful annealing of the oligonucleotides was determined by electrophoresis on an agarose gel and confirmation of a size shift of the annealed product in comparison to both individual starting oligonucleotides.

ChIP enriched DNA samples and respective Inputs were Kinase and Pfu polymerase treated (both Fermentas) to produce blunt-ended DNA fragments. These were then ligated to adaptors (produced as above) via a T4 DNA ligase reaction (Fermentas) at room temperature for one hour. Ligated DNA material was purified using an Enzymatic Reaction Purification Kit (Qiagen,). An aliquot of each respective Input or ChIP sample was diluted 1:5 and amplified by PCR for a range of cycles (17-25) to determine an appropriate number of cycles that resulted in amplification of the DNA without obvious bias towards smaller or larger DNA fragments. Once an appropriate number of cycles was chosen, 25 separate PCR amplifications were performed before a single reaction was size separated on an agarose gel and visualized to confirm successful amplification. A negative control reaction, containing no template DNA, was performed for all samples to ensure that there was no amplification of non-specific DNA contamination. PCR reactions were set-up as 1:5 diluted ChIP or Input DNA, 1x Taq Buffer (Fermentas), 2.5mM $MgCl_2$ (Fermentas), 2.5mM dNTPs (Fermentas), 0.4nM OL1 Primer and 0.1U Recombinant

Taq polymerase (Fermentas) with cycling parameters of 95°c for 10 minutes, followed by the appropriate number of cycles of 95°c for 1 minute, 65°c for 1 minute and 72°c for 1 minute, before a final incubation of 72°c for 10 minutes. Following confirmation of successful amplification, replicate reactions for individual samples were pooled and DNA purified by PCR purification Kit (Qiagen). The DNA was quantified with a Nanodrop 1000 (Thermo Scientific) and 500ng of each sample was size separated by agarose gel electrophoresis and visualized to ensure that the DNA was of mono and dinucleosomal fragment length.

2.7.5.2 Cy3/Cy5 labeling of LM-PCR amplified ChIP material

Input and ChIP samples were labeled with Cy5 or Cy3 dUTP nucleotides (Amersham, catalogue numbers PA53022 and PA55022) respectively using a BioPrime Array CGH Genomic Labeling Module (Invitrogen).

2μg of each DNA sample was combined with Random Primers (final concentration 1x) and incubated at 96°c for 5 minutes to denature the double stranded DNA. The denatured DNA was added to a reaction containing final concentrations of 1x dNTP mix, 22μM Cy3 or Cy5 labeled dUTP and 40U Exo-Klenow polymerase and incubated at 37°c for 3 hours to perform a linear amplification of the DNA that included incorporation of the fluorescent dUTP nucleotides. DNA was recovered using BioPrime Purification Columns (Invitrogen). Successful amplification of the material and incorporation of Cy3 or Cy5 dUTP was determined by Nanodrop 1000 (Thermo Scientific, Microarray setting) and reading of absorbance at 260nm, 550nm and 450nm respectively.

2.7.5.3 Custom ChIP-chip microarray design

Agilent microarray design, processing and data analysis were performed in collaboration with Dr R Jenner at University College London.

The microarrays used were Agilent Custom ChIP-on-chip microarrays (Agilent Custom SurePrint G3 ChIP-on-chip, 4x180K features) and each custom tiling array contained approximately 140,000 60-mer oligonucleotides. For regions covered on the array probe sets were spaced, on average, 250 base pairs apart along the human genomic sequence. The probes covered a variety of genes with known functions in ASM along with adjacent genes, which were included as controls. The probes were designed against build 36 (hg18) of the human genome according to previously

published criteria (Lee et al. 2006). Briefly, this involved removing all non-repeat masked genomic regions that were less than 100 base pairs as it is difficult to design high quality probes against such small regions. Probes were then chosen to be complimentary to non-repeat masked sequences of genes of interest using the ArrayOligoSelector (AOS) programme, with a number of minor modifications (Lee et al. 2006). AOS scores potential probes based on four different criteria and the following matrices were used to select probes of appropriate quality; a GC content of 30-100%, a self-binding score of less than 100, a complexity score of less than or equal to 24 and a uniqueness score of greater than or equal to -40. Potential probe sets were then selected such that the average spacing between probe sets in terms of genomic coordinates was 250 base pairs.

2.7.5.4 Hybridization, washing and scanning of Agilent Custom ChIP-on-chip microarrays

Cy5 and Cy3 labeled DNA samples were hybridized to Agilent Custom ChIP-on-chip microarrays using a Mammalian ChIP-on-chip Protocol (Agilent) and all reagents used were, unless otherwise stated, from Agilent. 2.5μg of amplified and labeled ChIP DNA was combined with an equal amount of labeled DNA from the corresponding Input sample before being added to 5μg Cot-1 DNA, Agilent Blocking Agent and Agilent Hybridization Buffer (both 1x final concentration). The samples were denatured at 95°c for 3 minutes before an incubation of 30 minutes at 37°c. Each combined Cy3-labeled ChIP and Cy5-labeled Input sample was then loaded onto a microarray and fixed within an array gasket before being hybridized for 24 hours at 20 RPM and 65°c.

Following the 24 hours incubation the microarray gaskets were disassembled in Oligo aCGH/ChIP-on-chip Wash Buffer 1. The microarrays were washed in the same buffer for 5 minutes before being transferred to Oligo aCGH/ChIP-on-chip Wash Buffer 2, which had been pre-heated to 31°c, for a subsequent 5 minutes wash. The microarrays were then loaded into Agilent Scanning Cassettes and scanned using an Agilent DNA Microarray Scanner BA. PMT settings were set manually to normalize bulk signal in the Cy3 and Cy5 channel and scans were automatically aligned and then manually examined for abnormal features.

2.7.5.5 ChIP-chip data processing

Data was extracted from ImageFile using FeatureExtractor before the default Agilent CGH Normalisation protocol was performed. This involved a background correction achieved by taking the average intensity of the 1500 negative control probes tiled on the microarray and subtracting this value from each probe set. To correct for different amounts of ChIP-enriched DNA compared to the Input sample the negative control subtracted median intensity value of the ChIP-enriched DNA channel was divided by the median of the Input DNA channel. The corrected ChIP-enriched DNA signals were then converted to browser extensible data (.bed) files and visualised within the UCSC Genome Browser.

Chapter 3 – Profiling miRNA expression in ASMCs isolated from healthy or asthmatic individuals

3.1 Introduction

3.1.1 microRNAs

microRNAs (miRNAs) are 20-24 nucleotide (nt) non-coding RNAs that exert a post-transcriptional regulation on specific mRNAs. They were officially recognized as an independent gene class in 2001 (Lau et al. 2001) (Lagos-Quintana et al. 2001) (Lee & Ambros 2001) and the latest release of miRBase contains over 1500 validated or predicted human miRNA genes [miRBase 18, www.mirbase.org]. It has been proposed that miRNAs could confer regulation on over 60% of human mRNAs (Kertesz et al. 2007), suggesting that they signify a relevant and extremely important development in our understanding of the regulation of gene expression.

3.1.2 miRNA derivation and biogenesis

3.1.2.1 miRNA genes and nuclear processing

The majority miRNA genes are transcribed by RNA polymerase II as primary transcripts known as pri-miRNAs, which contain the classical features of RNA polymerase II derived transcripts including a 5' methyl cap and polyadenylated tail (Lee et al. 2004). A smaller number of miRNA genes are transcribed by RNA polymerase III (Borchert et al. 2006). miRNA genes can be located in a number of genomic contexts; they can reside as a single miRNA which is transcribed into a pri-miRNA or they can be found as clusters that are transcribed as a single pri-miRNA, from which individual miRNAs are processed. Alternatively, a subset of miRNAs, known as miRtrons, are excised from the introns of protein coding genes by the cellular splicing machinery (Ruby 2007).

Early studies suggested that levels of pri-miRNAs did not always correlate with the level of mature miRNA (Tam 2001), which indicated that there were additional stages of regulation in miRNA biogenesis. Two seminal papers enlightened the area of pri-miRNA processing and showed it to be heavily reliant on the fact that the sequence of pri-miRNA transcripts results in the formation of stem-loops within the RNA molecule. Lee *et al.* identified an RNase III enzyme, Drosha, which is responsible for the cleavage and release of the stem-loop from the pri-miRNA molecule (Lee et al. 2003). Mutagenesis experiments indicated that the formation of double stranded RNA (dsRNA) in the stem of the hairpin loop was essential for Drosha mediated cleavage, rather than the specific sequence or the formation of the loop itself. Gregory *et al.* showed that Drosha was found in two main complexes, a large multi-component protein complex and a smaller minimal complex containing only Drosha and the dsRNA binding protein, DiGeorge syndrome critical region 8

(DGCR8). It was shown that the minimal complex was sufficient and necessary for pri-miRNA processing both *in vitro* and *in vivo* (Gregory et al. 2004). Features important for processing are now known to include a hairpin-loop in the pri-miRNA greater than 9nt in length (Zeng & Cullen 2005) and a 6-11nt stretch of unstructured nucleotides either 5' or 3' to the hairpin-loop (Zeng et al. 2005). The specific site of cleavage has been shown to be ~11nt from the stem-loop/ssRNA junction (Han et al. 2006). The essential role of Drosha in miRNA processing is demonstrated through studies showing that the p68 and p72 DEAD-box RNA helicase subunits of Drosha are essential for embryonic survival (Fukuda et al. 2007). Despite our understanding of the features of pri-miRNA processing perhaps the most important aspect, namely its regulation, is still unclear. mRNAs form secondary structures, many of which will resemble the features of a pri-miRNA. How the process is regulated to ensure that only *bone fide* pri-miRNA molecules are targeted is still poorly understood. The crystal structure of DGCR8 interacting with a pri-miRNA was produced in 2007 and indicated that a single DGCR8 molecule binds to each side of the stem-loop (Sohn et al. 2007). More recently it has been proposed that recognition of a pri-miRNA requires the co-operative binding of three DGCR8 molecules to the stem-loop (Faller et al. 2010). This work, however, is ongoing and knowledge as to the regulation of Drosha mediated cleavage remains limited.

Although the minimal Drosha/DGCR8 complex is sufficient for pri-miRNA cleavage there are other factors that confer additional levels of regulation. The best studied of these is the regulation of let-7 production by lin-28. let-7 is expressed at high levels in nearly all differentiated cells, however, it is not present in embryonic cells. Thomson *et al*. were the first to demonstrate that pri-let-7 is present in embryonic cells, suggesting that may be subject to post-transcriptional regulation (Thomson et al. 2006). It was subsequently shown that recombinant lin-28 blocks the processing of pri-let-7, whilst knocking down lin-28 facilitates let-7 expression (Viswanathan et al. 2008). This effect is mediated by lin-28 binding to the stem-loop of let-7 and preventing Drosha mediated cleavage (Newman et al. 2008). It is likely that many proteins are involved in regulating pri-miRNA processing, probably in a miRNA specific manner.

3.1.2.2 Export of pre-miRNAs from the nucleus

Following nuclear processing of pri-miRNA transcripts to short hairpin loops, known as pre-miRNAs, the pre-miRNA molecules are exported into the cytoplasm by

a complex made up of Exportin-5 (XPO-5) and Ran-GTP (Yi et al. 2003). Important features allowing the recognition of correctly processed pre-miRNAs by XPO-5 include a defined length of dsRNA and 3' overhangs (Lund et al. 2004) (Lund & Dahlberg 2006) (Zeng & Cullen 2004).

3.1.2.3 Cytoplasmic pre-miRNA processing

Once in the cytoplasm, the exported pre-miRNAs are cleaved by a second RNase III endonuclease known as Dicer (Zhang et al. 2002), resulting in the formation of 21-26nt duplex miRNA molecules with 3' overhangs. Dicer functions in a complex known as the RNA-induced silencing complex (RISC)-loading complex (RLC), which commonly includes transactivation-response RNA-binding protein (TRBP), protein activator of PKR (PACT) and a single member of the Argonaute (AGO) family of proteins. TRBP and PACT do not contribute catalytically to the processing of pre-miRNAs but rather act to stabilize Dicer. The essential role of Dicer in miRNA biogenesis is demonstrated by the fact that its deletion results in a large decrease or complete loss of mature miRNAs (Hutvágner et al. 2001) and the demonstration that mice lacking DICER are non-viable (Bernstein et al. 2003).

AGO proteins are essential for facilitating the action of miRNAs as they are required to anchor the miRNA:mRNA interaction and are believed to provide the catalytic activity required for target regulation. The number of AGO proteins is highly variable across species, with *S. pombe* expressing only one whilst *C. elegans* expresses 27 variants. Both mouse and humans encode 8 AGO proteins within their genome. Sequence homology studies allow the 8 human AGO proteins to be divided into two distinct families. AGO 1-4 are termed as AGO proteins and are required for miRNA function whilst AGO 5-8 are more similar to the *D. melanogaster* PIWI proteins. These AGO proteins are required for the function of piRNAs, which are involved in the silencing of transposable elements within the human genome (Sasaki et al. 2003).

AGO proteins are characterised by the presence of Piwi-argonaute-zwille (PAZ) and PIWI domains (Cerutti et al. 2000). PAZ domains contain a conserved hydrophobic cavity that recognizes the characteristic 2nt 3'overhang products of Dicer cleavage (Lingel et al. 2004) (Ma et al. 2004) and are thus responsible for anchoring the miRNA within the AGO protein. PIWI domains are located at the C-terminal end of AGO proteins and resemble the RNase H enzyme in structure. It is this domain that

is believed to facilitate the endonucleolytic function of AGO proteins (Song et al. 2004). In addition, X-ray crystallography of prokaryote AGO has determined the structure of a conserved domain between the PIWI and PAZ domains, known as the MID domain (Parker et al. 2005) (Yuan et al. 2005). This domain contains a highly basic pocket believed to be important in anchoring the 5' end of the short oligonucleotides, miRNAs in the case of AGO, within the protein.

Dicer cleaves the pre-miRNA hairpin and removes the loop, resulting in the production of a ~22nt miRNA duplex with a 2nt overhang at each 3' end. Following cleavage of the pre-miRNA molecule Dicer, TRBP and PACT dissociate from the miRNA duplex. The miRNA duplex is then unwound into its constituent functional strand, which is complimentary to the mRNA target, and the passenger miRNA* strand. The differentiation between the guide and passenger strand is proposed to be determined by the thermodynamic stability of the base pairs at either end of the duplex, with the miRNA strand which has the less stable base pairing at its 5' end loaded into RISC (Khvorova et al. 2003). Until recently it was believed that the guide strand was incorporated into RISC whilst the passenger strand was degraded (Schwarz et al. 2003). A group of recent reports, however, have indicated that the process may not be as simple as previously envisaged. High depth sequencing in both mouse and drosophila has shown that some miRNA* species are abundant in certain cell types and in some cases they are more abundant than the complimentary miRNA strand (Ro et al. 2007) (Okamura et al. 2008). The process of miRNA duplex sorting is more thoroughly understood in drosophila, with three recent studies providing insight into the process. These reports showed that miRNA*s are commonly modified by 2'-O-methylation at their 3' ends and that they are preferentially incorporated into AGO2 complexes, unlike the miRNA strands, which are typically incorporated into an AGO1 complex. Of particular note are reporter assays performed by Czech *et al.*, which showed that depletion of Drosha in S2 cells led to the de-repression of both miRNA and miRNA* reporters. This suggests that miRNA*s can repress mRNA targets and thus greatly increases the potential regulatory capability of miRNAs (Okamura et al. 2008) (Czech et al. 2009) (Ghildiyal et al. 2010). It should be noted that the increased complexity and redundancy of mammalian AGO proteins suggests that any analogous sorting mechanism is likely to be more intricate.

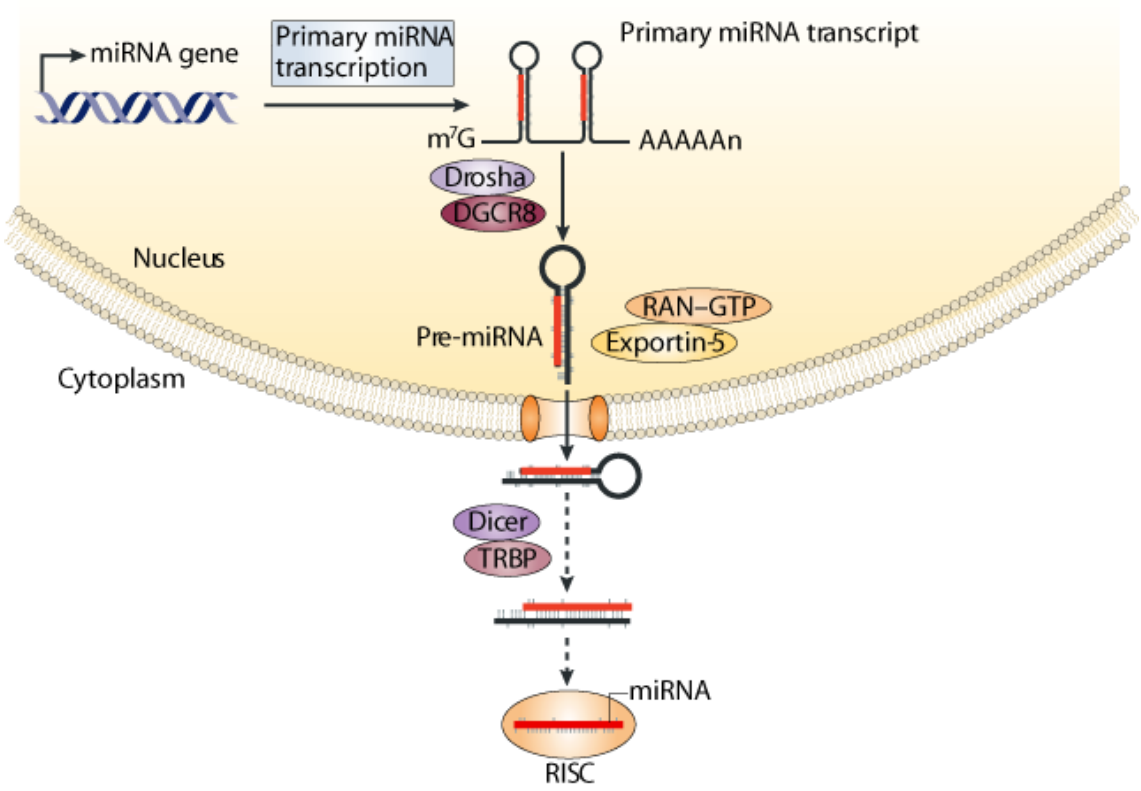

Figure 3.1.1 – The biogenesis and function of miRNAs – Primary miRNA transcripts are processed to pre-miRNA stem-loops of ~60nt in length by Drosha. The pre-miRNA is exported from the nucleus by Exportin before being further processed to a ~21nt mature RNA duplex. The functional strand of the miRNA duplex is loaded into the RNA-induced silencing complex (RISC) and mediates the repression of target mRNAs by mRNA degradation or translation inhibition**.** Figure adapted from Lodish *et al.* 2008.

3.1.3 miRNA target recognition

3.1.3.1 Positioning of miRNA target sites within mRNAs

Once incorporated into RISC miRNAs facilitate the down-regulation of specific mRNA targets through partial base pairing. The majority of miRNA target sites have been identified within the 3' untranslated region (UTR) of mRNAs. A major reason for the strong bias towards 3'UTR target sites is that the original discovery of the miRNAs lin-4 and let-7 in *C.elegans* was accompanied by evidence that their target sites resided in the 3'UTR of their validated biological targets (Lee et al. 1993b). It has been proposed that miRNAs may be restricted to targeting the 3'UTRs of mRNAs due to their mechanism of action. Gu *et al.* suggested that the ability of a miRNA to mediate repression of a target reporter was lost when the miRNA target site was repositioned within the open reading frame (ORF) by disruption of the initial stop codon (Gu et al. 2009). It is clear that the initial evidence from *C.elegans* stuides

does not dictate that all other miRNA target sites should be restricted to 3'UTRs. Results from microarray studies where miRNAs have been transfected into human cells have identified a subset of mRNAs with potential target sites within the ORF, however, these have often not been followed up because they were believed to be rare events with uncertain consequences *in vivo* and because of concerns over the off-target consequences involved with over-expression approaches (Lim et al. 2005) (Grimson et al. 2007). More recent data using the Photoactivatable-Ribonucleoside-Enhanced Crosslinking and Immunoprecipitation (PAR-CLIP) technique to identify the position of AGO, and thus miRNA binding sites in target mRNAs, has shown that approximately 50% of AGO binding events occur within the ORF of mRNAs, whilst 46% occur in the 3' UTR and 4% in the 5'UTR (Hafner et al. 2010). This data suggests that miRNA-mediated post-transcriptional regulation may be more widespread than was previously predicted by 3'UTR restricted analyses.

3.1.3.2 Base pairing between miRNAs and mRNAs

Evolutionary evidence suggests that the 5' end of miRNAs is important for their function, as it is the only region of the miRNA to be conserved to a greater extent than would be expected by chance (Lewis et al. 2003). The two major determinants of a functional miRNA:mRNA interaction are believed to be base-pairing between nucleotides 2-8 of the miRNA, known as the seed, and the mRNA target in addition to the change in free energy state between the separated miRNA and mRNA and the miRNA:mRNA duplex (Doench & Sharp 2004) (Lewis et al. 2005). There are, however, additional features that also contribute to miRNA targeting. It has been shown that 3' base pairing along the miRNA has the capacity to compensate for weak seed matches (Brennecke et al. 2005). Both lin-4 and let-7 have been shown to mediate down-regulation through target sites that contain mismatches in the seed region and G:U wobbles (Ha et al. 1996) (Vella et al. 2004) and there are now a variety of recognized matches between the seed region of the miRNA and the mRNA that are capable of mediating repression (Figure 3.1.2) (Bartel 2009). As evidence of alternative modes of action, Shin *et al*. have recently examined mRNA expression array data following miRNA over-expression by transfection and identified a class of miRNA:mRNA interactions that lack both perfect seed pairing and 3'-compensatory pairing. Instead this class of interactions has 11-12 contiguous base pairs in the centre of the miRNA which is proposed to facilitate mRNA cleavage analogous to siRNA action (Shin et al. 2010). The current understanding of potential miRNA:mRNA interactions is depicted in Figure 3.1.2.

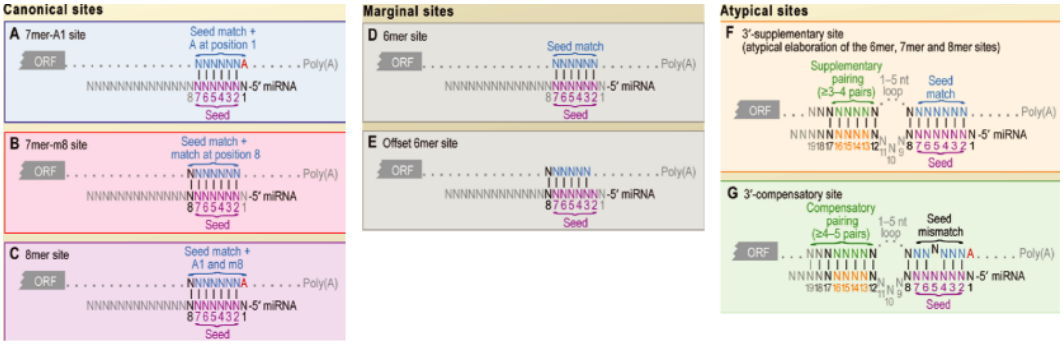

Figure 3.1.2 – Types of miRNA target sites - A-C - Indicate 7-8nt seed matches with vertical dashes representing Watson-Crick base pairing. **D-E** - Marginal sites with 6nt base pairing within the seed region. **F-G** – Sites in which 3' pairing is able to either increase the efficacy of a seed match or compensate for weak base pairing within the see region. Figure adapted from (Bartel et al. 2009).

3.1.3.3 3'UTR context and additional features

Didiano *et al*. demonstrated that seed matches between the miRNA, lsy-6, and its endogenous target, cog-1, were insufficient to predict functional down-regulation of the target (Didiano & Hobert 2006). Subsequent studies have determined that two non-sequence specific contextual features, rather than seed matches, are the critical determinants of lsy-6 mediated repression of cog-1 (Didiano & Hobert 2008). This data is a noteworthy demonstration of the role that the secondary structure of a mRNA may play in concealing miRNA target sites (Robins et al. 2005). Grimson *et al*. have proposed a number of features, in addition to the presence of a seed-match, that are important to mediate a functional miRNA:mRNA interaction (Grimson et al. 2007). These include target site location relative to the stop codon, AU-richness around the target site and preferential base-pairing to nucleotides 13-16 of the miRNA.

3.1.3.4 Prediction of miRNA targets through bioinformatics

A common strategy used to identify the potential mRNA targets of a particular miRNA is to use target identification algorithms based upon previously validated miRNA:mRNA interactions. These algorithms utilise the fact that miRNAs target mRNAs through base-pairing, meaning that a list of criteria to identify potential targets can be generated. Three of the most commonly used algorithms are TargetScan (Lewis et al. 2005), miRANDA (Enright et al. 2003) and PITA (Kertesz et al. 2007). Although the use of these algorithms is widespread it is important to note

that there are a number of limitations and issues associated with their implementation. Perhaps the most noteworthy of these is that, due to the assessment of conservation performed during the analysis, all the algorithms are restricted to searching for target sites within 3' UTRs. As described in Chapter 3.1.3.1, there is now a large amount of evidence indicating that miRNA target sites can be located throughout an mRNA, meaning that the prediction algorithms will not report a large number of potential target sites. In addition, all the algorithms are restricted to searching for base-pair matches to the miRNA seed within the 3'UTR and only specific, simple variations are permitted. This means that different target sites, for example those reliant on 3' supplementary pairing, may not be predicted. Increasing evidence has demonstrated that the secondary structure of the mRNA will profoundly influence the accessibility of potential miRNA target sites, however, of the major algorithms only PITA takes this into account.

More technical issues with the implementation of predictive algorithms are that they rely on differing assumptions and processes to generate a list of potential targets. TargetScan and miRANDA, for example, use the Ensembl or UCSC database of 3' UTRs respectively. When the TargetScan algorithm is applied to both databases only a 47% overlap in predicted targets is returned, whilst the same analysis for miRANDA results in a 65% overlap (Ritchie et al. 2009). This indicates that, unsurprisingly, the starting database used to define 3' UTRs has a profound impact on the potential targets recovered.

Despite the issues surrounding predictive algorithms of miRNA targets they are commonly used to identify potential targets and, if combined with data concerning co-expression of mRNAs, can offer a potential starting point when attempting to identify miRNA targets.

3.1.4 Mechanisms of miRNA-mediated regulation

The mechanism by which endogenous miRNAs mediate repression of their mRNA targets is controversial. Exogenously provided siRNAs facilitate the direct cleavage of their mRNA targets. This is known as Slicer activity and is mediated through the high level of complementarity between the siRNA guide strand and mRNA target (Martinez & Tuschl 2004). Binding of a fully complementary miRNA or siRNA to an mRNA target results in displacement of the 3' binding of the short oligonucleotide within the PAZ domain of the AGO protein, which is believed to be required for

Slicer activity. The importance of extensive base pairing between the siRNA and mRNA to mediate cleavage is demonstrated by the fact that engineering an exogenous siRNA so that the duplex it forms with its target contains central mismatches inhibits cleavage (Martinez & Tuschl 2004); whilst mutating let-7 so that it forms perfect duplexes with specific targets caused the targets to be cleaved (Hutvágner et al. 2001).

Mammalian miRNAs typically exhibit much lower levels of complementarity to their mRNA targets in comparison to exogenous siRNAs (discussed in Chapter 3.1.3). As such there are very few reports of endogenous mammalian miRNAs stimulating direct cleavage of their targets (Yekta et al. 2004) (Davis et al. 2005). It is likely that miRNA-loaded AGO proteins do not stimulate target cleavage as the interrupted pairing between the miRNA and target mRNA permits continued association of the 3' end of the miRNA with the PAZ domain and that this somehow inhibits the endonucleolytic activity. *In vitro* studies using RNA substrates complementary to exogenous siRNAs (Liu et al. 2004) or endogenous miRNAs (Kong et al. 2008) (Meister et al. 2004) have identified AGO2 as the only human AGO protein with Slicer activity. Assuming that each enzyme was correctly reconstituted in these *in vitro* assays, this suggests that endonucleolytic cleavage is not required for the function of endogenous miRNAs.

Initial evidence from *C.elegans* indicated that the most likely mode of action of miRNAs was one of translational repression with no influence on mRNA levels; as it was shown that the miRNA lin-4 decreased the level of lin-14 protein whilst having no detectable affect on mRNA levels (Lee et al. 1993). Furthermore, it was shown that the association of lin-14 mRNA with polyribosomes appeared unchanged following lin-4 mediated inhibition of protein expression (Olsen & Ambros 1999). The broad nature of this mechanism was given support by the fact that mRNA levels of a separate lin-4 target, lin-28, did not alter when lin-4 blocked lin-28 protein accumulation (Moss et al. 1997) (Seggerson et al. 2002). In addition, a large number of studies using over-expression of miRNAs and analysis of specific targets have shown that target protein levels decreased following over-expression of the miRNA, with no alteration in mRNA levels (Martin et al. 2006b) (Deshpande et al. 2009). The majority of evidence indicates that miRNA-induced translational repression occurs at the level of translation initiation. It has been shown that tethering either of the translation initiation factors eukaryotic initiation factor (eIF)-4E or eIF-4G to an

mRNA renders it resistant to miRNA mediated repression, suggesting that miRNAs may prevent recognition of the 5' cap by the cap binding protein (Pillai et al. 2005). It has been speculated that AGO proteins contain potential binding sites for 5' methyl cap structures (Djuranovic et al. 2010) suggesting that this may be the mechanism by which AGO proteins facilitate translational inhibition. In addition Mathonnet *et al*. have shown that *in vitro* repression of mRNA targets by let-7 is initiated by let-7 mediated recognition of the 5' cap (Mathonnet et al. 2007).

It is not definitive that miRNA-mediated repression has no influence on target mRNA levels and there have been many reports indicating that miRNAs do in fact decrease the level target mRNA. A study by Bagga *et al*. showed that regulation by let-7 and, in contrast to the evidence from Lee *et al.* and Wightman *et al*., lin-4 miRNAs in *C.elegans* resulted in target mRNA degradation (Bagga et al. 2005). Potential reasons for these different data are that the initial studies by Lee *et al.* and Wightman *et al.* were generated using RNase protection assays, which do not demonstrate the existence of full-length, intact mRNA molecules whereas Bagga *et al*. used Northern blotting to identify specific full-length mRNAs.

An important study from Guo *et al.* in 2010 suggested that mRNA degradation is the major mechanism of miRNA mediated repression in mammalian cells. Using both RNA-sequencing and ribosome profiling as read-outs of mRNA levels and translational efficiency respectively, it was demonstrated that mRNA degradation was responsible for the majority of the miRNA-mediated target repression (Guo et al. 2010).

The increasing evidence that mRNA levels are affected by miRNA-mediated regulation has lead to the emergence of a two-step model for the mechanism of down-regulation (Djuranovic et al. 2011). This involves an initial inhibition of translation, most likely through a mechanism that involves the prevention of 5' cap recognition, which then indirectly leads to degradation of the mRNA. Recent experimental data from a *D. melanogaster* system has been published in support of this mechanistic model (Djuranovic et al. 2012). This temporal action of regulation may explain some of the variation in reported mechanisms of miRNA action, as the time point analysed may influence the readout generated and individual miRNA:mRNA interactions may have differing kinetics of translational inhibition and subsequent mRNA degradation.

3.1.5 Relevance of miRNAs to disease

Despite their recent discovery there is already a large body of literature detailing altered miRNA expression and function in a variety of disease settings. Of relevance to asthma there are a number of reports detailing the altered expression of miRNAs and subsequent deregulation of mRNA targets in both mouse models and *in vitro* studies (Pagdin & Lavender 2011) and these will be discussed further in Chapter 3.3.

Exciting data is emerging regarding the potential for miRNAs as both therapeutic and diagnostic targets. The liver-specific miRNA, miR-122, has an essential role in the regulation of cholesterol metabolism and it has been shown that systemic administration of a cholesterol-linked antagomir to miR-122 reduces plasma cholesterol levels and cholesterol synthesis in a murine model of hypercholesterolaemia (Esau et al. 2006). In addition to its role in lipid biosynthesis, miR-122 is essential for Hepatitis C virus (HCV) accumulation in cultured liver cells. It has recently been shown that treating chronically HCV-infected chimpanzees with a 3 week regime of high-dose anti-miR-122 results in a significant decrease in HCV RNA serum after 3 weeks, improving to a 2.6 order of magnitude decrease after 14 weeks of treatment (Lanford et al. 2010). This is very promising evidence for the efficacy of miRNA-based therapies in a primate-based disease model and anti-miR-122 therapies are currently in Phase II clinical trails.

Perhaps a more immediate way of exploiting miRNAs is through molecular diagnostics, particularly risk stratification and outcome prediction. miR-155 and miR-let7a-2 expression, for example, correlate with poor overall survival in lung adenocarcinoma patients (Yanaihara et al. 2006), whilst a five-miRNA signature (miR-137, mir-372, miR-182*, miR-221 and let-7a) has been shown to correlate with disease-free survival in non-small cell lung cancer (NSCLC) patients (Yu et al. 2008). A further feature of miRNAs is that they are stable and detectable in blood plasma and serum by qPCR or array hybridization. Indeed, Chen *et al*. have recently shown that the expression profile of serum miRNAs can serve as a NSCLC fingerprint (Chen et al. 2011) suggesting that miRNAs may serve as useful biomarkers for non-invasive diagnostics.

3.1.6 Aims of the chapter

As discussed during this chapter introduction, miRNAs represent a recent addition to our understanding of the regulation of gene expression. The aims and objectives of this chapter were therefore to generate a profile of miRNA expression in cultured ASMCs to begin to investigate if altered miRNA expression levels may contribute to the phenotypic differences between healthy and asthmatic ASM that were discussed in Chapter 1. Of particular importance was to compare the expression levels of individual miRNAs between healthy and asthmatic ASM and attempt to validate any potentially differential expression identified between the phenotypic groups.

3.2 Results

3.2.1 Preparation and labeling of RNA samples for Affymetrix GeneChip® miRNA microarray expression profiling

Affymetrix GeneChip® miRNA microarray expression profiling was performed to compare the expression of miRNAs in cultured ASMCs isolated from healthy or moderate asthmatic individuals (as defined in Chapter 2.1.1). An initial screen was performed to compare miRNA expression in three healthy and three moderate asthmatic primary explant ASMC cultures (all samples were from male volunteers, healthy mean age - 29 ± 6.65 SD, moderate asthmatic mean age – 39 ± 16.64 SD). RNA was isolated at passage number 3 or 4 of the original explant culture, prior to the initiation of this project, and subsequently stored at -80°c (described in Chapter 2.3.1). Upon initiation of this project the RNA samples were DNase treated and RNA quality was determined by Agilent Bioanalyser analysis to confirm that all samples had 'RNA Integrity' values of greater than 7, which is the threshold for RNA integrity recommended by the KCL Genomics Centre for microarray studies (Figure 2.1).

Following confirmation that all samples were of an appropriate quality for microarray experiments total RNA from each sample was labeled using a Genisphere FlashTag Biotin HSR RNA labeling system (as described in Chapter 2.5.1.1). Efficient labeling of all RNA samples was confirmed by an ELOSA assay (detailed in Chapter 2.5.1.2), as recommended by the manufacturer. This involved the addition of streptavidin-bound horseradish peroxidase to an aliquot of each biotin labeled RNA sample. The optical density of each sample following addition of tetramethylbenzidine substrate was measured and readings of 0.1OD or greater above that of the negative control, which contained no RNA or spike-in controls, were taken to represent efficiently labeled RNA, as recommended by the manufacturer. All six RNA samples used in subsequent microarray experiments were found to be successfully labeled (Figure 3.2.1).

Following confirmation of efficient labeling of RNA from all samples, microarrays were hybridized and scanned as detailed in Chapter 2.5.1.3 and 2.5.1.4.

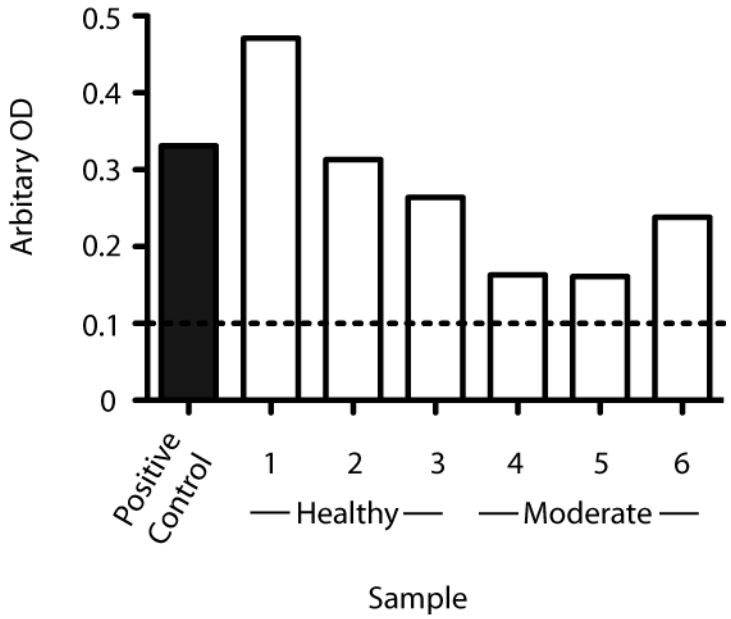

Figure 3.2.1 - All RNA samples used in Affymetrix GeneChip® miRNA expression arrays were efficiently labeled - Total RNA samples isolated from three healthy and three moderate asthmatic ASMC cultures were labeled using the Genisphere FlashTag Labeling System. An aliquot of each sample was treated with streptavidin-horseradish peroxidase and vigorously washed before the addition of TMB substrate. The metabolism of TMB by horseradish peroxidase and concomitant colour generation was measured by absorbance at a wavelength of 450nm. The dotted horizontal line represents an OD reading of greater than 0.1 above the negative control, which corresponds to the manufacturers recommendation for successful labeling.

3.2.2 Initial microarray quality control performed using the Affymetrix miRNA QC Tool

Data generated from the Affymetrix GeneChip® miRNA microarrays were imported into the Affymetrix miRNA QC Tool as .cel files and the default workflow analysis was run as described in Chapter 2.5.1.5. It should be noted that all normalised intensity values discussed in the following section are $\log_{(2)}$ transformed. Initial analyses involved performing quality control checks to ensure consistent intensity profiles across all microarrays and to identify any grossly erroneous general intensity levels that may be indicative of an issue during the hybridization or scanning procedures.

Initially, the normalised intensity values for probe sets complimentary to control oligonucleotides that were spiked into the samples during RNA labeling and microarray hybridization were analysed. This was performed to ensure that values for corresponding probe sets were similar across microarrays and to allow the identification of any obvious anomalous results. Normalised intensity values for control oligonucleotides with varying GC contents that were spiked into the RNA samples during the labeling procedure (Chapter 2.5.1.1) demonstrated similar values across the microarrays, indicating that consistent labeling was achieved across all samples (Figure 3.2.2, Panel A). Further, control oligonucleotides added to the samples during the hybridization procedures also generated similar normalised intensity values across each individual microarray (Figure 3.2.2, Panels B and C). This indicated consistent hybridization of all microarrays was achieved and indicated that the direct comparison of individual probe sets between microarrays was valid.

Further to the analysis of normalised intensity values for individual probe sets, the range of intensities across each complete microarray was analysed to evaluate the overall consistency between each microarray within the experiment. Box and whiskers plots were generated to depict the range of normalised intensities generated by the Affymetrix Bio hybridization controls that were spiked into the RNA samples prior to microarray hybridization (Figure 3.2.3). These plots summarize the distribution of normalised intensities generated by these spike-in controls by indicating the minimum and maximum values, the median value and the 25^{th} and 75^{th} percentile. This allows potential outlier samples with distributions that differ in comparison to the other samples to be readily identified. All of the

plots depicted in Figure 3.2.3 demonstrated a similar profile of normalised intensities and this hence indicated that none of the samples were outliers. A similar analysis for the total probe content of the microarrays again indicated a similar intensity profile for all microarrays, suggesting that no outliers were present (Figure 3.2.4).

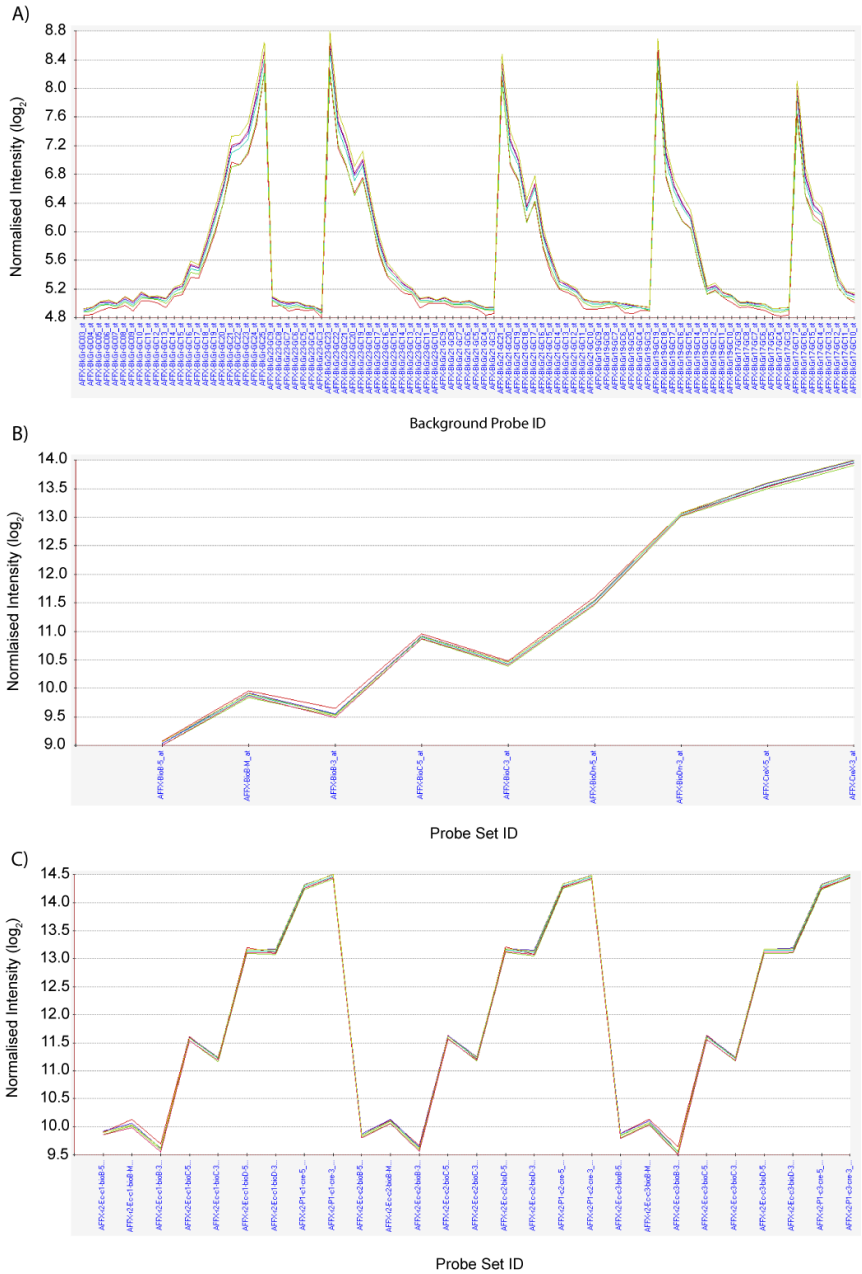

Figure 3.2.2 - Hybridization and scanning of Affymetrix miRNA arrays is consistent across samples - Quality control of Affymetrix miRNA arrays performed in the Affymetrix miRNA QC Tool demonstrates the mean intensities for probe replicates complementary to Genisphere spike-in controls added during the labeling protocols (**A**) and Affymetrix Bio-hybridization controls added during the hybridization (**B** and **C**). The Y-axis demonstrates the normalised probe intensities and the X-axis details individual probe descriptions. Each coloured line represents an individual replicate.

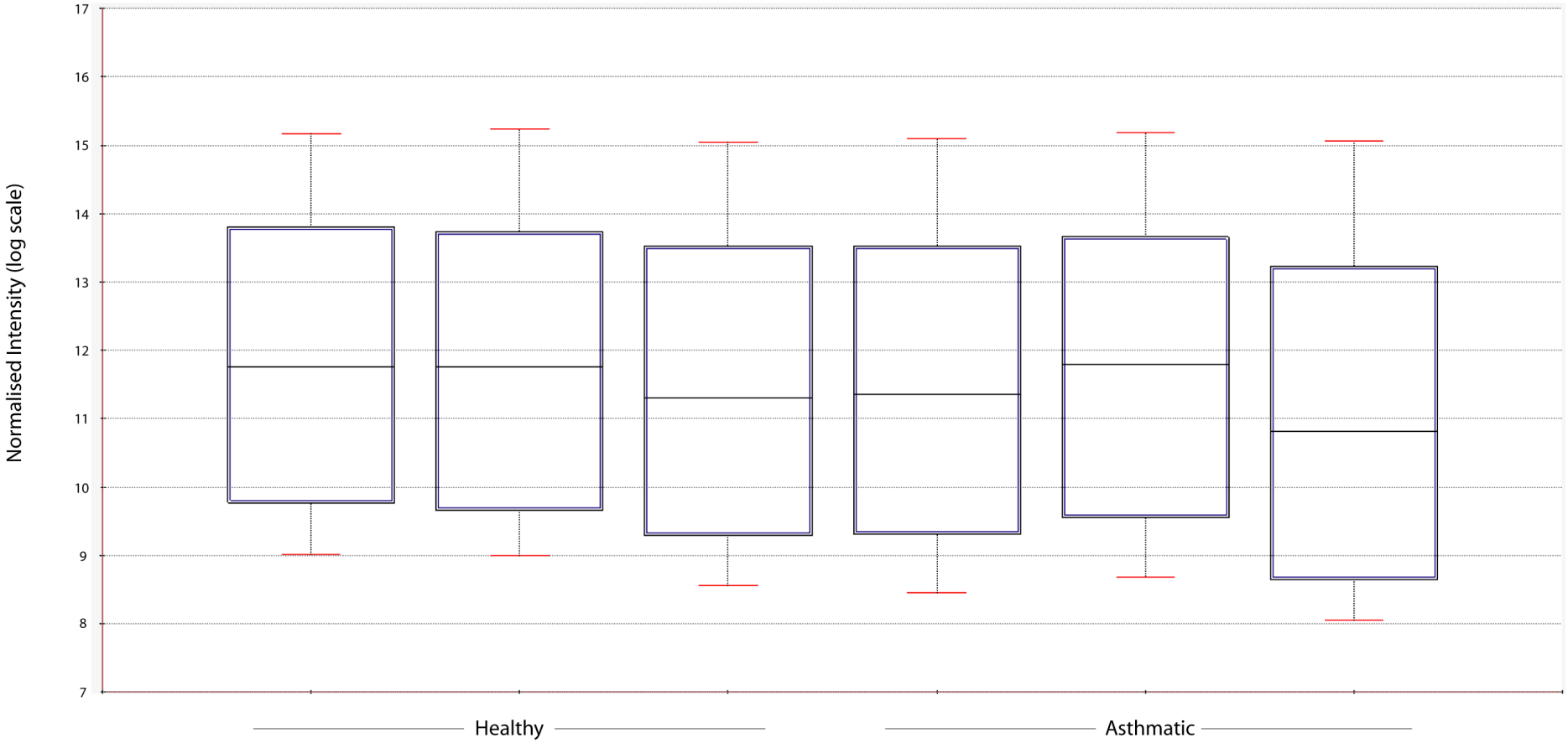

Figure 3.2.3 – Affymetrix Bio hybridization control oligonucleotides have a consistent inter-array profile of detections – Quality control of miRNA arrays performed in the Affymetrix miRNA QC Tool demonstrates the normalised intensity profile of Affymetrix Bio hybridization control oligonucleotides added to the total RNA samples prior to microarray hybridization. Each box and whiskers plot represents a separate biological replicate with the central line of the box representing the median intensity level and the top and bottom of the box corresponding to the 25th and 75th percentiles respectively. The top and bottom of the whiskers correspond to the highest and lowest detected spike-in respectively.

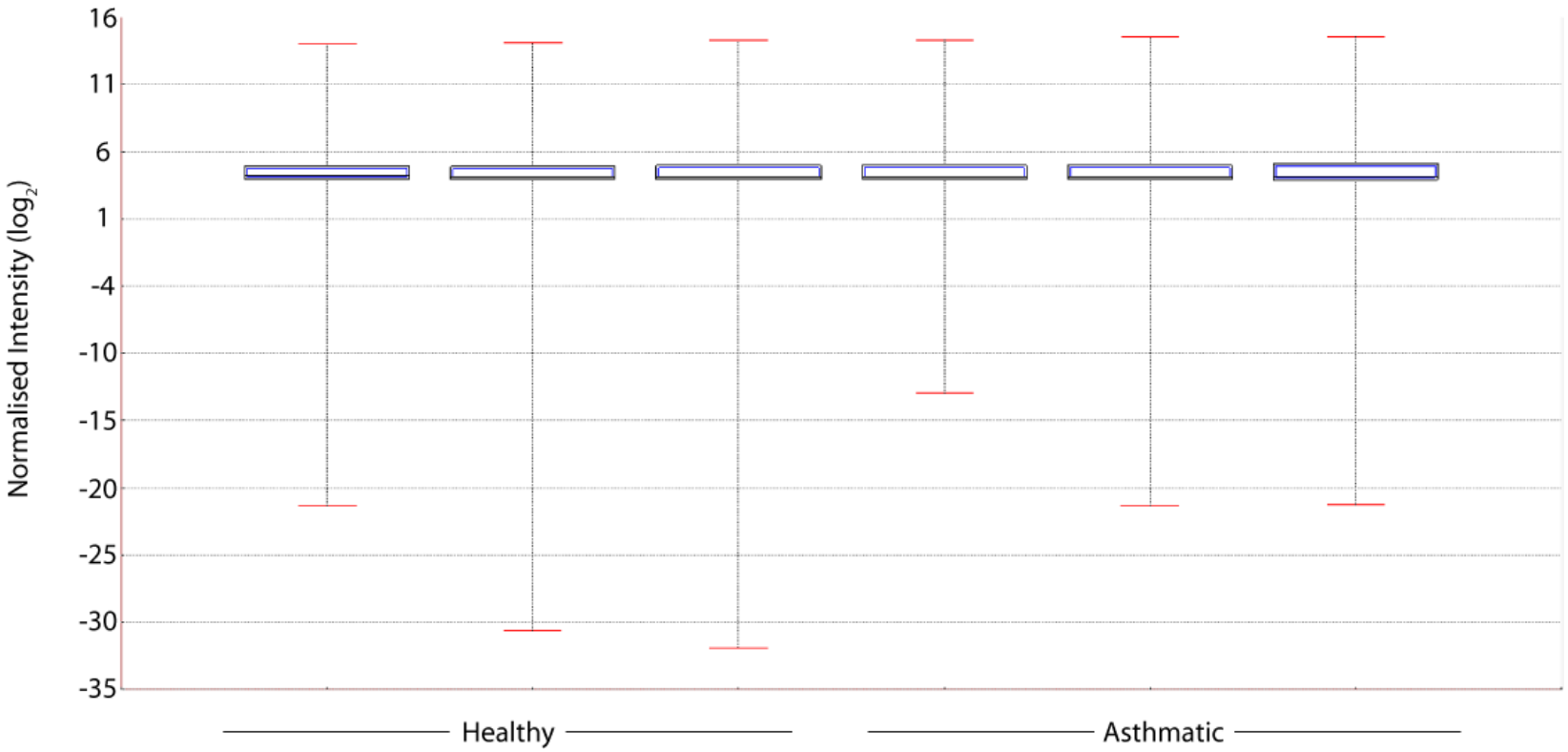

Figure 3.2.4 - The total array content intensity profiles are similar for all healthy and moderate asthmatic RNA samples – Quality control of Affymetrix miRNA arrays performed in the Affymetrix miRNA QC Tool demonstrates the intensities of replicate probes complimentary to small RNAs assayed on the Affymetrix miRNA Expression array. Each box and whiskers plot indicates the range of detected intensities for small RNAs in each biological replicate performed. The central line of the box represents the median intensity level whilst the top and bottom of the box correspond to the 25th and 75th percentiles respectively. The top and bottom of the whiskers correspond to the highest and lowest detected spike-in respectively.

A box and whiskers plot describing the profile of intensities generated by background control oligonucleotides indicated that these control probes had similar normalised intensity values to the majority of general content probes present on the microarray (Figure 3.2.5). The majority of detected intensities for both background control and general content probe sets were close to $\log_2(4.5)$, which is the threshold below which a Wilcoxon-rank test performed in the Affymetrix miRNA QC Tool calls the majority of probe sets as being undetectable above general background. The Wilcoxon-rank test compares the intensity value for a given miRNA probe to a set of control probes with a similar GC-content that do not bind to any known miRNA sequence and the detection of the target miRNA is defined as true or false based upon its statistical significance above the background value. The null hypothesis of the test is that there is no difference between the intensity values of the test and background probes and a result of $p>0.05$ is therefore defined as an absence of detectable expression and $p<0.05$ as detectable expression. A determination of false does not mean that a miRNA is not expressed, but rather that it is below the limit of detection for the microarray. Although the result is generated as a p-value, normalised intensity values of less than $\log_2(4.5)$ are generally defined as absent. This analysis indicated that the majority of probes present within the total content of the microarray, which predominantly represent miRNAs, were not detected at intensity levels greater than those of the background control probes and thus suggested that the majority of miRNAs with complimentary probe sets tiled on the microarrays were undetectable in RNA isolated from cultured ASMCs. It should be noted that the analysis performed in the Affymetrix miRNA QC Tool includes all the probe sets present on the Affymetrix GeneChip® miRNA expression array and as such includes probe sets directed against other species in addition to human. When analyzing only the normalised intensities of probe sets directed against human miRNAs, however, an average of 600 human miRNAs per sample, out of a total of 847 assayed, were reported as false by the Affymetrix miRNA QC Tool.

Analysis of the general expression profile of human miRNAs within cultured ASMCs was performed by determining the average detection of each miRNA across all six samples (Appendix I). These analyses were encouraging as let-7a, let-7b, let-7c, let-7d and let-7e, members of the let-7 family of miRNAs that are known to be broadly expressed at a high level across a number of cell types, were found to be within the top thirty miRNAs in terms of their relative abundance within the cultured ASMCs. In addition a number of miRNAs with previously reported roles in smooth muscle

differentiation and function, for example miR-100, miR-143, miR-145 and miR-21 were found to be highly abundant across all samples. The miRNA with the highest level of average detection was miR-1826, which has been shown to function as a tumour suppressor through the downregulation of VEGFc, β-catenin and MEK1 (Hirata et al. 2012).

It was therefore determined that all the RNA samples and microarrays were of sufficient quality, based upon the criteria described by Genisphere and Affymetrix, to be used in downstream comparative analyses.

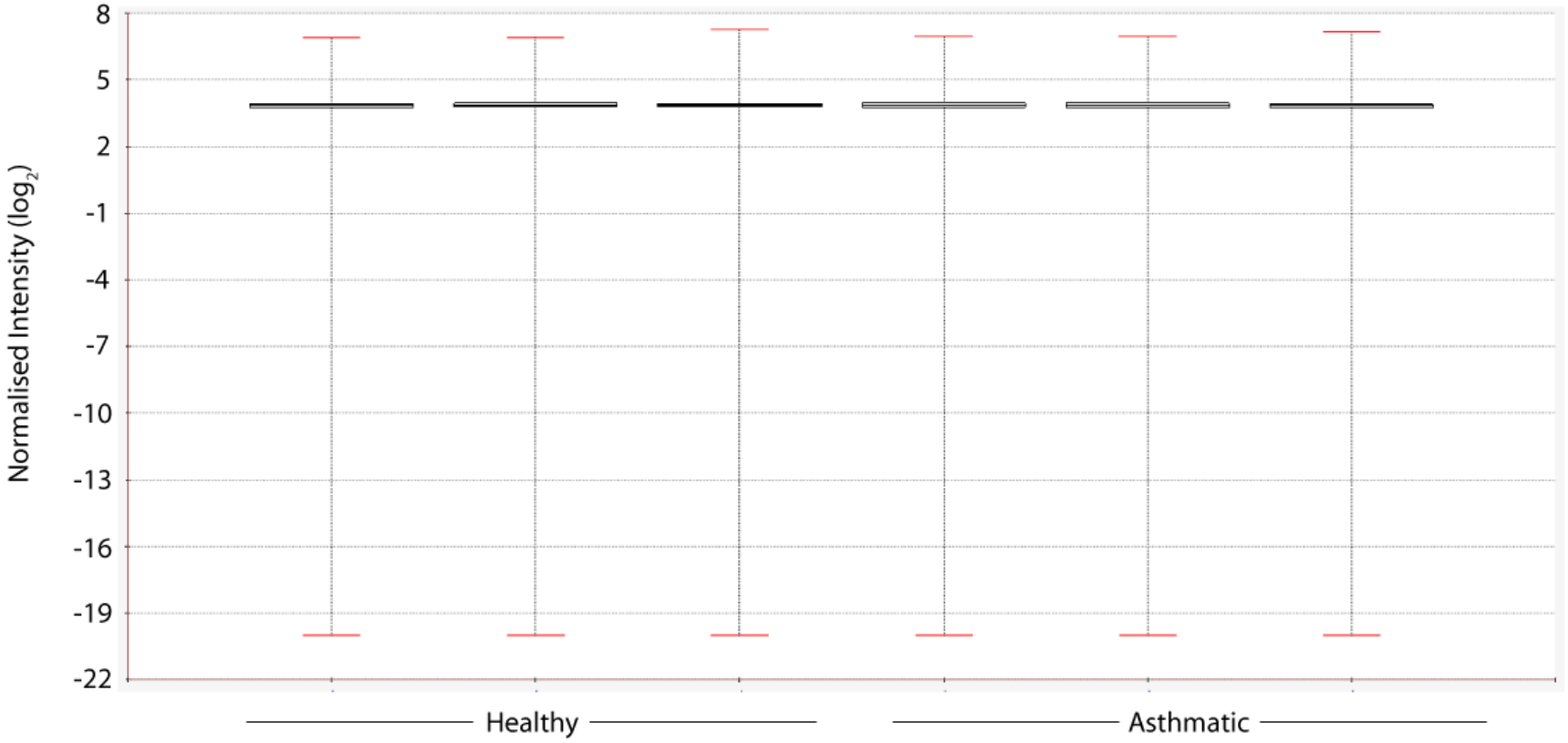

Figure 3.2.5 - Box and whiskers plot to show the normalised intensity profile of background control probes - Quality control of Affymetrix miRNA arrays performed in Affymetrix miRNA QC Tool demonstrates the intensities of background control probes. Each box and whiskers plot indicates the range of detected intensities for background probes in each biological replicate performed. The central line of the box represents the median intensity level whilst the top and bottom of the box correspond to the 25th and 75th percentiles respectively. The top and bottom of the whiskers correspond to the highest and lowest detected spike-in respectively.

3.2.3 Comparative analysis of miRNA expression between cultured ASMCs isolated from healthy or moderate asthmatic individuals

The Affymetrix miRNA QC Tool allows the rudimentary comparison of probe set intensities from two microarrays within an experiment through the generation of MvA plots. Figure 3.2.6 shows such an MvA plot comparing the normalised intensity values of miRNA probe sets from a single healthy and single moderate asthmatic ASMC culture. This plot indicates that there is little variation in miRNA expression between the two samples as the majority of the data points fall on, or very close to, the line of x=0, which indicates no difference between the two samples.

The variation between individual samples was also visualized in the Affymetrix miRNA QC Tool by generating Pearson's correlation coefficients for all possible sample pairs (Table vii). This analysis generates a value between -1 and +1, which represent a perfect negative or positive correlation between two variables. All values generated for comparisons between the six samples analysed were close to +1 and demonstrated a very strong positive correlation between samples, indicating that an individual miRNA is likely to have similar levels of abundance in different biological replicates. This was a further indication that the general miRNA expression profile was very similar for cultured ASMCs isolated from healthy or moderate asthmatic individuals.

	Healthy 1	Healthy 2	Healthy 3	Asthmatic 1	Asthmatic 2	Asthmatic 3
Healthy 1	1.00	0.99	0.99	0.98	0.98	0.96
Healthy 2	0.99	1.00	0.99	0.99	0.98	0.96
Healthy 3	0.99	0.99	1.00	0.99	0.98	0.99
Asthmatic 1	0.98	0.99	0.99	1.00	0.98	0.98
Asthmatic 2	0.98	0.98	0.98	0.98	1.00	0.96
Asthmatic 3	0.96	0.96	0.99	0.98	0.96	1.00

Table vii – Pearson's correlation coefficient values for inter-array comparisons performed in the Affymetrix miRNA QC Tool – The table shows the Pearson's correlation coefficient values generated following the comparison of indicated pairs of ASMC cultures in terms of small RNA expression. A Pearson's correlation coefficient of +1 represents a perfect positive correlation.

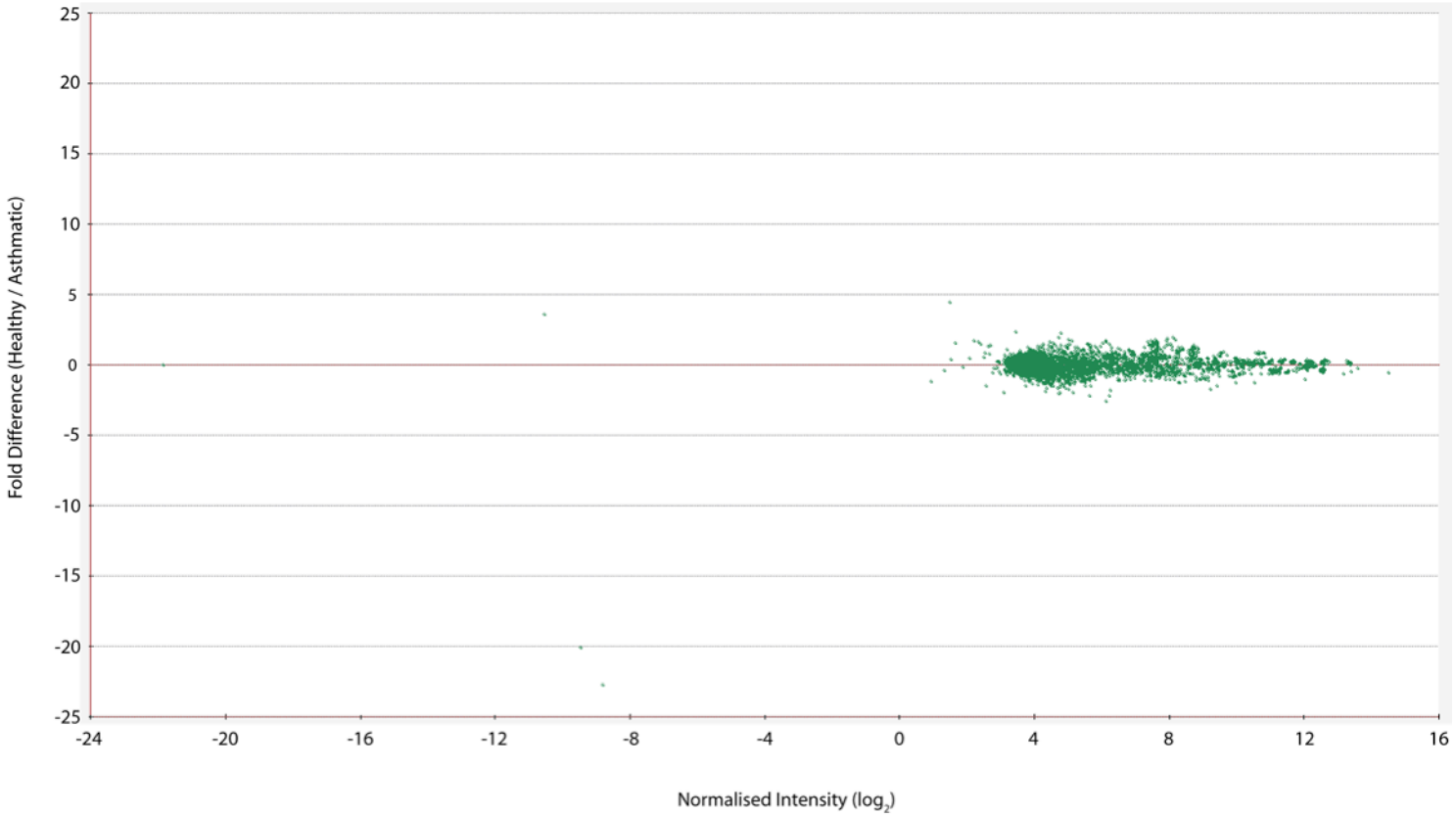

Figure 3.2.6 - Initial comparative analysis of a single healthy and a single asthmatic RNA sample indicates no gross differences in small RNA expression – A representative MvA plot generated by the Affymetrix miRNA QC Tool demonstrates the comparative expression of small RNAs in cultured ASMCs isolated from either a healthy or a moderate asthmatic individual. The Y-axis shows the fold difference in expression, with positive values indicating probe sets with a higher intensity in the healthy sample and negative values indicating those with a higher intensity in the asthmatic sample. The X-axis demonstrates the normalised intensity of probe sets for an individual RNA. Each dot on the scatter graph indicates the average intensity value for a single small RNA.

Although the data analysis performed in the Affymetrix miRNA QC Tool enabled the general profile of small RNA expression to be interrogated, it was insufficient to allow the identification of individual miRNAs that might have been differentially expressed between the cultured ASMCs isolated from healthy and moderate asthmatic individuals. Due to this restriction the raw data were imported into Partek Genomics Suite 2.0 as .cel files and processed through the default miRNA workflow (described in Chapter 2.5.1.6). A variety of filtering steps and comparative analyses were then performed to identify miRNAs that demonstrated potential differential expression between cultured ASMCs isolated from healthy or moderate asthmatic individuals.

Following importation of the data into Partek Genomics Suite the probe sets were filtered such that subsequent analysis would only include probe sets directed against human miRNAs. This filtering step was performed because the Affymetrix GeneChip® miRNA expression arrays contain probe sets directed against multiple species including human, mouse, rat, canine and rice. Although cross-species comparison can increase confidence in results, especially if there are nucleotide substitutions between species, the data is much easier to manipulate and interpret if the analysis is restricted to probe sets designated as human. This is evidenced by the fact that there are 847 probe sets directed against human miRNAs compared to 3135 in total. The fact that many of the 3135 total probe sets are duplications across species increases the complexity.

The global expression profile of human miRNAs was analysed by performing Principal Component Analysis (PCA) to compare the variation between individual samples (Figure 3.2.7). PCA is used to transform a set of observations, in this case the normalised intensity values of probe sets, into a set of vector components that allow the data to be visualized in a three-dimensional space. The axes of the graph indicate uncorrelated contributions to the total variance within the data and the space between individual samples indicates the difference in overall expression profile between the samples. In terms of microarray data, PCA is usually used to determine if certain treatment conditions or disease groups are more similar than others. In the case of this analysis, the fact that the phenotypic groups were not separated along any of the three axes indicated that there were not global differences in miRNA expression between disease states. This analysis therefore

corroborates the Pearson's correlation coefficients generated in the Affymetrix miRNA QC Tool (Table vii).

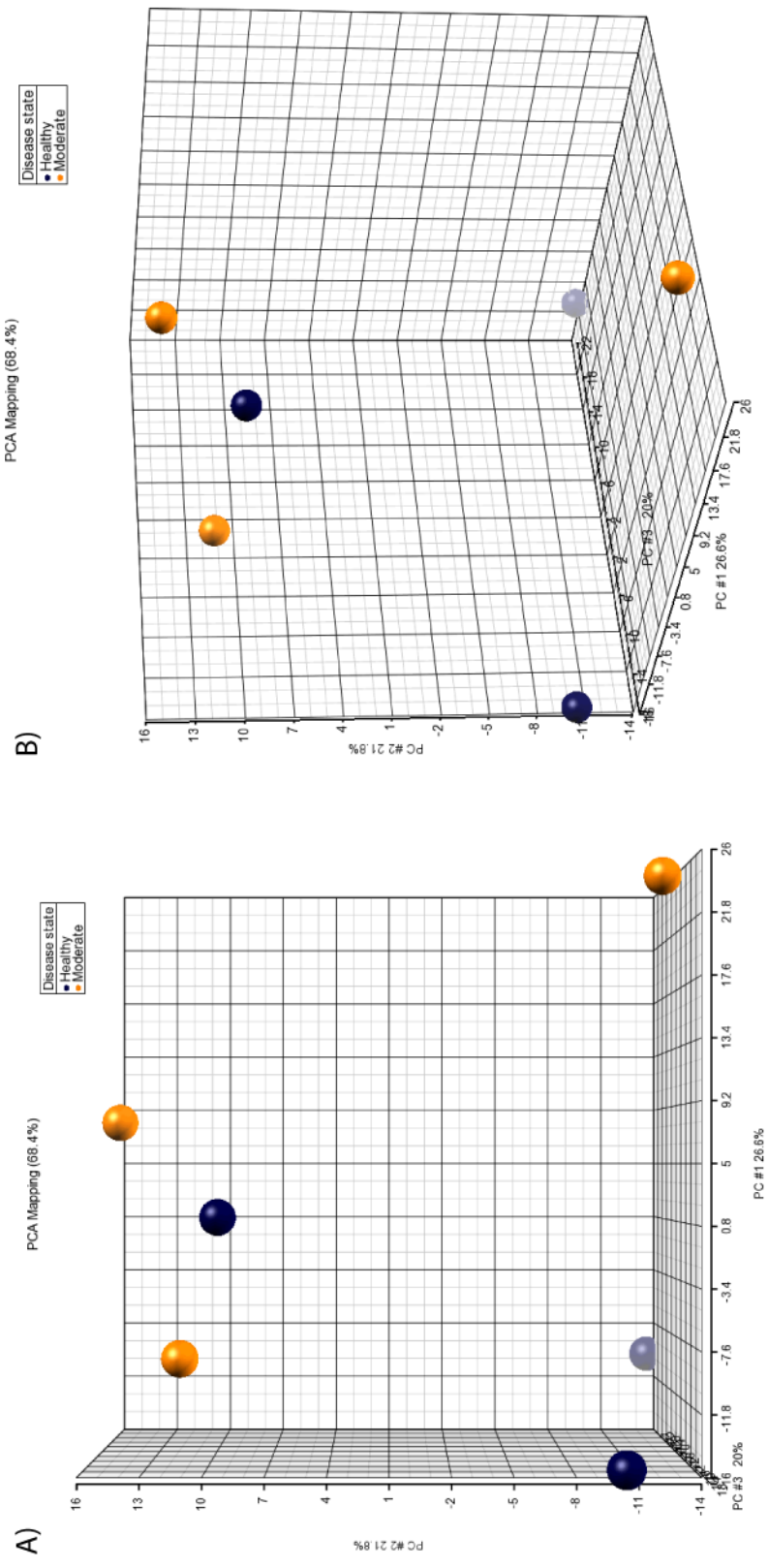

Figure 3.2.7 - Principal component analysis is unable to differentiate cultured ASMCs from healthy or moderate asthmatic individuals based upon their small RNA expression profile - Raw .cel files generated by the Affymetrix GCOS software were imported into Partek Genomics Suite and analysed using the default miRNA expression workflow. Principal component analysis was performed on probe sets directed against human miRNAs. **A)** Shows the principal component analysis plot through the X and Y planes and **B)** is the same plot rotated by 45°about the Y-axis. Dark blue and orange dots represent individual healthy and moderate asthmatic replicates respectively.

The total profile of miRNA expression in ASMCs isolated from healthy or asthmatic individuals was also visualized by implementing hierarchical clustering using Euclidean Dissimilarity and Average Linkage to generate a dendogram (Figure 3.2.8). This analysis clusters the samples by a lack of similarity in the total miRNA expression profile and the samples that are more similar therefore cluster closer together. This analysis was unable to define separate clusters for cultured ASMCs isolated from either healthy or moderate asthmatic individuals based upon their miRNA expression profile. In fact, sample 'Healthy 3' was most similar in miRNA expression profile to 'Asthmatic 1' and these two samples were subsequently most similar to 'Asthmatic 2' followed by 'Healthy 2' and 'Healthy 1'. The most different sample was 'Asthmatic 3'. It should be noted that the differences depicted in this analysis are relative within the data set, meaning that any differences shown may be very small in terms of absolute values. This analysis does, however, give a further indication that there were not global differences in the miRNA expression profile of the three healthy and three moderate asthmatic ASMC cultures analysed.

3.2.4 Identification of miRNAs demonstrating altered expression in cultured ASMCs isolated from healthy or moderate asthmatic individuals

To identify individual miRNAs with potential differential expression between cultured ASMCs isolated from either healthy or moderate asthmatic individuals analysis of variance (ANOVA) was performed. As an increasing viewpoint within the miRNA field is that small changes in the expression level of a miRNA can have profound affects on downstream targets and biological processes (Guo et al. 2010) it was decided that the initial analysis should include miRNAs that demonstrated an average difference in expression of greater than 1.5-fold between cultured ASMCs isolated from healthy or moderate asthmatic individuals. This analysis generated a list of 218 probe sets, 107 of which had higher expression in cultured ASMCs isolated from moderate asthmatics and 111 in those from healthy individuals (Appendix II). When hierarchical clustering using Euclidean Dissimilarity and Average Linkage was performed to cluster these 218 probe sets sample 'Healthy 3' clustered with the moderate asthmatic samples rather than remaining two healthy replicates (Figure 3.2.9). It should be noted that the positioning of the samples across the horizontal plane of the dendogram (Figure 3.2.9) is not reflective of their miRNA expression and that branch points can be rotated without altering the data. What the clustering does indicate, however, is the samples 'Healthy 3' and

'Asthmatic 1' were more similar to one another than to any of the remaining samples when comparing only the miRNAs that demonstrated an average difference in expression of greater than 1.5-fold between the phenotypic groups.

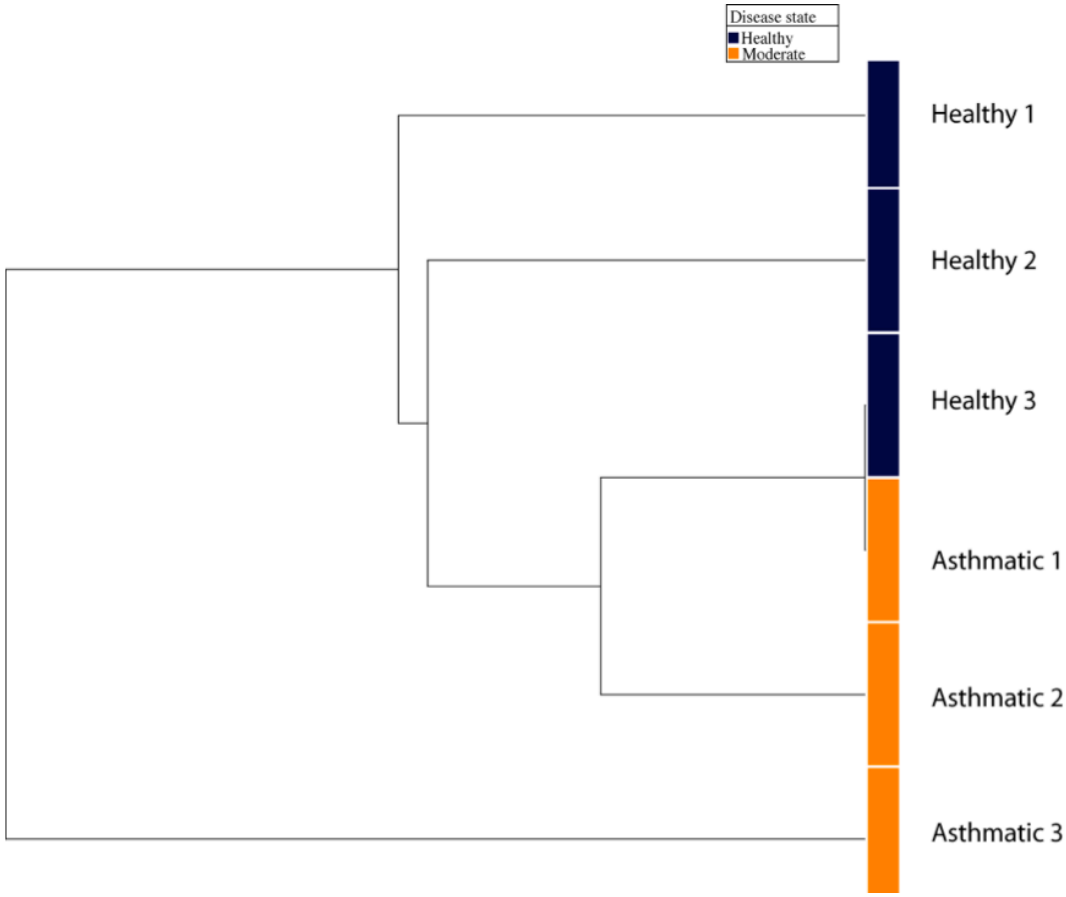

Figure 3.2.8 - Unsupervised hierarchical clustering is unable to differentiate cultured ASMCs isolated from healthy or moderate asthmatic individuals based upon their miRNA expression profile - Raw .cel files generated by the Affymetrix GCOS software were imported into Partek Genomics Suite and analysed by the default miRNA expression analysis workflow. Intensity levels for all human miRNA probe sets were clustered in an unsupervised manner using Euclidean Dissimilarity and Average Linkage.

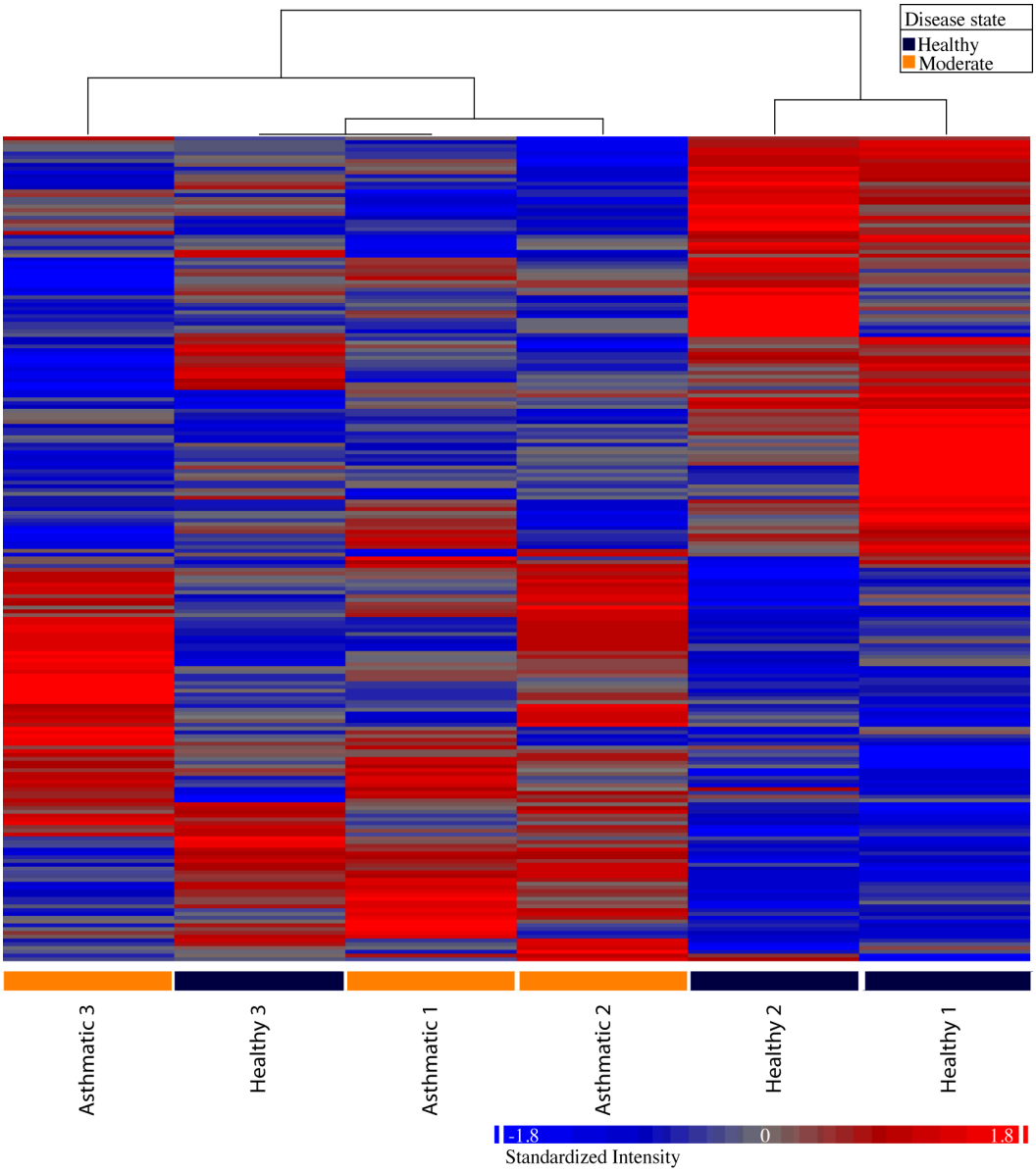

Figure 3.2.9 - Hierarchical clustering of miRNAs with a difference in expression of greater than 1.5-fold between cultured ASMCs isolated from moderate asthmatic patients compared to those from healthy individuals – Expression levels of miRNAs were compared in moderate asthmatic and healthy replicates by ANOVA before Euclidean Dissimilarity and Average Linkage were used to cluster those miRNAs that demonstrated a difference in expression of greater than 1.5-fold. A total of 218 probesets directed against human miRNAs showed a fold difference in expression of greater than 1.5-fold, with 107 and 111 probesets demonstrating higher expression in the asthmatic and healthy samples respectively. The heatmap is coloured by relative difference in expression, with red indicating increased expression and blue decreased expression. The strength of the colour represents the magnitude of the relative difference in expression with a stronger colour representing a larger difference.

The miRNAs with differential expression were further defined by restricting the gene list to those miRNAs that demonstrated an average difference in expression of greater than 1.5-fold between the healthy and asthmatic samples that was significant at a $p<0.05$, as determined by the ANOVA. This additional threshold reduced the list of miRNAs with a potential differential expression to 37, with 18 having a statistically significant higher average expression level in the healthy samples and 19 higher in the moderate asthmatic samples (Table viii). When hierarchical clustering, using Euclidean Dissimilarity and Average Linkage, of these 37 miRNA genes was performed sample 'Healthy 3' again clustered with the moderate asthmatic samples rather than the remaining healthy replicates (Figure 3.2.10). For many of the miRNAs that demonstrated a differential average expression in the healthy compared to the moderate asthmatic samples, for example miR-218-2, miR-488*, miR-423-5p, miR-1257, miR-939, miR-330-3p, miR-214* and miR-181c*, the expression level of that particular miRNA in 'Healthy 3' was more similar to the moderate asthmatic samples than to 'Healthy 1' or 'Healthy 2'. Only a minority of the identified miRNAs demonstrated a consistent difference in expression levels between the phenotypic groups. These miRNAs included miR-155, miR-93, miR-17*, miR-99b*, miR-1264, miR-125b-1*, miR-584 and miR-992 which were detectable at a higher level in the healthy samples and miR-1284, miR-769-5p, miR-34b, miR-889, miR-362-3p and miR-548d-3p, which were detectable at higher levels in the moderate asthmatic samples.

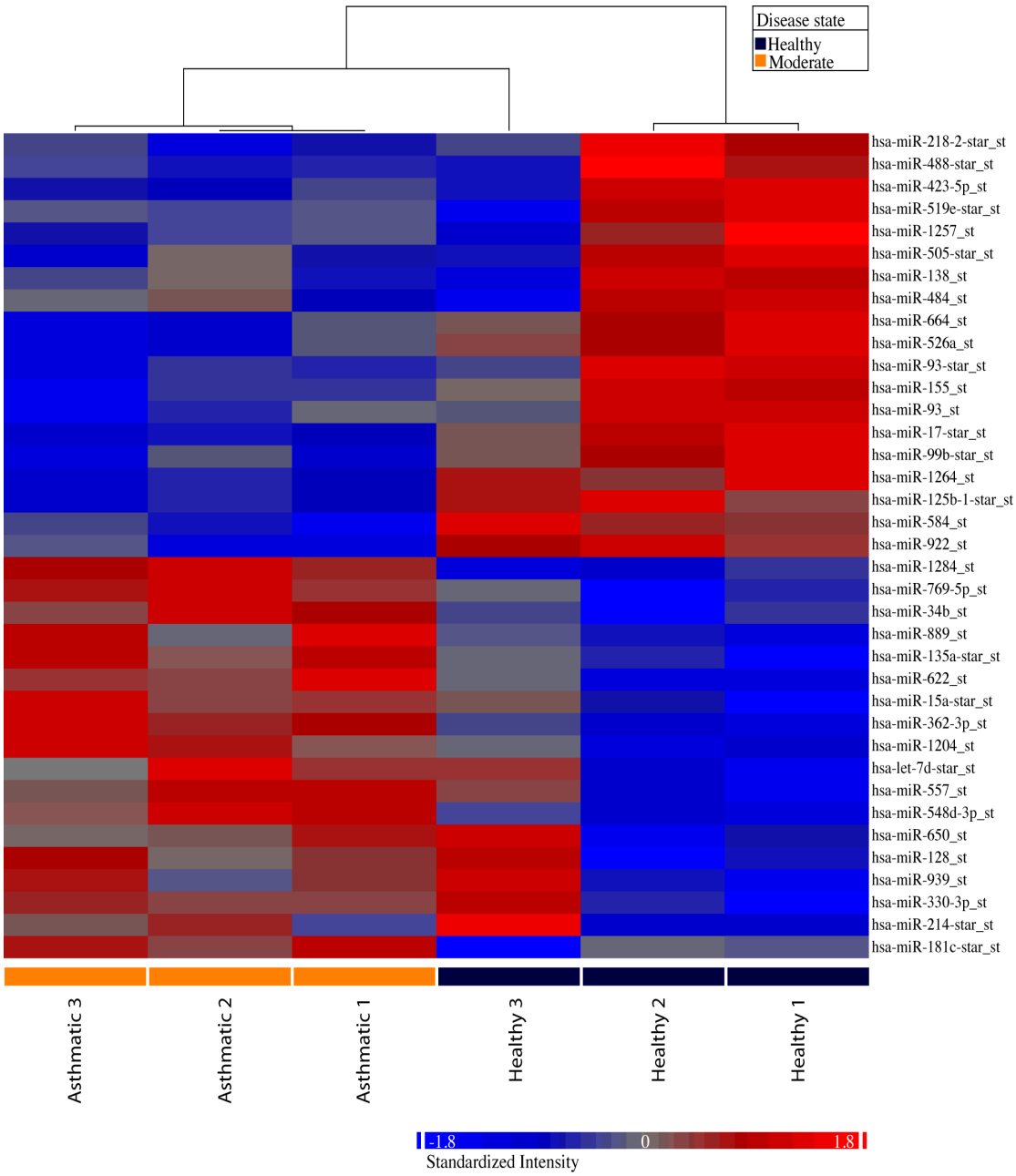

Figure 3.2.10 - Hierarchical clustering of the 37 miRNAs that demonstrated differential expression between cultured ASMCs isolated from healthy or moderate asthmatic individuals that was greater than 1.5-fold and significant at p<0.05 as determined by ANOVA – Expression levels of miRNAs were compared between moderate asthmatic and healthy samples by ANOVA. Euclidean Dissimilarity and Average Linkage were used to cluster those small RNAs that demonstrated a difference in expression that was greater than 1.5-fold and significant at $p<0.05$. A total of 37 probesets directed against human miRNAs passed these thresholds, with 18 and 19 probesets demonstrating higher expression in the asthmatic and healthy samples respectively. The heatmap is coloured by relative difference in expression, with red indicating increased expression and blue decreased expression. The strength of the colour represents the magnitude of the relative difference in expression with a stronger colour indicating a larger difference.

miRNA	p-value	Fold-Change	Direction of change
hsa-miR-17-star_st	0.000600082	3.25043	Healthy up vs Moderate
hsa-miR-155_st	0.022613	3.19565	Healthy up vs Moderate
hsa-miR-584_st	0.0485421	2.92857	Healthy up vs Moderate
hsa-miR-664_st	0.0280203	2.68862	Healthy up vs Moderate
hsa-miR-138_st	0.0186382	2.45935	Healthy up vs Moderate
hsa-miR-1257_st	0.0480535	2.1446	Healthy up vs Moderate
hsa-miR-1264_st	0.022613	1.98243	Healthy up vs Moderate
hsa-miR-93_st	0.00795574	1.96836	Healthy up vs Moderate
hsa-miR-218-2-star_st	0.019144	1.88239	Healthy up vs Moderate
hsa-miR-125b-1-star_st	0.0327697	1.84828	Healthy up vs Moderate
hsa-miR-99b-star_st	0.0233029	1.75556	Healthy up vs Moderate
hsa-miR-488-star_st	0.0194346	1.7309	Healthy up vs Moderate
hsa-miR-505-star_st	0.0348294	1.68301	Healthy up vs Moderate
hsa-miR-526a_st	0.0257118	1.59683	Healthy up vs Moderate
hsa-miR-519e-star_st	0.00371451	1.56464	Healthy up vs Moderate
hsa-miR-93-star_st	0.0428375	1.56293	Healthy up vs Moderate
hsa-miR-922_st	0.0435139	1.54631	Healthy up vs Moderate
hsa-miR-484_st	0.0463345	1.50405	Healthy up vs Moderate
hsa-miR-423-5p_st	0.00413081	1.50253	Healthy up vs Moderate
hsa-miR-214-star_st	0.0498476	-1.54065	Healthy down vs Moderate
hsa-miR-939_st	0.0468749	-1.68162	Healthy down vs Moderate
hsa-miR-330-3p_st	0.0417987	-1.72259	Healthy down vs Moderate
hsa-miR-1284_st	0.0097613	-1.76251	Healthy down vs Moderate
hsa-miR-650_st	0.0381242	-1.89542	Healthy down vs Moderate
hsa-let-7d-star_st	0.0444071	-2.07359	Healthy down vs Moderate
hsa-miR-135a-star_st	0.0387714	-2.084	Healthy down vs Moderate
hsa-miR-1204_st	0.0176738	-2.09261	Healthy down vs Moderate
hsa-miR-181c-star_st	0.0351941	-2.14799	Healthy down vs Moderate
hsa-miR-362-3p_st	0.00171051	-2.17816	Healthy down vs Moderate
hsa-miR-769-5p_st	0.0251811	-2.20762	Healthy down vs Moderate
hsa-miR-548d-3p_st	0.0169308	-2.25869	Healthy down vs Moderate
hsa-miR-15a-star_st	0.0326716	-2.29567	Healthy down vs Moderate
hsa-miR-622_st	0.0265693	-3.04139	Healthy down vs Moderate
hsa-miR-889_st	0.0497449	-3.36351	Healthy down vs Moderate
hsa-miR-128_st	0.0338725	-3.62733	Healthy down vs Moderate
hsa-miR-34b_st	0.0463163	-3.77843	Healthy down vs Moderate
hsa-miR-557_st	0.0156561	-3.96221	Healthy down vs Moderate

Table viii – ANOVA identified 37 miRNAs with a difference in expression level of greater than 1.5-fold and statistical significance of $p<0.05$ between the healthy and moderate asthmatic ASMC cultures analysed – ANOVA was performed in Partek Genomics Suite 2.0 to compare the expression level of miRNAs in cultured ASMCs isolated from either healthy or moderate asthmatic individuals. 37 miRNAs were found have a difference in average expression of greater than 1.5-fold that was statistically significant at a value of $p<0.05$, with 18 and 19 probesets demonstrating higher expression in the asthmatic and healthy samples respectively.

One advantage of the Affymetrix miRNA QC Tool in comparison to Partek Genomics Suite is that it uses a Wilcoxon-rank test (as described in 3.2.2) to compare the intensity value for a given miRNA probe to a GC-content matched control probe and then defines detection of an individual miRNA as true or false based upon its statistical significance above background. Figure 3.2.11 shows the correlation between the average normalised intensity values for probe sets directed against human miRNAs in the six biological replicates as determined by the Affymetrix miRNA QC Tool and Partek. There was a very good correlation between the two, which is reflective of the fact that the normalisation procedures performed are very similar. There was a slight skew at low intensity values due to the fact that the miRNA QC Tool, but not Partek, performs a small constant addition during the data processing procedure. The majority of the probe sets with a normalised intensity value of less than 3 in Partek are defined as false by the miRNA QC Tool and it was therefore decided to remove these miRNAs from subsequent analysis as they are likely to either not be expressed in the cultured ASMCs or to be expressed at a level that would make it difficult to determine any differential expression in subsequent validation experiments. Following the removal of miRNAs for which the average normalised intensity was less than three in the phenotypic group with the highest average intensity only 17 miRNAs remained, 9 of which were detectable at a higher average level in the healthy samples and 8 in the moderate asthmatic samples (Table ix). These miRNAs included miR-155, miR-138 and miR-93, which were detectable at a statistically significant lower level in the moderate asthmatic samples and miR-128, miR-769-5p and miR-181c* which were detectable at statistically higher levels in the asthmatic samples.

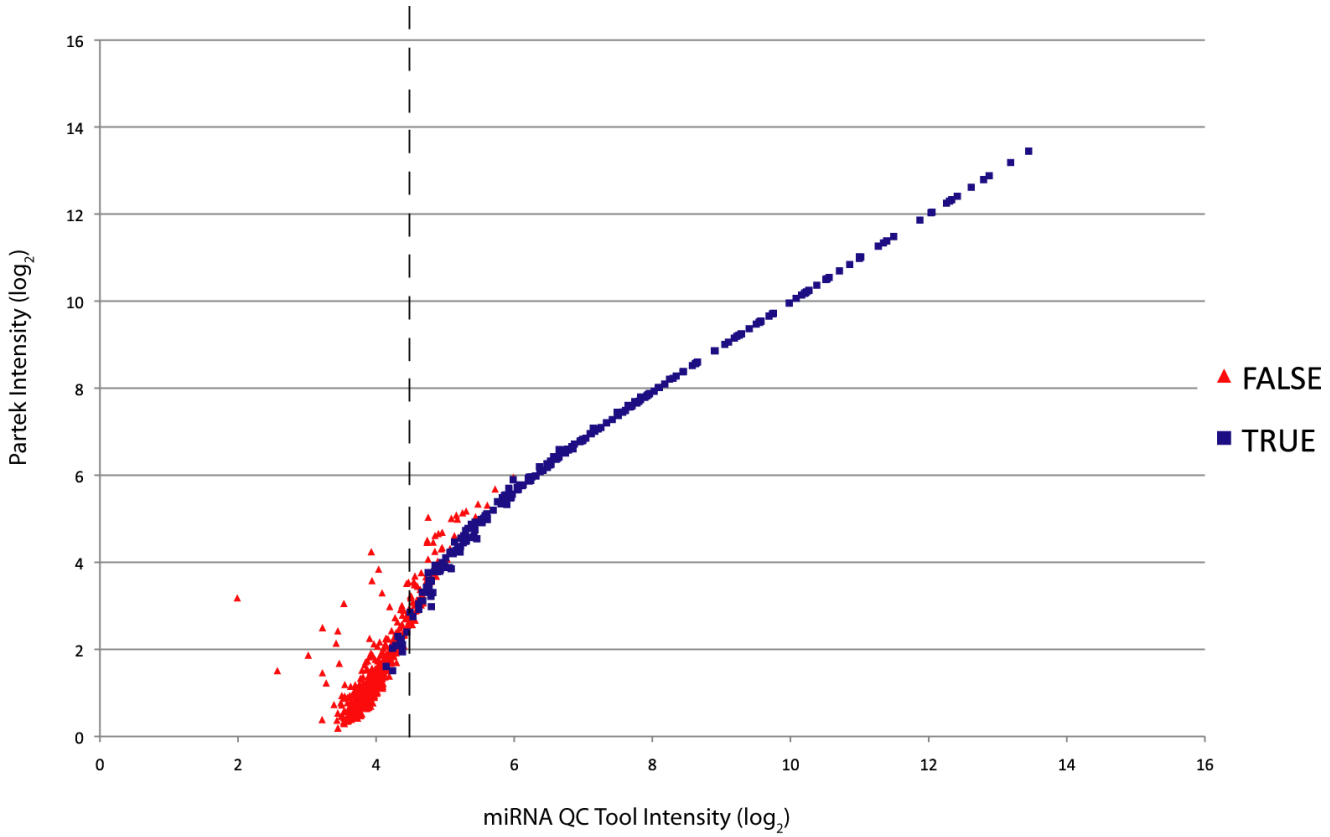

Figure 3.2.11 – The normalisation strategies used in the Affymetrix miRNA QC Tool and Partek Genomics Suite result in similar intensity values for human miRNA probe sets – Log_2 transformed normalised intensity values for human miRNA probe sets generated from the Affymetrix miRNA QC Tool and Partek Genomics Suite are shown on the X and Y axes respectively. Red triangles represent those probe sets classified as absent in the QC Tool whilst the blue squares represent those probe sets classified as present. The hashed vertical line represents the cut-off below which the majority of the probe sets were classified as absent as defined by a Wilcoxon-Rank test performed in the Affymetrix miRNA QC Tool.

Probeset ID	p-value	Fold-Change	Direction of change
hsa-miR-155_st	0.022613	3.19565	Healthy up vs Moderate
hsa-miR-138_st	0.0186382	2.45935	Healthy up vs Moderate
hsa-miR-93_st	0.00795574	1.96836	Healthy up vs Moderate
hsa-miR-125b-1*_st	0.0327697	1.84828	Healthy up vs Moderate
hsa-miR-99b-star_st	0.0233029	1.75556	Healthy up vs Moderate
hsa-miR-505-star_st	0.0348294	1.68301	Healthy up vs Moderate
hsa-miR-93-star_st	0.0428375	1.56293	Healthy up vs Moderate
hsa-miR-484_st	0.0463345	1.50405	Healthy up vs Moderate
hsa-miR-423-5p_st	0.00413081	1.50253	Healthy up vs Moderate
hsa-miR-214-star_st	0.0498476	-1.54065	Healthy down vs Moderate
hsa-miR-939_st	0.0468749	-1.68162	Healthy down vs Moderate
hsa-miR-330-3p_st	0.0417987	-1.72259	Healthy down vs Moderate
hsa-let-7d-star_st	0.0444071	-2.07359	Healthy down vs Moderate
hsa-miR-135a-star_st	0.0387714	-2.084	Healthy down vs Moderate
hsa-miR-181c-star_st	0.0351941	-2.14799	Healthy down vs Moderate
hsa-miR-769-5p_st	0.0251811	-2.20762	Healthy down vs Moderate
hsa-miR-128_st	0.0338725	-3.62733	Healthy down vs Moderate

Table ix – miRNAs called as detectable by the Affymetrix miRNA QC Tool and identified as being differentially expressed between healthy and moderate asthmatic ASMCs – miRNAs defined as being detected above background and identified as differentially expressed by an ANOVA comparing expression in healthy and asthmatic ASMCs using using thresholds of a difference in expression of greater than 1.5-fold and $p<0.05$.

3.2.5 qPCR validation of miRNAs with potential differential expression between cultured ASMCs isolated from healthy or moderate asthmatic individuals

Due to the fact that the miRNA microarray experiments were used as preliminary screens, with only three biological replicates analysed for both healthy and moderate asthmatic groups, a subset of those miRNAs that demonstrated a potential difference in expression between the healthy and moderate asthmatic samples were investigated further through RT-qPCR studies. This analysis was performed using

the same six RNA samples used for the microarray analysis, plus an additional four or five samples for both healthy and moderate asthmatic ASMC cultures.

Due to the preliminary nature of the initial screen performed it was decided to validate the expression of miRNAs that demonstrated varying characteristics of differential expression between cultured ASMCs isolated from healthy or moderate asthmatic individuals. miR-155 and miR-93 were investigated further as both demonstrated a statistically significant diminished relative level of expression in the cultured ASMCs isolated from moderate asthmatic individuals compared to healthy individuals (Table ix). In addition, miR-20a and miR-146a were analysed in RT-qPCR assays as they displayed a difference in expression of greater than two-fold between the moderate asthmatic and healthy cells which was not significant at $p<0.05$ as determined by the ANOVA (Appendix II). Closer inspection, however, demonstrated that both miR-20a and miR-146a had consistent differences in relative adundance between biological replicates of either healthy or moderate asthmatics but that there was variation in the relative expression levels within the phenotypic group, which likely accounted for the lack of statistical significance. It was therefore decided that it would be interesting to use miR-20a and miR-146a as models to determine if a number of miRNAs that displayed a suggestion of differential expression that appeared reproducible but was influenced by intra-group variation could be confirmed by RT-qPCR in an increased number of biological replicates. miR-335 was validated as a miRNA with a potentially higher level of expression in asthmatic ASM compared to healthy ASM is it displayed a consistently higher normalised intensity in the moderate asthmatic samples when compared to the healthy samples. Similar to miR-20a and miR-146a, however, this difference was not determined as statistically significant primarily because of the variation between the replicates and therefore may be significant if an increased number of biological replicates were to be used. Each of the miRNAs validated by RT-qPCR was determined as detectable above background levels by the Wilcoxon-Rank test performed in the Affymetrix miRNA QC Tool. The relative expression levels the miRNAs validated by RT-qPCR, as determined for each individual biological replicate during the microarray studies, are demonstrated in Figure 3.2.12.

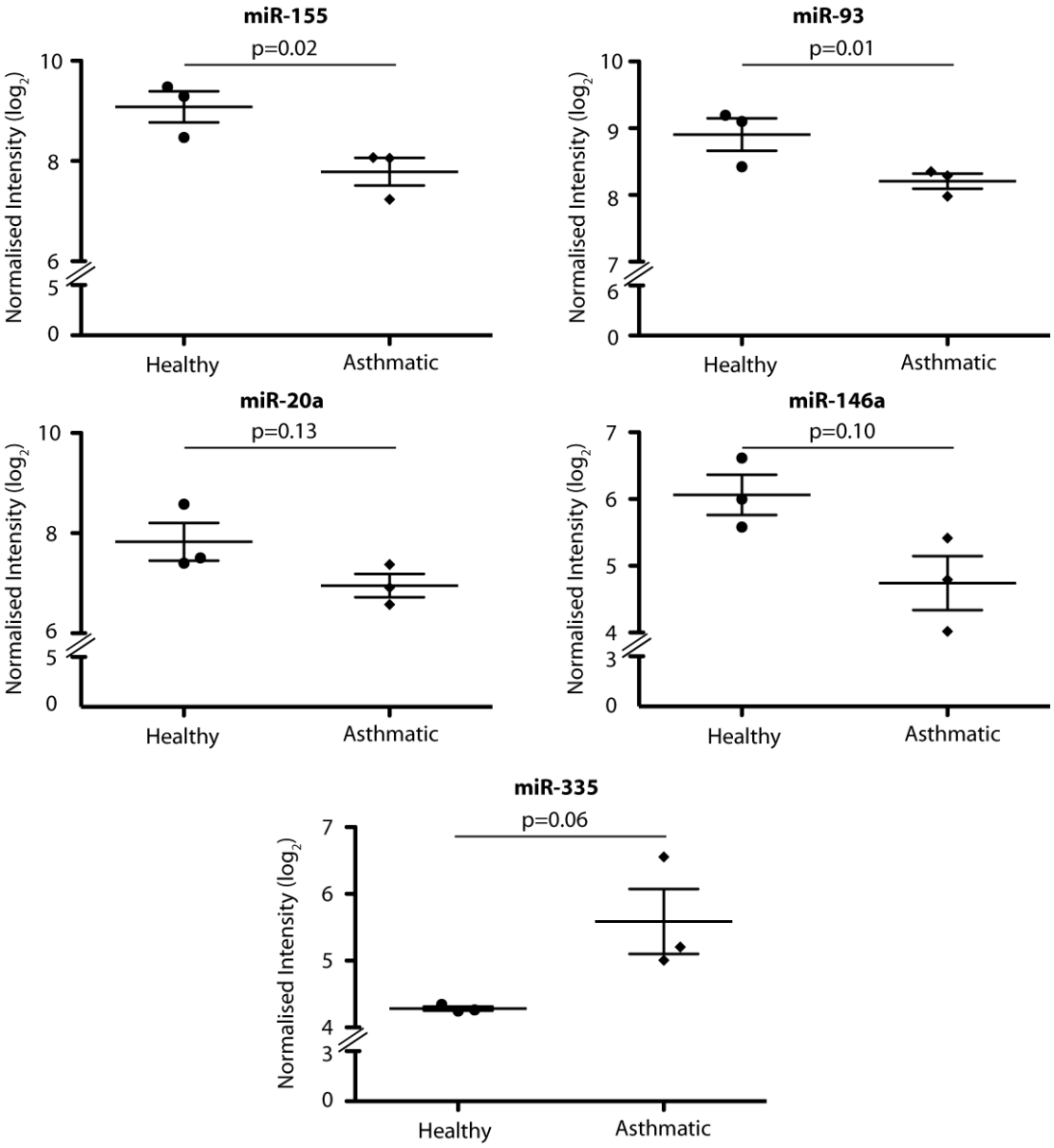

Figure 3.2.12 – Normalised intensity values of miRNAs chosen for RT-qPCR follow-up studies – The normalised intensity values as generated by Partek Genomics Suite for a chosen miRNA in each biological replicate. The x-axis demonstrates the normalised intensity signal (log_2 transformed) and error bars represent SEM. Statistical significance was determined by ANOVA in Partek Genomics Suite 2.0.

RT-qPCR was performed (as described in Chapters 2.3.2 and 2.3.4) on an additional number of biological replicates (for volunteer details see Table x) to validate the expression of miR-155, miR-146a, miR-20a and miR-93, which suggested lower abundance in the moderate asthmatic samples in the microarray analysis compared to healthy samples and miR-335, which suggested the opposing trend (Figure 3.2.12). In general the results of the RT-qPCR validations recapitulated those of the microarray studies, both in terms of the direction of change in relative expression levels and the magnitude of any change (Figure 3.2.13). miR-155 demonstrated a statistically significant lower level of abundance in the moderate asthmatic compared to the healthy samples, with a consistently low relative expression level determined in all of the asthmatic samples tested. Although there was some variation in the relative expression levels of mature miR-155 detected in the healthy samples, the average difference in expression was found to be significant as determined by a Mann-Whitney U test. miR-146a also demonstrated a statistically significant lower level of abundance in the moderate asthmatic compared to healthy samples, although the relative levels were more varied than those of miR-155 and there was a greater overlap between the healthy and moderate asthmatic samples. miR-20a demonstrated a trend towards a lower level of abundance in the moderate asthmatic samples, however, the difference was not statistically significant. One of the healthy samples demonstrated a relative expression level of miR-20a that was far greater than the remaining healthy samples and this clearly influences the mean relative expression level. A number of the remaining healthy samples, however, also had an increased relative miR-20a expression level when compared to the moderate asthmatic samples. miR-93 demonstrated a trend towards a lower level of expression in the moderate asthmatic samples, however, this was not statistically significant. miR-335 showed no difference in average expression between the healthy and moderate asthmatic samples. Interestingly, the relative expression levels of the moderate asthmatic samples fell into two groups that demonstrated either a high or low level of relative expression. There was no obvious correlation between the expression levels of any of the miRNAs and either gender or age.

	Healthy	**Moderate Asthmatic**
Gender (Male/Female)	5/3	6/2
Age (Mean/StDev)	30 ± 7.8	39 ± 12.7

Table x – Details of volunteers from whom bronchial biopsies were taken to generate the ASMC cultures used in the RT-qPCR miRNA expression profiling

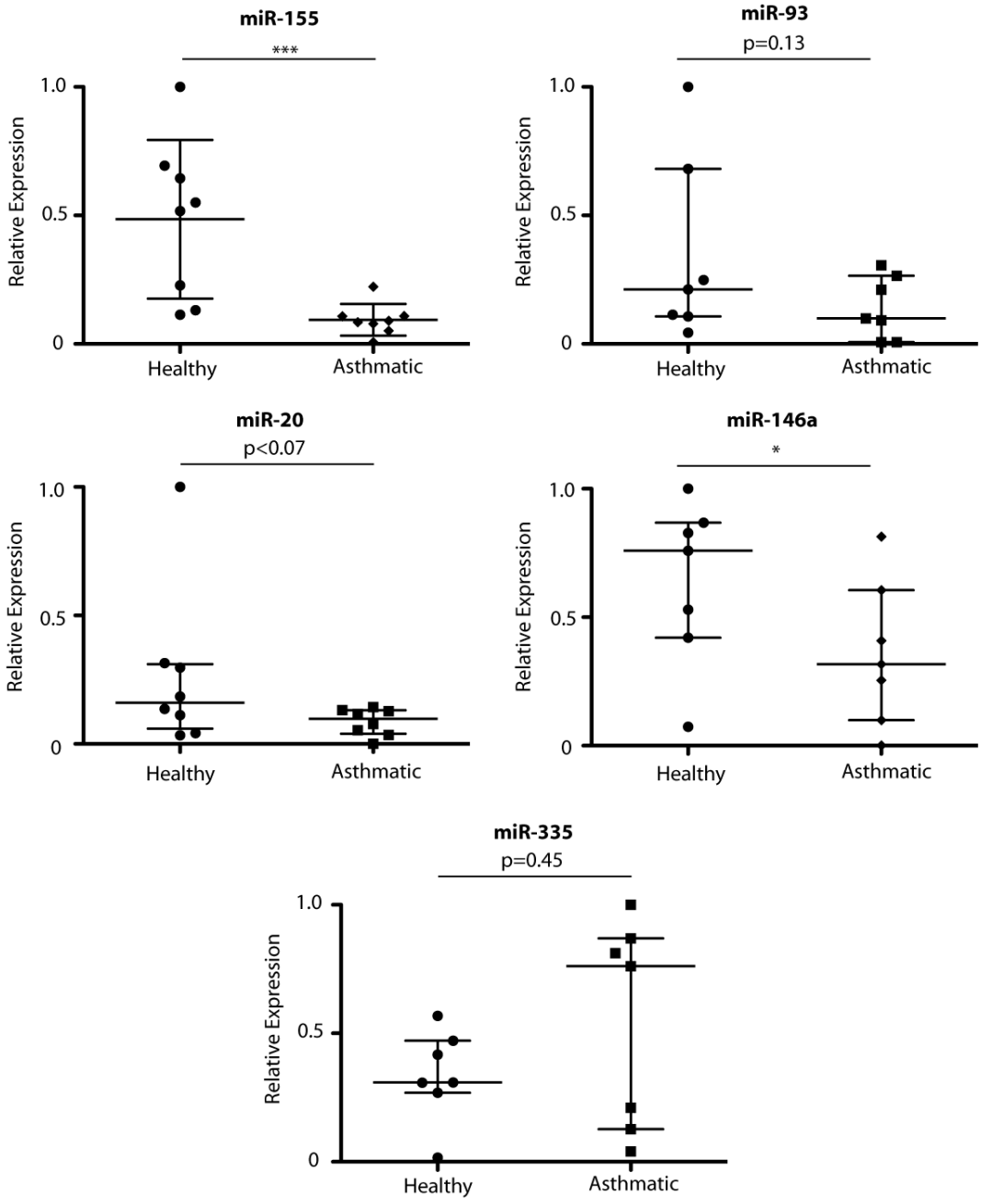

Figure 3.2.13 - RT-qPCR analysis of a subset of miRNAs that demonstrated potential differential expression between cultured ASMCs isolated from healthy individuals compared to those isolated from moderate asthmatic individuals – Cultured ASMCs isolated from either healthy or moderate asthmatic individuals were growth arrested by a 72 hour incubation in serum-free media. RNA was harvested from $5x10^5$ cells and DNase treated before miRNA-specific stem loop RT-qPCR was performed. Relative levels of each indicated miRNA were determined by ΔΔCt methodology using RNU6B as the endogenous control and expression levels are presented relative to the individual sample with the highest level of expression. *** $p<0.0005$ and * $p<0.05$ as determined by a Mann-Whitney U Test, the horizontal line represents the median sample for each miRNA and the whiskers represent the inter-quartile range of the relative expression levels, n=7 or 8 for each miRNA.

3.3 Discussion

3.3.1 Summary of results

The aim of the experiments described in this chapter was to determine if there was evidence for differential expression of miRNAs between cultured ASMCs isolated from healthy or moderate asthmatic individuals. The experimental strategy undertaken was to perform an initial preliminary screen using three biological replicates for both healthy and moderate asthmatic ASM samples before candidate miRNAs with potential differential expression were validated using RT-qPCR as an independent experimental read-out. The main findings of this study were that miR-155 and miR-146a had diminished abundance in the assayed cultured ASMCs isolated from moderate asthmatic compared to healthy individuals.

The microarray data were initally quality checked using the Affymetrix miRNA QC Tool, according to the manufacturers instructions. These quality control tests included determining that control probes generated equal intensity values across all individual microarrays performed within the experiment (Figure 3.2.2) and that the range of detected intensities for both the total content of the microarrays and the background control probes was similar for all microarrays performed (Figures 3.2.3-3.2.5). All of the quality control measures indicated that the labelling, hybridization and detection of each of the six samples was successful and that each could therefore be included in downstream analysis.

In addition to quality control tests, rudimentary comparative analyses were also performed using the Affymetrix miRNA QC tool. These included the generation of MvA plots to compare the intensity levels of probes on individual microarrays (Figure 3.2.6) and the generation of Pearson's correlation coefficient values to describe the overall similarity between individual microarray comparisons (Table vii). Both of these approaches indicated that there was very little difference in the overall expression profile of small RNAs in healthy and asthmatic ASMCs. It should be noted that the Affymetrix GeneChip® miRNA expression arrays used in these experiments contain probe sets directed against multiple species and it is not possible to restrict analyses to human miRNAs using the Affymetrix miRNA QC Tool. A number of the probesets are directed against species-specific sequences and the high level of similarity across microarrays may therefore be influenced by the large number of undetectable probesets that are simply directed against sequences not expressed by human cells. The fact that an average of 600 out of 847 human miRNAs assayed on each microarray were undetectable, however, implies that the

majority of human miRNAs assayed on the microarray are not expressed in ASM (Chapter 3.2.2).

To enable more sophisticated analysis of potential differential miRNA expression between healthy and asthmatic ASMCs the microarray intensity data was imported into Partek Genomics Suite 2.0. Analysis of the general profile of miRNA expression in cultured ASMCs indicated that miRNAs such as the let-7 family of miRNAs, miR-100, miR-21 and the miR-143/145 cluster were expressed at high levels within the cultured ASMCs (Appendix I). This was encouraging, as a number of these miRNAs have described roles in smooth muscle biology (see Chapter 3.3.3).

Comparative analysis by both PCA (Figure 3.2.7) and unsupervised hierarchical clustering (Figure 3.2.8) indicated that there were not gross differences in the expression profile of miRNAs in healthy and asthmatic ASMCs, as neither method was able to discriminate between the phenotypic groups. This result was not surprising as it is likely that any differences between healthy and asthmatic ASM will be subtle, as implicated by the controversy in the literature regarding a number of aspects of an altered ASM phenotype in asthma (Chapter 1.5.1). Further, the fact that an average of 600 out of 847 human miRNAs assayed were undetectable in each sample means that the analyses determining global expression profiles will be greatly influenced by this large number of miRNAs that were undetectable in each sample (see Chapter 3.2.2). ANOVA identified a number of candidate miRNAs with potential differential expression between the cultured healthy and asthmatic ASMCs assayed. A number of thresholds were applied to identify candidate miRNAs with potential differential expression, including using cut-offs on fold change alone (Appendix II and Figure 3.2.9), fold-change and p-value (Table viii and Figure 3.2.10) and fold-change, p-value and a statistically significant level of expression (Table ix). Using thresholds of an average fold difference in expression of greater than 1.5-fold between the phenotypic groups at a $p<0.05$ and a signal that was detectable above background levels 17 miRNAs were identified. These included miR-155, miR-138 and miR-93, which were detectable at lower levels in the moderate asthmatic compared to the healthy samples and miR-128, miR-769-5p and miR-181c* which showed the opposite trend (Table ix).

Independent RT-qPCR validation studies were performed on a number of miRNAs identified at various stages of the analysis. These included miR-155 and miR-93,

which were differentially detectable at a level greater than 1.5-fold between the healthy and asthmatic ASMCs and this difference was deemed statistically significant (Table ix). Due to the preliminary nature of the microarray screen miR-20a, miR-146a and miR-335, which all suggested differential expression that was not statistically significant (Appendix II and Figure 3.2.12), were also followed-up by RT-qPCR. The results of the RT-qPCR validation indicated that miR-155 and miR-146a were expressed at a statistically significant lower level in the moderate asthmatic ASMCs assayed compared to those isolated from healthy individuals, whilst miR-20a and miR-93 demonstrated a trend towards lower expression in asthmatic ASMCs that was not statistically significant. miR-335 demonstrated no difference in expression between the healthy and asthmatic ASMCs (Figure 3.2.13). It is important to note the variation in relative abundance of each miRNA between biological replicates as it indicates the need to assay a number of biological replicates to increase confidence in the results generated. As an example of this, two of the three healthy samples analysed on the microarray profiling demonstrated high levels of miR-155 expression and an increased number of biological replicates indicated that whilst there was variation in the level of miR-155 expression in ASMCs isolated from healthy individuals, the median level of abundance was greater than that in ASMCs isolated from moderate asthmatic individuals (Figure 3.2.13). In contrast to this, all three of the moderate asthmatic samples analysed during the microarray studies demonstrated relatively high abundances of miR-335 expression (Figure 3.2.12). During RT-qPCR validation experiments, however, it was demonstrated that the relative abundance of miR-335 in ASMCs isolated from moderate asthmatic individuals was varied and there was an equal chance of detecting a high or low level of expression (Figure 3.2.13). These data therefore demonstrate the importance of performing independent validations of microarray results when the power of the initial study is limited. Closer inspection of the individual biological replicates assayed did not indicate general trends in overall miRNA expression, meaning that certain individuals did not demonstrate consistently high or low expression of all miRNAs.

None of the miRNAs analysed by qPCR analysis are derived from the same pri-miRNA transcript and hence no potential differences in expression levels could be explained by a differential transcriptional regulation of a single locus.

3.3.2 Caveats and limitations

A consideration when analysing the results described in this chapter is the nature of the ASMC model from which the RNA was derived. This point is clearly important for all studies throughout the thesis in which ASMCs are used, particularly when comparisons between healthy and asthmatic ASMCs are performed rather than the use of an exogenous treatment. The explant culture method (described in 2.1.1) used to isolate the ASMCs has been utilised in a large number of published studies (Hirst 2000) (Chan 2006) and includes staining to confirm the expression of smooth muscle proteins including α-SMA, desmin, and calponin. There is, however, controversy as to the extent to which the cultured ASMCs truly represent *in vivo* cells (Wenzel 2006). In addition, the attempts to identify endogenous differences between ASMCs isolated from healthy and asthmatic volunteers detailed in this chapter rely on the fact that any differences must be retained throughout an extended culture period. In opposition to this argument, however, any differences that are identified during the extended culture period are more likely to represent stable or endogenous differences, rather than those that are a response to the inflammatory milieu of the asthmatic lung. It must therefore be noted that although these cells represent a relatively accessible model system, it cannot be presumed that they completely replicate ASMCs as they are found *in vivo*. This issue was noted during the project and it was hoped that the study could be replicated in laser microcapture sections of ASM bundles. Due to various issues, however, this was not possible. It would be very useful to use an *in situ* hybridization approach to determine if there was endogenous expression of miR-155 in ASM bundles within bronchial biopsies. In addition, such an *in situ* hybridization approach would also enable the identification of other cell types within the airways in which miR-155 was expressed and allow the determination of the relative level of miR-155 expression between different cell types.

Due to limitations in the resources available for this microarray study a preliminary experiment analysing three healthy and three moderate asthmatic ASMC cultures was performed. The rationale was that any candidate miRNAs demonstrating potential differential expression would then be confirmed during independent RT-qPCR studies. This approach has produced useful data as miR-155, for example, has been shown to be expressed at lower levels in the assayed ASMCs derived from asthmatic compared to healthy individuals by two independent experimental approaches. The preliminary nature of the microarray studies, however, demands

that caution must be taken when analysing the results. The major manifestation of this is the lack of statistical power. It was not possible to perform multiple testing corrections following the ANOVA as the small number of replicates meant that none of the data would pass a multiple testing correction. This means that there will be a number of miRNAs that are identified as differentially expressed between the healthy and asthmatic ASMCs that are false positives. It is because of this fact that it was essential to perform RT-qPCR validations of potential differential expression prior to downstream investigations. Using the data generated in this chapter as preliminary data to perform power calculations that could direct a potential comprehensive microarray analysis indicates that a total of 25 samples per phenotypic group would be required to detect over 90% of the miRNAs with differences in expression levels of greater than 1.5-fold at thresholds of $p<0.05$. If a 2-fold difference in expression were used, with the same statistical thresholds, approximately 15 samples per phenotypic group would be required to detect 90% of the miRNAs demonstrating differential expression (power calculations performed in Partek Genomics Suite 2.0). Although this analysis indicates that the microarray profiling performed in this chapter is not sufficient to detect the totality of subtle differences in miRNA expression between healthy and asthmatic ASMCs, it is possible to detect larger differences in expression, for example that of miR-155, if the microarray analysis is combined with subsequent RT-qPCR validation in an increased number of biological replicates.

Due to the fact that the microarray studies were performed as a screen to identify potentially interesting miRNAs for further investigations, the list of miRNAs that were validated by RT-qPCR is not comprehensive but rather a subset of miRNAs displaying varying characteristics of differential expression. It is clear that other miRNAs not assayed in RT-qPCR studies may potentially be important. Some of the miRNAs, for example miR-155 and miR-93, had very strong indications of differential expression between the ASMCs isolated from healthy or moderate asthmatic volunteers (Table ix and Figure 3.2.12). Other miRNAs, for example miR-146a, miR-20a and miR-335 had a suggestion of differential expression that was not deemed as statistically significant due to either a small average difference between the healthy and asthmatic samples or variation within the phenotypic group. If an increased number of replicates had been assayed during the initial microarray studies more confidence could have been taken in choosing the miRNAs to validate during RT-qPCR studies. It was decided not to choose candidate miRNAs from solely

from Table ix as it was deemed important to identify if miRNAs with a suggestion of differential expression in the microarray screens could be confirmed by RT-qPCR. The fact that miR-146a was shown to demonstrate a diminished relative expression level in moderate asthmatic compared to healthy ASMCs gives a level of credence to this approach (Figure 3.2.13).

3.3.3 Relevance of results

Although miRNAs were initially reported only relatively recently (see Chapter 3.1.1.), their significance and importance in the regulation of gene expression can be determined from the large number of studies investigating the influence of miRNAs in a wide variety of disease settings. At the time of writing, however, the dataset produced in Chapter 3.2 was the first attempting to compare the expression of miRNAs in isolated healthy and asthmatic ASMCs.

There are a small number of reports investigating miRNAs in the context of ASM, with the majority focusing on changes in miRNA expression following an exogenous stimulus. Chiba *et al.* have reported that IL-13 treatment of human bronchial smooth muscle cells causes a decrease in the expression of miR-133a and that artificial inhibition of miR-133a function in smooth muscle cells through the use of antagomirs results in an increase in the expression of RhoA, a known pro-contractile protein (Chiba 2009). The results generated during the studies described in this chapter, however, indicated that miR-133a was detectable in only one of the six RNA samples analysed (Appendix I).

Two separate studies have investigated the influence of proinflammatory cytokine treatment on the expression of miRNAs in primary human ASMCs. Larner-Svensson *et al.* reported an IL-1β dependent induction of miR-146a, which correlated with the release of IL-6 and IL-8 from the ASMCs. Further mechanistic studies, however, indicated that the increase in miR-146a expression was not causative of the increase in IL-6 and IL-8 expression (Larner-Svensson 2010). In the second study, human ASMCs were treated with a combination of IL-1β, TNFα and IFNγ and it was determined that the abundance of miR-25, miR-40*, miR-188 and miR-320 decreased following proinflammatory cytokine treatment (Kuhn 2010). Further mechanistic studies of miR-25 determined the potential for miR-25 to regulate a number of molecules with known roles in ASM biology, including CCL5, CCL26, TNFα and myosin heavy chain. Of the miRNAs identified by Kuhn *et al.*, miR-25,

miR-140* and miR-320a were detectable in all the samples analysed during Chapter 3.2, whilst miR-188 and miR-320b, miR-320c and miR-320d were not detectable in any. Neither miR-25, miR-140* or miR-320a demonstrated any evidence of differential expression between ASMCs isolated from healthy or asthmatic volunteers.

Mohammed *et al.* have reported an interesting study in which they exposed human ASMCs to 1 hour of cyclic stretch and compared miRNA expression before and after stretch (Mohamed et al. 2010). miR-26a was found to be upregulated following stretch and further studies indicated that miR-26a contributed to the stretch-induced hypertrophy of the ASMCs through the targeted downregulation of glycogen synthase kinase-3β. miR-26a was found to be expressed in all healthy and asthmatic ASM cultures analysed in Chapter 3.2 (Appendix I), however, it did not demonstrate any evidence of differential expression.

A large amount of data is available regarding the role of miRNAs in cardiac and vascular smooth muscle. A high impact study published in 2009 described an influential role for the co-transcribed miRNAs, miR-143 and miR-145 in the differentiation of both cardiac and vascular smooth muscle cells (Cordes et al. 2009). It was shown that miR-143 and miR-145 were direct transcriptional targets of serum response factor and myocardin and that they acted co-operatively to target a number of factors involved in smooth muscle function, including Kruppel-like factor 4, myocardin and Elk-1. This initial report has been followed by a number of studies describing a role for miR-143 or miR-145 in various aspects of smooth muscle biology, including contraction, injury response and plasticity (Boettger et al. 2009), (Xin et al. 2009) (Elia 2009), (Wang et al. 2010b). Collison *et al.* have published a particularly interesting study regarding miR-145 in the context of asthma (Collison 2011). In this report the authors demonstrated that a general inhibition of miR-145 in a house dust-mite induced model of allergic airways disease results in a decrease in airway inflammation that is comparable to glucocorticoid treatment. This implies an *in vivo* role for miR-145 in allergic airways disease, however, it should be noted that the cell type influenced is unclear. In the miRNA microarrays performed in Chapter 3.2 both miR-143 and miR-145 were expressed at a high level, suggesting they have functional roles in airway smooth muscle (Appendix I). Neither of the miRNAs, however, demonstrated evidence of differential expression.

In addition to smooth muscle biology it is important to analyse the data from chapter 3.2 in the context of the asthma disease setting. As would be expected, a large amount of the data concerning the role of miRNAs in asthma is focused around their influence on cytokine expression and signaling. miR-21 has been shown to be upregulated in an IL-13 driven mouse model of asthma and was found to repress IL-12p35 expression and thus contribute to a bias towards a Th2 immune response (Lu et al. 2009). It has subsequently been shown that ablation of miR-21 expression resulted in an increase in signaling through the IL-12/IFNγ pathway and a decrease in lung eosinophilia in an ovalbumin-driven murine model of asthma (Lu et al. 2011). Of particular interest to the study described in Chapter 3.2, miR-21 has also been shown to mediate the TGF-β and 'bone morphogenetic protein' induced contractile phenotype of vascular smooth muscle (Davis et al. 2008). miR-126 was required for Th2 effector function in an acute TLR4-driven murine model of asthma (Mattes et al. 2009) whilst inhibition of miR-126 function in a chronic model resulted in decreased eosinophilia but no alteration in airway wall remodeling (Collison 2011). In the microarray results presented in Chapter 3.2, miR-21 was detectable in RNA derived from cultured ASMCs whilst miR-126 was not (Appendix I). There was, however, no evidence for the differential expression of miR-21.

Data from the only study to date examining miRNA expression from lung biopsies of healthy and asthmatics reported no differential expression (Williams et al. 2009). This data, however, only analysed the expression of 227 out of over 700 annotated human miRNA genes. The data also focused on heterogeneous cell populations isolated from biopsies rather than specific cell types and may therefore have potentially missed changes in miRNA expression in individual cell types. In addition, the study focused on mild asthmatics and it may be that a more severe phenotype is required to identify potential differences in miRNA expression.

The miRNA with the highest level of differential expression between the assayed healthy and asthmatic ASMCs was miR-155, which was detectable at a level 3-fold lower in asthmatic compared to healthy ASMCs (Figure 3.2.13). Rodriguez *et al*. have described the phenotype of a total miR-155 knock-out mouse, the most striking feature of which was the spontaneous development of lung remodeling and fibrosis by 320 days of age (Rodriguez et al. 2007). Many of the features of this lung remodeling are very similar to those reported in murine models of allergic airways disease in which remodeling occurs. This was very encouraging evidence that the

diminished abundance of miR-155 in asthmatic ASMCs may potentially have a pro-asthmatic function. It was therefore decided to further investigate the functions of miR-155 in ASMCs.

Chapter 4 – Investigating potential targets of miR-155 in cultured ASMCs

4.1 Introduction

The following chapter details investigations to identify potential targets for miR-155, a miRNA that was identified as being differentially expressed in cultured ASMCs isolated from moderate asthmatic compared to healthy individuals (Figure 3.2.13), in cultured ASMCs.

4.1.1 Genomic location and derivation of miR-155

The *BIC* locus was originally noted as a common retroviral integration site in avian leucosis virus (ALV)-induced B cell lymphomas (Clurman & Hayward 1989). Initial analysis of the locus indicated that it did not contain an open-reading frame and lead to the hypothesis that it may function as an untranslated RNA (Tam et al. 1997). The human *BIC* gene is located at chromosome 21q21 and consists of three exons (Figure 4.1), it was fully characterised by Tam *et al*. in 2001 who confirmed that the locus was not protein coding. Comparison of BIC cDNAs from human, mouse and chicken identified a region of 138 nucleotides with 78% homology that mapped to the final exon of each gene. This region of homology was predicted by bioinformatics analysis to form an imperfect RNA duplex with a similar structure in all three species (Tam 2001) and shortly afterwards the sequencing of short RNAs from various mouse tissues demonstrated that one branch of the BIC RNA stem-loop contained the sequence of mature miR-155 (Lagos-Quintana et al. 2002). miR-155 is most highly expressed in lymphoid tissues such as the spleen and thymus, however, its expression is also noted in other organs, for example the lungs, kidneys and liver (Lagos-Quintana et al. 2002) (Tam 2001) (Martin et al. 2006).

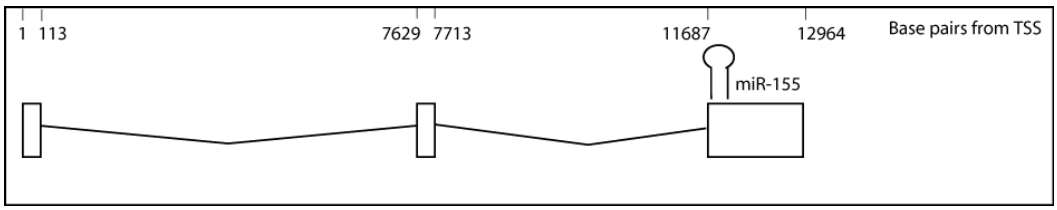

Figure 4.1 – Gene structure of human *BIC* – The human *BIC* gene is located at chromosome 21q21 and consists of three exons. The miR-155 sequence is located at the 5' end of the third exon. Blocks represent exons and connecting lines represent introns. The numbers represent the number of base pairs from the annotated transcriptional start site.

4.1.2 The function of miR-155

miRNAs predominantly function through the post-transcriptional downregulation of specific mRNAs (detailed in Chapter 3.1). The first reported target of miR-155 was Angiotensin II Type 1 receptor (AT1R), which was shown through luciferase reporter assays and mutagenesis to be a direct target of miR-155. The regulation of endogenous AT1R was subsequently inferred by a decrease in the detection of radiolabelled ligand binding to AT1R following the over-expression of miR-155 in fibroblasts (Martin et al. 2006b). Interestingly, a silent polymorphism caused by a single nucleotide substitution within the 3'UTR of *AT1R* had been shown to associate with cardiovascular disease, however, its position within the gene made it difficult to ascertain the functional significance. Two reports published at a similar time showed that the base pair mutation resulted in disruption of the miR-155 binding site within the 3'UTR of AT1R, leading to increased protein levels (Martin et al. 2007) (Sethupathy et al. 2007).

The majority of work investigating the function of miR-155 has subsequently focused on inflammation and cancer, with a variety of potential targets reported across a number of cell types and systems.

4.1.2.1 miR-155 and inflammation

Rodriguez *et al*. have described the phenotype of a mouse knock-out of miR-155, the most striking feature of which was the spontaneous development of lung remodeling and fibrosis by 320 days of age (Rodriguez et al. 2007). This remodeling involved collagen deposition, an increased cell mass of sub-bronchiolar myofibroblasts and an increase in the amount of ASM, along with an increase in the number of leukocytes in the BAL. In addition the miR-155-/- mice had several immune defects including reduced production of IgM and switched antigen-specific antibodies following tetanus toxin fragment C immunization, reduced production of IL-2 and IFNγ by splenocytes and impaired antigen-presentation by dendritic cells. Further, during *in vitro* differentiation experiments naïve miR-155-/- CD4+ cells cultured in either neutral or weakly Th2 polarizing conditions showed an increased propensity to differentiate towards a Th2 phenotype, a phenomenon the authors suggest is caused by a loss of miR-155 mediated regulation of the Th2-inducing transcription factor, c-maf. Additional reports on the phenotype of the miR-155-/- mouse have detailed reduced extrafollicular and germinal centre responses and a failure to produce high-affinity IgG1 antibodies, which is suggested to be mediated

by miR-155 regulation of the PU.1 transcription factor (Thai et al. 2007). This finding was also reported independently in a murine model where miR-155 was specifically knocked-out in B cells (Vigorito et al. 2007). There is also evidence that miR-155 directs the down-regulation of Activation-Induced Cytidine Deaminase (AID) (Dorsett et al. 2008), a critical enzyme that is essential for antibody class switching in B cells.

Levels of miR-155 are increased following the activation of a number of immune cells, including macrophages (O'Connell et al. 2007), dendritic cells (Martinez-Nunez et al. 2009), CD4+ effector T cells (Haasch et al. 2002) and regulatory T cells (Kohlhaas et al. 2009), suggesting that it has a broad range of functions across a variety of myeloid and lymphoid cells. In terms of disease relevance, the lung remodelling apparent in the miR-155-/- mouse suggests that miR-155 may have causative roles in the establishment of pulmonary fibrotic conditions, including asthma. In addition, increased expression of miR-155 has been reported in both the synovial fibroblasts and surrounding tissue in Rheumatoid Arthritis patients. This increased expression is augmented by *in vitro* treatment with LPS, IL-1β and TNFα and is associated with a decrease in the expression of MMP1 and MMP3 (Stanczyk et al. 2008). Further, miR-155-/- mice are resistant to the establishment of experimental autoimmune encephalomyelitis (EAE), a murine model of multiple sclerosis (O'Connell et al. 2010), (Murugaiyan et al. 2011). This resistance is conferred by an inability of the miR-155-/- mice to generate a Th17 mediated immune response. The data from mouse models summarised above are particularly interesting as there are reports of abnormalities caused by both an increase and a loss of miR-155 expression, suggesting that it has cell-type or stimulation-specific roles in various contexts.

4.1.2.2 miR-155 and cancer

In addition to its role in the immune system miR-155 is a widely-reported oncogene, continuing from the initial reports of the *BIC* locus as a common ALV-induced B cell lymphoma integration site before the function of the gene was understood (Clurman & Hayward 1989). There are now a number of reports detailing increased expression of miR-155 across a variety of malignancies, including both leukaemias and solid tumours (Faraoni et al. 2009) and miR-155 is viewed as a promising biomarker for disease sub-typing and designing treatment plans. Immunohistochemical studies of Diffuse Large B-cell Lymphomas (DLBCL), for

example, have demonstrated they can be classified into two distinct molecular subtypes, either germinal centre B cell-like (GCB) or activated B cell-like (ABC). miR-155 expression has been shown to correlate very well with ABC, suggesting that levels of miR-155 expression may be useful for both the diagnosis and prognosis of DLBCL (Lawrie et al. 2007).

The evidence for the oncogenic role of miR-155 appears to favour an anti-apoptotic function. O'Connell *et al.* have demonstrated that the over-expression of miR-155 in heamatopoeitic stem cells (HSCs) results in the establishment of a myeloproliferative disorder (O'Connell et al. 2008). Following the demonstration that the pro-apoptotic tumour suppressor gene, Src homology-2 domain-containing inositol 5-phosphatase 1 (SHIP1), was a direct target of miR-155 (Costinean et al. 2009) it has been shown that miR-155 induces an *in vitro* myeloproliferative disorder via the down-regulation of SHIP1 (O'Connell et al. 2009). Further, there is also evidence that miR-155 mediated repression of SHIP1 is important in the etiology of ABC-DLBCL (Pedersen et al. 2009). In addition to SHIP1, miR-155 has been shown to regulate the expression of additional pro-apoptotic genes, including tumour protein 53-induced nuclear protein 1 (Gironella et al. 2007) and JARID2 (Bolisetty et al. 2009). There is also evidence that miR-155 may play a role in metastasis. Kong *et al.* have reported that TGFβ-induced epithelial-mesenchymal transition (EMT), a process that is important in the metastasis of many advanced malignancies, is dependent upon miR-155 regulation of RhoA to disrupt tight junction formation (Kong et al. 2008).

4.1.3 Aims of the Chapter

Following the determination of decreased miR-155 abundance in cultured ASMCs isolated from asthmatic compared to healthy individuals (Figure 3.2.13) the aim of this chapter was to investigate potential targets for miR-155 in cultured ASMCs.

A number of experimental approaches were undertaken, including:

i) the identification of candidate miR-155 targets with known pro-asthmatic functions in ASMCs through target identification algorithms and literature searches,

ii) the determination of the functionality of predicted miR-155 targets through luciferase assays,

iii) investigations into the regulation of endogenous candidate mRNA and protein targets by miR-155 in cultured ASMCs,

iv) the unbiased determination of potential endogenous targets of miR-155 in human ASMCs through mRNA microarray studies.

4.2 Results

4.2.1 Confirmation of a diminished abundance of mature miR-155 and BIC in cultured ASMCs isolated from moderate asthmatic compared to healthy individuals

RNA was harvested from ASMC cultures isolated from eight healthy and eight moderate asthmatic volunteers as described in Chapter 3.2.5 (Figure 4.2.1). RNA isolation and DNase treatment were performed at culture passages 3-5 of the initial explant culture, whereupon RNA was stored at -80°c until RT-qPCR analysis. Separate RT-qPCR analysis (described in Chapter 2.3.1, 2.3.2 and 2.3.4) was performed using RNU6B or let-7b as endogenous control genes to increase confidence that the results generated were not an artifact of differences in the expression of the control gene between samples. Relative quantification using both RNU6B and let-7b as the endogenous control demonstrated a statistically significant diminished abundance of mature miR-155 in cultured ASMCs isolated from moderate asthmatics compared to healthy individuals (Figure 4.2.1 A) and B)).

RT-qPCR was also performed (described in Chapter 2.3.5) to assess the levels of the miR-155 housing transcript, BIC, in cultured ASMCs isolated from healthy or moderate asthmatic individuals. The qPCR forward and reverse primers are targeted against sequences in the second and third exons of the BIC transcript respectively (see Figure 4.1) and the assay therefore detects the levels of mature BIC transcript. This analysis demonstrated a statistically significant lower level of BIC transcript in cultured ASMCs isolated from moderate asthmatics compared to those from healthy individuals (Figure 4.2.1 C)). This suggests that a mechanism influencing the transcription or stability of the BIC transcript is responsible for the lower levels observed in moderate asthmatic ASMCs.

Following the determination of diminished abundance of both BIC RNA and mature miR-155 in cultured ASMCs isolated from moderate asthmatics compared to healthy individuals subsequent experiments were performed to identify targets for miR-155 in ASMCs.

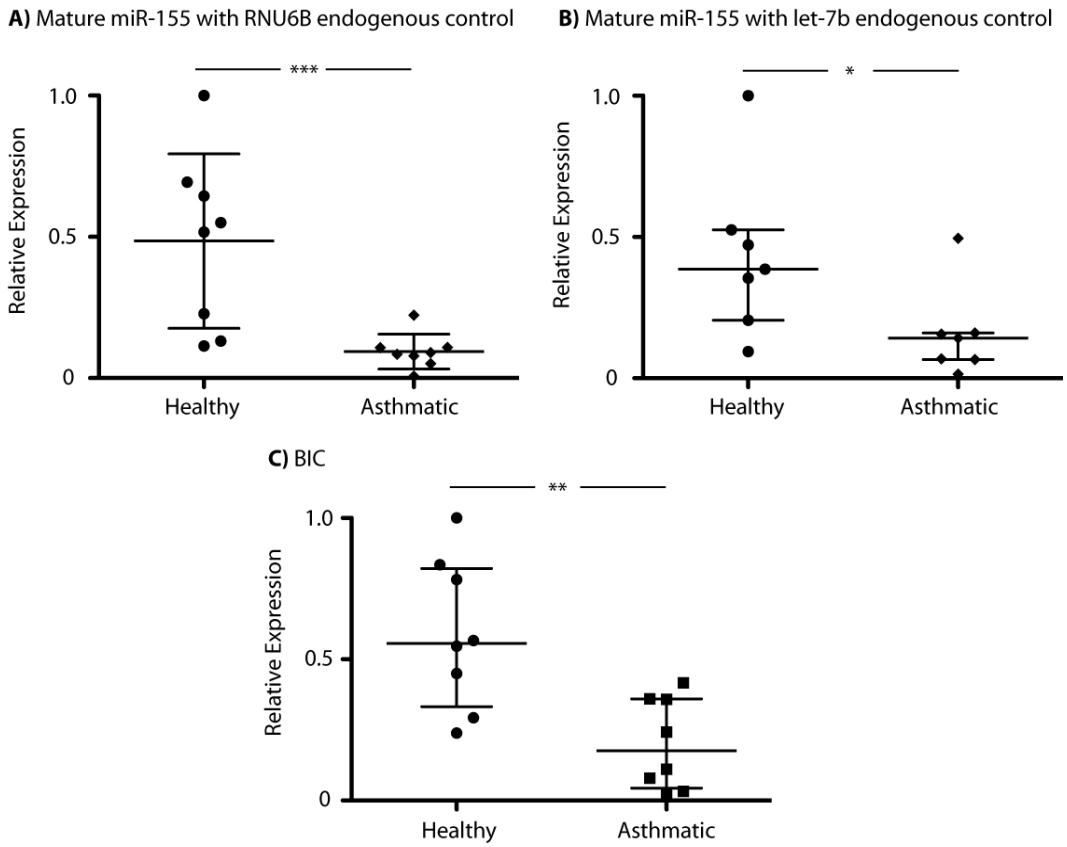

Figure 4.2.1 - Mature miR-155 and its housing transcript BIC are expressed at lower levels in cultured ASMCs isolated from moderate asthmatic compared to healthy individuals – Cultured ASMCs isolated from either healthy or moderate asthmatic individuals were growth arrested by a 72 hour incubation in serum-free media. RNA was harvested from $5x10^5$ cells and DNase treated before RT-qPCR was performed for mature miR-155 or the full BIC transcript. Relative levels of the mature miR-155 transcript were determined by ΔΔCt methodology using **A)** RNU6B or **B)** let-7b as the endogenous control. Expression levels are shown relative to the sample with the highest miR-155 expression. **C)** Relative BIC levels as determined through ΔΔCt methodology using 18S as the endogenous control gene. Expression levels are shown relative to the sample with the highest level of BIC expression. The horizontal bar represents the sample with the median relative expression level and the whiskers represent the interquartile range, n=7 or 8, *** $p<0.0005$, ** $p<0.005$, *$p<0.05$ as determined by a Mann-Whitney U test.

4.2.2 Investigations to identify endogenous targets for miR-155 in cultured ASMCs using a candidate gene approach

The initial approach chosen to identify targets for miR-155 in cultured ASMCs was a candidate gene approach. Potential miR-155 targets were chosen for further investigation based on a combination of predicted targets from the miRNA target prediction algorithms TargetScan, miRANDA and PITA in combination with literature searches for previously reported mRNA targets of miR-155 in other cell types and the identification of potential targets known to be expressed in ASM (see Table xi). It should be noted that target identification algorithms identify many potential targets for miR-155, for example TargetScan reports 440 potential targets and miRANDA reports over 5000. A small subset of potential targets were therefore chosen for further investigation based upon validated expression of the mRNA in cultured ASMCs and a potential role in pro-asthmatics pathways. Of the potential targets that were investigated the majority were predicted by at least one algorithm and had previous evidence of being miR-155 targets. RhoA was the only potential target not predicted by any of the bioinformatics algorithms, however, because it had previously been shown to be a miR-155 target in epithelial cells (Kong et al. 2008) and has important roles in ASM physiology (Chapter 1.5.2.2) it was deemed that it would be an interesting potential target to investigate. It is noted that the list of candidate miR-155 targets investigated is not extensive and that there were a large number of potential targets with similar attributes to those chosen that were not investigated further.

Gene	TargetScan	miRANDA	PITA	Literature
BACH1	YES	YES	YES	YES (Skalsky 2007)
H6PD	NO	NO	NO	NO
ETS	YES	YES	YES	YES (Romania 2008)
FOS	YES	NO	YES	YES (Gottwein 2007)
JARID2	YES	YES	YES	YES (Bolisetty 2009)
MYLK	YES	YES	YES	NO
RhoA	NO	NO	NO	YES (Kong 2008)
Septin 11	YES	YES	YES	NO

Table xi – The occurrence of candidate miR-155 target genes in bioinformatics predictions – Shows the occurrence of candidate miR-155 target genes chosen for further investigation in target prediction algorithms and any prior reports of miR-155 specific regulation reported in the literature. In addition the occurrence of BACH1 and H6PD, used as a positive and negative control respectively, is also shown.

4.2.2.1 Determination of predicted miR-155 target efficacy through luciferase assays

miRNA target prediction algorithms generate lists of potential targets that generally contain hundreds of results for a particular miRNA. It was therefore decided that the activity of potential miR-155 target sites should be tested through *in vitro* dual luciferase reporter assays. DNA fragments centering on the predicted miR-155 target site within the 3'UTRs of indicated genes were cloned downstream of the luciferase coding sequence in the pGL4.13 expression plasmid (described in Chapter 2.4.1). In addition to predicted miR-155 target sites, a 500 base pair fragment from the 3' UTR of Hexose-6-phosphate dehydrogenase (H6PD), which contains no predicted miR-155 target sites as determined by Targetscan, PITA or miRNADA, was cloned as a negative control. The cloning strategy used was to synthesis primers with Xba1 restriction sites at the 5' termini to enable sub-cloning of the target sequence directly 3' of the luciferase open-reading frame in the pGL4.13 vector. Of the cloned regions, only RhoA contained an internal Xba1 restriction site and hence these primers were synthesised with an Fse1 restriction site on the 5' end and inserted into the pGL4.13 vector using these restriction sites. A $CaCl_2$ mediated transfection protocol was optimized to facilitate the transfection of pGL4.13 plasmids into HEK293 cells alongside pre-miR-155 (see Chapter 2.2.3). Pre-miR-155 acts as a miR-155 mimic and facilitates over-expression of miR-155 (Figure 4.2.2).

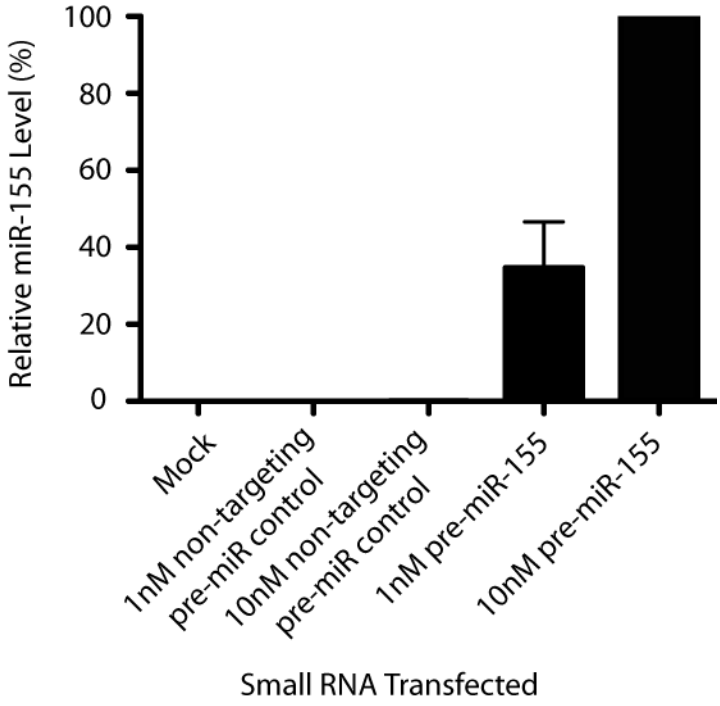

Figure 4.2.2 - $CaCl_2$ mediated transfection of pre-miR-155 facilitates the over-expression of miR-155 in HEK293 cells – HEK293 cells were transfected with either non-targeting pre-miR-Control or pre-miR-155 using $CaCl_2$ methodology and incubated for 24 hours before RNA was harvested. RT-qPCR was performed and results are shown following correction for RNU6B as the endogenous control. Expression levels are expressed relative to cells transfected with 10nM pre-miR-155. Error bars represent SEM, n=3.

Dual luciferase reporter assays were initially performed (described in Chapter 2.4.2) using pGL4.13 plasmids with either a 500 base pair fragment of H6PD or BTB and CNC homology 1 (BACH1) cloned downstream of the luciferase coding sequence. The H6PD 3'UTR contains no predicted miR-155 target sites, as previously stated, whilst the cloned region of the BACH1 3'UTR contains three predicted miR-155 target sites and has previously been reported to be a miR-155 target (Skalsky 2007) and therefore acted as a positive control. Analysis of pGL4.13-H6PD and pGL4.13-BACH1 demonstrated that the dual luciferase assay was suitable to detect miR-155 mediated repression as the pGL4.13-BACH1 plasmid had lower levels of luciferase activity when co-transfected with either 1nM or 10nM pre-miR-155, whilst no difference in luciferase activity was determined when either no small RNA or a non-targeting control pre-miR was co-transfected (Figure 4.2.3, Panel A). The pGL4.13-H6PD construct, however, showed no alteration in luciferase activity irrespective of the small RNA that was co-transfected (Figure 4.2.3, Panel B).

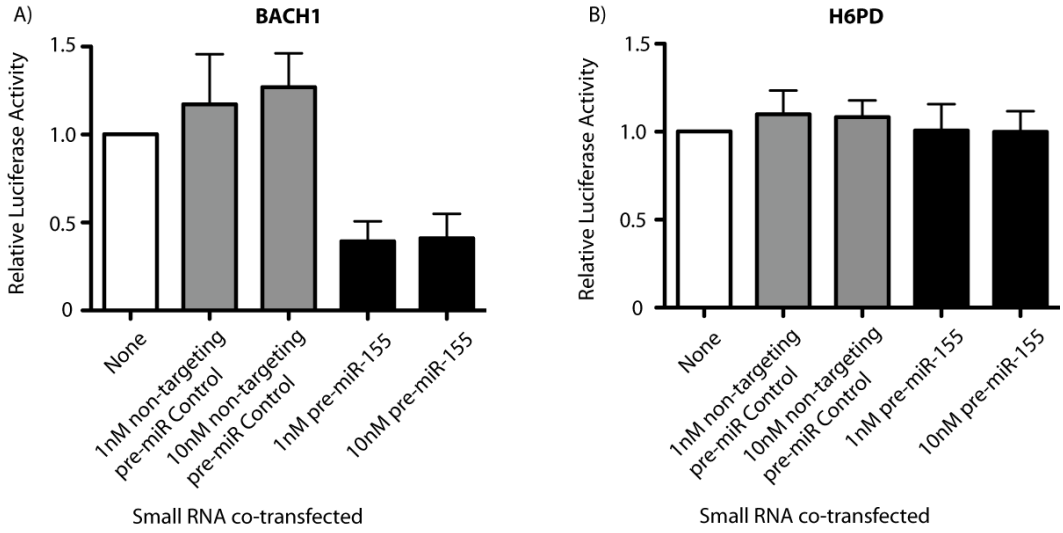

Figure 4.2.3 – The over-expression of miR-155 in HEK293 cells allows the determination of miR-155 mediated regulation of a co-transfected pGL4.13 luciferase expression plasmid – pGL4.13 luciferase expression plasmids with a fragment from the 3'UTR of either **A)** BACH1, which contains three predicted miR-155 target sites or **B)** H6PD, which contains no predicted miR-155 target sites, cloned directly 3' of the luciferase coding sequence were transfected into HEK293 cells. In addition co-transfection with no small RNA, non-targeting pre-miR-Control or pre-miR-155 was performed. Following a 24 hour incubation the cells were lysed and luciferase activity assessed using the Promega Dual Luciferase Reporter Assay. Results are expressed relative to the luciferase activity of cells with no small RNA transfected after subtraction of background luciferase activity and correction for Renilla luciferase activity as a transfection control. Error bars represent SEM, n=3.

Once it was determined that the dual luciferase assay was suitable for screening potential miR-155 target sites a panel of cloned regions from the 3'UTRs of six candidate genes, each containing a predicted miR-155 target site, was screened for miR-155 mediated repression (Table xi). The results of the dual luciferase assays indicated that, in this assay set-up, the majority of predicted miR-155 binding sites were able to mediate a reduction in luciferase activity in a miR-155 specific manner (Figure 4.2.4). Of the potential miR-155 target sites tested, only pGL4.13-ETS did not show evidence of miR-155 mediated repression of luciferase activity. The remaining candidate target sites from Fos, JARID2, myosin light chain kinase (MYLK), RhoA and Septin-11 all showed trends towards a decrease in luciferase activity when co-transfection with pre-miR-155 rather than no small RNA or non-targeting control pre-miR was performed (Figure 4.2.4).

The results gained from the dual luciferase assays indicated that the majority of predicted miR-155 target sites were able to mediate a reduction in luciferase activity in this assay set-up and confirmed the efficacy and specificity of the pre-miR-155. It was therefore decided that it would be more informative to investigate the regulation of potential endogenous targets of miR-155 in cultured ASMCs.

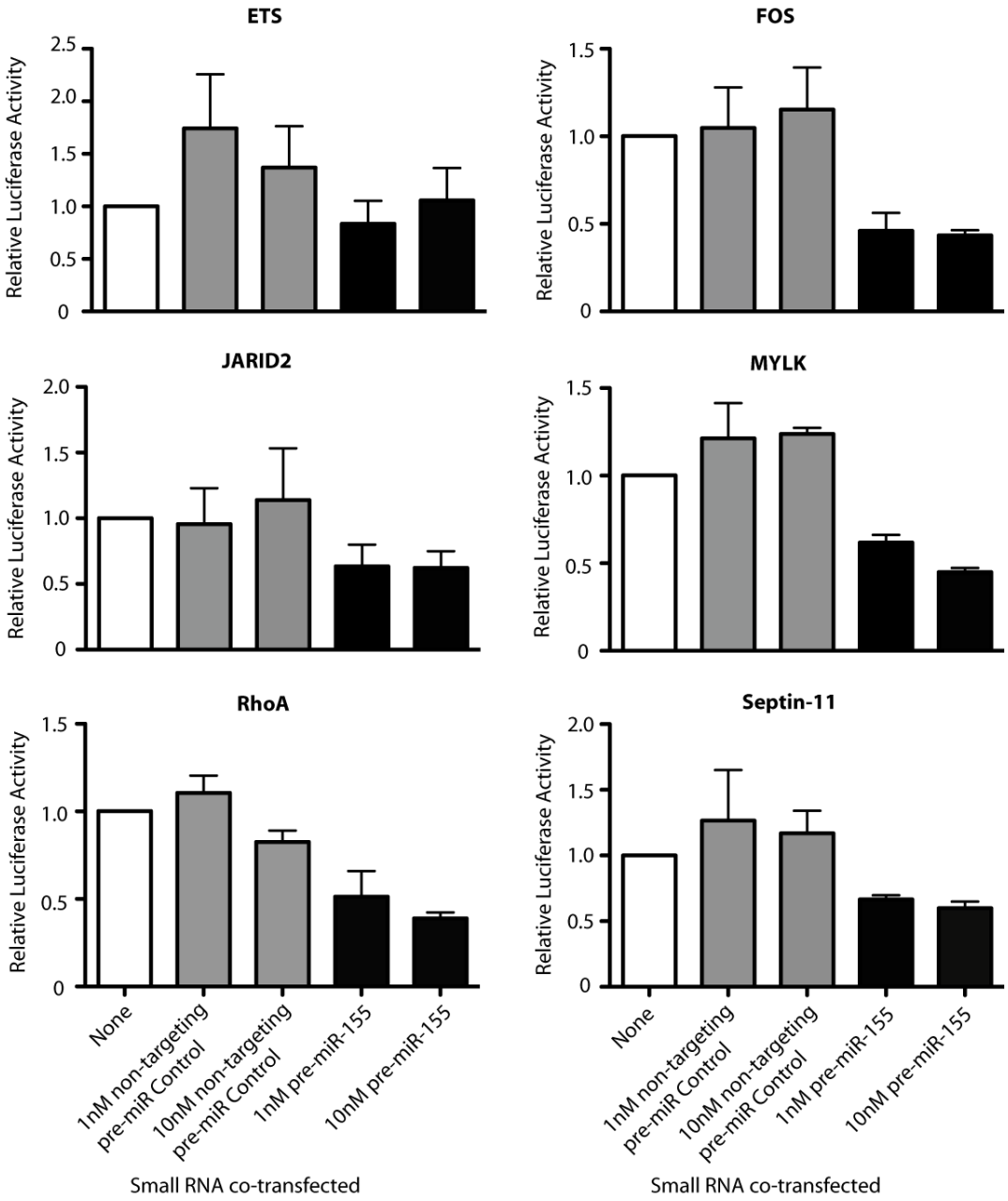

Figure 4.2.4 - The majority of predicted miR-155 target sites facilitate miR-155 mediated regulation during *in vitro* luciferase assays – Predicted miR-155 target sites within the 3'UTRs of candidate target genes were cloned directly downstream of the pGL4.13 Firefly luciferase coding sequence. Each individual plasmid was co-transfected into HEK293 cells in parallel with pRL-TK as a transfection control and either no small RNA, non-targeting control pre-miR or pre-miR-155 using $CaCl_2$ methodology. Following a 24 hour incubation the cells were lysed and luciferase activity assessed by the Promega Dual Luciferase Reporter Assay. Results are expressed relative to the luciferase activity of cells with no small RNA transfected after substraction of background luciferase activity and correction for Renilla luciferase as a transfection control. The small RNA transfected is indicated on the X-axis of the bottom graph in each column. Error bars represent SEM, n=3.

4.2.2.2 Optimization of a protocol to use small RNAs to manipulate the levels of mature miR-155 in cultured ASMCs

To assess miR-155 mediated regulation of endogenous mRNAs or proteins in cultured ASMCs, a protocol first had to be optimized to enable the efficient transfection of small RNAs. It was particularly important to repress miR-155 activity through the use of single stranded antagomirs (anti-miRs), in addition to over-expressing miR-155 through the use of pre-miR-155. This was required to increase confidence that any potential regulation observed was specific and not an artifact of over-expression. All experiments described in the following sections were performed using cultured ASMCs isolated from healthy individuals.

Small RNAs were transfected into cultured human ASMCs using Lipofectamine 2000 methodology (see 2.2.1) and successful transfection was routinely assessed by flow cytometry as described in section 2.2.2. Figure 4.2.5 shows a representative result gained 24 hours post Lipofectamine 2000 mediated transfection of small RNAs into the cultured ASMCs. A gating strategy based on forward scatter and staining for Invitrogen Live/Dead stain was used to assess live cells for the positive transfection of fluorescein amidite (FAM)-labeled non-targeting pre or anti-miR controls (Figure 4.2.5, Panel A). The Invitrogen Live/Dead stain is an amine reactive fluorescent dye that is only able to bind to the cell-surface amines of live cells with intact membranes, resulting in a moderate level of fluorescence. In cells with compromised membranes, however, the dye reacts with free amines both on the cell surface and in the cell interior, yielding a greater level of fluorescence. Live cells were assessed for positive FAM signal compared to mock transfected cells. Transfection of 20nM pre-miR routinely resulted in 70-80% of cells being positively transfected (Figure 4.2.5, Panel C) whilst transfection of 100nM anti-miR routinely resulted in 50-60% of cells being positively transfected (Figure 4.2.5, Panel D).

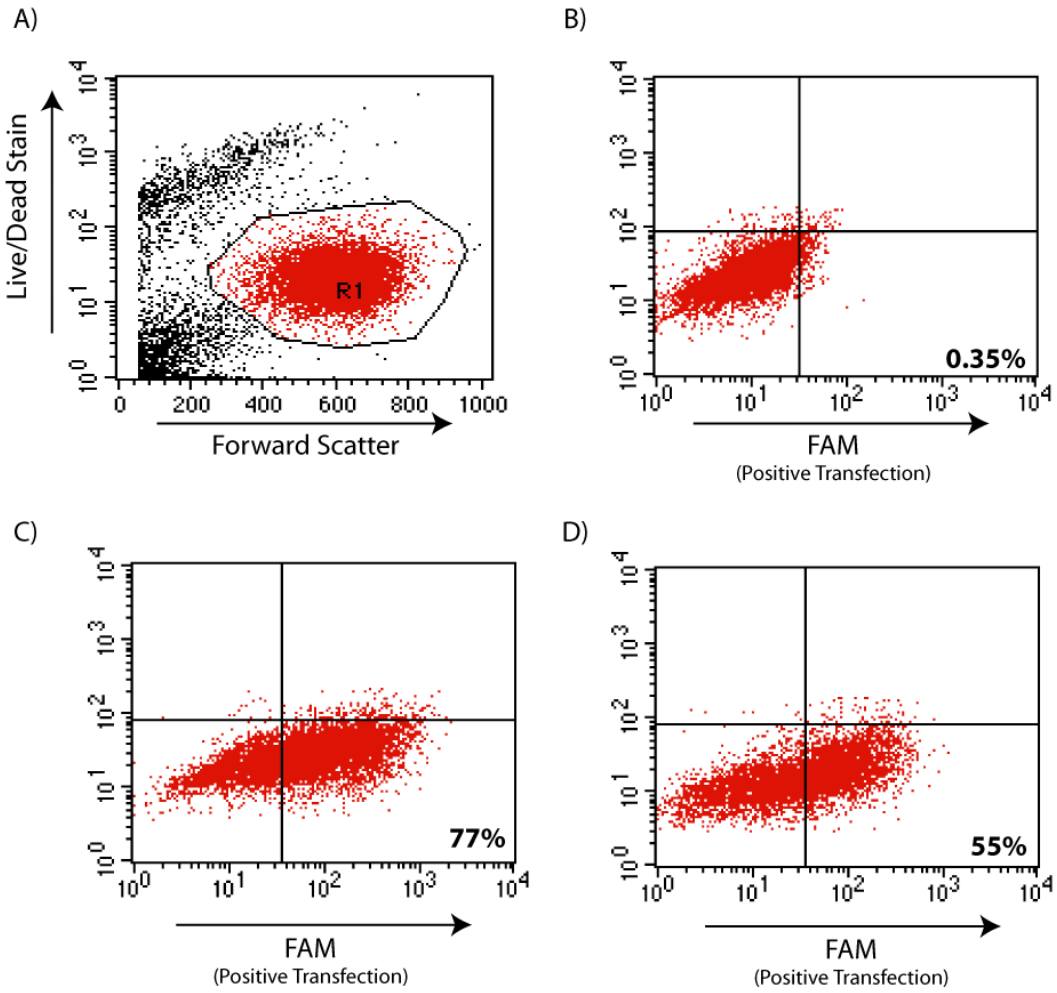

Figure 4.2.5 - Lipofectamine mediated transfection of small RNAs into cultured ASMCs – ASMCs were growth arrested by serum starvation for 72 hours before Lipofectamine 2000 mediated transfection of FAM-labeled non-targeting pre-miR or anti-miR control was performed to ascertain transfection efficiency. Following a 24 hour incubation the cells were harvested by Trypsin-EDTA and assessed for successful transfection by flow cytometry. **A)** Mock transfected sample showing the gating strategy for live cells, **B)** mock transfected cells, **C)** cells transfected with 20nM FAM-labeled pre-miRNA control and **D)** cells transfected with 100nM FAM-labeled anti-miR control. Plots are representative from one of six experiments.

Following the demonstration that Lipofectamine 2000 was a suitable method by which to transfect cultured ASMCs a range of concentrations of small RNAs was used to determine the most suitable concentration of either pre-miR or anti-miR to gain a percentage of positively transfected cells that was sufficient for downstream analysis. Figure 4.2.6 demonstrates the percentage of positively transfected cells (as determined using the flow cytometry analysis detailed in Figure 4.2.5) 24 and 72 hours post-transfection with a range of concentrations of FAM-labeled non-targeting pre-miR or anti-miR control. This analysis demonstrated a reasonable

concentration response for the pre-miR (Figure 4.2.6, Panel A), with increases in the concentration of pre-miR resulting in an increase in the percentage of positively transfected cells. This was not the case for the anti-miR transfections, however, as a detectable percentage of positively transfected cells was not achieved until transfection of 100nM anti-miR (Figure 4.2.6, Panel B). Although no intermediate concentration between 10nM and 100nM anti-miR was tested in this experiment it was decided to focus on using 100nM anti-miR as lower concentrations would be likely to result in the percentage of positively transfected cells being too low to adequately interrogate in downstream analyses. It should be noted that the percentage of positively transfected cells for a given concentration of small RNA was consistently lower at 72 hours compared to 24 hours post-transfection (Figure 4.2.6, Panels A and B).

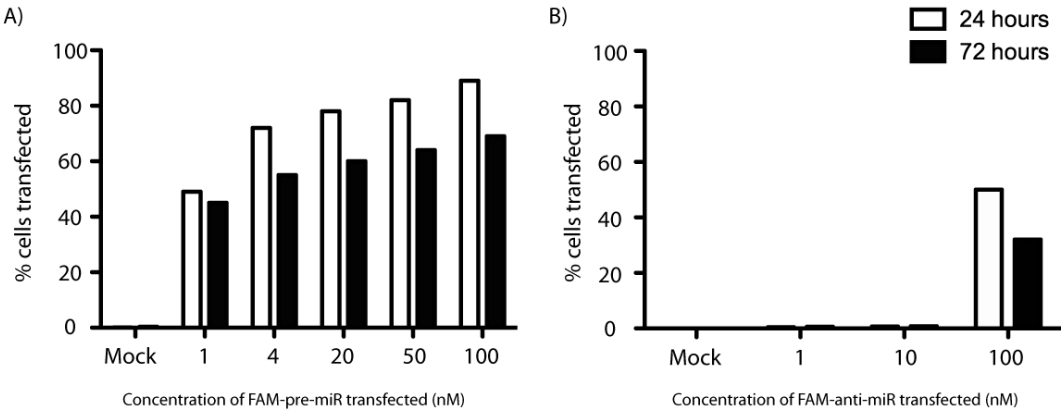

Figure 4.2.6 – Assessment of the optimal concentration of pre-miR and anti-miR for ASMC transfections – ASMCs were growth arrested by serum starvation for 72 hours before Lipofectamine 2000 mediated transfection of **A)** FAM-labeled non-targeting pre-miR or **B)** FAM-labeled non-targeting anti-miR. Following a 24 or 72 hour incubation cells were harvested with Trypsin-EDTA and assessed for successful transfection as determined by a positive FAM signal in flow cytomtery (n=1).

Concentrations of 4nM and 20nM pre-miR and 100nM anti-miR were used in subsequent analyses as these were deemed to be the minimum concentrations required to gain an acceptable percentage of positively transfected cells whilst limiting any potential toxicity. The affect of transfecting these concentrations of pre-miR-155 and anti-miR-155 on the levels of detectable mature miR-155 in the total cell population was assessed by RT-qPCR (described in sections 2.3.1, 2.3.2 and 2.3.4). Transfection of 4nM or 20nM pre-miR-155 resulted in a large increase in the level of detectable mature miR-155, with an approximate 600-800 fold increase at 6, 24 and 72 hours post-transfection with 20nM pre-miR-155 (Figure 4.2.7) and an

approximately 200 fold increase at the same time points post-transfection with 4nM pre-miR-155 (Figure 4.2.7). Due to this large increase it was important to be able to perform reciprocal experiments where miR-155 activity was disrupted. This was achieved by transfection of 100nM anti-miR-155, which resulted in a near complete loss of detectable mature miR-155 at 24 hours post-transfection (Figure 4.2.8).

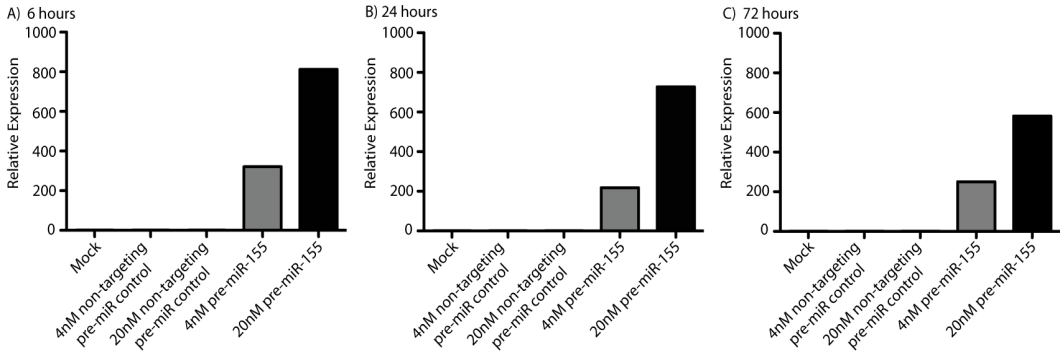

Figure 4.2.7 - Lipofectamine mediated transfection of pre-miR-155 into cultured ASMCs results in an increase the level of detected mature miR-155 - ASMCs were growth arrested by serum starvation for 72 hours before Lipofectamine 2000 mediated transfection of 4nM or 20nM non-targeting pre-miR control or pre-miR-155. Mock transfections with Lipofectamine only were also performed as controls. Following an **A)** 6 hour, **B)** 24 hour or **C)** 72 hour incubation RNA was harvested and RT-qPCR performed. Results are analysed using ΔΔCt methodology through normalisation to RNU6B RNA as the endogenous control and expression levels are presented relative to the mock transfected sample for each specific time point post-transfection. Graphs are representative of 4 or 5 separate transfections.

To determine if the transfection of small RNAs into cultured ASMCs affected the viability of the cells the Live/Dead staining routinely performed during the flow cytometry assessment of transfection efficiency was assessed. The mean percentage of live cells counted at 6, 24 and 72 hours post-transfection was similar regardless of whether or not the cells were transfected with a small RNA (Figure 4.2.9) suggesting that the transfection of small RNAs had no gross affect on cell viability. In addition, no overt influences on cell proliferation or morphology were observed.

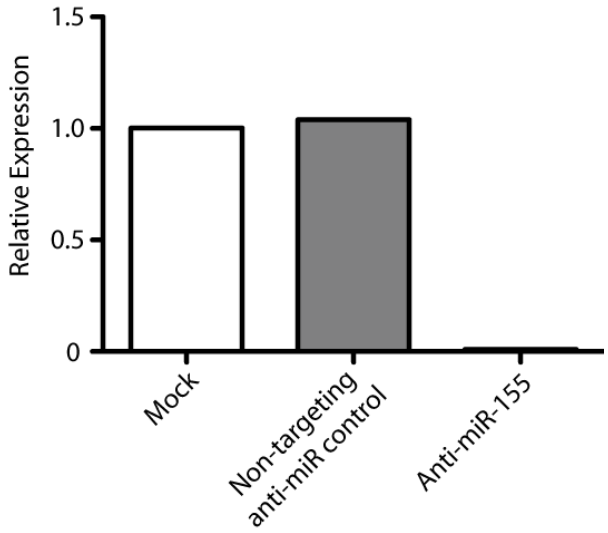

Figure 4.2.8 - Lipofectamine mediated transfection of anti-miR-155 into cultured ASMCs results in a decrease in the level of detected mature miR-155 - ASMCs were growth arrested by serum starvation for 72 hours before Lipofectamine 2000 mediated transfection of either 100nM non-targeting anti-miR control or 100nM anti-miR-155. Mock transfections with Lipofectamine only were also performed as controls. Following a 24 hour incubation RNA was harvested and RT-qPCR performed. Results are analysed using ΔΔCt methodology through normalisation to RNU6B RNA as the endogenous control and expression levels are presented relative to the mock transfected sample. Data are representative of 4 separate transfections.

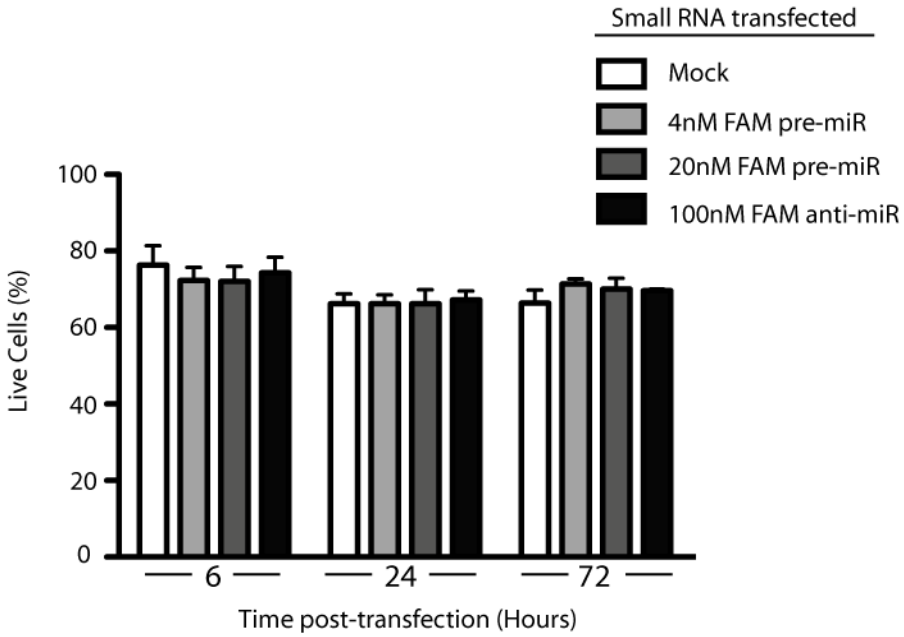

Figure 4.2.9 - Transfection of small RNAs does not influence the viability of cultured ASMCs – ASMCs were growth arrested by serum starvation for 72 hours before Lipofectamine 2000 mediated transfections. The cells were incubated for either 6, 24 or 72 hours post-transfection before being harvested with Trypsin-EDTA and assessed for viability using Invitrogen Live/Dead Staining Kit. Error bars represent SEM, n=5 for 24 hours and 4 for 6 and 72 hours.

4.2.2.3 Investigating a potential miR-155 mediated regulation of RhoA in cultured ASMCs

Following the determination that the abundance of miR-155 in cultured ASMCs could be successfully modulated by the transfection of small RNAs, the regulation of potential endogenous targets of miR-155 was analysed. The potential regulation of RhoA by miR-155 was investigated because it has previously been demonstrated to be a miR-155 target in epithelial cells (Kong et al. 2008) and because it has important roles in ASM physiology through the calcium sensitization pathway (Chapter 1.5.2.2).

Potential alterations in the level of RhoA mRNA at various timepoints post-transfection with pre-miR-155 were investigated through RT-qPCR studies (described in 2.3.3 and 2.3.4). These results were somewhat inconclusive, with an indication of a potential miR-155 mediated reduction in the level of RhoA mRNA 24 hours post-transfection with 20nM pre-miR-155 (Figure 4.2.10). This trend was not statistically significant when compared to either mock transfections or cells transfected with 20nM non-targeting pre-miR control. There was a trend towards a reduced level of RhoA mRNA at 72 hours post-transfection when comparing the pre-miR-155 and mock transfected samples, however, this was not statistically significant. Further, the level of detected RhoA mRNA in the pre-miR-155 transfected samples was very similar to that in the non-targeting control pre-miR transfected samples.

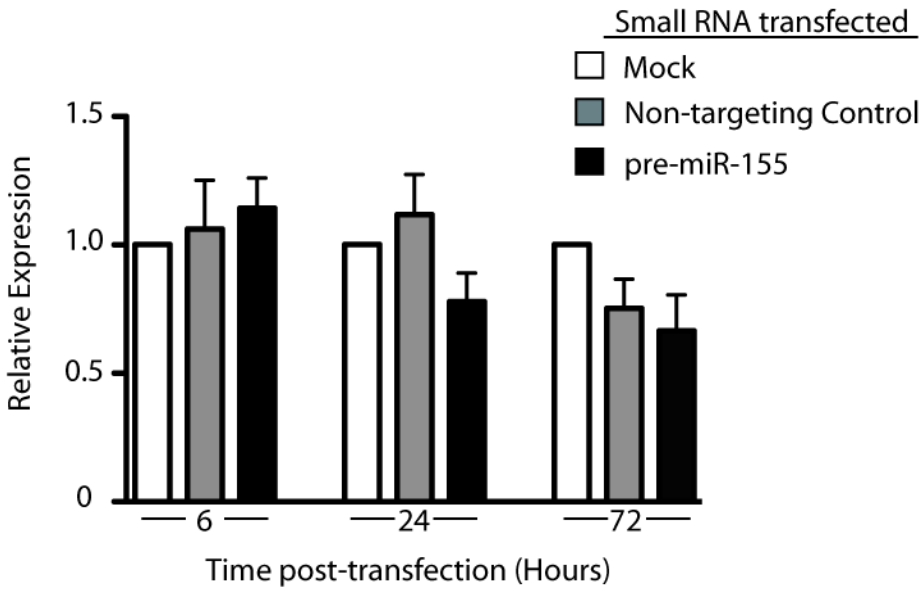

Figure 4.2.10 – Analysis of RhoA mRNA levels following miR-155 over-expression in cultured ASMCs - ASMCs were growth arrested by serum starvation for 72 hours before Lipofectamine 2000 mediated transfection of 20nM non-targeting pre-miR control or 20nM pre-miR-155. Following a 6, 24 or 72 hour incubation RNA was harvested and RT-qPCR performed. Results are analysed using ΔΔCt methodology through normalisation to 18S RNA as the endogenous control and expression levels are presented relative to the mock transfected sample for each time point post-transfection. Error bars represent SEM, n=4 for 6 and 72 hours and n=5 for 24 hours. Results were tested for statistical significance using Friedmann's Test with Dunn's Multiple Comparison Correction Test.

To further investigate the potential miR-155 mediated decrease in RhoA mRNA levels at 24 hours post-transfection the abundance of RhoA mRNA in cells transfected with 100nM anti-miR-155 was determined. This analysis was undertaken as it would be expected that a true miR-155 target would demonstrate a reduction in mRNA levels following miR-155 over-expression and increased mRNA levels following miR-155 antagonism. Determination of RhoA mRNA levels 24 hours post-transfection with 100nM anti-miR-155, however, indicated no difference between mock, non-targeting anti-miR control and anti-miR-155 transfected cells (Figure 4.2.11). This suggests that the level of RhoA mRNA is not directly regulated by miR-155 in cultured ASMCs.

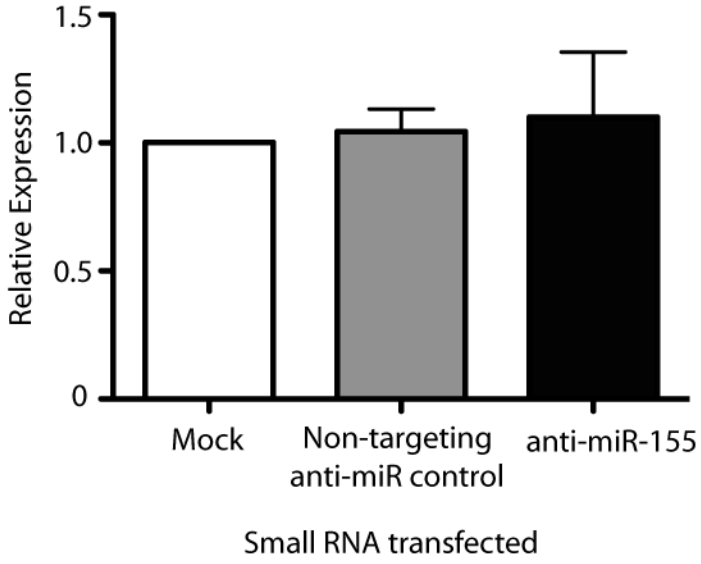

Figure 4.2.11 - Antagonism of miR-155 function in cultured ASMCs does not result in an increase in the abundance of RhoA mRNA - ASMCs were growth arrested by serum starvation for 72 hours before Lipofectamine 2000 mediated transfection of 100nM non-targeting anti-miR control or 100nM anti-miR-155. Following a 24 hour incubation RNA was harvested and RT-qPCR performed. Results are analysed using ΔΔCt methodology through normalisation to 18S RNA as the endogenous control and expression levels are presented relative to the mock transfected sample. Error bars represent SEM, n=4.

As discussed in Chapter 3.1.4, it is controversial as to whether the mechanism of miRNA-mediated target down-regulation occurs predominantly through an mRNA degradation or translational repression pathway. It was therefore important to determine that miR-155 was having no impact on the level of RhoA protein in cultured ASMCs. This was especially relevant as previous evidence from Kong *et al.* (Kong et al. 2008) has indicated that miR-155 caused a decrease in the level of RhoA

protein in epithelial cells with no affect on the level of RhoA mRNA. Western blots performed on cytoplasmic protein extracts (described in Chapter 2.3.1 and 2.3.2), however, indicated that there was no influence of pre-miR-155 (Figure 4.2.12) or anti-miR-155 (Figure 4.2.13) on the level of RhoA protein.

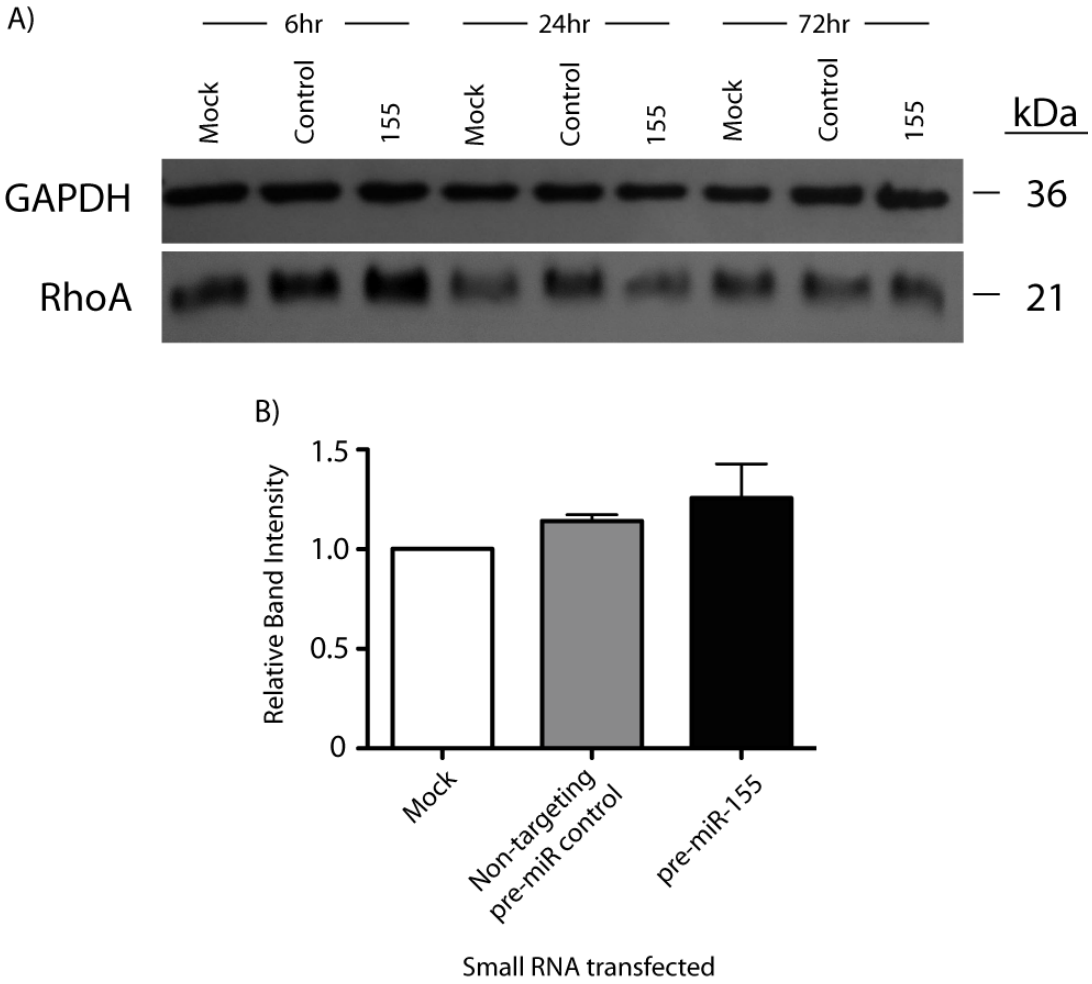

Figure 4.2.12 - Over-expression of miR-155 in cultured ASMCs does not cause a decrease in RhoA protein levels - ASMCs were growth arrested by serum starvation for 72 hours before Lipofectamine 2000 mediated transfection of 20nM non-targeting pre-miR control or 20nM pre-miR-155. Following a 6, 24 or 72 hour incubation protein was harvested using a NE-PER kit. 35μg of cytoplasmic protein extract per well was electrophorised through a polyacrylamide gel before transfer to a nitrocellulose membrane and determination of the level of RhoA and GAPDH by western blot. **A)** Shows a representative blot of RhoA and GAPDH protein for 1 experiment. **B)** Shows the mean relative expression of RhoA protein for 3 independent experiments when protein was harvested 24 hours post-transfection. Band intensities were calculated using ImageQuant software, before correction of RhoA levels for GAPDH as a loading control. Relative levels are expressed in relation to mock transfected samples. Error bars represent SEM, n=3.

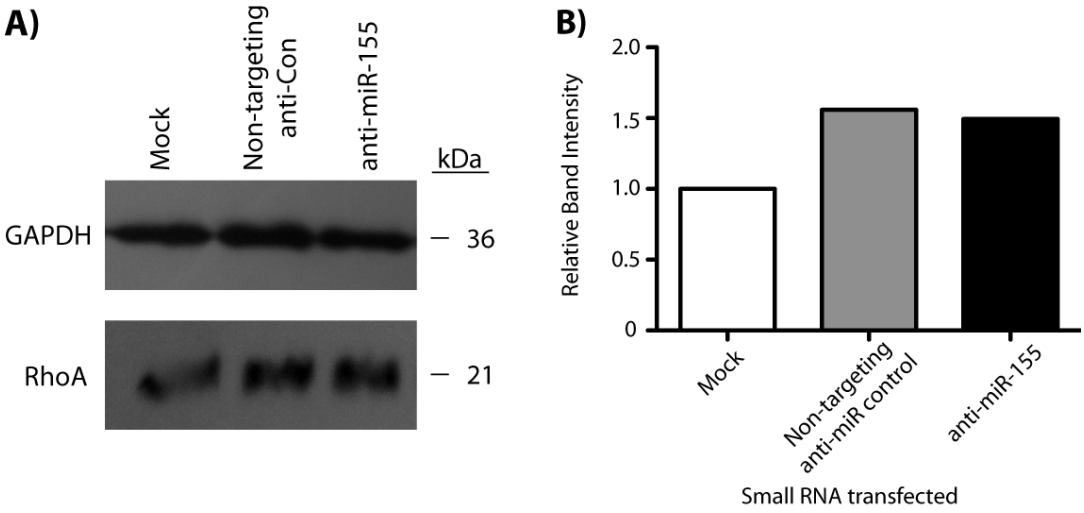

Figure 4.2.13 - Antagonism of miR-155 function does not result in an increase in the level of RhoA protein - ASMCs were growth arrested by serum starvation for 72 hours before Lipofectamine 2000 mediated transfection of 100nM non-targeting anti-miR control or 100nM anti-miR-155. Following a 24 hour incubation protein was harvested using a NE-PER kit. 35μg of cytoplasmic protein extract per well was electrophorised through a polyacrylamide gel before transfer to a nitrocellulose membrane and determination of the level of RhoA and GAPDH by western blot. **A)** Shows a representative blot of RhoA and GAPDH protein. **B)** Shows the densitometric analysis of bands performed using ImageQuant software. The intensity of the RhoA bands was corrected for GAPDH as a loading control and expression levels are expressed relative to a mock transfected sample. n=1.

Taken together the data are insufficient to support a potential miR-155 mediated regulation of RhoA in cultured ASMCs, rather the evidence generated suggests that there is no miR-155 mediated regulation occurring.

4.2.2.4 Investigating a potential miR-155 mediated regulation of MYLK in cultured ASMCs

In addition to RhoA, a potential miR-155 mediated regulation of MYLK in cultured ASMCs was investigated. MYLK was investigated further as it is predicted to be a miR-155 target in all target identification algorithms used (Table xi), has an essential role in the contraction of ASM and there are reports of differential expression in asthmatic compared to healthy ASM (Chapter 1.5.2.2).

The experimental strategy followed to determine a potential miR-155 mediated regulation of MYLK in cultured ASMCs was the same as that for RhoA. Initial investigations using pre-miR-155 to over-express miR-155 gave encouraging results, with a statistically significant diminished abundance of MYLK mRNA 24 hours post-transfection when comparing pre-miR-155 transfected cells to both mock and non-targeting control transfected cells (Figure 4.2.14). At 72 hours post-transfection there was also a statistically significant lower amount of MYLK mRNA in cells transfected with 20nM pre-miR-155 compared to mock transfections. There was, however, no difference in MYLK mRNA levels when comparing cells transfected with either pre-miR-155 or an equal concentration of non-targeting pre-miR control. In addition, the non-targeting pre-miR control resulted in a trend towards a decrease in the level of MYLK mRNA in comparison to the mock (Figure 4.2.14).

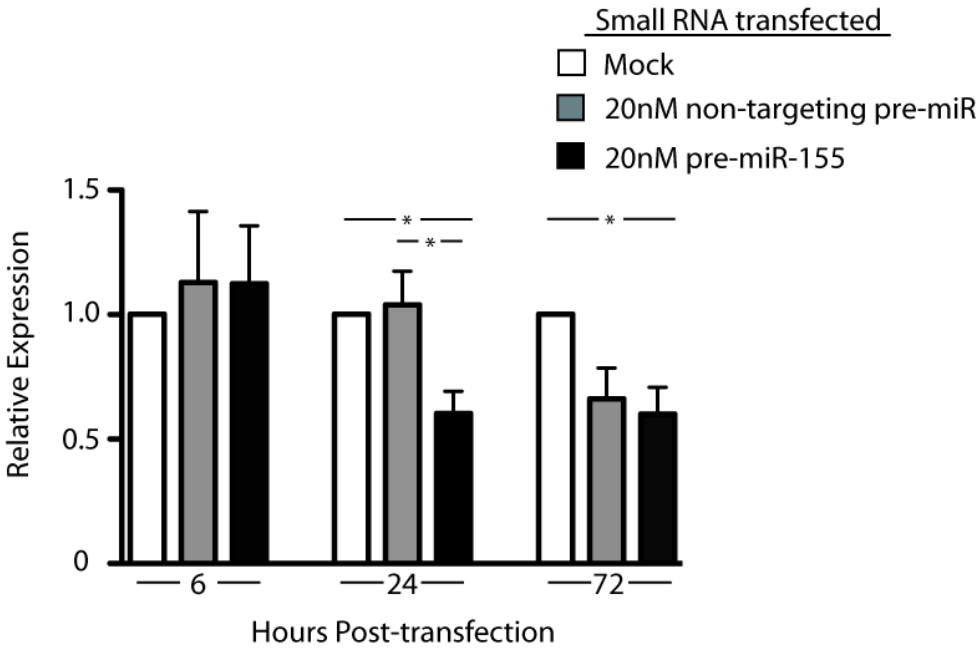

Figure 4.2.14 – Analysis of MYLK mRNA levels following miR-155 over-expression in cultured ASMCs - ASMCs were growth arrested by serum starvation for 72 hours before Lipofectamine 2000 mediated transfection of 20nM non-targeting pre-miR control or 20nM pre-miR-155. Following a 6, 24 or 72 hour incubation RNA was harvested and RT-qPCR performed. Results are analysed using ΔΔCt methodology through normalisation to 18S RNA as the endogenous control and expression levels are presented relative to the mock transfected sample for each time point post-transfection. Error bars represent SEM, n=4 for 6 and 72 hours and n=5 for 24 hours. * $p<0.05$ as determined by Friedman's Test with Dunn's Multiple Comparison Correction Test.

To ensure that the decrease in MYLK mRNA detected at 24 hours was not merely an artifact caused by the large miR-155 over-expression (Figure 4.2.7), MYLK mRNA levels were assessed in cDNA generated from cells 24 hours post-transfection with 100nM anti-miR-155. This analysis indicated that there was no difference in the level of MYLK mRNA in cDNA from mock, pre-miR-155 or non-targeting pre-miR control transfected cells (Figure 4.2.15).

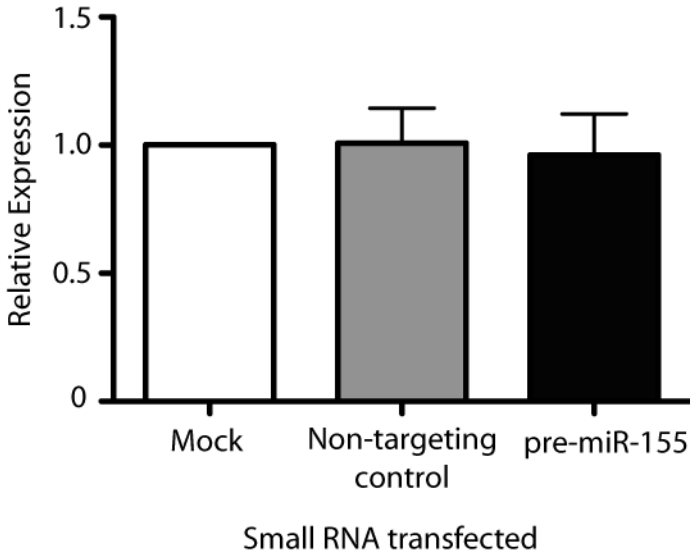

Figure 4.2.15 - Antagonism of miR-155 function in cultured ASMCs does not result in an increase in the level of MYLK mRNA - ASMCs were growth arrested by serum starvation for 72 hours before Lipofectamine 2000 mediated transfection of 100nM non-targeting anti-miR control or 100nM anti-miR-155. Following a 24 hour incubation RNA was harvested using TRIzol methodology and RT-qPCR was performed. Results are analysed using ΔΔCt methodology through normalisation to 18S RNA as the endogenous control and expression levels are presented relative to the mock transfected sample for each specific time point post-transfection. Error bars represent SEM, n=4. Results were tested for statistical significance using Friedman's Test with Dunn's Multiple Comparison Correction Test. n=4.

As for RhoA, a potential regulation of MYLK protein by miR-155 was then investigated (Figure 4.2.16). These investigations, however, revealed no indication of a miR-155 mediated regulation any of the major isoforms of MYLK at 130kDa, 210kDa or 225kDa, during either a timecourse following transfection of 20nM pre-miR-155 (Figure 4.2.16 (A)) or 24 hours post-transfection with 100nM anti-miR-155.

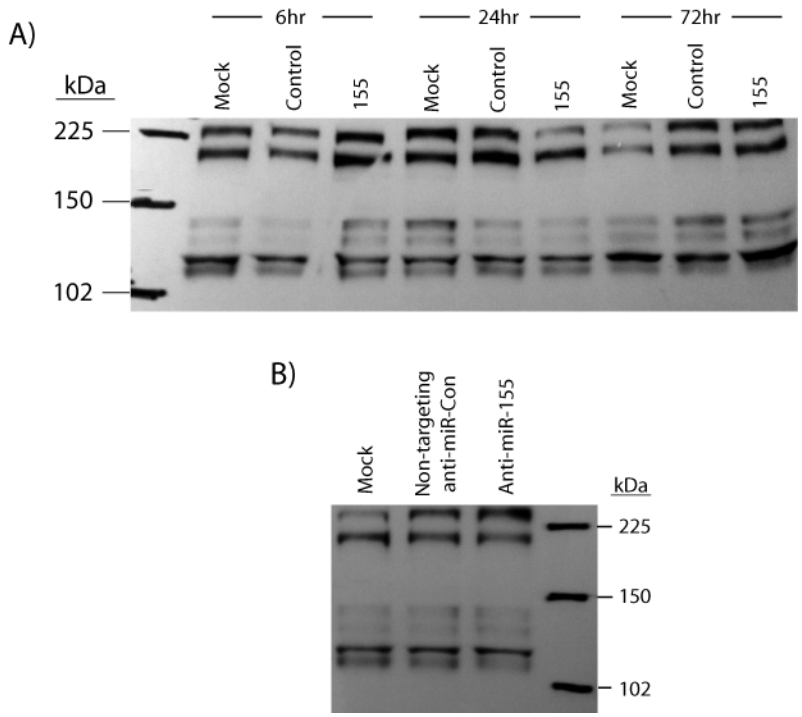

Figure 4.2.16 – Manipulation of the level of miR-155 in cultured ASMCs does not result in a clear alteration in the levels of MYLK protein - ASMCs were growth arrested by serum starvation for 72 hours before Lipofectamine 2000 mediated transfections were performed. **A)** Cells were mock transfected or transfected with 20nM non-targeting pre-miR control or pre-miR-155 and following a 6, 24 or 72 hour incubation protein was harvested using a NE-PER kit. 35μg of cytoplasmic protein extract per well was electrophorised through a polyacrylamide gel before transfer to a nitrocellulose membrane and probed with an anti-MYLK antibody. **B)** Cells were transfected as either mock or with 100nM non-targeting anti-miR control or anti-miR-155 before western blotting was performed as above.

4.2.3 Unbiased mRNA profiling of cultured ASMCs following modulation of miR-155 levels

After attempts to identify miR-155 targets in cultured ASMCs using a candidate gene approach were unsuccessful it became clear that it was an extremely inefficient and time-consuming approach. Increasing evidence has indicated that a number of miRNA targets are regulated through a mechanism that involves an mRNA degradation pathway (see Chapter 3.1.4) and because of this it was decided to perform unbiased microarray analysis of mRNA isolated from cultured ASMCs in which miR-155 had been over-expressed with pre-miR-155 or antagonized with anti-miR-155. The rationale of these investigations was to determine if specific effects of miR-155 over-expression and antagonism in cultured ASMCs could be determined by assaying mRNA levels. A particular aim was to determine if the reciprocal regulation of an individual mRNA was observed following miR-155 over-expression or antagonism. Further support for the discovery of a *bone fide* target would then be drawn from the identification of candidate genes with known or rationale pro-asthmatic functions or the identification of a miR-155 target sequence within the potential target. As such these analyses were primarily designed to ascertain whether this experimental strategy would be valuable for identifying potential targets for further analysis.

Affymetrix U133.2 GeneChip® mRNA Expression microarray analysis was performed using RNA previously isolated and archived from a single experiment in which cultured ASMCs were transfected with either 20nM non-targeting pre-miR control or 20nM pre-miR-155, 100nM non-targeting anti-miR control or 100nM anti-miR-155 or mock transfected (as described in Chapter 2.2.1). RNA was processed, labeled and hybridized to Affymetrix U133.2 Expression Arrays and data processing was performed in Partek Genomics Suite 2.0 (described in Chapter 2.5.2).

4.2.3.1 Quality control of microarrays

Initial analyses were performed in Partek to ensure consistency across the microarrays. As part of the labelling and hybridization procedures (see Chapter 2.5.2.1 and 2.5.2.2) Affymetrix control RNAs are spiked into each RNA sample at known concentrations. These control RNAs have corresponding probe sets on the microarray surface that do not bind to any known human RNA sequence. The intensity of these probe sets can therefore be used to determine consistency in RNA

labelling and hybridization across microarrays. Analysis of the normalised intensities of each of these control RNAs (Figure 4.2.17) demonstrated that individual probes gave similar intensities for individual microarrays, indicating that there were no gross differences in sample labeling and hybridization efficiencies. In addition, Affymetrix also recommends that the degradation of RNA samples be assessed by comparing the normalised intensity levels of probe sets directed against either the 5' or the 3' end of specific transcripts. This analysis indicated that none of the control probe sets had a difference in normalised intensity of greater than three-fold between the 3' and 5' directed probe sets (Figure 4.2.18). The threshold ratio is recommended by Affymetrix and samples generating ratios of greater than three are regarded as being unsuitably degraded. As such, all RNA samples were deemed to be of a sufficient quality for subsequent analysis. Figure 4.2.19 demonstrates the general normalised intensity profile of each microarray as a box and whiskers plot and indicates that the range of intensities was similar for all microarrays, giving a further indication of consistent labeling and hybridization of all samples.

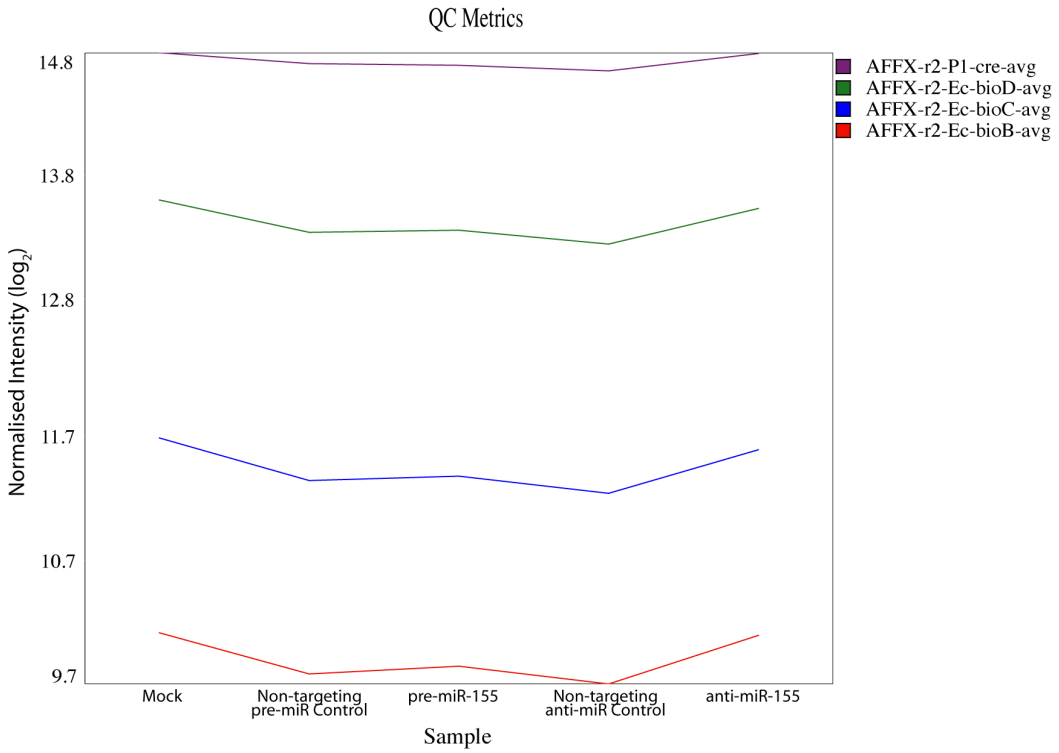

Figure 4.2.17 - Validation of efficient Affymetrix U133.2 microarray hybridization – Affymetrix Eukaryotic Hybridization Controls were spiked into the sample labelling and hybridization steps at known concentrations to ensure that labelling, hybridization and scanning occurred efficiently and consistently across all arrays. The Y-axis represents the normalised probe intensities (log_2) and each coloured line represents a separate spike-in control.

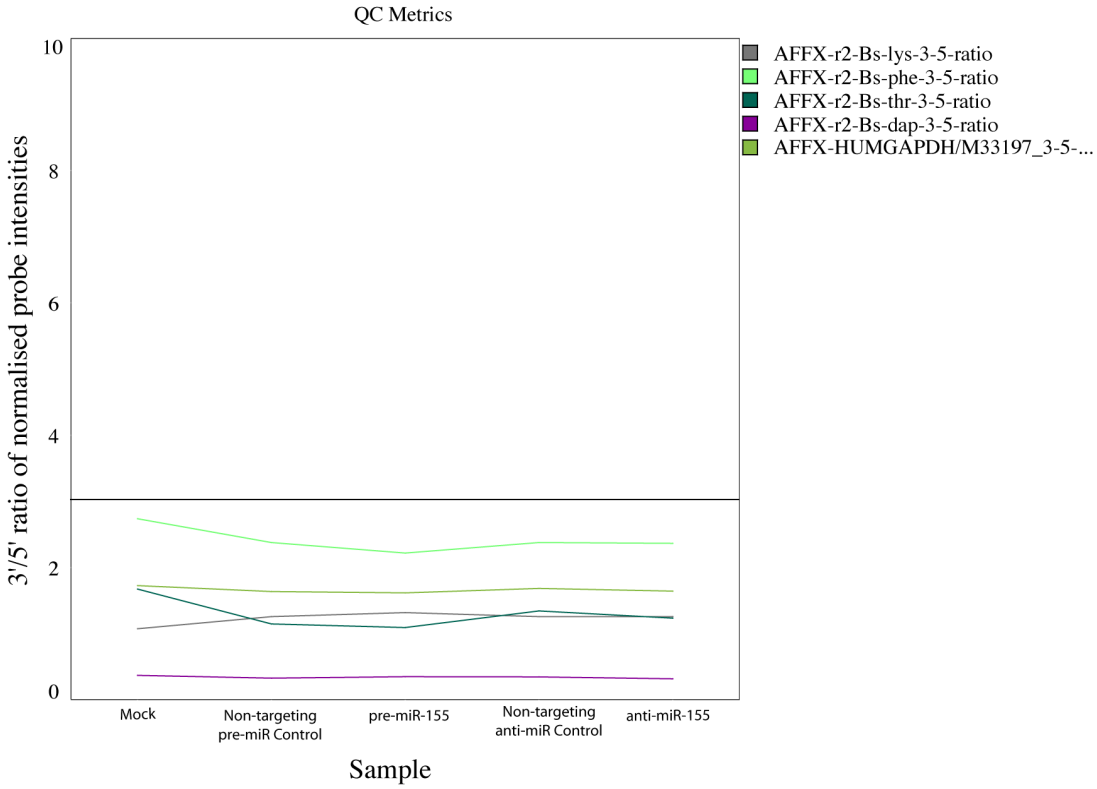

Figure 4.2.18 - The ratio of normalised intensities for probes directed against the 3' or 5' end of control transcripts indicates that the RNA samples have not degraded during labeling and hybridization procedures – Normalised intensity values for probes directed to either the 3' or 5' end of various control probes were assessed to determine if they produced an equal signal intensity. Ratios of 3' to 5' signal of greater than three (indicated by the horizontal line) represent RNA with levels of degradation above that deemed acceptable by the Affymetrix guidelines.

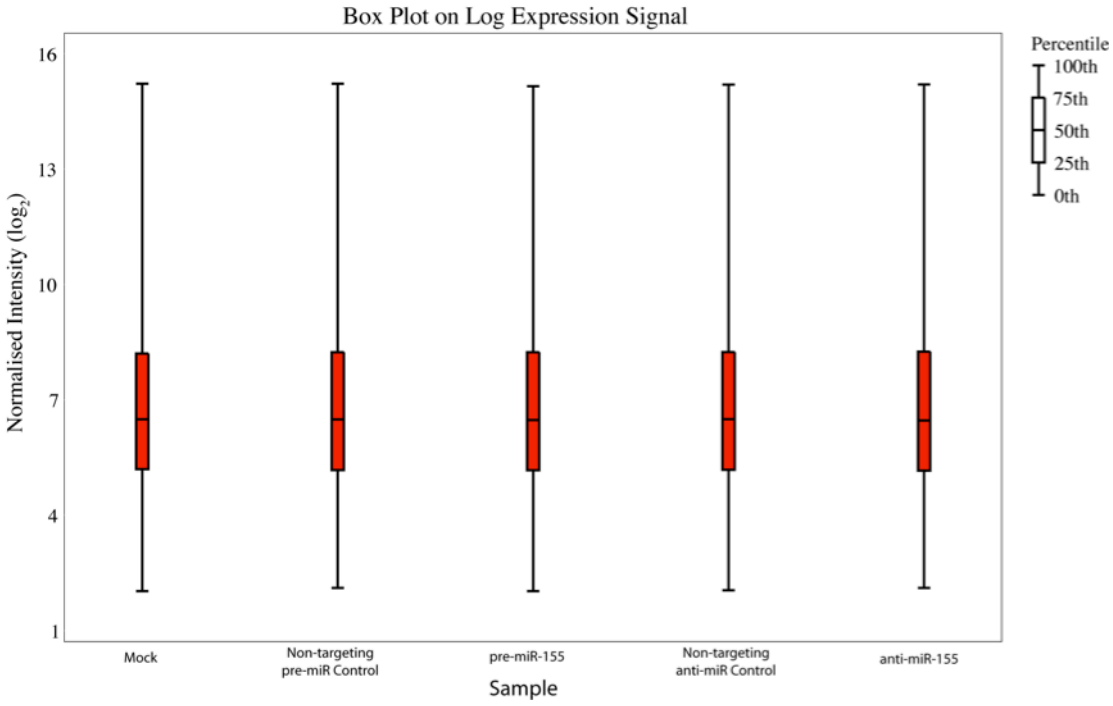

Figure 4.2.19 - The total array content intensity profile is similar for all samples analysed on the Affymetrix U133.2 microarrays – Quality control analysis performed in Partek Genomics Suite indicates the range of normalised intensities for all probe sets on the Affymetrix U133.2 microarrays.

4.2.3.2 Global differences in mRNA expression profiles following miR-155 modulation in cultured ASMCs

Analyses were performed to investigate differences in the global profile of mRNA expression in mock, 20nM non-targeting control pre-miR, 20nM pre-miR-155, 100nM non-targeting anti-miR control and 100nM anti-miR-155 transfected cultured ASMCs. Principal component analysis (PCA), which portrays the total variation within the data as three arbitrary vectors most completely describing the variation (discussed previously in Chapter 3.2.3), indicated that cells transfected with 20nM pre-miR-155 had the greatest difference in their global mRNA expression profile in comparison to the remaining samples (Figure 4.2.20). The sample showing the subsequent least similarity was the mock transfection, indicating that the transfection of any small RNA into the ASMCs had some consistent influences on gene expression. A similar analysis is depicted in Figure 4.2.21 whereby Euclidean Dissimilarity and Average Linkage have been used to construct a hierarchical clustering dendogram of the five samples. The resulting dendogram separates the samples based on a lack of similarity, such that the order in which the samples branch indicates their relative global similarity and the length of a branch represents the relative difference between the samples. This analysis again illustrated that the pre-miR-155 transfection, followed the mock were the least similar in comparison to the three remaining samples. Following this the anti-miR-155 was less similar to the two non-targeting control transfections than they were to one another. The fact that the 100nM anti-miR-155 transfection was most similar to the non-targeting control transfections suggests that it had few specific influences on global mRNA expression. It should be noted that the differences depicted in these analyses are relative within the data set, meaning that any differences shown may be very small in terms of absolute values.

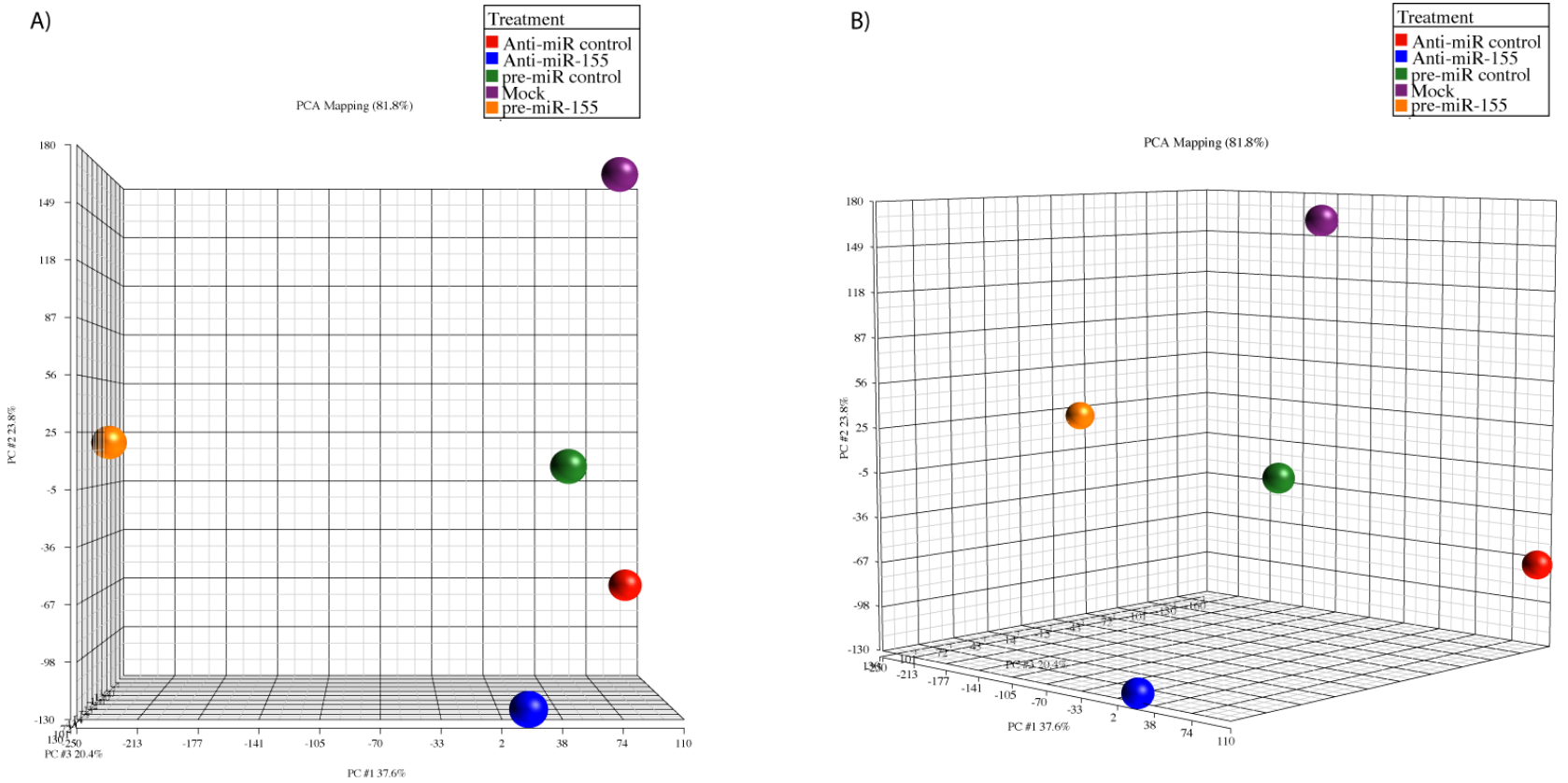

Figure 4.2.20 - Principal component analysis demonstrates that cultured ASMCs transfected with pre-miR-155 have the least similarity in mRNA expression profile compared to the alternative transfections – Principal component analysis demonstrates the variation within a data set. **A)** The X, Y and Z axes reflect independent contributions towards the total variation within the data. Each dot represents a single sample and the distance between dots is directly correlated to the total difference in expression patterns between those samples. **B)** Depicts the same data rotated 45° about the Y-axis.

Figure 4.2.21 - Unsupervised hierarchical clustering of total mRNA expression demonstrates that cells transfected with pre-miR-155 have the least similarity in comparison to the alternative transfections – Unsupervised hierarchical clustering using Euclidean Dissimilarity and Average Linkage was performed to determine the relative similarity in overall mRNA expression levels between mock, 20nM pre-miR-155, 20nM non-targeting pre-miR control, 100nM anti-miR-155 and 100nM non-targeting anti-miR control transfected samples. Branch points represent clustering of more similar samples.

4.2.3.3 Identification of individual mRNAs with potential differential expression following modulation of miR-155 levels in cultured ASMCs

To enable the identification of potential endogenous targets of miR-155 in cultured ASMCs individual contrast comparisons were performed. As these microarray studies were performed as a preliminary study in a single replicate no statistical analysis could be performed and the results in the following section are therefore based on a threshold value for a difference in expression between two transfection conditions.

A gene list containing all the probe sets that demonstrated a difference in normalised intensity of greater than two-fold between cells transfected with 20nM pre-miR-155 and those transfected with 20nM non-targeting control pre-miR was generated. Figure 4.2.22 demonstrates hierarchical clustering, as determined by Euclidean Dissimilarity and Average Linkage, of the 127 mRNAs that demonstrated a greater than two-fold difference in expression between cells transfected with 20nM pre-miR-155 or 20nM non-targeting control pre-miR. The relative expression

levels of these 127 mRNAs in the mock, non-targeting control anti-miR and anti-miR-155 transfected samples are also shown for comparison and indicate that the majority showed similar trends in all the samples when compared to the pre-miR-155 transfection.

4.2.3.3.1 Transcripts with decreased abundance following miR-155 over-expression

To identify mRNAs with decreased abundance following miR-155 over-expression a filtered list containing only those probe sets with a normalised intensity that was at least two-fold lower in the 20nM pre-miR-155 sample compared to the 20nM non-targeting control pre-miR transfection was then generated (Figure 4.2.23 and Table xi). These are the transcripts that are most likely to be direct targets of miR-155 in cultured human ASMCs as the canonical outcome of a miRNA:mRNA interaction is a decrease in the expression level of the mRNA. This analysis identified 37 probe sets, with the majority showing a decrease in the pre-miR-155 transfected sample in comparison to all the other transfection conditions (Figure 4.2.23). The general magnitude of changes in intensity was not large, with the greatest fold-decrease, that of FIP1L1, being approximately three-fold (Table xii). In order to gain further confidence that these differences were specific to pre-miR-155 transfection, the fold difference between cells transfected with 20nM pre-miR-155 and those that underwent a mock transfection were compared (Table xi). Interestingly, only probe sets directed against five mRNAs; KBTD10, LGSF10, KCND2, ITGA8 and ADAMTS5 had intensity values that were greater than two-fold lower following pre-miR-155 transfection in comparison to both mock and non-targeting control pre-miR transfections. A two-fold decrease in intensity is, however, an arbitrary threshold and if a 1.8-fold decrease in expression were used to compare the pre-miR-155 and mock samples, then 27 out of the 37 transcripts would be included. Further, all of the probe sets have a lower intensity in the pre-miR-155 sample compared to that of the mock, suggesting that they all have trends in the appropriate direction to indicate being a direct target of miR-155 in cultured ASMCs.

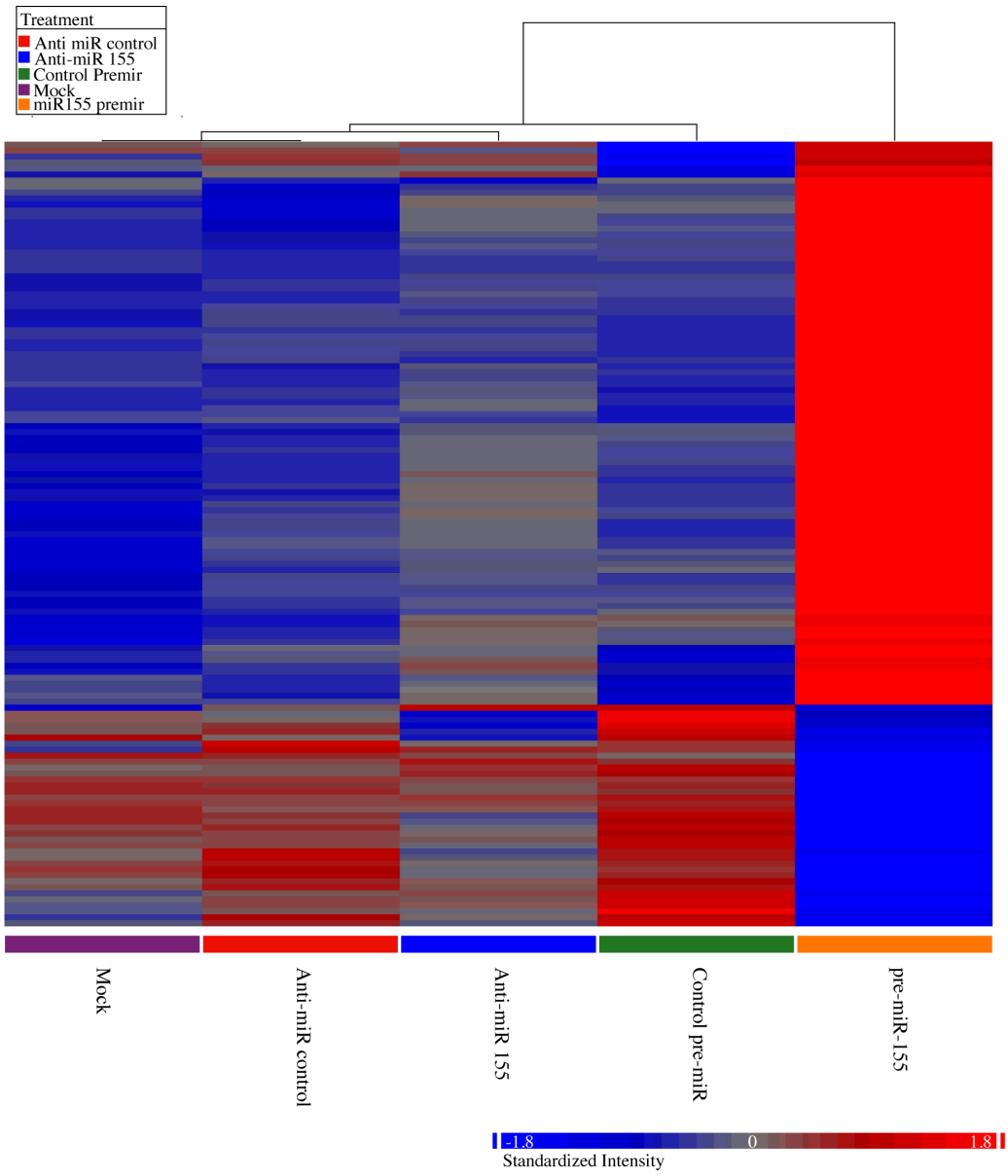

Figure 4.2.22 – Hierarchical clustering of the 127 probe sets that demonstrated a greater than two-fold difference in normalised intensity following transfection of 20nM pre-miR-155 compared to 20nM non-targeting pre-miR control – Expression levels of mRNAs were compared in cultured ASMCs transfected with either 20nM pre-miR-155 or 20nM non-targeting control pre-miR before Euclidean Dissimilarity and Average Linkage were used to cluster those mRNAs that demonstrated a difference in expression of greater than two-fold. The relative intensities of each probe set following mock, 100nM non-targeting control anti-miR and 100nM anti-miR-155 transfections are also included for comparison. All total of 127 probe sets showed a fold difference of greater than two-fold difference in normalised intensity, with 37 probe sets demonstrating a decrease in intensity following transfected with pre-miR-155 and 91 probe sets demonstrating an increase in intensity. The heatmap is coloured by relative difference in expression, with red indicating increased expression and blue indicating decreased expression. The strength of the colour represents the magnitude of the relative difference in expression with a stronger colour indicating a larger difference.

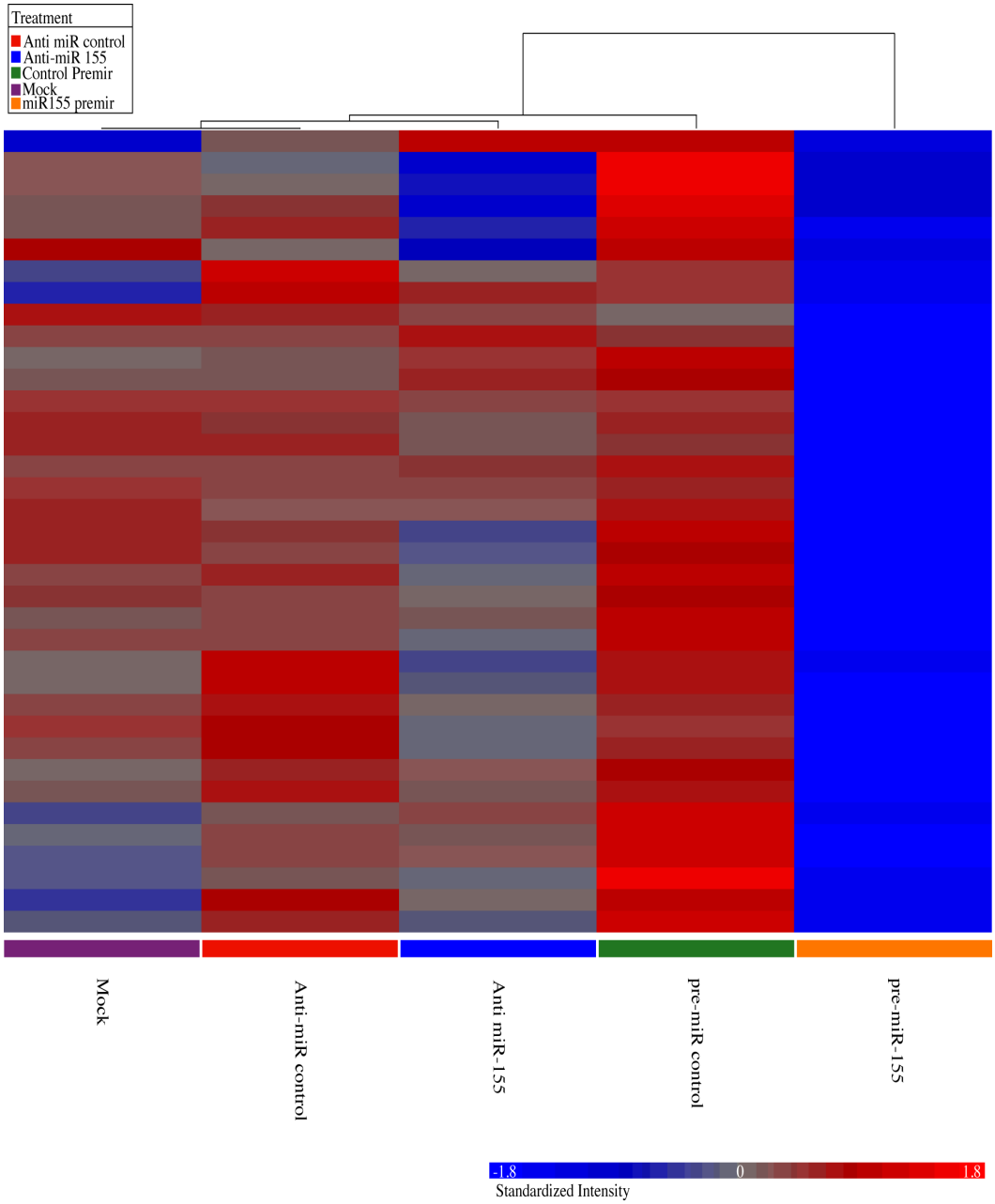

Figure 4.2.23 – Hierarchical clustering of the 37 probe sets that demonstrated a greater than two-fold decrease in normalised intensity following transfection with 20nM pre-miR-155 in comparison to 20nM non-targeting pre-miR control - Expression levels of mRNAs were compared in cultured ASMCs transfected with either 20nM pre-miR-155 or 20nM non-targeting control pre-miR before Euclidean Dissimilarity and Average Linkage were used to cluster those mRNAs that demonstrated a normalised intensity value that was at least two-fold lower following transfection with 20nM pre-miR-155. The relative intensities of each probe set following mock, 100nM non-targeting control anti-miR and 100nM anti-miR-155 transfections are also included for comparison. The heatmap is coloured by relative difference in expression, with red indicating increased expression and blue indicating decreased expression. The strength of the colour represents the magnitude of the relative difference in expression with a stronger colour indicating a larger difference.

Gene	Fold Change v Non-targeting Control	Fold Change v Mock
FIP1L1	3.01756	1.94054
KBTBD10	2.74785	2.5881
PCTK2	2.44799	1.4953
BC025664	2.2931	1.77312
MALAT1	2.28623	1.50398
CCND2	2.27764	1.53397
RAPGEF6	2.2674	1.79573
COL21A1	2.25223	1.97494
IGSF10	2.23272	2.08094
SLITRK6	2.2308	1.81272
PUS10	2.20533	1.37177
ZNF652	2.20204	1.78773
SNAP25	2.19306	1.91865
chr15:94554756-94556856	2.14844	1.79486
KIAA1211	2.1468	1.79544
KCND2	2.13827	2.04751
PAN3	2.13657	1.90256
BRWD1	2.11875	1.46855
G3BP1	2.1161	1.98357
ITGA8	2.10929	2.14221
NDUFS1	2.10658	1.97514
FILIP1	2.0985	1.63428
ZNF323	2.06606	1.44975
ABAT	2.04711	1.49667
ADAMTS5	2.04488	2.08358
SOX5	2.04167	1.51462
FAM164A	2.04113	1.91148
GAB2	2.03726	1.70246
CD24	2.0352	2.52899
ADAMTS5	2.03315	2.12286
MBNL1	2.02498	1.62783
ADAMTS5	2.02335	2.05641
EVI2A	2.02257	1.12439
C15orf5	2.01262	1.43461
NKTR	2.01128	1.33426
SEMA3A	2.00256	1.35622
KIAA2026	2.00048	1.8956

Table xii – Genes with a greater than 2-fold decrease in expression following transfection with 20nM pre-miR-155 - Indicates genes with a greater than 2-fold decrease in expression in the pre-miR-155 transfected sample compared to the non-targeting pre-miR control sample. The fold difference relative to Mock transfected cells is included for comparison.

4.2.3.3.2 Transcripts with increased abundance following miR-155 over-expression

A gene list of those probe sets that demonstrated an increase in normalised intensity of greater than two-fold between the 20nM pre-miR-155 transfected and 20nM non-targeting pre-miR control transfected samples was generated (Figure 4.2.24 and Table xiii). These genes are less likely to be direct targets of miR-155 in cultured human ASMCs as there are very few reports of miRNAs causing an increase in detectable levels of a target mRNA (Vasudevan et al. 2007).

This analysis identified 91 probe sets with a greater than two-fold increase in normalised intensity between the 20nM pre-miR-155 transfected and 20nM non-targeting pre-miR control transfected samples. Further analysis demonstrating that the majority of probe sets, 75 out of 91, also had a greater than two-fold increase in intensity when compared to the mock sample (Table xiii). Hierarchical clustering (Figure 4.2.24) indicated that the majority of probe sets showed an increase in normalised intensity following 20nM pre-miR-155 transfection in comparison to all alternative transfection conditions. There were, however, a number of probe sets that demonstrated increased normalised intensities following anti-miR-155 transfection in comparison to the mock transfection. The most striking feature of the gene list generated was the predominance of pro-inflammatory molecules, particularly chemokines. Seven chemokines are present on the gene list; CCL5, CXCL10, CCL8, CXCL11, CCL26, CXCL9 and CCL7 and all had a greater than two-fold increase in mRNA levels in the pre-miR-155 transfected sample compared to both the mock and non-targeting control pre-miR transfected samples. In addition to chemokines, there were a number of other pro-inflammatory molecules with increased mRNA levels following miR-155 over-expression. These included IDO1, ISG20, IRF1, ZC3HAV1, CD38, CR1L, TNFSF10, OASL, NOD2, CR1, PLA1A, MCF2, GBP4, GBP5, AGFG1, IL41L, ALCAM, LST-1 AND TNFAIP6. This increase in the mRNA levels of a large number of pro-inflammatory genes suggests that a major result of miR-155 over-expression in cultured ASMCs is the activation of a pro-inflammatory phenotype.

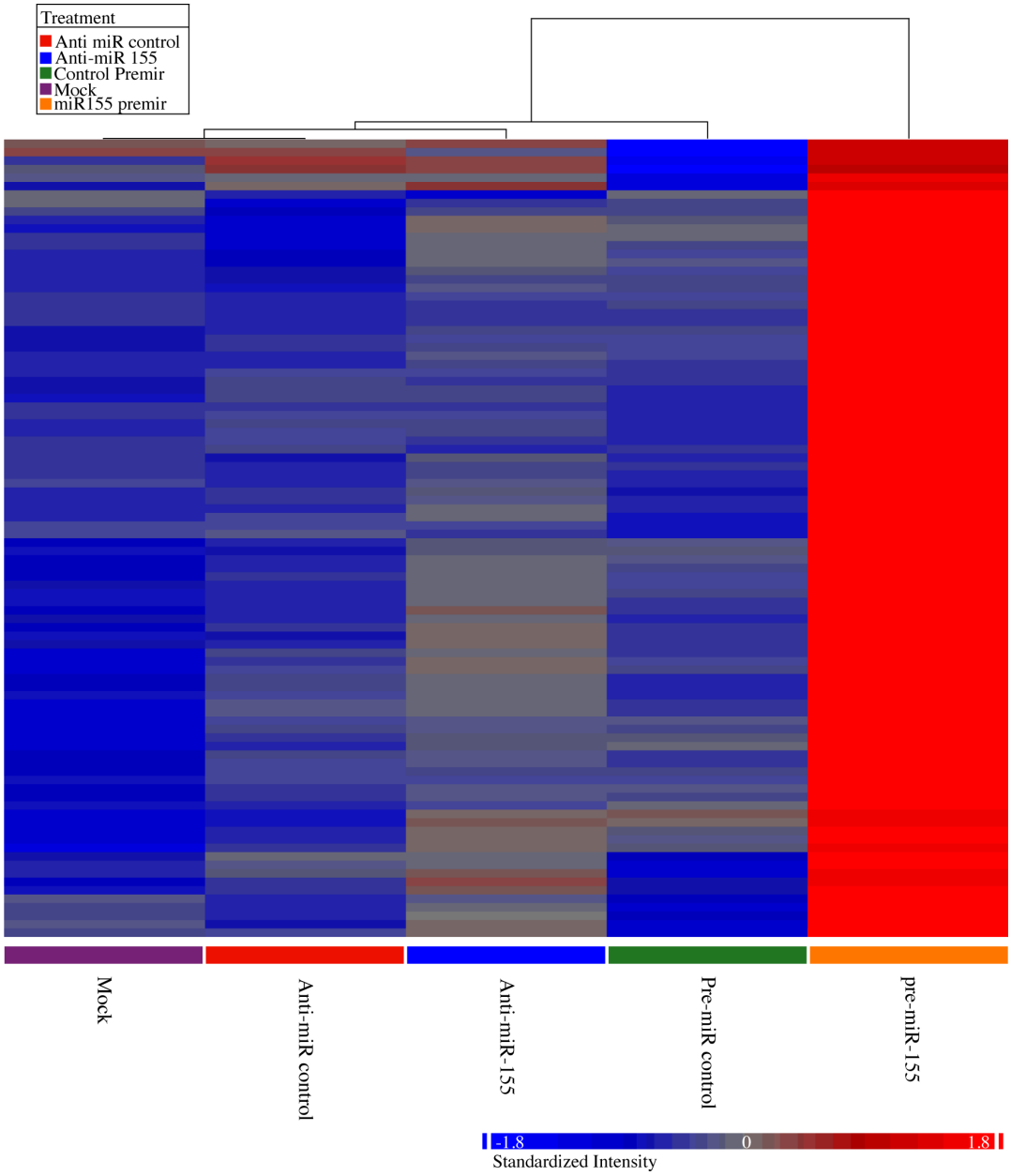

Figure 4.2.24 – Hierarchical clustering of the 91 probe sets that demonstrated a greater than two-fold increase in normalised intensity following transfection with 20nM pre-miR-155 in comparison to 20nM non-targeting pre-miR control – Expression levels of mRNAs were compared in cultured ASMCs transfected with either 20nM pre-miR-155 or 20nM non-targeting control pre-miR before Euclidean Dissimilarity and Average Linkage were used to cluster those mRNAs that demonstrated a normalised intensity value that was at least two-fold greater following transfection with 20nM pre-miR-155. The relative intensities of each probe set following mock, 100nM non-targeting control anti-miR and 100nM anti-miR-155 transfections are also included for comparison. The heatmap is coloured by relative difference in expression, with red indicating increased expression and blue indicating decreased expression. The strength of the colour represents the magnitude of the relative difference in expression with a stronger colour indicating a larger difference.

Gene	Fold Change v Non-targeting	Fold Change v Mock
KIF5C	5.98847	6.57523
IDO1	4.69136	5.11367
PMAIP1	4.44712	5.95504
CCL5	4.39149	5.02007
CXCL10	3.798	5.2261
GCH1	3.77368	4.52995
PMAIP1	3.62381	5.62405
DNER	3.33893	4.71107
TM7SF2	3.0544	3.0737
CCL8	3.03614	4.93214
ISG20	3.02472	3.38274
ZC3HAV1	2.9738	2.15602
IRF1	2.94669	2.92484
ISG20	2.91257	3.35001
GBP5	2.88829	2.69599
STX11	2.88225	2.90879
CXCL11	2.86884	7.18668
GBP4	2.83858	3.10279
TYSND1	2.82123	2.6898
CD38	2.78565	2.95523
FRMD3	2.77228	3.14394
C1orf173	2.74036	3.52967
FAM26F	2.68452	2.82849
CR1L	2.59184	3.43634
GOLGA4	2.57934	2.13817
ASPHD2	2.57861	2.85438
CCL26	2.55726	2.67385
TNFSF10	2.54987	2.96579
TYSND1	2.46371	2.66445
CXCL9	2.42823	2.65424
OASL	2.42606	2.87678
WARS	2.38233	2.91251
FAM26F	2.38097	2.39099
ENPEP	2.37872	1.88953
RHBDF2	2.35904	3.2418
PHACTR4	2.34419	2.13101
OASL	2.33566	2.67427
IRF1	2.33491	2.26655
TMEM171	2.33111	2.61686
FRMD3	2.32494	2.24395
TNFSF10	2.32104	2.83838
CSAG2 /// CSAG3	2.31819	3.09975
NOD2	2.31084	2.55666
SLC2A13	2.2619	2.80964
CR1 /// CR1L	2.24864	3.42512
NUDCD1	2.2343	2.148
PLA1A	2.2277	1.88997
FOSL1	2.22519	2.14761
SQRDL	2.21758	2.15536
LOC100131733	2.2132	2.13767
NCF2	2.21066	2.16498

GBP4	2.20991	3.13819
GDPD3	2.20973	2.03603
HRASLS2	2.20691	2.99329
WARS	2.17659	2.66823
NCRNA00103	2.1745	2.36287
ATF3	2.16423	2.45034
AGFG1	2.15959	1.27086
TNFSF10	2.14998	2.39969
IL4I1	2.13242	2.43875
MT1M	2.12688	2.57641
PCDH17	2.12462	2.06392
MSX1	2.10695	2.28529
FLJ32255	2.10306	2.41889
ALCAM	2.0968	1.38298
ATP10A	2.09412	1.56562
LST1	2.08848	1.92429
STAMBPL1	2.08115	2.21133
TNFAIP6	2.07527	2.10876
C10orf10	2.06986	1.75253
NFE2L3	2.06571	2.25562
RHEBL1	2.06404	2.28601
CCL7	2.06155	2.58944
HMOX1	2.05632	1.83502
HPSE	2.05529	2.06608
TNFAIP6	2.05525	2.16795
DISC1	2.04732	1.51682
CH25H	2.0371	2.32173
C9orf91	2.03159	1.83843
PDZD2	2.02978	2.55694
DUSP6	2.02758	2.68634
C10orf140	2.0226	2.79529
RXRG	2.01266	1.83288
LOC100128081	2.01226	1.22032
HMMR	2.00636	1.71596
ETV7	2.00585	2.32611
STAMBPL1	2.00227	1.95885
EHD4	2.00153	1.95977

Table xiii – Genes with a greater than 2-fold increase in expression following transfection with 20nM pre-miR-155 – Indicates genes with a greater than 2-fold increase in expression in cells transfected with pre-miR-155 compared to the non-targeting pre-miR control sample. The fold difference relative to Mock transfected cells is included for comparison.

4.2.3.4 Transcripts with altered abundance following miR-155 antagonism

As discussed in Section 3.3.3.2, the global effects of the anti-miR-155 transfection of cultured ASMCs did not appear to be gross, with the overall mRNA expression profile following anti-miR-155 transfection being most similar to that of cells

transfected with non-targeting control pre-miR or anti-miR (Figure 4.2.20 and 4.2.21). It would be a strong indication of a *bone fide* miR-155 target, however, if a transcript that was decreased following miR-155 over-expression was also increased following miR-155 antagonism. A list of probe sets with a normalised intensity that differed by a threshold of greater than 1.5-fold between cells transfected with 100nM anti-miR-155 and those transfected with 100nM non-targeting anti-miR control was therefore generated (Figure 4.2.25). A threshold of 1.5-fold was chosen because a 2-fold threshold, as was used in Section 4.2.3.3, resulted in no probe sets passing the filter. It was decided that a value of 1.5-fold should be used in order to generate a list of potential candidates for further investigation. Interestingly, hierarchical clustering of these probe sets demonstrated less consistent changes in relative intensity levels compared to the other transfection conditions than was observed when probe sets that altered following pre-miR-155 transfection were clustered (Figure 4.2.22). This indicated that some of the effects may be non-specific or at a magnitude that is difficult to distinguish from experimental variation.

4.2.3.4.1 Transcripts with increased abundance following miR-155 antagonism

37 probe sets demonstrated an increase in normalised intensity of greater than 1.5-fold in cells transfected with 100nM anti-miR-155 compared to those transfected with 100nM non-targeting anti-miR control (Figure 4.2.26 and Table xiv). Of these probe sets, however, none also showed a greater than two-fold decrease in mRNA levels following miR-155 over-expression (Table xii). This was unexpected as it was hoped that the use of miR-155 antagonism would allow true miR-155 targets to be identified by providing an additional comparison in order to counter any non-specific effects of the over-expression approach. The poor corroboration between probe sets that demonstrated an increase in normalised intensity following anti-miR-155 transfection and a decrease following pre-miR-155 transfection, combined with the poor consistencies in relative intensities when comparing anti-miR-155 transfections to the remaining samples (Figure 4.2.25), means that it is difficult to gain confidence in the validity of the results gained following the anti-miR-155 transfection.

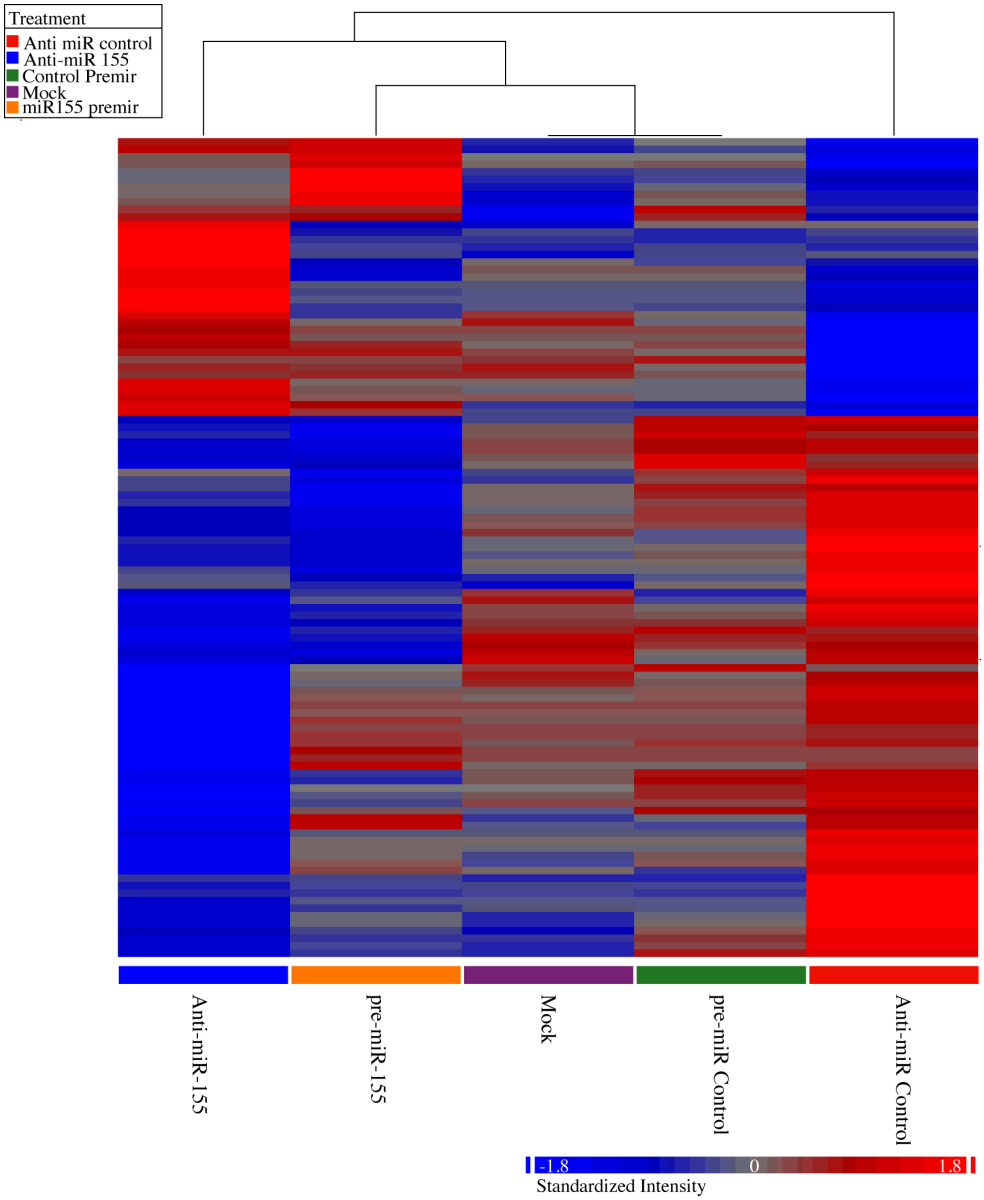

Figure 4.2.25 – Hierarchical clustering of the 109 probe sets that demonstrated a greater than 1.5-fold difference in normalised intensity following transfection with 100nM anti-miR-155 in comparison to 100nM non-targeting anti-miR control – Expression levels of mRNAs were compared in cultured ASMCs transfected with either 100nM anti-miR-155 or 100nM non-targeting control anti-miR before Euclidean Dissimilarity and Average Linkage were used to cluster those mRNAs that demonstrated a difference in expression of greater than 1.5-fold. The relative intensities of each probe set following mock, 20nM non-targeting control pre-miR and 20nM pre-miR-155 transfections are also included for comparison. A total of 109 probe sets showed a fold difference of greater than two-fold difference in normalised intensity, with 37 probe sets demonstrating a decrease in intensity following transfected with pre-miR-155 and 91 probe sets demonstrating an increase in intensity. The heatmap is coloured by relative difference in expression, with red indicating increased expression and blue indicating decreased expression. The strength of the colour represents the magnitude of the relative difference in expression with a stronger colour indicating a larger difference.

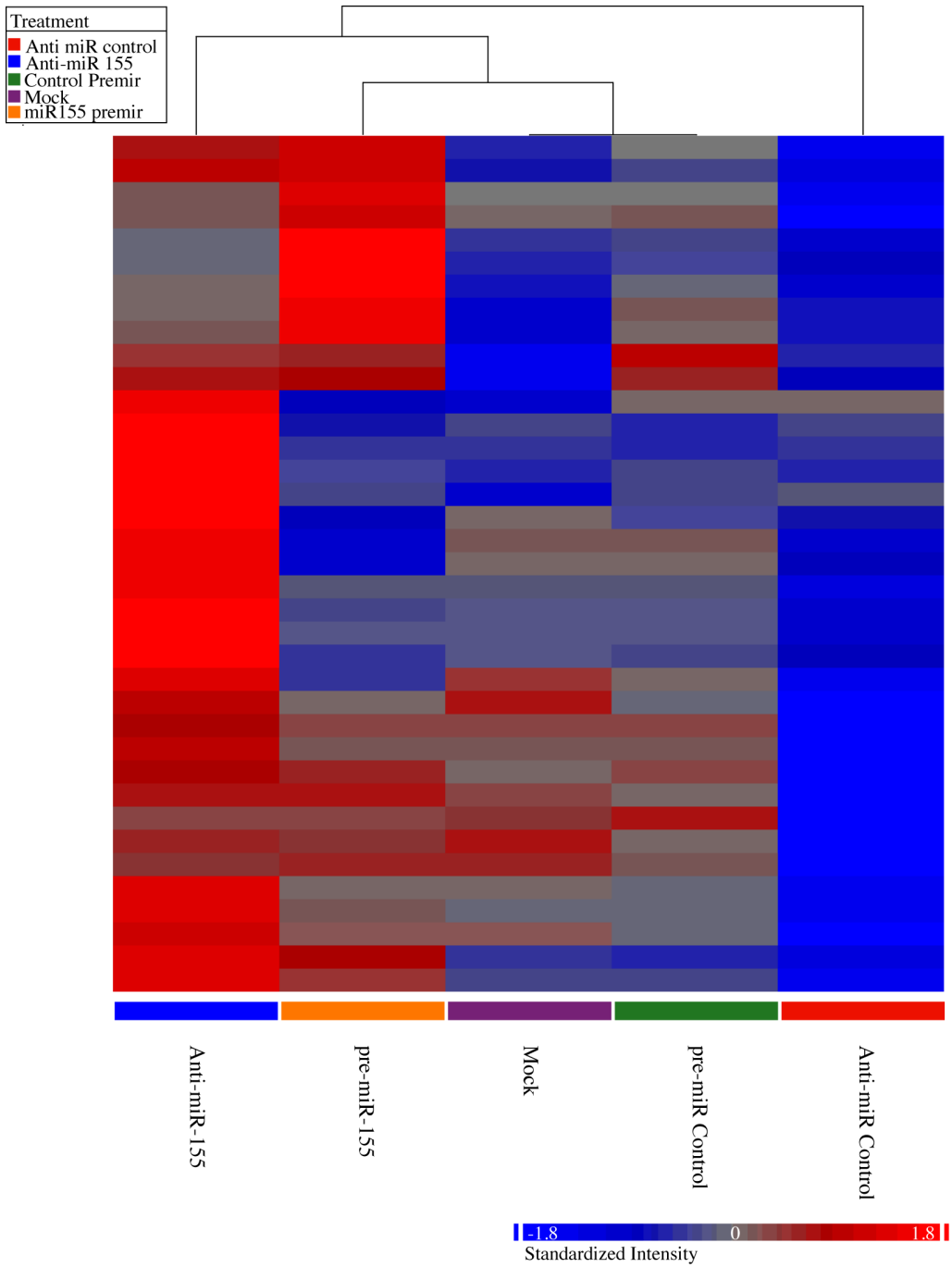

Figure 4.2.26 – Hierarchical clustering of the 37 probe sets that demonstrated a greater than 1.5-fold increase in normalised intensity following transfection with 100nM anti-miR-155 in comparison to 100nM non-targeting anti-miR control –Expression levels of mRNAs were compared in cultured ASMCs transfected with either 100nM anti-miR-155 or 100nM non-targeting control anti-miR before Euclidean Dissimilarity and Average Linkage were used to cluster those mRNAs that demonstrated an increase in expression of greater than 1.5-fold following transfection with 100nM anti-miR-155. The relative intensities of each probe set following mock, 20nM non-targeting control pre-miR and 20nM pre-miR-155 transfections are also included for comparison. The heatmap is coloured by relative difference in expression, with red indicating increased expression and blue indicating decreased expression. The strength of the colour represents the magnitude of the relative difference in expression with a stronger colour indicating a larger difference.

Gene	Fold Change v anti-miR Control	Fold Change v Mock
DENND1B	1.90558	1.49683
IZUMO1	1.88031	1.21482
CXCL11	1.86271	2.21709
BVES	1.77466	1.40741
CXCL11	1.77382	2.34534
ITIH4	1.71185	1.45323
SULT1C2	1.69592	1.52337
ZNF254	1.65587	1.67884
CCL5	1.65308	1.26519
MGC35361	1.62348	1.46431
KCNH5	1.61358	1.36567
chr7:156765361-156765870	1.61085	1.05554
ZNF385D	1.60425	1.09884
POU3F3	1.60338	1.03145
ISG20L2	1.60007	1.17335
CEP97	1.59519	1.40711
GMDS	1.59396	1.34775
MTND2	1.59393	1.03068
HPCAL4	1.57304	1.27089
CCL5	1.56823	1.30724
C7orf10	1.55904	1.87713
chr1:8223148-82234802	1.54769	1.08452
GPR84	1.54132	1.20296
LIMD1	1.53598	1.34756
CISD2	1.53597	1.01675
BPTF	1.53333	1.84283
ANO2	1.53171	1.28818
MMP1	1.53157	2.21117
SUSD5	1.52429	1.52429
FKSG2	1.52	1.12661
HRASLS2	1.51986	1.43679
GTF2F2	1.51392	1.13714
ABCC12	1.51044	1.22839
chr8:82,351,922-82,352,353	1.50938	1.02283
chr2:96,349,913-96,351,371	1.50262	1.01035
KIAA0564	1.50249	1.50249
HAUS6	1.50089	1.89748

Table xiv – Genes with a greater than 1.5-fold increase in expression following transfection with 100nM anti-miR-155 – Indicates genes with a greater than 1.5-fold increase in expression in cells transfected with anti-miR-155 compared to non-targeting anti-miR control. The fold difference relative to Mock transfected cells is included for comparison.

4.2.4 Further investigation of candidate miR-155 target genes identified during Affymetrix U133.2 microarray studies

Due to the lack of detectable global effects of miR-155 antagonism on mRNA levels in cultured ASMCs (Figures 4.2.20, 4.2.21 and 4.2.25) and a lack of corroboration between transcripts with altered mRNA levels following miR-155 over-expression and antagonism, it was decided to utilise samples isolated from previous transfection experiments to further investigate transcripts that demonstrated an altered level following pre-miR-155 transfections. These transcripts would then be investigated further by assaying cDNA isolated from cells transfected with anti-miR-155 from an increased number of replicates.

4.2.4.1 Validation of transcripts with increased abundance following miR-155 over-expression

It was decided that the striking number of pro-inflammatory transcripts that demonstrated increased levels following miR-155 over-expression (see Chapter 4.2.3.3.2) should be investigated further.

Initial analyses were focused on 24 hours post-transfection as this was the time point at which RNA used in the Affymetrix microarray experiments was isolated. cDNA generated from RNA isolated from previously performed transfections was used to perform RT-qPCR interrogation of a subsets of transcripts that demonstrated altered mRNA levels at 24 hours post-transfection with 20nM pre-miR-155. The majority of the mRNAs assayed showed very similar results, including a statistically significant increase in the level of mRNA in the pre-miR-155 transfected sample when compared to the mock (Figure 4.2.27). Of the mRNAs tested, only CCL11 and CCL13 did not give this result. CCL11 had no difference in expression between any of the transfection conditions whilst CCL13 showed a trend towards an increase between the pre-miR-155 and mock transfection that was not statistically significant. Apart from CCL11, the remaining transcripts all showed a trend towards an increase in mRNA levels in the pre-miR-155 transfected sample compared to the non-targeting pre-miR control transfected sample. Only in the case of CCL5 and CCL13, however, was this difference statistically significant. It is likely that the transfection of any small RNA had some influence on the levels of a number of these transcripts as CCL5, CCL26, CXCL10 and CXCL11 all showed a trend towards an increase in mRNA levels in the non-targeting pre-miR control transfected sample

compared to the mock. In addition to this, the two non-chemokine transcripts tested, IRF1 and CD38, also showed a similar trend.

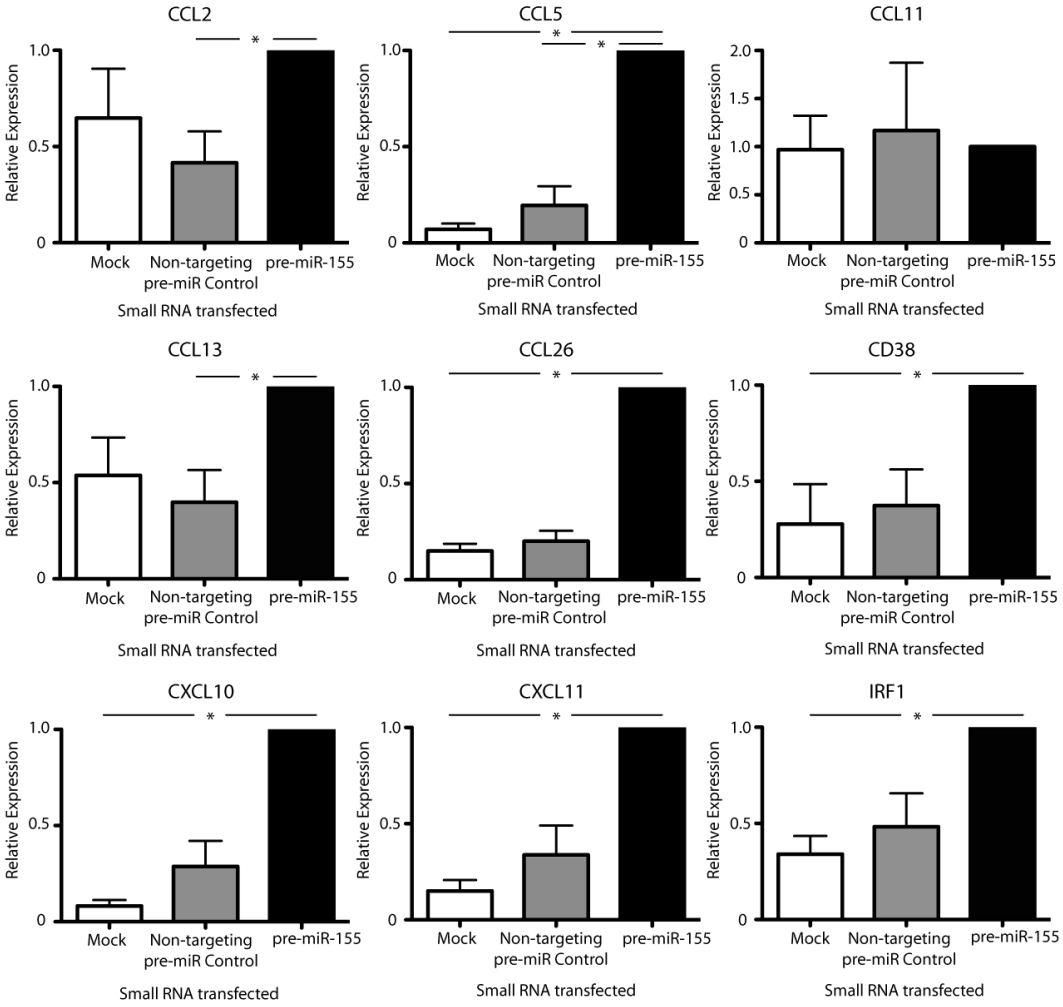

Figure 4.2.27 - Validation of mRNAs with increased abundance following miR-155 over-expression in cultured ASMCs - ASMCs were growth arrested by serum starvation for 72 hours before Lipofectamine 2000 mediated transfection of 20nM non-targeting pre-miR control or 20nM pre-miR-155. Following a 24 hour incubation RNA was harvested and RT-qPCR performed. Results are analysed using ΔΔCt methodology through normalisation to 18S RNA as the endogenous control and expression levels are presented relative to the 20nM pre-miR-155 transfected sample. Error bars represent SEM, n=5. * $p<0.05$ as determined by Friedman's Test with Dunn's Multiple Comparison Correction Test.

4.2.4.2 Investigating a potential miR-155 mediated regulation of CCL5 and CCL26 in cultured ASMCs

As CCL5 and CCL26 appeared to show the greatest increase in mRNA levels 24 hours post-transfection with pre-miR-155, it was decided that these should be further investigated as models of a potential miR-155 mediated pro-inflammatory response in cultured ASMCs.

A possible temporal influence on the regulation of CCL5 and CCL26 by miR-155 was investigated by assaying mRNA levels at 6 and 72 hours post-transfection and these results, in addition to those generated at 24 hours post-transfection (initially shown in Figure 4.2.27) are depicted in Figure 4.2.28. At 6 hours post-transfection there was a trend towards an increase in the mRNA of both chemokines following miR-155 over-expression. This was more striking for CCL26, as CCL5 mRNA levels demonstrated a relatively high level of variation. Neither of these comparisons, however, were statistically significant. At 72 hours post-transfection, there were again trends towards an increase in mRNA levels for both CCL5 and CCL26 following miR-155 over-expression. Once again, however, none of these comparisons reached statistical significance and the variation within the data makes it difficult to make strong statements about potential miR-155 mediated regulation at these timepoints.

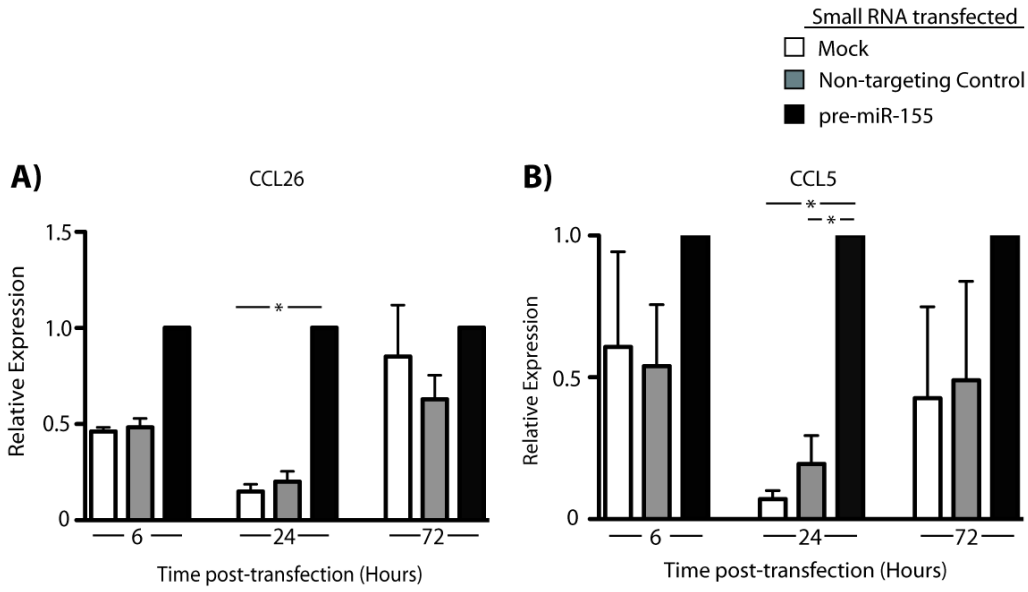

Figure 4.2.28 – Analysis of CCL5 and CCL26 mRNA levels following over-expression of miR-155 in cultured ASMCs - ASMCs were growth arrested by serum starvation for 72 hours before Lipofectamine 2000 mediated transfection of 20nM non-targeting pre-miR control or 20nM pre-miR-155. Following a 6, 24 or 72 hour incubation RNA was harvested and RT-qPCR performed. **A)** Shows the relative expression levels of CCL26 at the indicated times post-transfection and **B)** shows the same analysis for CCL5. Results are analysed using ΔΔCt methodology through normalisation to 18S RNA as the endogenous control and expression levels are presented relative to the 20nM pre-miR-155 transfected sample. Error bars represent SEM, n=4 for 6 and 72 hours and n=5 for 24 hours. *$p<0.05$ as determined by Friedman's Test with Dunn's Multiple Comparison Correction Test.

To investigate whether the miR-155 over-expression induced increase in CCL5 mRNA observed at 24 hours post-transfection was a specific effect or a potential artefact of the large over-expression of miR-155 (Figure 4.2.7) the level CCL5 mRNA following transfection with 4nM pre-miR-155 was assayed. It is clear that the transfection of 20nM pre-miR-155 resulted in a far greater increase in the level of CCL5 mRNA in comparison to the other transfection conditions (Figure 4.2.29 Panel A) and the difference between the 20nM pre-miR-155 transfections and both the mock and 4nM non-targeting control pre-miR were statistically significant following correction for multiple-testing. When the 20nM pre-miR-155 and 20nM non-targeting pre-miR control transfections were removed from the analysis, however, it appeared that there was a trend towards an increase in the level of CCL5 mRNA following 4nM pre-miR-155 transfection, although this was not statistically significant (Figure 4.2.29, Panel B).

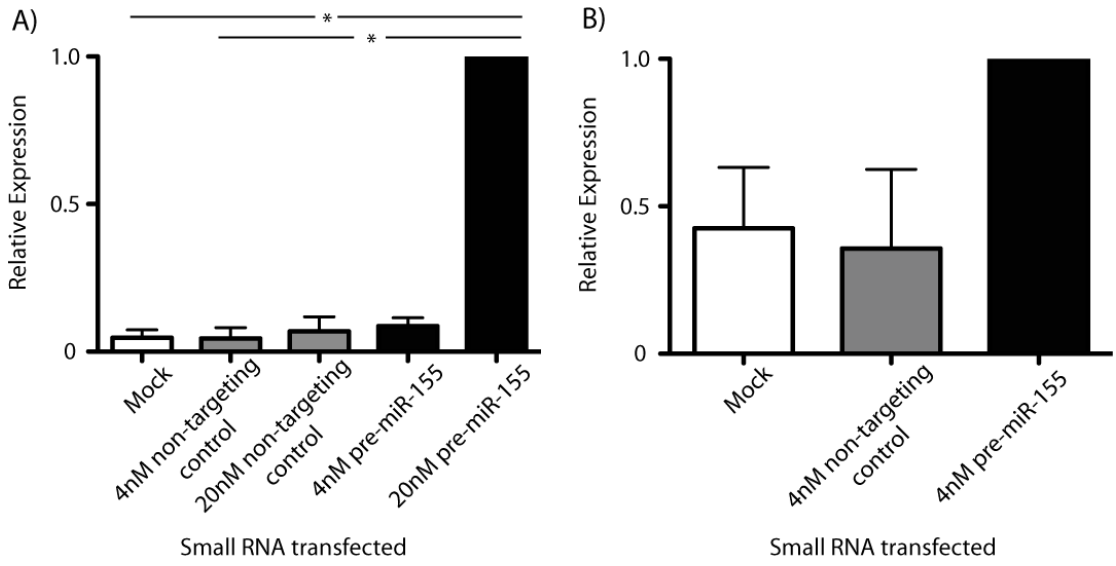

Figure 4.2.29 – Determination of whether the concentration of transfected pre-miR-155 influences the increase in CCL5 mRNA levels - ASMCs were growth arrested by serum starvation for 72 hours before Lipofectamine mediated transfection of 4nM or 20nM non-targeting pre-miR control or pre-miR-155. Following a 24 hour incubation RNA was harvested and RT-qPCR performed. **A)** Shows the relative expression of CCL5 mRNA 24 hours post-transfection presented relative to the 20nM pre-miR-155 transfected sample. **B)** Shows the relative expression of CCL5 mRNA 24 hours post-transfection relative to the 4nM pre-miR-155 samples, the 20nM pre-miR-155 sample is not included on this graph. Results are analysed using ΔΔCt methodology through normalisation to 18S RNA and expression levels are expressed relative to the to 20nM pre-miR-155 (A) or 4nM pre-miR-155 (B). Error bars represent SEM, n=3. Statistical significance was determined using a 2-way Friedmans Test (A) or Friedman's Test (B), both of which were corrected using Dunn's Multiple Testing Correction.

Although results from the microarray analysis indicated an increase in the level of CCL5 mRNA 24 hours post-transfection with anti-miR-155 (see Table xiv), the fact that the fold difference between the anti-miR-155 and the non-targeting anti-miR control was only 1.6-fold and the difference between the anti-miR-155 and the mock sample was only 1.2-fold (Table xiv), coupled with the large increase in CCL5 mRNA following pre-miR-155 transfection, indicated that this may be an erroneous result. It was therefore decided to assay the level of CCL5 mRNA 24 hours post-transfection with anti-miR-155 in an increased number of replicates. This analysis recapitulated the data of the original microarray screen, with a trend towards an increase in the level of CCL5 mRNA in the anti-miR-155 transfected sample when compared to both the mock and non-targeting control anti-miR transfection (Figure 4.2.30).

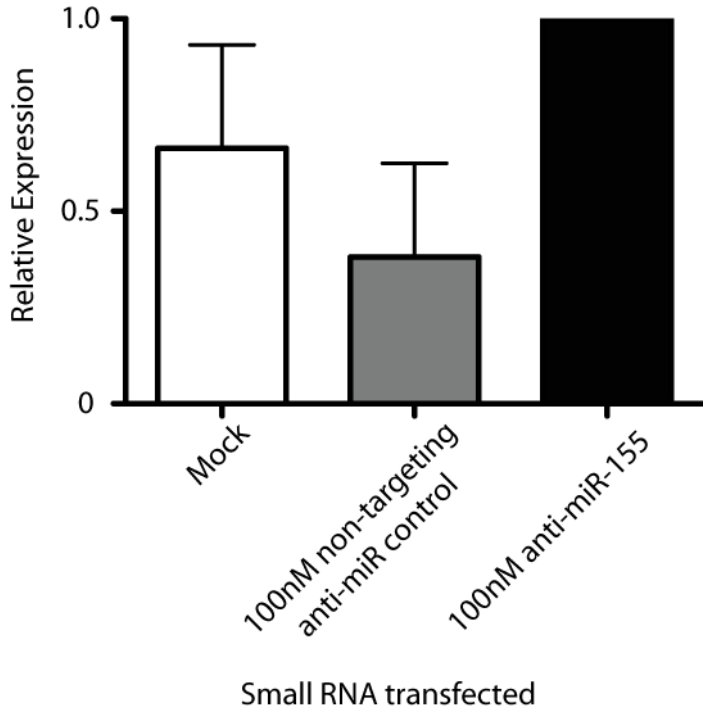

Figure 4.2.30 - CCL5 mRNA levels do not decrease following the antagonism of miR-155 function in cultured ASMCs - ASMCs were growth arrested by serum starvation for 72 hours before Lipofectamine 2000 mediated transfection of 100nM non-targeting anti-miR control or 100nM anti-miR-155. Following a 24 hour incubation RNA was harvested and RT-qPCR performed. Results are analysed using ΔΔCt methodology through normalisation to 18S RNA as the endogenous control and expression levels are expressed relative to the mock transfected sample. Error bars represent SEM, n=3.

The final option was to investigate a potential regulation of CCL5 protein levels to determine if the results observed in the mRNA studies were more pronounced at the protein level. To this end, an ELISA analysis was performed on supernatants archived from cultured ASMCs 24 hours post-transfection (performed as described in 2.2.1). The results of this analysis were very similar to those generated from mRNA analyses, with the largest increase in CCL5 mRNA occurring following transfection with 20nM pre-miR-155, however, there was also an increase following transfection with 100nM anti-miR-155 (Figure 4.2.31). It should be noted, however, that this ELISA analysis was only performed on a single replicate and additional experiments would be required for validation.

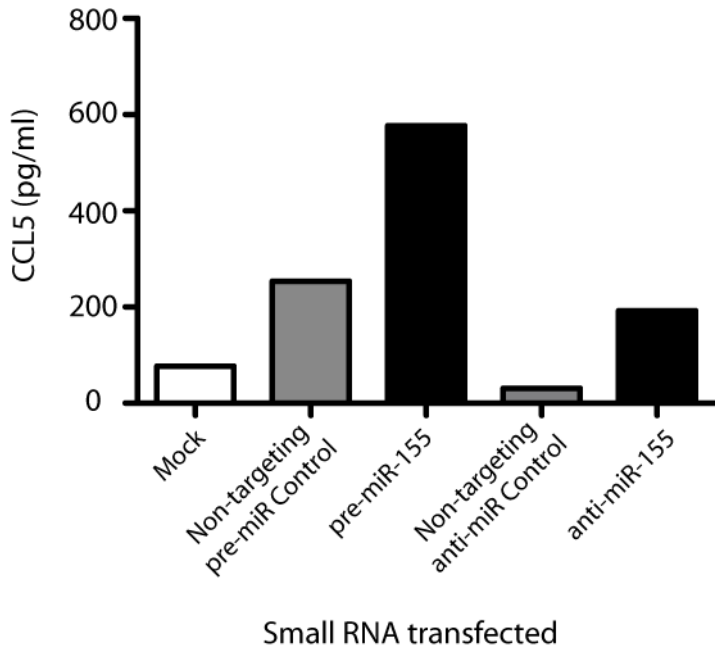

Figure 4.2.31 – Analysis of CCL5 protein levels 24 hours post-transfection with pre-miR-155 or anti-miR-155 - ASMCs were growth arrested by serum starvation for 72 hours before Lipofectamine 2000 mediated transfection of 20nM non-targeting pre-miR control, 20nM pre-miR-155, 100nM non-targeting anti-miR control or 100nM anti-miR-155. CCL5 protein levels in the culture supernatants was determined by ELISA, n=1.

4.2.4.3 Validation of candidate transcripts with decreased abundance following miR-155 over-expression

As stated in Chapter 4.2.3.3.1, transcripts that demonstrated a decrease in mRNA levels following over-expression of miR-155 are the most likely to be direct targets for regulation.

RT-qPCR validation was performed for BRWD1, COL21A1 and ZNF652 as these transcripts were predicted miR-155 targets as determined by at least one of the bioinformatics prediction algorithms. In addition FIP1L1, MALAT1 and ITGA8 were also investigated further. Of these potential candidate targets BRWD1, ITGA8, ZNF652 and COL21A1 showed similar results, with trends towards a decrease in mRNA levels following 20nM pre-miR-155 transfections compared to mock and non-targeting control transfections (Figure 4.2.32). The difference between the pre-miR-155 and mock transfections was statistically significant for BRWD1, ITGA8 and ZNF652 whilst the difference did not reach statistical significance in the case of COL21A1. None of the transcripts showed a statistically significant difference between the pre-miR-155 and non-targeting control pre-miR transfections, however, there was a trend towards lower mRNA levels in the pre-miR-155 transfections for all genes. MALAT1 showed no suggestion of consistent regulation across a number of replicates, whilst FIP1L1 showed a potential trend towards an increase in mRNA levels in both pre-miR-155 and non-targeting pre-miR control transfections when compared to the mock.

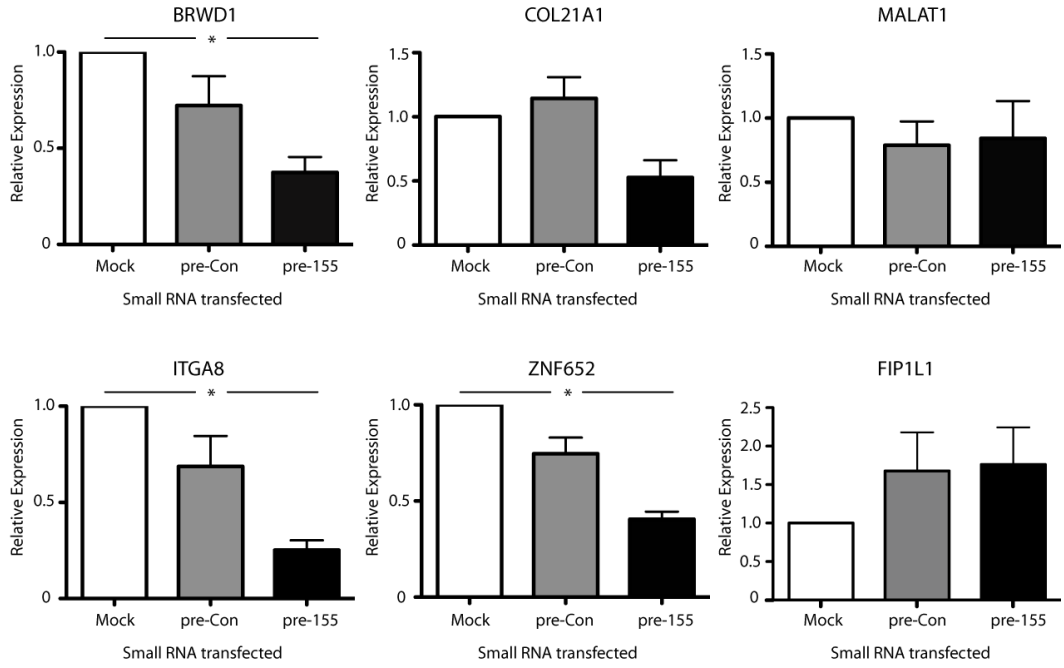

Figure 4.2.32 - Validation of mRNAs with decreased levels following miR-155 over-expression in cultured ASMCs - ASMCs were growth arrested by serum starvation for 72 hours before Lipofectamine 2000 mediated transfection of 20nM non-targeting pre-miR control or 20nM pre-miR-15. Following a 24 hour incubation RNA was harvested and RT-qPCR performed. Results are analysed using ΔΔCt methodology through normalisation to 18S RNA as the endogenous control and expression levels are presented relative to the mock transfected sample. Error bars represent SEM, n=5. * $p<0.05$ as determined by Friedman's Test with Dunn's Multiple Comparison Correction Test.

4.2.4.4 Interrogation of ZNF652 as a candidate for direct regulation by miR-155 in cultured ASMCs

ZNF652 is a zinc-finger transcription factor that was initially noted as a transcriptional repressor (Kumar 2006). It is predicted to be a miR-155 target by TargetScan and PITA and there is previous experimental evidence that it is a miR-155 target in luciferase-reporter based assays (Yin 2008).

As previously stated, there was a statistically significant diminished abundance of ZNF652 mRNA levels 24 hours post-transfection with 20nM pre-miR-155 in comparison to mock transfections and a trend towards decreased levels in comparison to non-targeting control pre-miR transfections (Figure 4.2.32). RT-qPCR indicated a trend towards a miR-155 mediated decrease in the level of ZNF652 mRNA at 6 hours post-transfection when comparing 20nM pre-miR-155 transfections to both mock and 20nM non-targeting control pre-miR transfections

(Figure 4.2.33). It should be noted, however, that this decrease did not reach statistical significance in the replicates analysed. This is most likely due to the variation in the relative level of mRNA in the non-targeting pre-miR control samples. By 72 hours post-transfection there was no evidence for miR-155 mediated regulation.

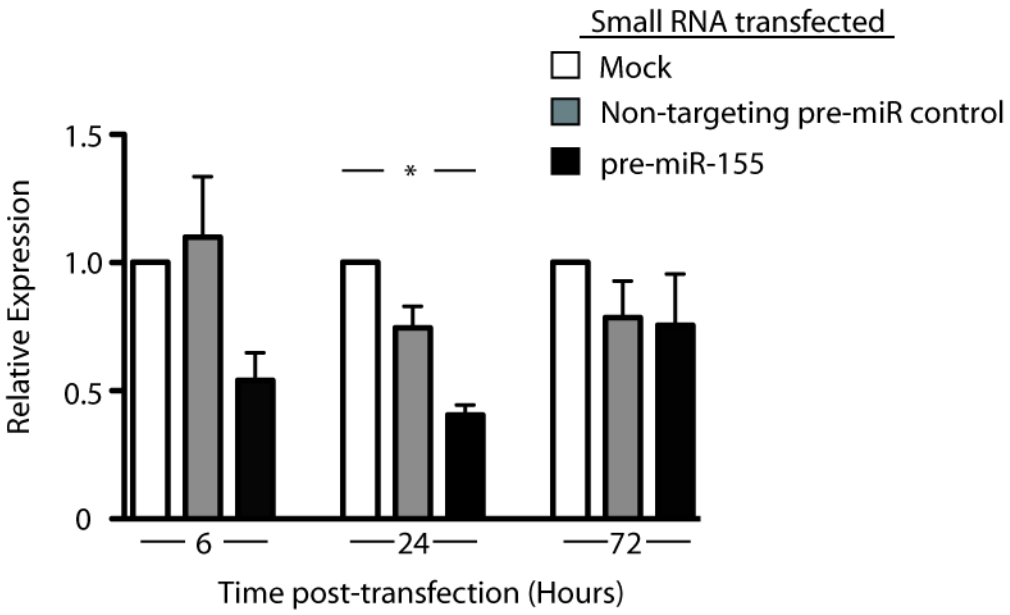

Figure 4.2.33 – Analysis of ZNF652 mRNAs levels following the over-expression of miR-155 in cultured ASMCs - ASMCs were growth arrested by serum starvation for 72 hours before Lipofectamine 2000 mediated transfection of 20nM non-targeting pre-miR control or 20nM pre-miR-155. Following a 6, 24 or 72 hour incubation RNA was harvested and RT-qPCR performed. Results are analysed using ΔΔCt methodology through normalisation to 18S RNA as the endogenous control and expression levels are presented relative to the mock transfected sample. Error bars represent SEM, n=4 for 6 and 72 hours and n=5 for 24 hours. * $p<0.05$ as determined by Friendman's Test with Dunn's Multiple Comparison Correction Test.

In terms of a concentration-responsiveness in the decrease in ZNF652 mRNA observed at 24 hours post-transfection, analysis of cDNA from cells transfected with 4nM pre-miR-155 resulted in no statistically significant difference between the relative mRNA levels following transfection with 4nM or 20nM pre-miR-155 (Figure 4.2.34). The mean relative level of mRNA was slightly lower following 20nM pre-miR-155 transfection when compared to 4nM pre-miR-155 and there was a trend towards a lower relative level of ZNF652 mRNA following 4nM pre-miR-155 transfection in comparison to both mock and non-targeting pre-miR control transfections. None of these trends, however, were statistically significant.

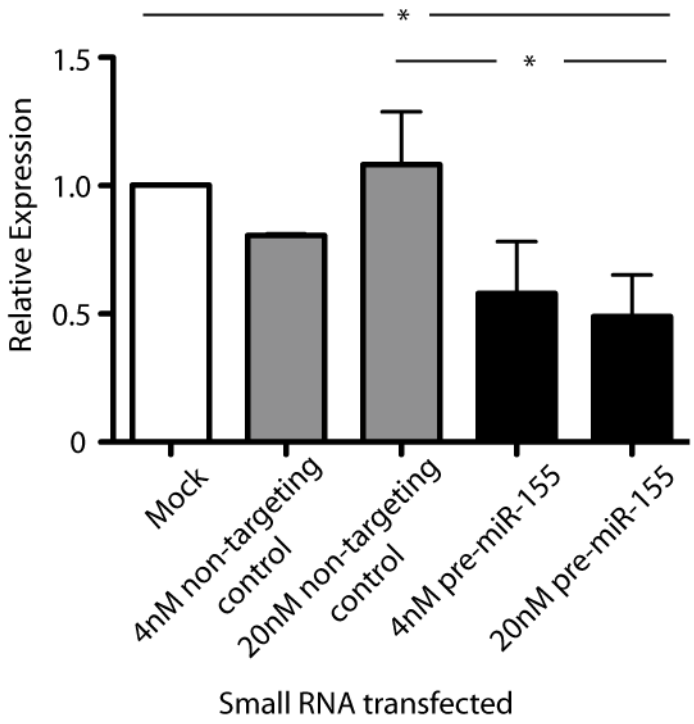

Figure 4.2.34 - Determination of whether the concentration of transfected pre-miR-155 influences the decrease in ZNF652 mRNA levels - ASMCs were growth arrested by serum starvation for 72 hours before Lipofectamine 2000 mediated transfection of 4nM or 20nM non-targeting pre-miR control or pre-miR-155. Following a 24 hour incubation RNA was harvested and RT-qPCR performed. Results are analysed using ΔΔCt methodology through normalisation to 18S RNA as the endogenous control and expression levels are presented relative to the mock transfected sample. Error bars represent SEM, n=3, * $p<0.05$ as determined by a 2-way Friedman's Test with Dunn's Multiple Comparison Correction Test.

Determination of ZNF652 mRNA levels 24 hours after transfection with anti-miR-155 demonstrated no statistically significant difference between 100nM anti-miR-155 transfection when compared to either mock or 100nM non-targeting control anti-miR transfections (Figure 4.2.35). There was, however, a slight trend towards an increase in the level of ZNF652 mRNA following miR-155 antagonism, which is what would be expected if ZNF652 was in fact a true endogenous target of miR-155 in cultured ASMCs.

Unfortunately, due to time constraints, no further investigations into possible endogenous targets of miR-155 in cultured ASMCs were possible.

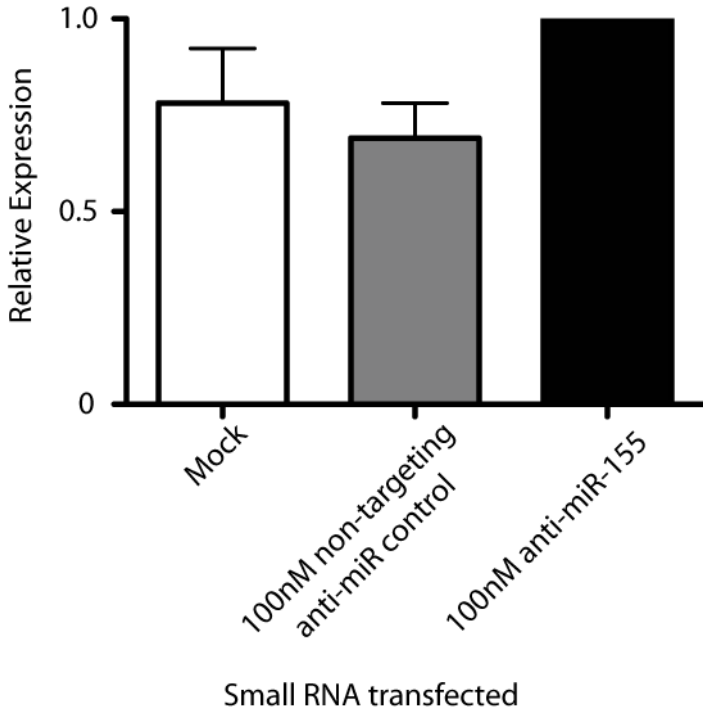

Figure 4.2.35 – Analysis of ZNF652 mRNA levels following the antagonism of miR-155 function in cultured ASMCs - ASMCs were growth arrested by serum starvation for 72 hours before Lipofectamine 2000 mediated transfection of 100nM non-targeting anti-miR control or 100nM anti-miR-155. Following a 24 hour incubation RNA was harvested and RT-qPCR performed. Results are analysed using ΔΔCt methodology through normalisation to 18S RNA as the endogenous control and expression levels are presented relative to the mock transfected sample. Error bars represent SEM, n=3.

4.3 Discussion

4.3.1 Summary and interpretation of results

The aim of the experiments described in this chapter was to identify endogenous targets for miR-155 in cultured ASMCs and to determine if the diminished abundance of miR-155 in cultured ASMCs isolated from asthmatic individuals, described in Chapter 3, may have pro-asthmatic functions. Unfortunately, despite attempting a variety of experimental strategies it was not possible to find strong evidence for an endogenous target of miR-155 in cultured ASMCs.

Initially it was confirmed that both mature miR-155 and its housing transcript, BIC, were detectable at lower levels in cultured ASMCs isolated from moderate asthmatics compared to healthy individuals (Figure 4.2.1). The fact that both the mature miRNA and the transcript from which it is derived were detected at lower levels suggests a causative mechanism at either the level of transcription of the locus or the stability of the subsequent transcript. Differential expression of both BIC and mature miR-155 has been reported in a variety of disease settings and model systems (see Chapter 4.1) and a number of factors have been identified as potential regulators of *BIC* transcription, with the majority of evidence derived from studies investigating B-cell receptor (BcR) signaling and the differentiation and activation of macrophages. van den Berg *et al.* identified an NFκB binding site in the putative *BIC* promoter (van den Berg et al. 2003) and it has subsequently been shown that increased *BIC* expression downstream of BcR signaling is mediated by factors including protein kinase C, NFκB and AP-1 (Kluiver et al. 2006) (Qinyan Yin 2008). The regulation of *BIC* transcription during macrophage differentiation has been proposed to involve the transcription factors, nuclear factor erythroid 2-related factor 1 and E twenty-six-like transcription factor 1 (Schmeier et al. 2009) whilst acute upregulation of *BIC* expression following macrophage activation has been shown to involve the MyD88/TRIF or JNK/NFκB signaling pathways, depending upon the nature of the stimulus (O'Connell et al. 2007) (Wang et al. 2010a). Interestingly, both IL-10 and glucocorticoids have been shown to inhibit the induction of miR-155 (McCoy et al. 2010) (Zheng et al. 2012). TGFβ, a factor with important roles in airway remodeling, has been reported to have varying influences on miR-155 levels, as it stimulated an increase in miR-155 expression in epithelial cells (Kong et al. 2008) but resulted in a reduction in detectable levels in lung fibroblasts (Pottier et al. 2009).

A variety of approaches were followed to determine potential mRNA targets for miR-155 in cultured ASMCs. Initially a candidate target approach was followed, whereby miRNA target-prediction algorithms, literature searches for previously validated miR-155 targets in other cell types and identification of potential targets with known roles in ASM biology were combined to select a panel of candidate genes to investigate (Table xi). Preliminary screening experiments suggested that the majority of predicted miR-155 target sites were able to facilitate miR-155 mediated regulation during *in vitro* luciferase reporter assays (Figure 4.2.4) and the potential regulation of endogenous mRNAs in cultured ASMCs was therefore investigated. A protocol was optimized to facilitate the transfection pre-miRs and anti-miRs into cultured ASMCs, which enabled the over-expression and inhibition of miR-155 respectively (Figures 4.2.7 and 4.2.8). This protocol was confirmed to result in good percentages of positively transfected cells (Figure 4.2.5) without influencing the viability of the cells at the time points that assays were performed (Figure 4.2.9). The analysis of potential endogenous targets of miR-155 focused on RhoA and MYLK, two proteins with known pro-contractile functions in ASM (see Chapter 1.5.2.2.). The hypothesis driving these investigations was that a diminished abundance of miR-155 in asthmatic ASMCs may release a repression on RhoA and/or MYLK which would shift the ASMCs towards a pro-contractile phenotype. Despite assaying mRNA and protein levels at a variety of timepoints post-transfection with pre-miR-155 or anti-miR-155, no convincing evidence for a miR-155 specific regulation of either RhoA or MYLK was generated (Figures 4.2.10 – 4.2.16). Of the evidence that was generated, it appeared that assaying mRNA or protein levels at 24 hours post-transfection allowed the greatest opportunity to detect miR-155 specific effects. The 6 hour timepoint appeared too early to identify any regulation, whilst assaying 72 hours post-transfection appeared to be influenced by non-specific effects of the non-targeting control transfection (Figure 4.2.10 and 4.2.14). Despite some encouraging evidence regarding a potential regulation of both RhoA and MYLK mRNA at 24 hours post-transfection with 20nM pre-miR-155 (Figure 4.2.10 and 4.2.14) there was no evidence of an influence on the total level of either protein (Figure 4.2.13 and 4.2.16) or of a reciprocal regulation of the mRNA following anti-miR-155 transfection (Figure 4.2.11 and 4.2.15). The possible reasons for a lack of detectable regulation following anti-miR-155 treatment are discussed in detail later. In terms of a lack of a detectable influence of miR-155 over-expression on the protein levels of either RhoA or MYLK there are likely to be two possible explanations. This first of which is that the diminution of mRNA

observed at 24 hours post-transfection with pre-miR-155 is only a trend for RhoA, which does not reach statistical significance, whilst for MYLK there is approximately half the abundance of RNA following pre-miR-155 transfection compared to non-targeting control pre-miR. Neither of these decreases is large in terms of magnitude and it may be that they are within the region of transcriptional noise and that there is no affect on the level of detectable mature protein. The second explanation is that a longer timecourse is required to identify an affect on protein levels due to the half-life of the protein. The half-life of MYLK, for example, is reported to be approximately five days and it has been shown that there is residual protein detectable sixteen days following a temporal conditional knock-out of the locus in mice (He et al. 2008). Due to the suspected non-specific effects noted at 72 hours post-transfection, however, longer timepoints were not investigated during these experiments.

The failure to identify candidate genes that demonstrated miR-155 mediated regulation lead to a change in experimental approach. Increasing evidence has indicated that a number of miRNA targets are regulated through a mechanism that involves degradation of the mRNA ((Guo et al. 2010), see Chapter 3.1.4) and because of this it was decided to perform unbiased microarray analysis of mRNA isolated from cultured ASMCs that had been subject to either mock transfection, transfection with pre-miR-155, anti-miR-155 or their respective non-targeting controls. The experiment described in Chapter 4.2.3 was intended as a preliminary screen to determine if this approach was suitable for identifying potential targets of miR-155 in cultured ASMCs. It is clear that performing the experiment in an increased number of biological replicates would enable a much higher degree of confidence in potential identified targets to be ascertained. Global expression profiling of transcript levels by both PCA and unsupervised hierarchical clustering indicated that, of the five samples analysed, cells transfected with pre-miR-155 had the greatest difference in their global mRNA expression profile in comparison to the remaining samples (Figure 4.2.20 and 4.2.21). The sample with the subsequent highest divergence in mRNA expression profile was the mock, followed by the anti-miR-155 transfection and finally the non-targeting controls. It should be noted that the differences depicted in these analyses are relative within the data set, meaning that any differences shown may be very small in terms of absolute values.

The small relative effects of anti-miR-155 noted in the global expression profiling analyses were confirmed when analysing changes in expression at the level of individual transcripts (Figure 4.2.26 and Table xiv). There were no mRNAs that demonstrated a greater than 2-fold difference in expression when comparing the anti-miR-155 transfected sample to the non-targeting control anti-miR and there was also poor consistency in the difference in detected levels of transcripts between the anti-miR-155 sample and the remaining samples (Figure 4.2.22). It would be expected that a true target of miR-155 would have increased levels of detectable transcript following anti-miR-155 transfection when compared to the other conditions. In addition, it was very disappointing to determine that no mRNAs that were detected at an increased level following anti-miR-155 transfection were also detected at a decreased level following pre-miR-155 transfection.

There are a variety of potential explanations for the lack of detectable changes in the transcript profile of cultured ASMCs following anti-miR-155 transfection reported in Chapter 4.2.3.3. It is possible that the percentage of cells positively transfected with the anti-miR (Figure 4.2.5) was too low for influences on the level of transcripts to be identified in total cell population based RNA assays. It is also possible that the decrease in the level of mature miR-155 measured during the RT-qPCR control step was an artifact of the experimental approach (Figure 4.2.8) and it is noted that there is discrepancy between the 55% transfection efficiency reported (Figure 4.2.5) and the close to 100% knock-down of miR-155 expression (Figure 4.2.8), which is suggestive of potential issues within the experiment. It is possible that a large proportion of the anti-miR-155 used in the transfection was not taken into the cells but rather remained on the plate. It cannot be determined whether this anti-miR-155 was completely removed by the PBS washes and media change included in the transfection protocol (see Chapter 2.2.1). As there is no denaturation step included in the stem-loop specific mature miRNA RT-PCR protocol (see Chapter 2.3.2) it may be that residual anti-miR-155 anneals to mature miR-155 during the RT-PCR protocol rather than within the cell itself. This would inhibit the primers annealing to mature miR-155 and lead to an over-representation of the level miR-155 loss. A second hypothesis is that due the use of a lipid mediated transfection protocol the anti-miR-155 is taken into the cell and retained in endosomes. This would result in the anti-miR-155 being unable to physically interact with endogenous miR-155, which functions in the cytoplasm as part of the RISC complex, and inhibit its function in the cell. Upon lysis of the cell during the RNA isolation procedure, however, the

anti-miR-155 would be liberated from the endosomes and able to bind to miR-155 during the RT-qPCR protocol, thus preventing its detection. It should be noted that the use of anti-miRs at comparable concentrations is widespread within the miRNA field and has been utilized in a vast number of publications in which miRNA targets have been identified. Whether anti-miRs function through directing the degradation of target mRNAs or sequestering them, either within the cell or during subsequent assays, is unclear. A third possibility is that the influence of anti-miRs may be very subtle. It is an increasing viewpoint that, in many cases, miRNAs provide a weak dampening of target gene expression (Su et al. 2011) and that cases where alterations in the level of a specific miRNA result in an overt change in the phenotype of differentiated cells, for example miR-195 in cardiac smooth muscle (van Rooij et al. 2006), are less common than originally anticipated. It may therefore be the case that a large number of repetitions would be required to distinguish a subtle regulation from experimental noise. Further support for this viewpoint is drawn from the finding that the vast majority of miRNA knock-outs in model organisms have no obvious phenotypic effect (Miska et al. 2007) and that a particular stress is required for an effect to be observed. It may therefore have been useful to use a stimulus with relevance to asthma, for example Th2-signature cytokines or pro-remodeling signals, and to investigate the influence this had on the miRNA signature of ASMCs. A final hypothesis is driven by the range of relative expression levels of miR-155 reported in healthy ASMCs (Figure 4.2.1). More pronounced results may have been achieved if an ASM culture displaying high relative levels of miR-155 expression was used in experiments during which miR-155 activity was antagonized as a higher basal level of expression may have made any effects more obvious.

The PCA and unsupervised hierarchical clustering analyses of the total transcript profiles following transfections (Figures 4.2.20 and 4.2.21) indicated that cultured ASMCs transfected with pre-miR-155 had the most divergent mRNA expression profile in comparison to the other samples. It is noted, however, that only a single biological replicate of this experiment was performed on the microarray platform and because of the lack of any convincing effects of the anti-miR-155 transfection, off-target effects of the pre-miR-155 over-expression cannot be discounted.

The greatest influence of the pre-miR-155 transfection appeared to be the 91 transcripts that were detected at increased levels in the pre-miR-155 transfected

sample compared to the non-targeting pre-miR control sample (4.2.24 and Table xiii). The most likely scenario for a miRNA causing an increase in the level of a particular mRNA is that, under basal circumstances, the mRNA is repressed by a negative regulator and that the miRNA targets this negative regulator and thus releases repression of the mRNA that is subsequently detected as being increased. There are reports of miRNAs causing the direct upregulation of target mRNAs, however, these reports appear to be specific, isolated cases (Vasudevan et al. 2007), (Ørom et al. 2008) (Ma et al. 2010). miR-155 has previously been reported to have pro-inflammatory functions in a variety of cell types and disease models (O'Connell et al. 2010) (Cardoso et al. 2011) (Su 2011) and it was noted that a number of transcripts detected at increased levels following miR-155 over-expression in cultured ASMCs were pro-inflammatory. Specifically there were a large number of chemokines that were detected at increased levels (Table xiii). Evidence as to the role of miR-155 in regulating the expression of chemokines is unclear as there are reports of miR-155 stimulating both increases (Bhattacharyya et al. 2011) and repression of chemokine expression (Nie et al. 2004) (Tang et al. 2010). Seven chemokines demonstrated increased abundance following miR-155 over-expression (Table xiii); CCL5, CXCL10, CCL8, CXCL11, CCL26, CXCL9 and CCL7 all displayed a greater than two-fold increase in mRNA levels in the pre-miR-155 transfected sample compared to both the mock and non-targeting control pre-miR transfected samples. Due to the fact that chemokines genes are often found in clusters the change in expression levels of genes surrounding some of these chemokine genes was investigated. *CCL7, CCL8* and *CCL11* are located in a gene cluster with *CCL1, CCL2* and *CCL13* and subsequent analysis indicated that although CCL1, CCL2 and CCL13 did not pass the initial filtering threshold of a greater than two-fold increase in expression between the pre-miR-155 and non-targeting pre-miR control, CCL2 and CCL13 showed a 1.8-fold and 1.7-fold increase following pre-miR-155 transfection, respectively. CCL1 was not expressed in cultured ASMCs. The genes that flank either side of this chemokine cluster, *ACCN1* and *TMEM132E,* were detected at only very low levels and did not display any evidence of miR-155 mediated regulation, suggesting that the influence of miR-155 over-expression on the chemokine loci is a specific one. RT-qPCR validation indicated that the increase in the chemokine levels following miR-155 over-expression was reproducible in a miR-155 specific manner across a number of biological replicates (Figure 4.2.27). Further time-course and concentration-response experiments were performed to analyse the regulation of CCL5 by miR-155. CCL5 was chosen for further

investigation as it appeared to have the most robust increase in expression following miR-155 over-expression and has also been implicated in the pro-asthmatic phenotype of ASM (Berkman et al. 1996) (Chhabra et al. 2007). These analyses demonstrated a trend towards an increase in CCL5 levels following miR-155 over-expression at all time points analysed, however, this was only statistically significant at 24 hours (Figure 4.2.28). In addition, the use of 4nM rather than 20nM pre-mR-155 did not result in a statistically significant increase of CCL5 levels compared to other transfection conditions, however, there was a trend towards an increase when comparing 4nM pre-miR-155 to 4nM non-targeting pre-miR control and the mock transfection (Figure 4.2.29). The mRNA data was confirmed by analysis of the levels of CCL5 protein in the cell culture supernatants following transfections, which showed very similar trends to the mRNA data (Figure 4.2.31). It is noted, however, that this experiment was only performed as a single replicate and hence strong conclusions cannot be drawn from it. Further, the lack of any reciprocal regulation of CCL5 following miR-155 antagonism means that it is not possible to confirm that this is not an off-target or non-specific effect.

A potential explanation for this broad increase in expression of inflammatory mediators following miR-155 over-expression is that miR-155 targets a negative regulator of the inflammatory phenotype and hence when miR-155 is over-expressed to a high degree the negative regulator is diminished to very low levels. When miR-155 is antagonized, however, it may be that further increases in the levels of the negative regulator had no detectable effects on the levels of chemokine transcripts as transcription of the loci was already suppressed to basal levels. A potential candidate for this negative regulator is SHIP1, as it has previously been shown to be a target of miR-155 (O'Connell et al. 2009) and has also been shown to be involved in the regulation of chemokine expression in epithelial cells (Bhattacharyya et al. 2011). It is difficult, however, to place this potential regulation into the context of asthma as the pathway would seem to be counterintuitive. The expression of miR-155 was diminished in ASMCs isolated from asthmatic compared to healthy individuals (Figure 4.2.1) and this would therefore imply that asthmatic ASMCs were less pro-inflammatory than those of healthy individuals.

37 transcripts were identified as having a greater than two-fold decrease in abundance following pre-miR-155 compared to non-targeting pre-miR control transfections (Figure 4.2.23 and Table xiii). This list of transcripts appeared to

contain genes with a broad range of functions, including structural proteins such as COL21A1 and ITGA8, transcriptional regulators such as ZNF652 and BRWD1 and non-coding RNAs such as MALAT1 and FIP1L1. When comparing this list of transcripts to potential miR-155 targets predicted by TargetScan, PITA and miRANDA only COL21A1 was predicted by all three algorithms. In addition, ZNF652, BRWD1, SEM3A, RAPGEF6 and ZNF323 were predicted by at least one algorithm. This is slightly surprising, as one would expect transcripts with a greater than 2-fold difference in expression to be direct targets of miR-155 and therefore contain predicted target sites. There are a number of possible reasons for this lack of corroboration between the predicted targets and those transcripts found to be decreased following miR-155 over-expression. All the algorithms used search exclusively within the 3' UTR for potential miRNA binding sites, however, recent data has shown that binding sites are not restricted to the 3'UTR (Hafner et al. 2010). Within the list of decreased transcripts, many may contain miR-155 binding sites in positions other than the 3'UTR. ITGA8, for example, has an 8-mer seed match within the final exon of the mRNA. It may also be the case that non-canonical binding sites are used in the number of interactions (see Chapter 3.1.3). As the target-prediction algorithms are restricted to searching for small variations of complimentary base pairing around the miRNA seed, these non-canonical binding sites may be missed. In addition, it is likely that because only a single replicate was performed on the microarray platform a number of direct targets for miR-155 did not reach the threshold of 2-fold difference in this single experiment and are therefore absent from further analysis.

RT-qPCR validation of potential direct targets for miR-155 in cultured ASMCs indicated that BRWD1, ITGA8 and ZNF652 were reproducibly detected at statistically significant lower levels following pre-miR-155 transfections compared to mock transfections. Although there was also a trend towards in decrease in the pre-miR-155 compared to the non-targeting pre-miR control transfections, this difference was not statistically significant for any of the transcripts analysed (Figure 4.2.32). Further analysis was performed to determine if ZNF652 was a direct target for miR-155 in cultured ASMCs and although potentially encouraging results were gained (Figure 4.2.33 – 4.2.35), time restrictions meant that a comprehensive analysis could not be completed.

It is therefore with regret that the work undertaken during this project has been unable to determine a *bone fide* endogenous target for miR-155 within ASMCs.

4.3.2 Future Work

Initial future work on this project could involve completing a comprehensive analysis of ZNF652 as a potential miR-155 target. This should involve similar experiments to those performed when investigating RhoA and MYLK as possible targets and it would be particularly important to determine evidence for the regulation of ZNF652 by miR-155 at the protein level. In addition, it would then be important to continue and identify the functional effects of any potential regulation of ZNF652. ZNF652 would appear to be an interesting potential target for miR-155 as it has previously been described as a transcriptional repressor (Kumar 2006) and there is experimental evidence that it is a miR-155 target in luciferase reporter based assays (Yin 2008). The report from Kumar *et al.* in 2006 was the first report detailing ZNF652 and at present only two targets for ZNF652, growth-factor independent 1 (GFI1) and transcription factor 12 (TCF12), have been identified (Kumar 2006) (Kumar et al. 2008). A recent report detailing the genome-wide binding of ZNF652 in a breast cancer cell line will hopefully allow the identification of additional targets (Kumar et al. 2011). Interestingly, genome-wide association studies have correlated a single nucleotide polymorphism (SNP) upstream of the *ZNF652* locus to the development of hypertension (Newton-Cheh et al. 2009). As hypertension is also a disease in which smooth muscle plays an important role, it may be speculated that this is suggestive of a potential role for ZNF652 in smooth muscle biology.

Alternative strategies could be used to modulate the levels of miR-155 within the cultured ASMCs and to identify potential targets. It may have been beneficial to use cells from moderate asthmatic individuals, which have lower basal levels of miR-155 expression (Figure 4.2.1), as the target cells to transfect with pre-miR-155. The rationale of this approach is that a lower basal level of miR-155 may have made any effect of the over-expression easier to detect. In terms of the modulation of miR-155 levels, it may be beneficial to use a lentiviral approach to over-express and inhibit miR-155 in cultured ASMCs. A particular benefit of this approach would be that expression plasmids could be used that contained either a miR-155 mimic or a miR-155 inhibitor in addition to a green-fluorescent protein (GFP) gene. Co-expression of the GFP protein would enable positively transduced cells to be sorted prior to

functional assays and ensure that pure populations of cells in which miR-155 had been modulated were analysed. Further, if an appropriate promoter element was used to drive expression of the miR-155 mimic, more physiological levels of over-expression may be achievable compared to those generated by the transfection of discrete miR-155 mimics. The strategy of lentiviral transductions was not used during this study due to considerations of both the financial costs involved and the technical challenges within the timescale of the project. In addition, lentiviral approaches are most beneficial when stable regulation of endogenous gene expression is required over an extended time period. It was felt that for the purposes of these experiments a transient regulation of miR-155 expression levels would be sufficient. In this regard, however, the use of stable modulations of miR-15 levels facilitated by a lentiviral approach may have enabled longer timepoints to be analysed for potential protein regulation (see Figure 4.2.12 and 4.2.16).

Alternative approaches to identify miR-155 targets include a large-scale analysis of protein levels by 'stable isotope labeling by amino acids in cell culture' (SILAC), following modulation of miR-155 expression levels (Vinther 2006) (Selbach et al. 2008). This technique involves modulating endogenous levels of a miRNA during a culture period in heavy media containing radiolabeled amino acids. Levels of radiolabeled peptides are then compared to levels of non-labeled peptides isolated from cells cultured in normal media with no manipulation of miRNA expression levels through a mass spectrometry assay. The advantages of this approach in comparison to mRNA microarrays are that it will detect regulation at the level of both mRNA stability and rate of translation as it assays protein levels. Disadvantages include the cost and accessibility of the technology. In addition the read-outs are currently less comprehensive in terms of the number of proteins analysed compared to transcriptome anlaysis, with the broadest analysis reported to assay approximately 5000 proteins (Selbach et al. 2008). The technique has been used to identify targets of miR-155 in HEK293 cells, and this analysis identified 46 putative miR-155 targets in this cell type (Lößner et al. 2011). None of these targets, however, were decreased in abundance following miR-155 over-expression in cultured ASMCs (Table xii). A second alternative approach for the identification of potential miR-155 targets in ASMCs is the PAR-CLIP approach first described by Hafner *et al.* ((Hafner et al. 2010), see Chapter 3.1.3.1). This technique involves the immunoprecipitation of the RISC complex, generally through the AGO component, and sequencing the RNA recovered to identify transcripts that are associated with

RISC. In addition, a cross-linking step performed during the assay enables the position of RISC binding and therefore potential target sequences to be identified. The technique therefore enables the identification of direct targets for of miRNA-mediated regulation along with the position of the miRNA target sequence within the transcript.

Other potential future work may involve attempting to identify a potential functional effect following the modulation of miR-155 levels in cultured ASMCs. There are a wide variety of assays that could be performed in order to investigate the functional role of miR-155, including investigations into proliferation, calcium homeostasis, contraction and the secretion of inflammatory mediators. The range of potential functional assays for ASMCs, however, means that a wide variety of assays may have to be attempted and this would have obvious implications in terms of both the availability of cells and the reagents required. It should also be noted that these assays are likely to require caution, as the influence of a single miRNA within differentiated cell types is increasingly viewed as being a subtle control on the regulation of gene expression (Su et al. 2011) (Miska et al. 2007). It may therefore be difficult to detect a functional effect following manipulation of miR-155 levels. In support of this experimental approach, however, is a recent report by Sato *et al.* describing a model of fibroblast differentiation in the presence of IL-4 (Sato et al. 2011). It was shown that fibroblasts that had differentiated in the presence of IL-4 demonstrated a decreased abundance of miR-155 and that modulation of miR-155 levels in fibroblasts had profound affects on contraction, migration and fibronectin production, however, no direct targets of miR-155 that may mediate these functional effects were identified. This report is of further relevance to the work described in this chapter as the diminished expression of miR-155 was retained following the removal of the IL-4 signal and the results are therefore analogous to the decreased abundance of miR-155 described in asthmatic ASM following a period of *in vitro* culture. It is tempting to speculate that the increased levels of IL-4 present in the inflammatory milieu of the asthmatic lung may have a role in regulating miR-155 expression in ASMCs.

Chapter 5 – Profiling histone methylations in cultured ASMCs

5.1 Introduction

5.1.1 Hierarchical organization of chromatin structures

5.1.1.1 The nucleosome

Each human cell contains approximately 2 meters of DNA (Lodish et al. 2000). It is clear that this DNA must undergo a large degree of compaction to physically fit into the nucleus. Additionally, however, this compaction must be dynamic, such that regions of DNA can be made accessible to facilitate essential metabolic processes such as DNA replication and gene transcription.

The compaction of DNA is achieved by the formation of a hierarchically organized structure known as chromatin. The fundamental unit of chromatin is the nucleosome, the crystal structure of which was solved by Luger *et al.* in 1997 using nucleosomes isolated directly *ex vivo* (Luger et al. 1997). The structure, with a resolution of 2.8Å, shows that the nucleosome consists of core histone proteins, known as Histone 2A (H2A), H2B, H3 and H4. The core histones are organized as two H3H4 dimers with a H2A/H2B dimer associated on either side. This octamer of histone proteins forms a globular protein core that associates with approximately 147 base pairs (bp) of DNA, with the DNA wrapping around the nucleosome 1.7 times in a left-hand turn (Figure 5.1.1). In addition to the core histones, linker histone (H1/H5) binding associates an additional 20 bp of DNA to produce a nucleosome containing 167bp DNA (Noll & Kornberg 1977) (Allan et al. 1980).

Figure 5.1.1 – Ribbon traces of a nucleosome particle - ribbon traces for the 146bp DNA (brown and turquoise) associated with the eight core histone proteins (blue:H3, green:H4, yellow:H2A and red:H2B). The two views are down the DNA superhelix axis for the left particle and perpendicular to it for the right. Figure taken from Luger et al. 1997.

In addition to the canonical core histones there are also a range of histone variants, the most common of which are centromeric H3 (CenH3), H3.3, H2A.Z and H2A.X (Talbert & Henikoff 2010). These variants are structural alternatives of corresponding core histones and are often precisely positioned to promote specific processes. CenH3, for example, is essential for the establishment of kinetochores and therefore has an integral role in cell division (Santaguida & Musacchio 2009). H3.3 and H2A.Z have both been described to enrich at the promoters of genes within euchromatic regions (Ahmad & Henikoff 2002) (Schwartz & Ahmad 2005) (Raisner et al. 2005) (Barski et al. 2007). Early data from model organisms suggested that the presence of H2A.Z correlated with transcriptional competency (Allis et al. 1980) and more recent genome-wide studies in mammalian cells have indicated a positive correlation between the presence of H2A.Z and the transcriptional activity of a gene (Barski et al. 2007). H3.3 is deposited at gene promoters following transcriptional induction of the locus (Tamura et al. 2009) (Placek et al. 2009) and its presence may have a role in the propagation of an active transcriptional state (Jin et al. 2009). The function of H3.3 and H2A.Z at promoters is incompletely understood. It has been proposed that nucleosomes containing both H3.3 and H2A.Z are enriched around transcriptional start sites and that their decreased stability compared to canonical nucleosomes facilitates transcription (Jin et al. 2009). *In vitro* studies have produced varying results regarding the stability both H3.3 and H2A.Z in comparison to their canonical partners (Abbott 2001) (Zhang et al. 2005) (Park et al. 2004), (Thakar et al. 2009) and it has been proposed that the effect may be mediated by cooperativity between the two variants or a decrease in the ability of H3.3 to associate with H1 linker histones (Braunschweig et al. 2009). H2A.Z has been reported to 'slide' along DNA in a thermally driven process and this characteristic may have a role in facilitating transcription (Flaus et al. 2004). As a demonstration of how incomplete our understanding of the role of variant histones is, H3.3 has been shown to enrich in regions of pericentric heterochromatin and telomeres (Wong et al. 2008), whilst H2A.Z is enriched at the promoters of both active and non-active genes in euchromatic regions (Raisner et al. 2005) and is required for the repression of a number of euchromatic genes (Meneghini et al. 2003). It is clear therefore that there is much to learn regarding the function of histone variants.

Although the structure of the core nucleosome is well defined and understood, the nature of higher-order chromatin structures is in many cases controversial. The obvious necessity for further compaction of DNA, along with structures such as

metaphase chromosomes and lampbrush chromosomes, makes it clear that higher order structures must exist. The mechanism by which this compaction is facilitated, however, is unclear.

5.1.1.2 The 'beads-on-a-string' structure

Following the association of DNA with histones to form nucleosomes, the next level of chromatin organization is widely accepted to be a 'beads-on-a-string' fibre, whereby a 'string' of linker DNA joins 'beads' of individual nucleosomes. Adjacent nucleosomes are separated by linker DNA, which may vary in length between 0 and 80 bp in both a species and tissues specific manner (Prunell & Kornberg 1982). Studies isolating chromatin from nuclei and then reducing the ionic concentration *in vitro* have allowed such a beads-on-a-string structure to be visualized, indicating that it may be a component of chromatin structure (Thoma et al. 1979). Attempts to identify a beads-on-a-string structure *in vivo*, however, have proved extremely difficult. This has lead to conjecture that the structure may merely represent an intermediate state of compaction that does not exist stably *in vivo*. Recent data from Santangelo *et al.*, however, has indicated the presence of a native beads-on-a-string structure (Santangelo et al. 2009). Here the authors use comparisons of micrococcal nuclease and DNase I digestion of native chromatin to identify the presence of an open beads-on-a-string structure within the *IL4* gene of *in vitro* differentiated Th2 cells that is not present in Th1 cells, suggesting that the formation of a 'beads-on-a-string' structure may indeed be a stable state of chromatin compaction in cells.

5.1.1.3 30nm chromatin fibres

Interaction between nucleosomes is believed to facilitate further compaction of the 'beads-on-a-string' structure into a 30nm fibre. Early electron microscope studies of native chromatin isolated from nuclei inspired the proposal of two models for the formation of this structure. The first model is a solenoid structure whereby adjacent nucleosomes are connected by a linker DNA of 6-8 nucleotides, resulting in a helical path that can be formed regardless of variation in individual nucleosome length (Widom & Klug 1985). The second proposal is a zig-zag, or 2-start turn, helical structure in which adjacent nucleosomes are connected by straight sections of linker DNA, meaning that the resulting fibre formation is sensitive to differences in individual nucleosome length (Williams et al. 1986). It was proposed that a possible explanation for the variation in observations of the 30nm fibre structure was the intrinsic heterogeneity of using chromatin isolated *ex vivo.* To overcome this

potential issue more recent studies have used DNA sequences with strong nucleosomal positioning elements to reconstitute nucleosomal repeat lengths *in vitro.* Dorigo *et al.* used the Widom 601 nucleosome binding DNA sequence to reconstitute short nucleosomal lengths and reported the spontaneous formation of structures similar to the proposed two-start helix without a requirement for linker histones (Dorigo et al. 2004) (Schalch et al. 2005). Concerns raised about these reports, however, included the fact that the length of nucleosomal array used was too short to enable the formation of a solenoid structure and that the structures were solved in high concentrations of Mg^{2+} that are very uncommon physiologically. Indeed, a separate study from Robinson *et al*. used nucleosomal repeats of differing lengths and although they were unable to solve the complete structure, the dimensions greatly favoured a solenoid rather than zig-zag structure. Furthermore, when linker histones were not included the nucleosome repeat length formed a ladder structure very similar to that reported by Schalch *et al.* (Robinson et al. 2006).

5.1.1.4 Higher-order structures

The mechanisms facilitating the compaction of chromatin above the 30nm-fibre become increasingly controversial and poorly understood, however, the existence of structures such as metaphase chromosomes indicates that further compaction can take place. Textbook images (see Figure 5.1.2) often depict a radial loop model in which the 30nm chromatin fibre is anchored by axial folding around scaffolding proteins such as topoisomerase 2, condensin I and condensin II to form scaffold-associated regions. A number of approaches to disrupt proteins thought to be essential for the formation of scaffold-associated regions have, however, resulted in no disruption to metaphase chromosomes. This has lead to uncertainty within the field as to the precise mechanisms involved in facilitating further compaction of chromatin (Belmont 2006).

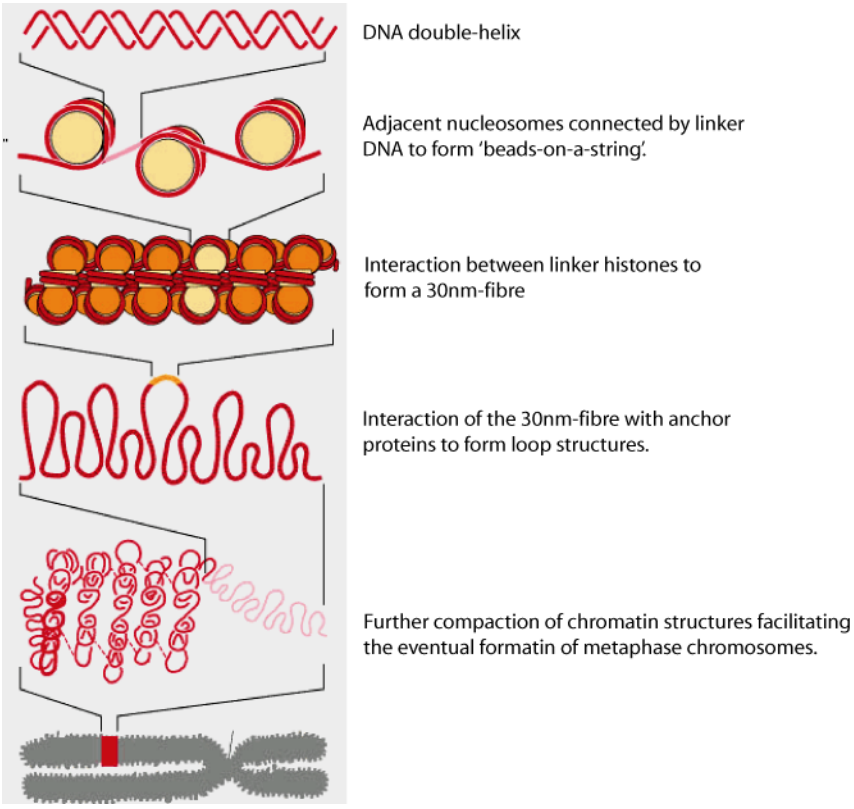

Figure 5.1.2 – Hierarchical formation of chromatin structures – A number of protein:protein interactions facilitate the organization of hierarchical structures facilitating compaction of DNA into the nucleus of a eukaryotic cell. Image taken from Alberts et al 2002.

5.1.2 Histone modifications

As stated previously, the structure of individual nucleosomes and their constituent histones is now well understood. An important feature of the nucleosome structure is that the unstructured N-terminal tails of the core histones protrude beyond the associated DNA (Figure 5.1.1) (Luger et al. 1997). These N-terminal tails, and to a lesser extent the C-terminal tails and core regions, of histones are subject to extensive post-translational modifications, with over 70 residues reported to undergo modifications in specific circumstances. This variation in the modification state of histones contributes to the regulation of gene expression through influencing the compaction of local chromatin structures and facilitating the targeted recruitment of specific transcription factors and co-factors in a controllable manner.

5.1.2.1 Acetylation of histone lysine residues

Acetylation was first described in 1964 by Allfrey *et al.* (Allfrey et al. 1964). The modification is caused by the addition of an acetyl group to the ε-amino group of a lysine residue (Figure 5.1.3). The acetylation of core histones results in the neutralisation of the positively charged lysine, leading to a weakening of the interaction between the histone and the negatively charged phosphate backbone of DNA (Puig et al. 1998). A variety of studies have indicated that this results in increased accessibility of DNA for transcription factors (Lee et al. 1993) (Juan et al. 1994), however, the majority of these studies have been performed *in vitro* and there are reports to dispute this phenomenon (Lutter et al. 1992). Despite this, the majority of evidence supports the role of acetylation in active transcription and correlative evidence shows that acetylation of core histones is generally associated with regions of chromatin from which active transcription occurs, whilst hypoacetylation is associated with regions not permissive for transcription (Kurdistani et al. 2004). Examples of the functional influences of specific acetylation events include histone 4 lysine 16 acetylation (H4K16Ac) preventing the formation of 30nm-like fibres, ensuring nucleosomes retain an 'open' structure (Shogren-Knaak et al. 2006) and acetylation of H4K56, present within the globular core of the histone, which facilitates the accessibility of DNA around mononucleosomes (Neumann et al. 2009).

The process of histone acetylation is dynamic, with the level of acetylation determined by actions of enzyme families with opposing functions. The addition of acetyl groups to lysine residues is catalysed by histone acetyl-transferases (HATs) whilst their removal is facilitated by histone deacetylases (HDACs). HATs are described as Type A or Type B family members. Type B HATs are localised in the cytoplasm and are responsible for the acetylation newly synthesized H4 at K5 and K12, which is required for the deposition of these histones in chromatin, after which the marks are removed (Parthun 2007). Type A HATs are more diverse and are responsible for the nuclear modification of histones. They are often divided into four main families, based upon homology of the HAT domain and conformational structure. These groups comprise the GCN5/PCAF, MYST, p300/CBP and RH-109 families (Marmorstein & Trievel 2009). Of these families the GCN5/PCAF and MYST families have homologs that are conserved from yeast to man, whilst the p300/CBP family and RH-109 family are metazoan and yeast specific respectively. HATs are often found within large multi-protein complexes that act to influence their

substrate specificity. The yeast HAT GCN5 has been shown to acetylate free histones when acting as a holoenzyme, however, when present within the SAGA complex, GCN5 is able to efficiently acetylate histones within a nucleosome (Grant et al. 1997). In addition to the acetylation of histones, HATs have been shown to acetylate non-histone proteins, for example the tumour suppressor p53 (Gu & Roeder 1997).

HDACs are classified into two broad families based upon sequence similarity and co-factor dependency. Classical HDACs, including HDAC1 and 2, have a high level of sequence similarity and require Zn^{2+} as a co-factor for deacetylation. The Sir2-related protein families (Sirtunin), however, have no sequence similarity to the classical family members and rely upon NAD^{+} rather than Zn^{2+} as a cofactor (Marmorstein & Trievel 2009). HDACs are believed to have relatively little intrinsic substrate specificity, with a single enzyme being capable of deacetylating multiple sites within a histone. It is therefore proposed that the specificity of HDACs is governed by other factors within large multiprotein complexes. Further complication is added as multiple HDACs are often found within the same complexes, for example HDAC1 and HDAC2 are found within the NuRD, Sin3a and Co-REST complexes, making it difficult to distinguish the contribution of individual HDAC proteins (Zhang et al. 1998) (Denslow & Wade 2007) (Nicolas et al. 2007) (Tahiliani et al. 2007).

5.1.2.2 Methylation of histone lysine residues

In addition to acetylation, histone lysine residues can also be methylated. Lysine methylation has an added degree of complexity compared to acetlyation as an individual lysine residue can be mono, di or trimethylated (me1, me2 and me3) (Figure 5.1.3). Unlike acetylation, the functional outcomes of histone lysine methylation are not facilitated by an alteration in the interaction between DNA and histone proteins, but rather through the recruitment of specific effector proteins containing domains that recognize specific methylation modifications. This concept is integral to our current understanding of the role of histone modifications in the control of gene expression and is discussed in Chapter 5.1.4.

The methylation of lysine residues is catalysed by Histone Lysine Methyltranferases (HKMTs). The first human HKMT to be discovered was an enzyme involved in H3K9 methylation, known as SUV39H1 (Rea et al. 2000). It was identified as a homologue of the *D. melanogaster* Su(var) 3-9 protein, a member of a family of three proteins

that contained an evolutionary conserved 130 amino acid sequence, known as a SET domain. Since the initial discovery of SUV39H1, more than 50 HKMTs have been identified and all except Dot1 contain the conserved SET domain (van Leeuwen et al. 2002). The majority of identified HKMTs can be classified into one of six families based upon sequence homology within and around the SET domain (Upadhyay & Cheng 2011). It should be noted that a number of HKMTs, including SET7 and SET9, which deposit the well-studied H3K4 methylation marks, do not fit into this family classification due to differing sequences flanking the SET domain. Unlike HATs, HKMTs have very strict substrate specificity. This is relatively simple in model budding yeast systems used to study histone modifications as H3K4, H3K36 and H3K79 are specifically targeted by KMT2/SET1, KMT3A/SET2 and KMT4/Dot respectively (Allis et al. 2007). In mammals, however, HKMTs usually catalyse the deposition of a specific methylation mark onto a specific lysine, for example KMT3A (Setd2) catalyses the tri-methylation of H3K36 and its depletion in cultured cells results in an acute loss of H3K36me3 with no affect on H3K36me1 or H3K36me2 (Edmunds et al. 2008).

A major alteration in our appreciation for the role of histone methylation in the regulation of gene transcription has been stimulated by the discovery of histone demethylases. The discovery of histone demethylases has shown that histone lysine methylation is a dynamic process and thus could be regulated by signaling pathways in order to influence the transcriptional state of target genes. Histone lysine demethylases (HKDMs) are of two general classes. The first class are amine oxidases and include the first HKDM to be discovered, LSD1 (Shi et al. 2004). These enzymes utilize a flavin adenine cofactor to form an imine intermediate, which then undergoes hydrolysis. Their requirement for a protonated nitrogen, however, means that they can only target the removal of me1 and me2 modification states. The second class of HKDMs are JmjC domain-containing proteins exemplified by JHDM1 (Tsukada et al. 2006). These enzymes are members of the Cupin superfamily of proteins and are iron and α-ketogluarate dependent oxygenases that can catalyse the removal of all three methylation states.

5.1.2.3 Other histone modifications

In addition to the widely studied acetylation and methylation of lysine residues, histones are subject to a variety of other modifications. Methylation of arginine residues is a common modification at H3R2, R8, R17 and R26 and H4R3 and there

are reports that it has roles in defining regions both active and repressed transcription (Kouzarides 2007). Phosphorylation of histones at serine, threonines and tyrosine residues is believed to induce a negative charge on the histones and thus induce alterations in local chromatin structure. In addition, ADP ribosylation, ubiquitylation, SUMOylation and the addition of β-N-acetylglucosamine groups to amino acids of core histone proteins have all been reported (Kouzarides 2007).

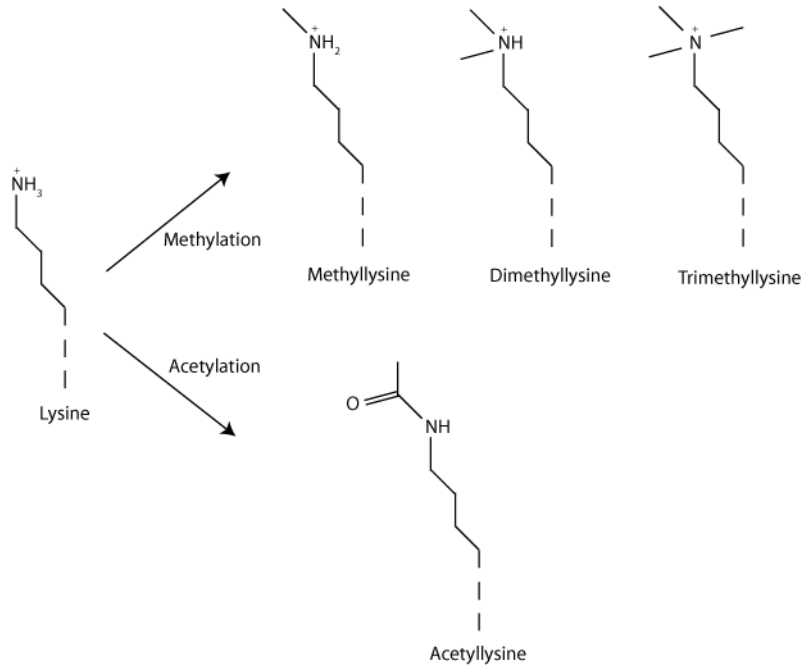

Figure 5.1.3 – Structure of a lysine residue and the impact of methylation and acetylation modifications

5.1.3 Histone modifications demarcate specific functional regions of chromatin

Recent experimental approaches allowing the simultaneous analysis of multiple loci across the genome have facilitated the identification of signatures, comprising a combination of histone modifications and the binding of specific proteins, which demarcate particular functional domains within chromatin. These studies have confirmed previously identified features, such as general hyperacetylation across regions of transcriptional activity (Birney et al. 2007), whilst they have also allowed more specific features to be annotated. The transcriptional start sites (TSS) of genes undergoing active transcription are enriched in H3K4me3 with H3K4me1/2 flanking both the upstream and downstream regions of this enrichment (Barski et al. 2007). Further analysis has indicated that these marks indicate genes that are undergoing transcription initiation and that addition modifications are present at loci undergoing productive transcriptional elongation. H3K36me3, for example, is enriched across the gene body of loci undergoing productive transcription (Barski et al. 2007), with recent data indicating that this enrichment is specific to exons (Kolasinska-Zwierz et al. 2009) and is potentially intrinsically linked to functional co-transcriptional splicing (Kim et al. 2011). It has been proposed that the specific enrichment of H3K36me3 across exons is an indirect reflection on an increase in the level of nucleosome occupancy across exons compared to introns (Schwartz et al. 2009). H3K79 methylation is also enriched across the body of genes undergoing active transcriptional elongation, providing an additional marker to distinguish between productive and unproductive transcription (Morillon et al. 2005). *Wang et al*. have proposed that promoters of actively transcribed genes are associated with a module of approximately 17 histone modifications and that the addition of further modifications to this module facilitates increases in transcription levels (Wang et al. 2008). Silent genes, in contrast to actively transcribed genes, are associated with a loss of acetylation and high level of H3K27me3 and H3K9me3 (Barski et al. 2007).

Analysis of multiple genomic regions has also allowed the identification of regulatory regions that are not associated with the promoter region of a gene. Data from the Encyclopedia of DNA Elements (ENCODE) Project, analysing the functional elements across 30Mb (~1%) of the human genome, have indicated that 53% of the regulatory regions within the genome, as determined by sites of DNase I hypersensitivity and H3 or H4 hyperacetylation, are located more than 2.5kb from annotated TSSs and are thus regarded as distal regulatory regions (Birney et al.

2007). Different classes of distal regulatory regions can be discriminated by signature combinations of histone modifications and the binding of protein factors. Insulators, for example, are associated with H3Ac and the protein CCCTC-binding factor (CTCF) (Birney et al. 2007). Guelen *et al*. have shown that regions demarcated by CTCF often associate with the nuclear lamina, suggesting that these regulatory regions may be important in the formation of higher-order chromatin structures and the division of chromatin into large domains whose transcriptional activity can be independently regulated (Guelen et al. 2008). Distal enhancer regions are demarcated by H3K4me1 (Heintzman et al. 2007), H3 Acetylation (Birney et al. 2007), the H2A variant H2A.Z (Birney et al. 2007) and the transcriptional coactivator p300 (Visel et al. 2009). Current models propose that distal enhancers function through a 'loop-model', whereby regulatory elements distal to core promoters in the linear DNA sequence are brought into proximity of the gene they regulate by interactions between factors bound at the enhancer and promoter. The resulting interactions allow increased levels of transcription from the particular gene. Interestingly, a recent study has suggested that enhancer regions with the potential to be active in a particular cell type are permanently demarcated with H3K4me1 and following the transition to an active enhancer they are modified to H3K4me3 (Pekowska et al. 2011).

5.1.4 Recognition of modified histone residues

The discovery of a number of protein domains able to recognize specifically modified histones has promoted the viewpoint that the specific modification of histones allows the recruitment of defined effector proteins in a manner that is rapidly and dynamically controllable by upstream signaling pathways.

5.1.4.1 Recognition of acetyl-lysine

In addition to influencing the structure of chromatin, acetyl-lysine is specifically recognized by proteins containing the bromodomain formation of protein folds. The first bromodomain to be described was that of p300/CBP-associated factor (PCAF), the mammalian homologue of the yeast HAT GCN5, which binds H4K16Ac. Crystal structures showed that this domain was formed of a left-handed, anti-parallel four-helix bundle with a hydrophobic binding pocket at one end (Dhalluin et al. 1999). Binding of acetyl-lysine residues was shown to be mainly mediated by hydrophobic interactions, with a specific hydrogen bond formed between the acetyl arbonyl and an amide nitrogen of a conserved asparagine residue within the binding pocket. The

fact that PCAF also contains a HAT domain indicates a potential mechanism for the dispersal of acetylation from an initially modified region. Evidence for a direct role of acetyl-lysine in the recruitment of the transcriptional initiation machinery has also emerged. Transcription initiation factor TFIID subunit 1 (TAF1), the largest subunit of Transcription Factor II D, contains a double bromodomain that binds to multiply acetylated H4 peptides. The crystal structure of the double bromodomain has shown the two binding pockets are separated by a gap of ~25Å, suggesting preferential binding to peptides with acetylated lysines seven residues apart (Jacobson et al. 2000). In support of this, of the binding partners tested *in vitro*, the strongest interaction was between TAF1 and H4 peptides acetylated at K5 and K12. This interaction suggests a mechanism by which acetyl-lysine may influence the recruitment of the transcription initiation machinery to TSSs.

5.1.4.2 Recognition of methyl-lysine

The addition of increasing numbers of methyl groups to lysine residues, from me1 to me3, causes an increase in the hydrophobicity and cation radius of the residue. As such, tri-methyl lysine requires a binding partner with similar hydrophobic properties and the ability to accommodate the positive charge of the methyl-lysine. In view of this, the domains currently reported to bind methyl-lysine share the characteristics of a binding pocket formed of aromatic residues, with increasing methylation states having a greater reliance on cation-π type interactions, rather than hydrosteric interactions to facilitate binding (Taverna et al. 2007) (Hughes et al. 2007).

5.1.4.2.1 Royal superfamily domains

The initial methyl-lysine recognition domain to be described was identified as a region of sequence homology between hetrochromatin-1 (HP-1) and Polycomb (Pc), two proteins involved in epigenetic repression (Paro & Hogness 1991). This domain was subsequently termed a chromodomain. Further analysis has determined that HP1 binds H3K9me3 specifically (Lachner et al. 2001), (Bannister et al. 2001), whilst Polycomb has been shown to recognise H3K27me3 (Min et al. 2003). Structural studies of the HP1 chromodomain have determined that it binds H3K9me3, but not unmethylated H3K9, via a binding pocket of three aromatic residues that form cation-π interactions with the methyl groups (Jacobs & Khorasanizadeh 2002) (Nielsen et al. 2002). The ability of HP1 and Pc to recognize different methylated lysine residues is facilitated by the extended binding pocket of

Pc, which allows the interaction with five additional residues of the histone peptide (Fischle et al. 2003).

Chromodomains have also been reported in proteins associated with active transcription. Chromodomain-helicase-DNA-binding protein 1 (CHD1), a protein that facilitates ATP-dependent nucleosome assembly and mobilization at sites of active transcription (Lusser et al. 2005), contains a double chromodomain at its N-terminal region. This double chromodomain is able to bind H3K4me2 or me3, but not monomethylated or unmethylated K4 (Flanagan et al. 2005). As for HP1 and Pc, the interaction is facilitated by cation-π interactions between aromatic residues of the chromodomain, in this case tryptophans, and the methyl groups. JMJD2A, a HKDM discussed in Chapter 5.1.2.2, also contains a double chromodomain capable of recognizing H3K4me3 (Huang et al. 2006). This ability of a HKDM to be targeted to sites of active initiation of transcription suggests a potential mechanism for regulating the control of gene transcription.

Members of the Royal superfamily are also able to recognize lower methylation states. P53-binding protein (53BP1), a protein involved in the repair of doublestrand DNA breaks (Sanders et al. 2004), is able to bind H4K20me1/2 through a tandem tudor domain. Structural studies have shown that this tandem chromodomain forms two separate binding pockets, unlike the single binding pocket of the double chromodomains (Botuyan et al. 2006).

5.1.4.2.2 Plant Homeodomain (PHD) Fingers

In addition to members of the Royal superfamily of domains, PHD fingers have evolved in a convergent manner to recognize methyl-lysine. As an example of PHD recognition of methyl-lysine, the PHD finger of Bromodomain PHD finger transcription factor (BPTF), the largest subunit of the nucleosome remodeling factor (NURF) (Tsukiyama & Wu 1995), is capable of specifically binding to H3K4me2/3 (Wysocka et al. 2006). The crystal structure of the BPTF PHD finger interacting with a H3K4me3 peptide has indicated that the binding is facilitated by the H3K4me3 peptide inserting into the PHD finger and extending it, thus forming extensive contacts with the internal surface of the PHD finger (Li et al. 2006). Vermeulen *et al.* have used a stable isotope labeling by amino acids in cell culture (SILAC) protocol to identify factors that bind H3 peptides containing the H3K4me3 modification (Vermeulen et al. 2007). These studies reported very interesting findings, as TFIID

was shown to preferentially interact with H3K4me3 through the PHD finger of TAF3, providing an additional functional link between the presence of H3K4me3 at the transcriptional start site of active genes and the transcriptional machinery.

5.1.5 The influence of multiple histone modifications

The complexity produced by the modification of histones is increased by interactions between individual modifications. Certain modifications preclude others, most obviously in the case of distinct modifications on the same residue, whilst some histone modifying enzymes are reliant on the prior deposition of a separate mark to perform their function. In addition, many regulatory proteins are found within large complexes containing recognition domains for a number of different histone modifications.

There are numerous examples of an initial histone modification being required for, or promoting, the deposition of a subsequent mark. The first evidence for such a mechanism was the demonstration that H3S10 phosphorylation stimulates the acetylation of H3K14 by GCN5 (Cheung et al. 2000). Additional examples include the requirement of H2B monoubiquitination for proper H3K4 methylation by the COMPASS complex (Lee et al. 2007b) and reports that mutations of H3K14, which prevents any acetylation events at this residue, result in the specific loss of H3K4me3 (Nakanishi et al. 2008). Yng1, a component of the NuA3 HAT complex, binds to H3K4me3 at TSSs via a PHD finger domain and thus facilitates the recruitment of the HAT complex and local acetylation of lysine residues (Martin et al. 2006a) (Taverna et al. 2006). H3K4me3 is also bound by complexes with HDAC activity, such as ING2, indicating that there are additional components of regulation and intricacies (Shi et al. 2006).

Certain modifications can preclude the deposition of others. H3R2me3, for example, prevents the methylation of H3K4 by Set1/COMPASS complexes in yeast and COMPASS-like complexes in mammals (Guccione et al. 2007) (Kirmizis et al. 2007), whilst the chromodomain containing protein, HP1, is unable to bind H3K9me when the adjacent S10 is phosphorylated in the context of either mitosis (Fischle et al. 2005) or active transcription (Mateescu et al. 2008).

A recent study by Zippo *et al.* investigating the regulation of the well-studied serum responsive gene *FOSL1* has emphasized the importance of the temporal deposition

of histone modifications (Zippo et al. 2009). It was shown that H3 phosphorylation is required for the acetylation of H4, which in turn allows the recruitment of the RNA polII elongation factor, P-TEFb. In addition, required phosphorylation events at the promoter and enhancer of *FOSL1* are performed by distinct kinases. Mitogen- and stress-activated protein kinase (MSK) 1/2 phosphorylated promoter proximal histones at early timepoints, whilst the subsequent phosphorylation of the enhancer region was performed by proto-oncogene serine/threonine-protein kinase (PIM) 1. To date, this is one of the best descriptions of the multiple enzymes that must be recruited to and function at distinct regulatory sites of a single gene to stimulate its transcription.

5.1.6 Complexes containing multiple modification recognition domains

The majority of examples discussed above describe instances whereby an initial modification either permits or prevents the recruitment of a secondary enzyme. Increasing emphasis is being placed on the potential for cooperative binding between multiple histone binding modules in an individual protein or a multi-protein complex. This interest has been stimulated in a large part by the fact that individual interactions between histone binding modules and modified histones are often too weak to facilitate the necessary targeting of effector proteins (Ptashne 2007) and the numerous examples of multiple readers for a single histone modification.

There are widespread examples of multiple histone binding modules targeting proteins or complexes. The double bromodomain of TAF1, for example, targets multiply acetylated H4 peptides (Jacobson et al. 2000) and the combined action of a PHD and chromodomain is required to direct the HDAC Rpd35 to regions of actively transcribed chromatin (Li et al. 2007). Despite this, there are relatively few reports suggesting true cooperativity. Lindroth *et al.* have demonstrated that the *A. thaliana* methyltransferase, CMT3, contains two chromodomains and is targeted to heterochromatic regions. It is only able to bind, however, when both H3K9 and H3K27 of the same peptide are trimethylated, with each individual interaction alone being too weak to permit binding (Lindroth et al. 2004). More recently, it has been reported that BPTF, which contains a PHD finger-linked bromodomain (Li et al. 2006) simultaneously recognizes H3K4me3 and acetylated lysines. Interestingly, it has been shown that although the acetyl-lysine binding is promiscuous in the absence of H3K4me3, binding of the PHD finger to H3K4me3 targets the

bromodomain to specific acetyl-lysine residues and that the dual affinity of the two interactions is greater than the sum of the individuals, suggesting true cooperativity (Ruthenburg et al. 2011).

Increasingly elegant *in vitro* experimental approaches are now being utilised to investigate both the binding of proteins to individual peptides compared to those in context of nucleosomes and the influence of multiple modifications on the recruitment of proteins. Bartke *et al.* and Nikolov *et al.* have used SILAC nucleosome affinity purifications (SNAP) and chromatin affinity purifications, respectively, to investigate both of these phenomena (Bartke et al. 2010) (Nikolov et al. 2011). Both reports used *in vitro* reconstituted nucleosomes with or without the presence of specific histone modifications to identify proteins that were able to bind specifically modified histones in the context of nucleosomes. A finding of particular interest was that the majority of proteins either bound to modified individual peptides or modified peptides in the context of a nucleosome, but that very few were able to target modified amino acids in both contexts. In addition to using the SNAP technique to identify proteins that bind to modified histones in the context of a nucleosome, Bartke *et al.* also used the system to look at the combinatorial influence of DNA methylation and histone methylation. DNA methylation involves the C5 methylation of DNA at cytosines within CpG dinucleotides. It is usually linked to transcriptional repression and is present throughout the genome (Bernstein et al. 2007). Recent genome-wide screens have demonstrated a very strong negative correlation between the presence of DNA methylation and H3K4me3 (Laurent 2010). Bartke *et al* demonstrated that the Origin Recognition Complex (ORC) bound to H3K9me3 or H3K27me3 modified histones and was localised to heterochromatic nuclear regions. Interestingly, the binding of the ORC was increased when H3K9me3 or H3K27me3 modified nucleosomes were associated with methylated DNA. In addition, the K36 demethylase KDM2A, which had previously been demonstrated to bind unmethylated CpGs through a CXXC-type zinc finger (Blackledge 2010), was shown to bind to K9me3-modified nucleosomes and this binding was disrupted by presence of methylated DNA. These experiments demonstrate that, although the use of single peptides has formed the foundation of our current knowledge of histone binding proteins, increasingly sophisticated approaches are required to identify more biologically relevant targets. In addition, the report of Bartke *et al.* has demonstrated that the influence of histone

modifications and DNA methylation is impacted by the wider context in which an individual modification is found.

5.1.7 Approaches used to study histone modifications

As discussed above, the post-translational modification of histones represents an important facet in the regulation of gene transcription through influences on chromatin structure, the demarcation of specific regulatory regions and the recruitment of specific transcription factors and co-factors. To determine the localisation of specific histone modifications a technique known as chromatin immunoprecipitation (ChIP) is utilised. ChIP involves the isolation of chromatin fragments from the cell type of interest at an appropriate size range to enable the accurate determination of the position of the nucleosome containing a modified histone. As nucleosomes associate with approximately 160bp of DNA this is often the size of fragment used to study histone modifications. The isolated chromatin is subject to immunoprecipitation with an antibody raised against the specific histone modification of interest, therefore, as with all protein studies, it is clear that ChIP is absolutely reliant upon the fidelity and specificity of the antibody used. In addition to DNA that has been subject to ChIP, a positive and negative control of Input DNA and isotype antibody control immunoprecipitated DNA are routinely analysed. Input DNA is chromatin that has not been exposed to antibody but has otherwise been treated in an identical manner to the ChIP sample. Its contents should therefore represent total fragmented genomic DNA and act as a control to allow determination of the recovery of DNA sequences from across the genome during the chromatin preparation procedure. Isotype antibody control immunopreciptiated DNA gives an indication of the level of non-specific interaction between sequences of DNA and the isotype of antibody, therefore giving a level against which specific enrichment of a DNA sequence in the ChIP sample can be determined.

A number of approaches can be used to identify the regions of DNA recovered from a specific ChIP and therefore determine the position of nucleosomes containing a histone marked with a specific modification. Quantitative PCR (qPCR) of ChIP material (ChIP-qPCR) allows the identification of specific DNA sequences associated with modified histones. By using specific primer sets, enriched recovery of a specific DNA sequence in the ChIP sample above the non-specific recovery of the control antibody sample can be determined. Advantages of the technique include its speed, price and the fact that little starting material is required. Disadvantages, however,

are that only a small number of regions are analysed, which can make it difficult to accurately judge specific enrichments, whilst the restriction of analyses to pre-determined regions for amplification can mean that important and interesting information is missed. ChIP followed by next-generation sequencing (ChIP-seq) utilises next-generation sequencing to identify all DNA recovered from a ChIP. These determined sequences are then aligned to the reference genome of the species of interest to map the position of modified nucleosomes (Kharchenko 2008). The main advantages of ChIP-seq are the unbiased identification of ChIP-enriched regions across the entire genome and the fact that the number of sequences analysed means that robust statistical analysis can be performed. Negatives, however, include the cost and the specific expertise required both to perform the experiment and to store and analyse the large amount of data produced. A third option to identify DNA isolated from ChIP experiments is to hybridize the DNA to a tiling array of predetermined oiligonucleotides (ChIP-chip). In many ways this approach represents a compromise between ChIP-qPCR and ChIP-seq as it allows the analysis of multiple gene loci but is ultimately still biased and limited by the content of the array. It is possible to run whole-genome tiling arrays, however, ChIP-seq usually offers a more economic option for this analysis.

In summary these approaches offer different options to study regions of DNA associated with modified histones, each of which has positives and negative aspects. The choice of which analysis to use should therefore be governed by the specific question to be answered in an individual investigation.

5.1.8 Identification of regions of enrichment in ChIP-seq experiments

As discussed above, the advent of ChIP-seq technology has facilitated the unbiased identification of regions in the genome associated with specific histone modifications. This powerful experimental technique, however, has generated a requirement for novel bioinformatics tools that are able to identify regions in the ChIP sample that are enriched above background levels. There are now a number of algorithms designed for this analysis, for example 'Model-based Analysis of ChIP-seq' (MACS) (Zhang et al. 2008) and 'Spatial clustering approach for the Identification of ChIP-Enriched Regions' (SICER) (Zang et al. 2009). These algorithms utilise a similar workflow to identify regions of enrichment in a ChIP sample compared to an Input control sample. Initially the reference genome is divided into windows of a given number of base pairs as determined by the user

according chromatin fragment size used in the initial ChIP. The uniquely aligned sequence reads generated from the ChIP and Input samples are then counted for each of these windows. ChIP enriched regions are defined as those windows with a statistically significant greater number of reads in the ChIP sample compared to the Input (Figure 5.1.4, A)).

SICER is particularly useful for the study of histone modifications as it can be customised to identify broad regions of enrichment. Functionally, SICER initially models the random distribution of reads across the genome for a defined number of uniquely aligned reads. Regions of enrichment in the ChIP sample are then identified by comparison to the random background model and the strength of the ChIP signal is compared to that of the Input control to determine statistical significance. The important feature facilitating the identification of broad regions of enrichment is that the user can define a maximum number of non-enriched windows between two windows that are classified as enriched. For values under this cutoff the region will be called as a single enrichment (Figure 5.1.4 B)). Broad regions of relatively low levels of enrichment over Input will often have gaps due to insufficient sequencing depth and this feature of SICER allows compensation for this phenomenon.

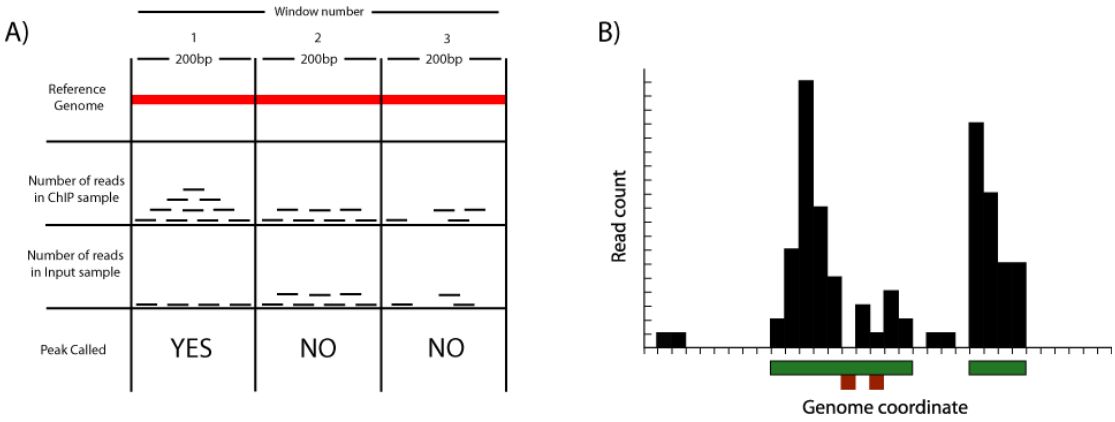

Figure 5.1.4 – A diagrammatic depiction of the action of ChIP-seq peak finding algorithm SICER – A) The reference genome (Red) is divided into 200bp windows (1, 2 and 3) and the number of uniquely aligned sequences generated from the Input control and specific ChIP samples are counted within each window. If there is a statistically significant greater number of aligned reads in the ChIP sample compared to the Input (window 1) then a peak is called. If there is no difference (window 2) or the difference is not significant (window 3) then no peak is called. **B)** SICER allows the identification of broad regions of enrichment as windows without a called enrichment are tolerated within a large peak region based on criteria defined by the user. Green bars indicate called peak regions and red bars indicate individual windows that do not display an enrichment but that fall within a larger peak region.

5.1.9 Aims of the chapter

The aim of this chapter was to investigate the role of histone modifications in regulating gene transcription in cultured ASMCs through the following experimental approaches:

i) the optimization of a protocol to enable the recovery of small mononucleosomal fragments of chromatin from cultured ASMCs,

ii) the validation of this chromatin through ChIP-qPCR to identify regions of expected histone modification enrichments,

iii) performing genome-wide ChIP-seq experiments to determine the enrichment of H3K4me1, H3K4me3 and H3K27me3 in healthy cultured ASMCs.

5.2 Results

5.2.1 Optimization and validation of a protocol to recover chromatin fragments of a defined size from cultured ASMCs and to enrich by ChIP for regions of DNA associated with specifically modified histones

As discussed in Chapter 5.1.3, the specific modification of particular histones provides a molecular signature that can demarcate functional and regulatory domains within chromatin. In order to identify regions of chromatin in ASMCs that are enriched for particular histone modifications a protocol was optimized to facilitate the recovery of small chromatin fragments from cultured ASMCs. The major requirements of this protocol were that it would enable the long-term storage of chromatin following its isolation and that the chromatin fragments generated would be sufficiently sized to facilitate accurate resolution in subsequent ChIP experiments. After various stages of optimization the protocol described in Chapter 2.6.1 was developed and subsequently used to isolate and archive chromatin from cultured ASMCs at passages 4-7 of the initial explant culture. Chromatin isolated using the described protocol routinely enabled the recovery of chromatin fragments of approximately 150 base pairs (bp), which corresponds to mononucleosomal size (Figure 5.2.1). This is the most appropriate size of starting material for the study of histone modifications as it enables the specific location of individual modified histones to be determined. Once isolated, the chromatin was stored at 4°c until all samples to be used in each experiment had been collected, whereupon all ChIPs were performed in a concurrent manner.

It was decided to study the profile H3K4me1, H3K4me3 and H3K27me3 enrichments as these modifications have well described correlative associations with particular classes of regulatory elements (Chapter 5.1.3). H3K4me3 is generally associated with TSSs from which transcription is currently initiating or has the potential to be initiated very rapidly. More recent data has suggested that H3K4me3 is also present at some active enhancer regions. H3K4me1 enrichment has been widely reported to demarcate enhancer regions and H3K27me3 has been reported to cover regions of the genome that are not permissive for active transcription.

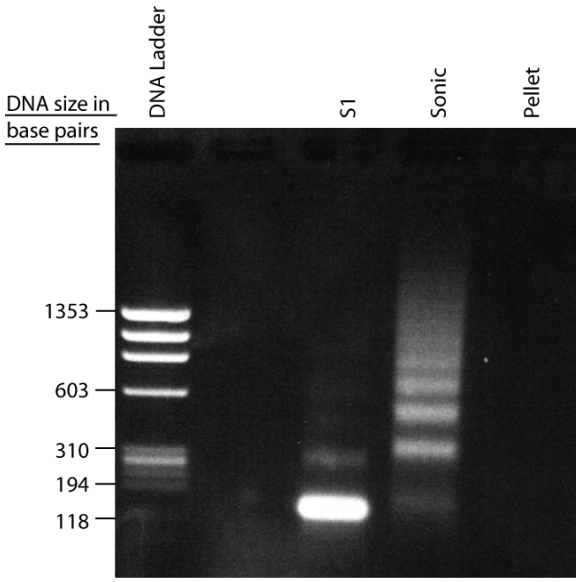

Figure 5.2.1 - Successful recovery of appropriately sized chromatin fragments from cross-linked cultured ASMCs – Approximately $15x10^6$ cultured ASMCs were serum starved for 72 hours before being cross-linked with 1% formaldehyde and harvested by Trypsin-EDTA treatment and gentle scraping. Cells were treated with detergent and centrifuged through a high concentration sucrose cushion to isolate nuclei, which were then treated with Nuclease T7. S1 represents material released by centrifugation performed immediately after Nuclease T7 treatment, whilst Sonic represents material released following sonication and centrifugation. The material in the Pellet is that not released following centrifugation. Results are representative from a single culture of ASMCs.

The ChIP protocol used in the following studies (described in Chapter 2.6.2) is routinely used in the Lavender laboratory to study both histone modifications and transcription factor binding in T-cells. In addition, the three antibodies used (see Table v) had previously been used and verified during T-cell studies. All ChIP experiments described in this chapter were performed using the 'S1' fraction of chromatin (Figure 5.2.1) and hence contained mainly mononucleosomal chromatin fragments. H3K4me3 and H3K27me3 ChIPs were analysed for efficiency and specificity by qPCR using primer sets directed against regions known to be enriched in the histone modification of interest. Specifically this constituted the 5' end of the housekeeping genes *RAD50* and *GAPDH* along with the smooth muscle-associated gene *smooth muscle-22*α for H3K4me3 and the neuronal specific genes *ARX* and *NKX2.3* for H3K27me3 (Figure 5.2.2, see Chapter 2.6.3). At the time of performing the H3K4me1 ChIPs, robust regions of enrichment within ASM chromatin were not known and hence these ChIPs were not quality checked in the same manner prior to larger scale analysis.

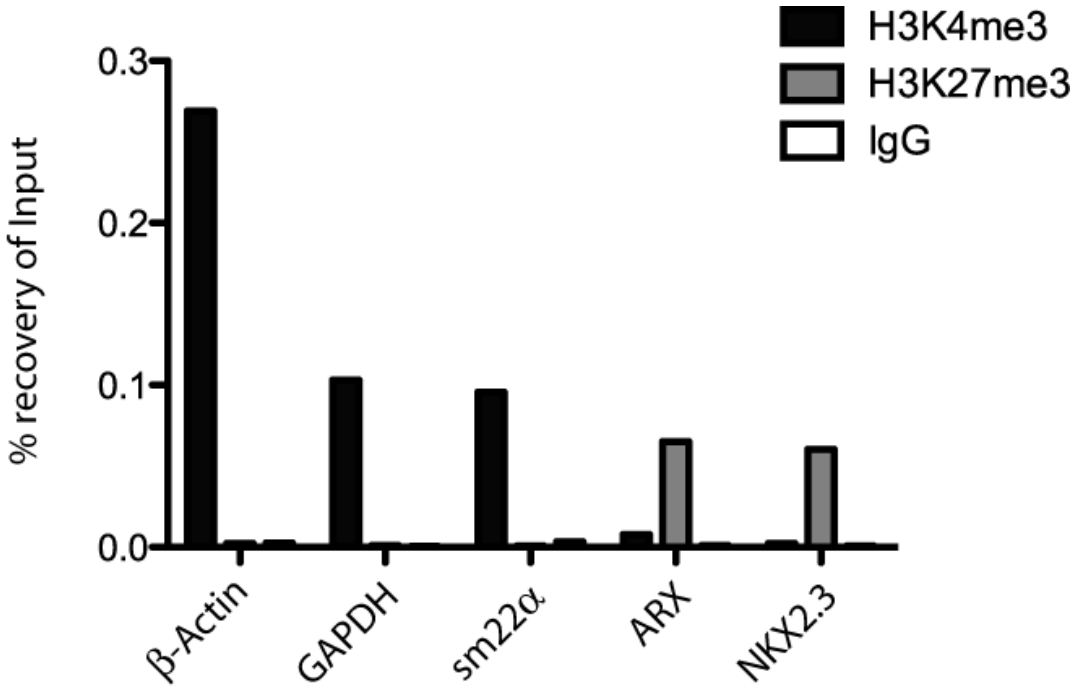

Figure 5.2.2 – qPCR validation of successful and specific H3K4me3 and H3K27me3 ChIPs – ChIPs were performed on chromatin isolated from formaldehyde cross-linked cultured ASMCs using either anti-H3K4me3, anti-H3K27me3 or isotype control IgG. DNA recovered from the ChIP was analysed by qPCR using primer sets proximal to the transcriptional start sites of β-actin, GAPDH, sm22α, ARX or NKX2.3. Results are expressed relative to the Input Ct value generated for each specific primer set and are representative from a single culture of ASMCs.

5.2.2 Profiling the genome-wide enrichments of H3K4me1, H3K4me3 and H3K27me3 in cultured healthy ASMCs

To analyse the profile of H3K4me1, H3K4me3 and H3K27me3 histone modifications in the most unbiased manner possible, ChIP-seq using Illumina next-generation sequencing was performed to identify regions enriched for each histone modification across the entire genome of a single healthy ASMC culture. ChIP-seq libraries were prepared from DNA isolated from H3K4me1, H3K4me3 and H3K27me3 ChIPs in addition to Input DNA that had not been immunoprecipitated (described in Chapter 2.6.4.1). Figure 5.2.3 shows an example of the amplification of a single ChIP-seq library including the removal, via size selection, of PCR amplification artefacts. This demonstrates that the material used for ChIP-seq analysis was of a defined size (~200bp inclusive of adaptor oligonucleotides), which was small enough to enable the accurate mapping of sequenced fragments relative to the reference genome.

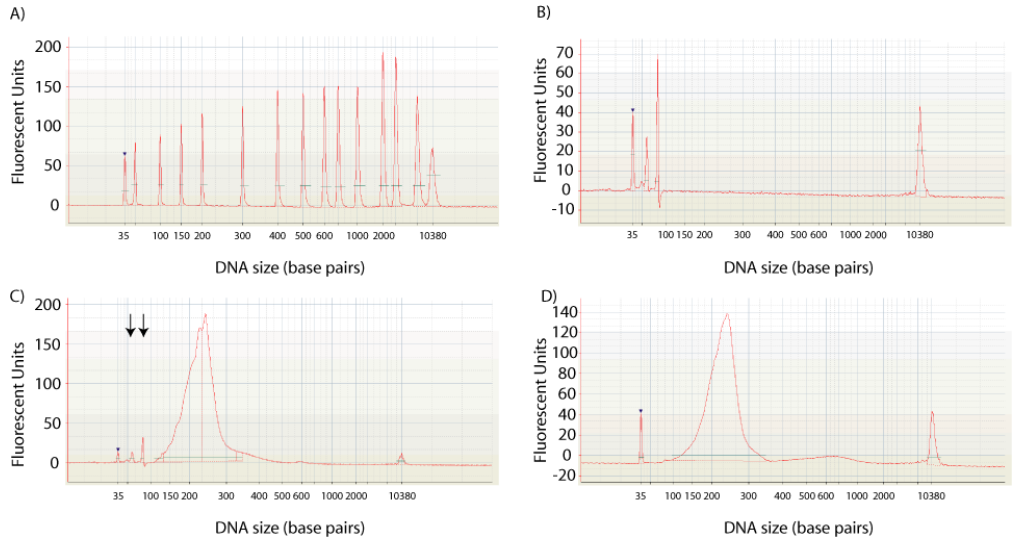

Figure 5.2.3 – Preparation of an Illumina ChIP-seq library – ChIP-seq libraries were prepared from DNA isolated by specific ChIPs using either anti-H3K4me3, anti-H3K4me1 or anti-H3K27me3 or from Input control DNA that had not been subjected to ChIP. Libraries were prepared according to the manufacturers instructions and aliquots were analysed at various steps using an Agilent Bioanalyser to confirm successful preparation of the libraries. **A)** Shows the DNA ladder run to enable the library to be accurately sized, **B-D)** show the profile of the H3K4me3 library at various stages during the process **B)** shows a library before PCR amplification, **C)** shows the profile of a library immediately following amplification, with the two arrowed peaks indicating PCR primers artefacts and **D)** shows the profile of the library following size-selection to remove the PCR primers.

Following the preparation of ChIP-seq libraries cluster generation, sequencing and alignment to the reference genome were performed as described in Chapter 2.6.4.2 and 2.6.4.3.

Figure 5.2.4 summarises the data generated from the four ChIP-seq libraries sequenced and shows that all libraries generated a similar number of total reads, ranging from 27,000,000 to 39,000,000. Following data processing through the Ilumina pipeline and Novoalign, the final number of uniquely aligned reads was 10,708,697 for Input, 10,860,220 for the H3K4me1 library, 9,430,075 for H3K4me3 and 9,994,756 for H3K27me3. The fact that all the ChIP-seq libraries generated a comparable number of aligned reads is important, as it means that samples can be compared to the Input sample without the complications and biases introduced by comparing samples with grossly different numbers of sequences. The final number of aligned reads is diminished in comparison to the initial number of sequences generated for a number of reasons including; the retention of only a single replicate of identical sequences that are likely to be an artefact of PCR amplification, a restriction allowing only two base pair mismatches per sequence compared to the reference genome and discarding of sequences that align to multiple locations within the genome.

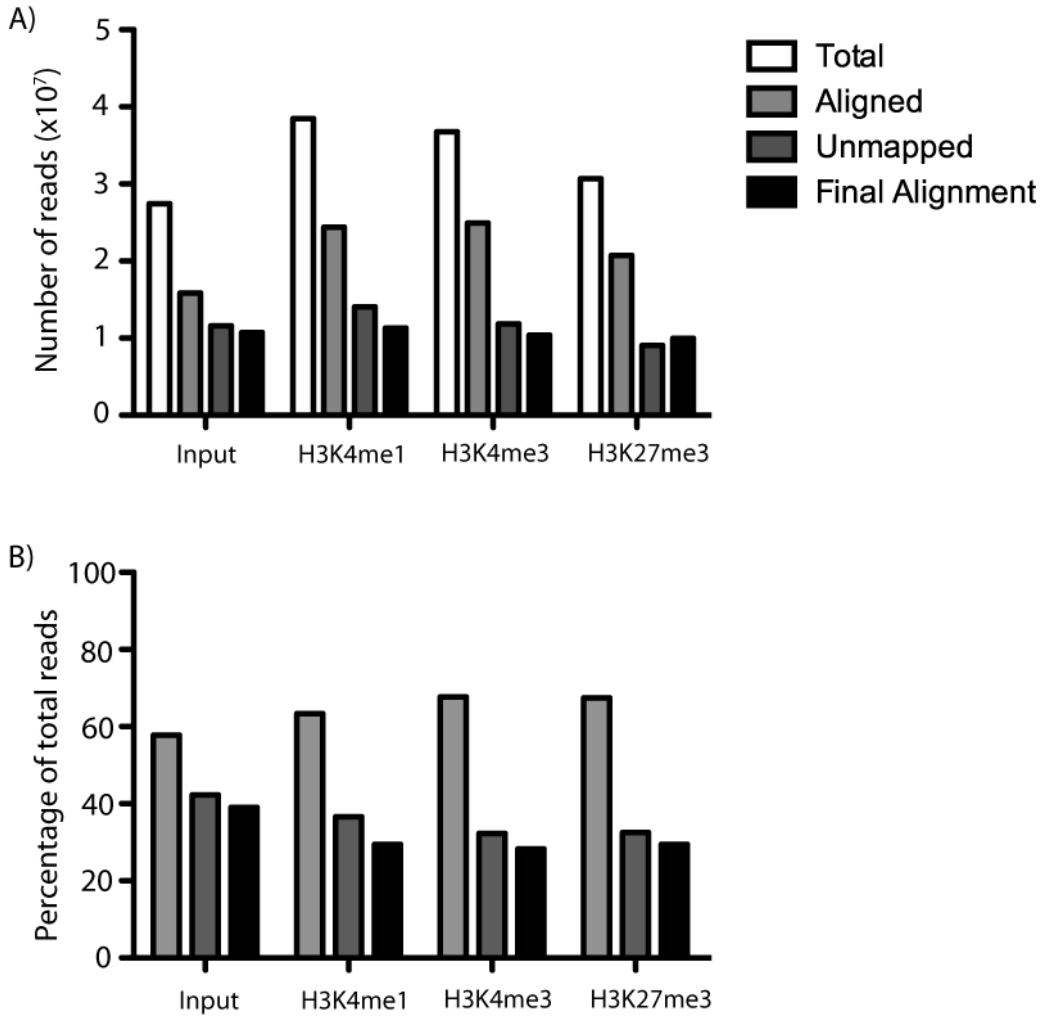

Figure 5.2.4 – Run statistics of Illumina next-generation sequencing of Input, H3K4me1 ChIP, H3K4me3 ChIP and H3K27me3 ChIP libraries – Four ChIP-seq libraries were sequenced using an Illumina GAIIx. Sequences were called and aligned to the reference human genome using Novoalign v2.07.07. **A)** Shows the total number of reads generated (white bars), those that were aligned to the reference genome (light grey bars) and those that could not be mapped to the reference genome (dark grey). The sum of aligned and unmapped reads is equal to the total number of reads generated for each library. The final alignment indicates the final number of reads used for downstream analysis following the removal of duplicate reads which are generated as a PCR artifact (black bars). **B)** Shows the same analysis but presented as the percentage of the total number of sequences generated.

5.2.3 Profiling H3K4me3 enrichments across the genome of a healthy ASMC culture

Illumina GAIIx sequencing of the H3K4me3 ChIP-seq library produced 36,787,141 total reads, of which 10,413,681 aligned uniquely to the reference genome (Figure 5.2.4). To identify regions of the genome that were enriched for histones demarcated with the H3K4me3 modification, the peak finding algorithm SICER was utilised, using a window and gap size of 200 base pairs (SICER analysis performed by Dr V Pullabhatla). Following 'peak calling' by SICER a total of 36,092 regions were identified as enriched for H3K4me3. To increase the stringency and ensure that only high quality peaks were analysed additional thresholds were then implemented. Initially the called peaks were sorted based upon p-value and arbitrary cut-offs were implemented at every 10-fold decrease in p-value. At each stage the 10 peaks with the highest remaining p-value were manually inspected on the UCSC genome browser to ensure that each of the 10 peaks was of high quality. This resulted in all peaks that had a p-value of greater than $1x10^{-10}$ being discarded. Further, to ensure that the potential for the false positive calling of peaks caused by comparisons in regions of the genome with a low number of Input reads was minimized, only peaks with at least 30 reads in the H3K4me3 ChIP sample were analysed further. It should be noted that although these procedures increased confidence that high quality peaks were subsequently analysed, there will inevitably be some false positive peaks retained and some false negatives discarded from the analysis. These thresholds resulted in 16,935 peaks being retained for downstream analysis (Figure 5.2.5).

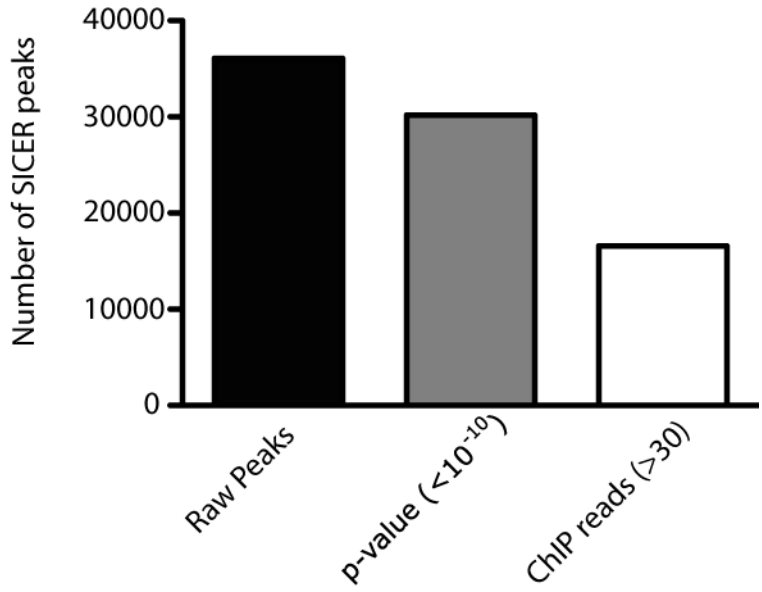

Figure 5.2.5 – Indicates the number of SICER called regions of H3K4me3 enrichment in the genome of cultured ASMCs – SICER was run using a window size and gap size of 200 base pairs to compare the final aligned sequences from the Input and H3K4me3 libraries and define regions that were enriched in the H3K4me3 library compared to background. The raw peaks (black bar) indicate the number of regions of enrichment initially called by SICER, these were then filtered based on p-value (grey bar) and subsequently the number of reads in the H3K4me3 library within the region of called enrichment (white bar).

5.2.3.1 Annotated TSSs in cultured ASMCs are enriched for H3K4me3

As discussed in Chapter 5.1.3, H3K4me3 is enriched at regions where transcription is actively initiating. To compare the profile of H3K4me3 enrichments in cultured ASMCs to previously published data sets (Barski et al. 2007) the 16,935 high quality peaks were classified according to the distance from the centre point of each called region of enrichment to the closest annotated gene in the RefSeq database (Figure 5.2.6). This analysis was completed using the GenomicAnnotation Tool in the ChIPseeqer-2.0 software (Giannopoulou & Elemento 2011) and demonstrated that over 70% of H3K4me3 peaks were associated with annotated TSSs (within 2kb). The number of peaks with defined locations is less than the number in the original input list as ChIPseeqer automatically disregards peaks located in 'black-listed' repetitive regions that are caused by sequence bias artefacts (Figure 5.2.6).

Further analysis performed using the Cis-Regulatory Element Annotation (CEAS) tool (liulab.dfci.harvard.edu/CEAS, performed by Dr. V Pullabhatla) allowed the profile of H3K4me3 enrichment across an average TSS to be constructed. This

analysis indicated that, on average, there is a large enrichment of H3K4me3 over the TSS of a gene that does not extend beyond 1kb downstream of the TSS (Figure 5.2.7). In addition there is a peak of H3K4me3 enrichment approximately 200bp downstream of the TSS, which is consistent with previous reports of a positioned first nucleosome in transcribed genes (Barski et al. 2007), (Schones et al. 2008).

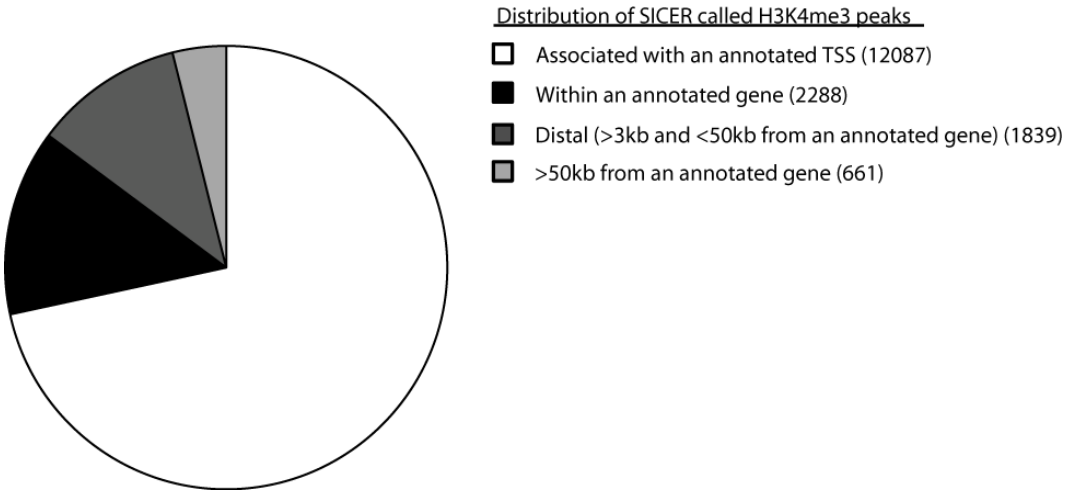

Figure 5.2.6 – Classifying the location of SICER called regions of H3K4me3 enrichment in relation to the closest gene – The 16,935 SICER called regions of H3K4me3 enrichment were classified based upon their linear distance from the closest annotated gene in the RefSeq database using the GenomicAnnotation Tool in ChIPSeeqer 2.0. Peaks were classified as those that were associated with annotated TSSs (white segment), those that were located within an annotated gene (black segment), those that were greater than 3kb but less than 50kb from an annotated gene (dark grey segment) and those that were located greater than 50kb from an annotated gene (light grey segment). The bracketed number represents the number of peaks in a classification.

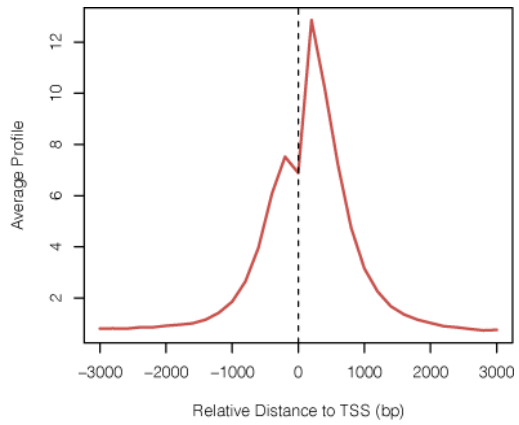

Figure 5.2.7 – Enrichment of H3K4me3 at an average TSS – Aligned sequences from the H3K4me3 ChIP library were analysed using the CEAS tool. The graphic is obtained from the CEAS output file and shows the average distribution of H3K4me3 sequences from 3kb downstream to 3kb upstream of the TSS of an average gene.

To enable the visualisation of specific genomic regions enriched for H3K4me3, the aligned reads generated from the H3K4me3 ChIP-seq library and the regions classified as being enriched for H3K4me3 by SICER were uploaded to the UCSC genome browser as .bigwig and .bed files respectively. Figure 5.2.8 shows a typical profile of H3K4me3 over three genes; *GAPDH, IFFO1* and *NOP2*. Analysis of Affymetrix U133.2 microarray expression data performed on three biological replicates of healthy cultured ASMCs in the Asthma, Allergy and Respiratory Science department prior to the initiation of this project (experiments performed by Dr V Kanabar, Dr C Karner and Dr D Cousins) indicated that each of these genes is detectable at differing levels relative to the mean expression of all genes in cultured ASMCs (Figure 5.2.8, A). Despite the fact that transcripts derived from *GAPDH, IFFO1* and *NOP2* were detected at varying relative levels, each has a SICER defined enrichment of H3K4me3 over the annotated TSS that does not extend into the body of the gene (Figure 5.2.8, B), similar to the average profile demonstrated in Figure 5.2.7.

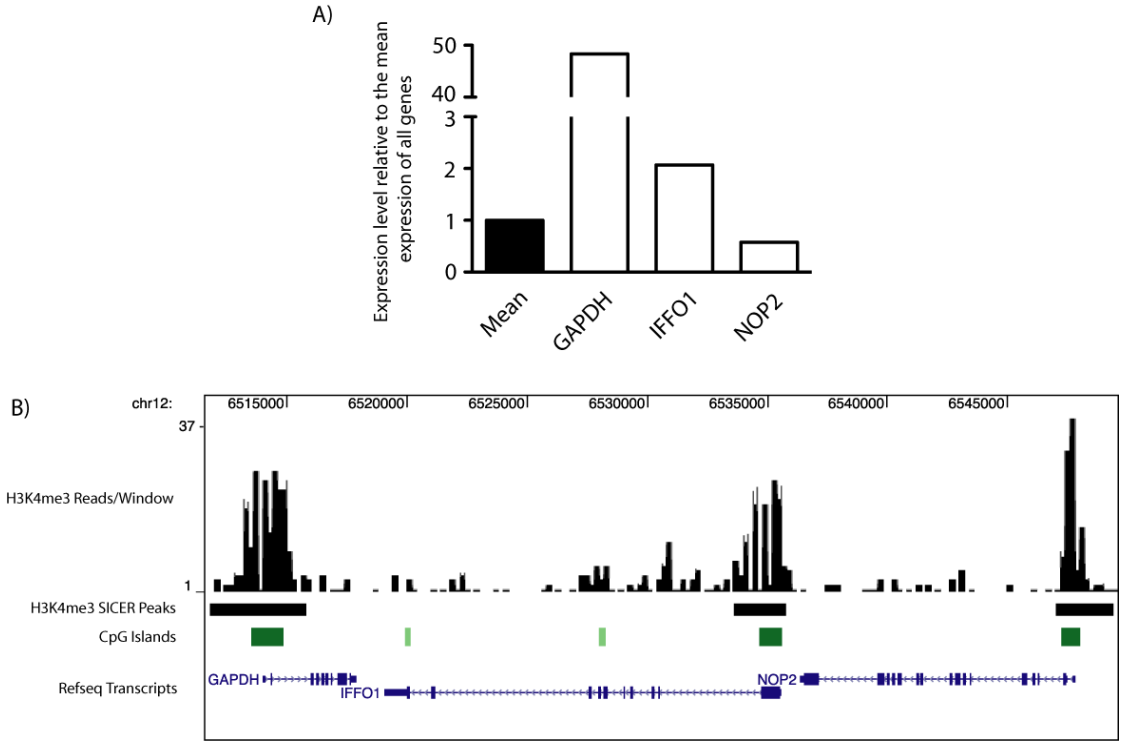

Figure 5.2.8 – Demonstrates the typical enrichment of H3K4me3 over the TSS of annotated genes – A) The average level of detectable transcripts from all genes in cultured ASMCs was calculated from intensity values generated from Affymetrix U133.2 expression arrays. The chart shows the mean expression of all genes and the relative expression of GAPDH, IFFO1 and NOP2. **B)** Aligned H3K4me3 reads were uploaded to the UCSC genome browser as a .bigwig file and regions called as enriched by SICER were uploaded as a .bed file. Regions of SICER called H3K4me3 enrichment and annotated CpG islands are depicted. Genome co-ordinates and annotated RefSeq transcripts are shown at the top and bottom of the figure respectively.

As genes with an enrichment of H3K4me3 at their TSS are likely to be actively transcribed, the relationship between the expression level of a transcript and the presence of a TSS-associated H3K4me3 enrichment was investigated. Expression levels of genes in cultured ASMCs were determined from the average detected expression levels of transcripts assayed on the Affymetrix U133.2 expression arrays performed prior to the initiation of this project. Each Affymetrix probe set was matched to the corresponding RefSeq IDs against which it was directed and the average relative intensity of each probe set was calculated across the three healthy biological replicates analysed. Refseq IDs directed against transcripts derived from the same locus were grouped and the Refseq ID generating the highest relative intensity for a given locus was retained and the remaining values discarded. This restriction was performed to ensure that the transcriptional potential of the locus rather than splice variations were analysed. The RefSeq IDs were ordered by their relative expression level and cross-referenced against a list containing all RefSeq IDs with a TSS-associated H3K4me3 enrichment, as defined by the GenomicAnnotation analysis performed in ChIPseeqer. 5 bins of Refseq transcripts were defined based upon their relative expression levels, with Bin A containing the 1000 transcripts with the highest level of detection and subsequent bins of 1000 transcripts taken at 3000 data point intervals until Bin E, which contains the 1000 transcripts with the lowest level of detection. The percentage of transcripts in each bin that had a TSS-associated region of H3K4me3 enrichment was then calculated. This analysis indicated that, on average, genes from which a higher level of transcript was detected were more likely to have a TSS-associated H3K4me3 enrichment, with the ~90% of the 1000 transcripts with the highest level of detectable transcript being directed against a gene with a SICER called enrichment of H3K4me3 at the TSS compared to only ~19% of the lowest 1000 (Figure 5.2.9).

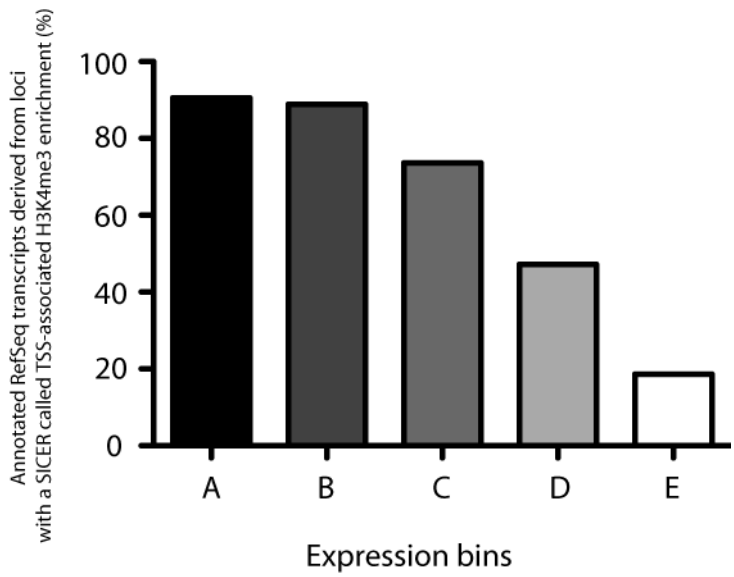

Figure 5.2.9 – Genes from which high abundance transcripts are derived are more likely to be demarcated with a TSS-associated region of H3K4me3 enrichment than genes producing low levels of transcripts – Loci that had a TSS-associated SICER-defined region of H3K4me3 enrichment were determined using the GenomicAnnotation Tool in ChIPSeeqer. These loci were compared to Affymetrix microarray expression data to determine the relationship between the abundance of a transcript and the presence of H3K4me3 enrichment at the gene TSS. 5 bins of Refseq transcripts were defined based upon expression levels, with Bin A containing the 1000 transcripts with the highest level of detection and subsequent bins of 1000 transcripts taken at 3000 data point intervals until Bin E, which contains the 1000 transcripts with the lowest level of detection. The percentage of transcripts in each bin that had a TSS-associated region of H3K4me3 enrichment was then calculated.

Previous studies have indicated that the number of reads from a H3K4me3 ChIP-seq sample that align to a particular gene (sequence tags) is correlated to the level of detectable transcript derived from that gene. To determine if this was true of the data generated for cultured ASMCs, a technical approach similar to those previously reported was utilised (Barski et al. 2007) (Araki et al. 2009). This involved calculating the normalised sequence tags within each individual TSS-associated region of H3K4me3 enrichment by dividing the number of reads within a peak by the total number of aligned sequences generated from the H3K4me3 ChIP-seq sample. The normalised sequence tag depth for each peak was then matched to the expression level of the respective transcript using RefSeq IDs, as described previously. The 17,000 transcript producing genes assayed on the Affymetrix U133.2 expression arrays were placed into bins of 1000 transcripts based upon their relative expression level and the mean normalised tag count and mRNA expression level of each bin was calculated. This analysis corroborated the data previously derived from different cell types (Barski et al. 2007) (Araki et al. 2009)

and indicated that the depth of normalised sequence tags within a TSS-associated H3K4me3 peak was reflective of the expression level of the most abundant transcript derived from that gene. This is demonstrated by the strong and highly statistically significant positive correlation between the mean normalised sequence tag depth and the mean transcript expression level of an expression bin as determined by Spearman's correlation analysis (Figure 5.2.10). This strong positive correlation occurred when all transcripts assayed on the Affymetrix U133.2 microarrays were analysed (Figure 5.2.10 (A)) and when only those genes that had been defined as been associated with a TSS-associated region of H3K4me3 enrichment through the ChIPseeqer analysis were analysed (Figure 5.2.10 (B)).

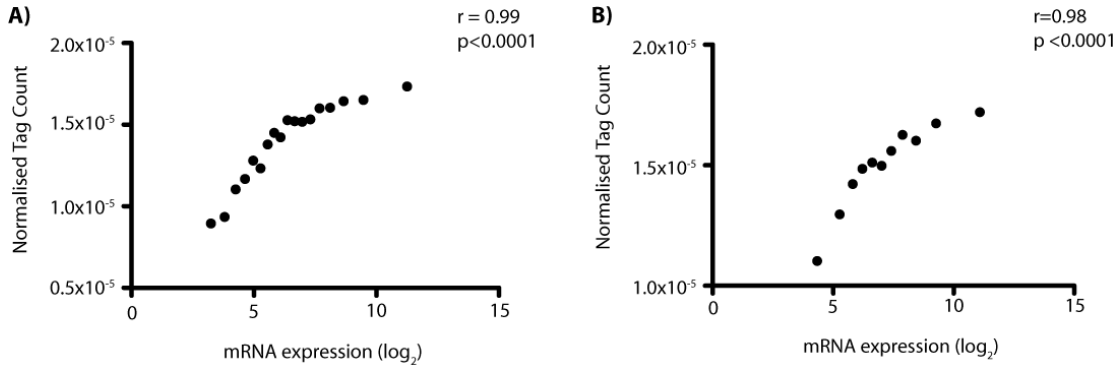

Figure 5.2.10 – The normalised tag count of a TSS-associated H3K4me3 enrichment positively correlates with the level of detectable transcript derived from that gene – Normalised tag counts for TSS-associated H3K4me3 enrichments were generated by dividing the number of aligned reads in each region of enrichment by the total number of aligned reads in the H3K4me3 ChIP-seq sample. TSS-associated regions of enrichment were matched to transcripts expression levels using RefSeq IDs. Bins of 1000 transcripts were defined based upon their relative expression levels and the mean normalised tag count and mean expression level for each bin was calculated. **A)** Demonstrates data for all transcript-producing loci analysed., **B)** Demonstrates data for loci with TSS-associated H3K4me3 enrichments only**.** The Y-axis indicates normalised tag count and the X-axis indicates the relative level of expression of the transcript bin (log_2). Correlation was calculated by determination of Spearman's correlation coefficient.

The profiling of H3K4me3 enrichments can provide information on the expression and regulation of a particular gene in a specific cell type. Figure 5.2.11 demonstrates the profile of H3K4me3 enrichments across the IL-16 locus in cultured ASMCs and *in vitro* differentiated Th2 cells. The Th2 cells were generated by Dr D Cousins according to a previously published protocol (Cousins et al. 2002) and H3K4me3 ChIP-seq profiling was performed by Dr A Kelly according to a

previously published protocol (Rani et al. 2011). IL-16 is a chemoattractrant factor for cells expressing CD4, including T cells, monocytes, eosinophils and dendritic cells (Cruikshank et al. 2000). This data shows that ASMCs and Th2 cells demonstrate enrichments of H3K4me3 at different annotated TSSs of the IL-16 locus, with the location of H3K4me3 peaks suggesting that ASMCs initiate transcription at a TSS approximately 100kb upstream of the TSS utilised in Th2 cells. Further investigations of individual loci where there is evidence for the differential use of TSSs may allow a greater understanding of both the regulation of particular genes within a cell type and the functional implications of this differential variant expression (see Chapter 5.3.1.1). Further, although Figure 5.2.11 demonstrates an example whereby both the TSSs used are annotated, there are 4843 regions of H3K4me3 enrichment at sites other than annotated TSSs in cultured ASMCs. These sites of enrichment may therefore represent unannotated TSSs, some of which may be smooth muscle or ASM specific.

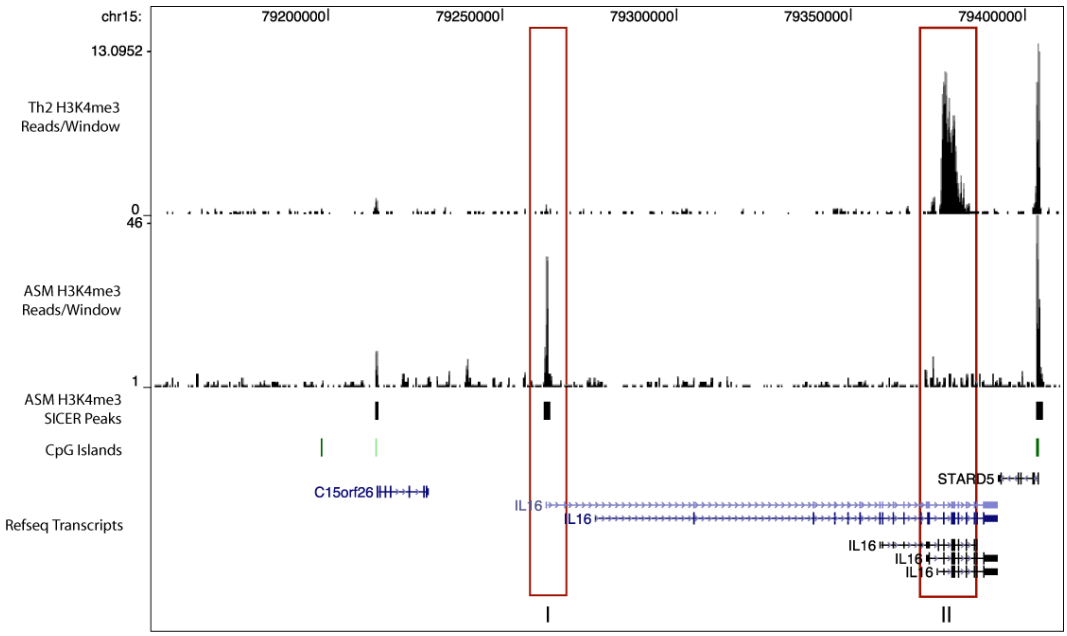

Figure 5.2.11 – Differing profiles of H3K4me3 enrichment across the IL-16 locus in culture ASMCs and *in vitro* differentiated Th2 cells – Aligned reads from ChIP-seq of H3K4me3 libraries generated from anti-H3K4me3 ChIPs in either *in vitro* differentiated Th2 or cultured ASMCs were uploaded to the UCSC genome browser as .bigwig files. SICER-called regions of H3K4me3 enrichment in cultured ASMCs are also shown. Box I demarcates a region of H3K4me3 enrichment in ASMCs over an annotated TSS for IL-16, indicating that this is the TSS utlilised in ASMCs. Box II demarcates a region of H3K4me3 enrichment in Th2 cells at a TSS close to the 3' end of the gene, indicating that this is the TSS utilised in Th2 cells.

5.2.3.2 H3K4me3 enrichments at sites other than annotated TSSs

Although the majority of literature regarding H3K4me3 describes its association with regions where transcription is actively initiating, increasing evidence indicates that it may also enrich at alternative sites within the genome, for example active enhancer regions (Pekowska et al. 2011). 4843 of the high quality regions of H3K4me3 enrichment (~28.6%) were found not to overlap with annotated TSSs and these may represent novel TSSs, as previously discussed, or alternatively may demarcate distinct regulatory regions (Figure 5.2.6).

2500 (14.8% of the total number of peaks) of the SICER called regions of H3K4me3 enrichment were located greater than 3kb from an annotated TSS (Figure 5.2.6). Of these distal regions of H3K4me3 enrichment, 1839 (10.9% of the total number of peaks) were located within 50kb of an annotated RefSeq transcript, whilst 661 (3.9% of the total number of peaks) were located more than 50kb from an annotated RefSeq transcript. In view of the recent data indicating that H3K4me3

may demarcate active regulatory regions, such as enhancers, it was decided that the potential for these distal sites of H3K4me3 enrichment to demarcate true regulatory regions should be investigated. The classical method for the identification of regulatory regions is the determination of regions of DNase I hypersensitivity. Unfortunately, due to restrictions on both time and resources it was not possible to produce this data set for cultured ASMCs during the timescale of this project. In addition, despite extensive searching, it was not possible to find a public dataset defining the regions of DNase I hypersensitivity in ASMCs on a genome-wide scale. An analysis was therefore performed to compare the regions of H3K4me3 enrichment in ASMCs to sites of DNase I hypersensitivity in aortic smooth muscle (AoSMC) that were available as a public dataset [GEO accession GSM816638]. This analysis was performed using the 'ComparePeakLists' tool in ChIPseeqer-2.0 and indicated that over 80% of SICER defined regions of H3K4me3 in ASMCs overlapped with a site of DNase I hypersensitivity in AoSMC (Table xv). The regions of H3K4me3 enrichment were further distinguished based upon their proximity to annotated TSSs. This analysis indicated that ~94% of TSS-associated regions of H3K4me3 enrichment overlapped with an AoSMC DNase I hypersensitivity site, compared to ~70% of regions between 3kb and 50kb from the closest annotated gene and ~51% greater than 50kb from the closest gene.

	Total Number of H3K4me3 peaks	Overlap with AoSMC DNase I sites (Number)	Overlap with AoSMC DNase I sites (%)
Overall	16935	14058	83.0
TSS	12089	11345	93.8
Within Gene	2288	1039	45.4
>3kb and <50kb	1840	1301	70.7
>50kb	661	340	51.4

Table xv – Greater than 80% of SICER-defined regions of H3K4me3 enrichment in cultured ASMCs overlap a DNase I hypersensitivity site from aortic smooth muscle cells – Regions of H3K4me3 enrichment that overlapped with defined regions of DNase I hypersensitivity in aortic smooth muscle were identified using the ChIPseeqer 'Find overlapping peaks tool'.

It is likely that a number of these distal regions of H3K4me3 enrichment represent unannotated TSSs, some of which may be potentially smooth muscle specific. Figure 5.2.12 demonstrates a region of H3K4me3 enrichment ~3kb upstream of the annotated TSS of *PRPF4B* gene, which encodes a kinase enzyme. This region of enrichment overlaps both an AoSMC DNase I hypersensitivity site and a CpG island and may therefore demarcate an unannotated, alternative TSS.

Figure 5.2.13 demonstrates a region upstream of *YY1*, a gene encoding a ubiquitously expressed transcriptional repressor (Shi et al. 1991), that contains three distinct regions of H3K4me3 enrichment. Two of these regions of enrichment (Box I and II) are centred at ~45kb and 25kb from the annotated TSS of *YY1* respectively and overlap both an AoSMC DNase I hypersensitivity site and a CpG island. The third region of H3K4me3 enrichment (Box III) is centred ~16kb from the annotated TSS of *YY1* and overlaps an AoSMC DNase I hypersensitivity site but not a CpG island. These regions of enrichment may represent alternative TSSs or, alternatively, may demarcate distinct regulatory regions. Further experimental investigations would be required to discriminate which of these two scenarios was correct.

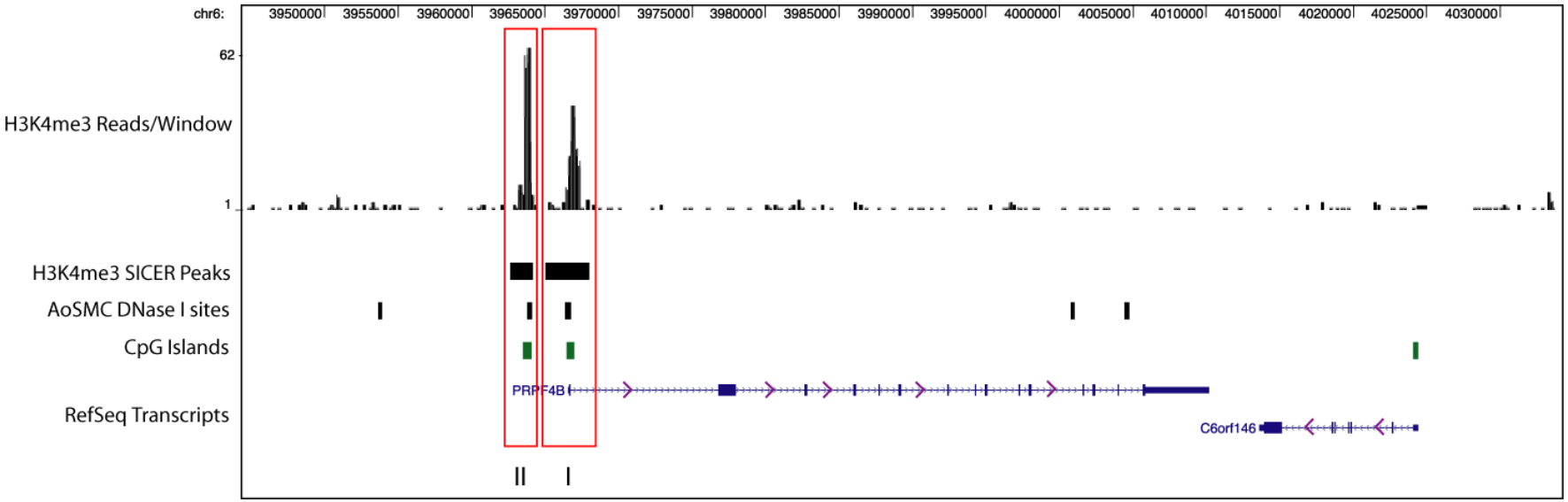

Figure 5.2.12 – Demonstrates an example of a region of H3K4me3 enrichment that is greater than 3kb from an annotated TSS and is likely to define an unannotated TSS – Aligned H3K4me3 sequences were uploaded to the UCSC genome browser as .bigwig files and regions defined as enriched for H3K4me3 by SICER were uploaded as .bed files. Regions of SICER defined H3K4me3 enrichment are depicted, along with annotated CpG islands and regions of DNase I hypersensitivity in aortic smooth muscle cells. Genome coordinates and annotated RefSeq transcripts are shown at the top and bottom of the figure respectively. Box I indicates a classical region of H3K4me3 enrichment that overlaps the TSS of a RefSeq annotated transcript along with a CpG island and a region of DNase I hypersensitivity in aortic smooth muscle. Box II indicates a SICER defined region of H3K4me3 enrichment that overlaps a CpG island and a region of DNase I hypersensitivity in aortic smooth muscle but does not overlap an annotated TSS.

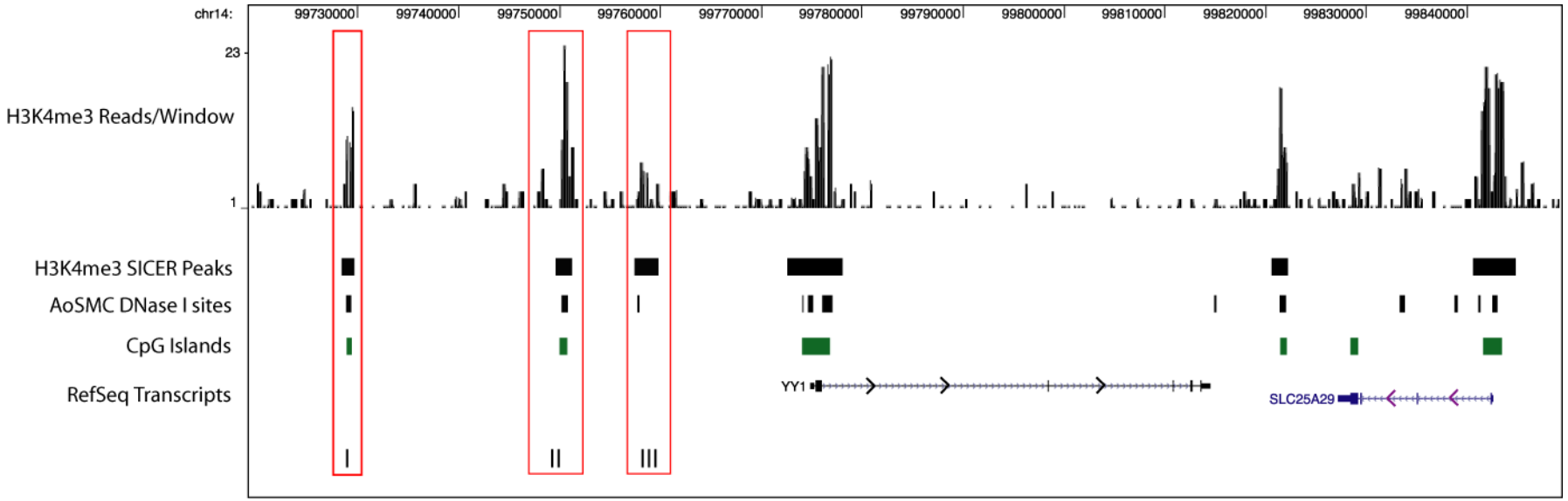

Figure 5.2.13 – Demonstrates an example of a region of H3K4me3 enrichment that is greater than 3kb from an annotated TSS and may demarcate a distal regulatory region – Aligned H3K4me3 sequences were uploaded to the UCSC genome browser as .bigwig files and regions defined as enriched for H3K4me3 by SICER were uploaded as .bed files. Regions of SICER defined H3K4me3 enrichment are depicted, along with annotated CpG islands and regions of DNase I hypersensitivity in aortic smooth muscle cells. Genome co-ordinates and annotated RefSeq transcripts are shown at the top and bottom of the figure respectively. Boxes I and II represent regions of H3K4me3 enrichment that overlap annotated CpG islands and aortic smooth muscle DNase I hypersensitivity sites whilst box III depicts a region of H3K4me3 enrichment that overlaps an aortic smooth muscle DNase I hypersensitivity site but not a CpG island.

5.2.4 Profiling H3K4me1 enrichments across the genome of a healthy ASMC culture

Illumina GAIIx sequencing of a H3K4me1 ChIP-seq library produced 38,458,785 total reads, of which 10,860,220 aligned uniquely to the reference genome (Figure 5.2.4). Following peak calling by SICER, using a window size of 200 base pairs and a gap size of 800 base pairs (performed by Dr V Pullabhatla), a total of 51,739 regions were identified as enriched for H3K4me1. The application of the same thresholds used to ensure only high quality peaks for H3K4me3 were analysed (see Chapter 5.2.3.) resulted in 23,528 H3K4me1 peaks being retained for downstream analysis (see Figure 5.2.14).

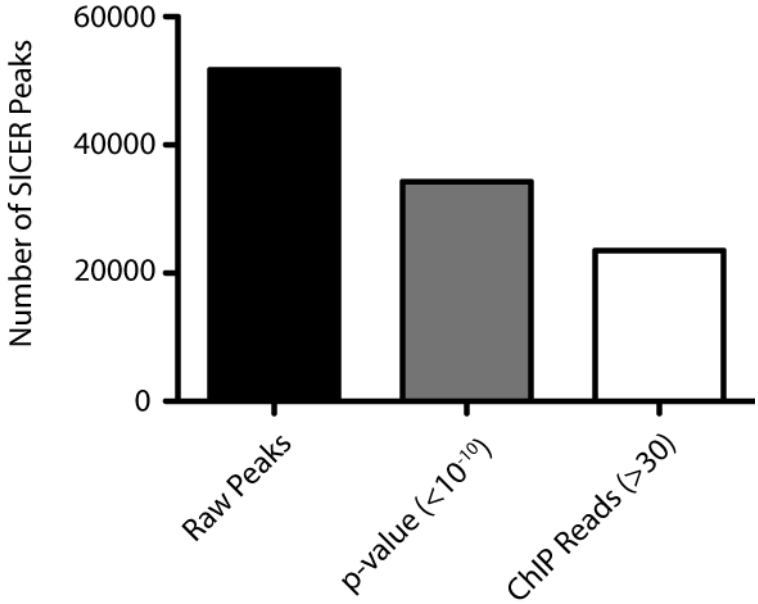

Figure 5.2.14 – The number of SICER called regions of H3K4me1 enrichment in the genome of cultured ASMCs – SICER was run using a window size of 200 base pairs and gap size of 800 base pairs to compare the final aligned sequences from the Input and H3K4me1 libraries and define regions that were enriched in the H3K4me1 library compared to background. The raw peaks (black bar) indicate the number of regions of enrichment initially called by SICER, these were then filtered based on p-value (grey bar) and subsequently the number of reads in the H3K4me1 library within the region of called enrichment (white bar).

As for H3K4me3, the regions determined by SICER to be enriched for H3K4me1 were classified depending upon the distance of the centre of the called region of enrichment to the closest annotated TSS in the RefSeq database (performed using GenomicAnnotation script in ChIPseeqer-2.0). This analysis identified in 5739 (22.4%) peaks that were associated with annotated TSSs, 10538 (44.9%) peaks that

were located within RefSeq genes and 7113 (30.3%) peaks that were located greater than 3kb upstream from the closest annotated RefSeq locus (Figure 5.2.15).

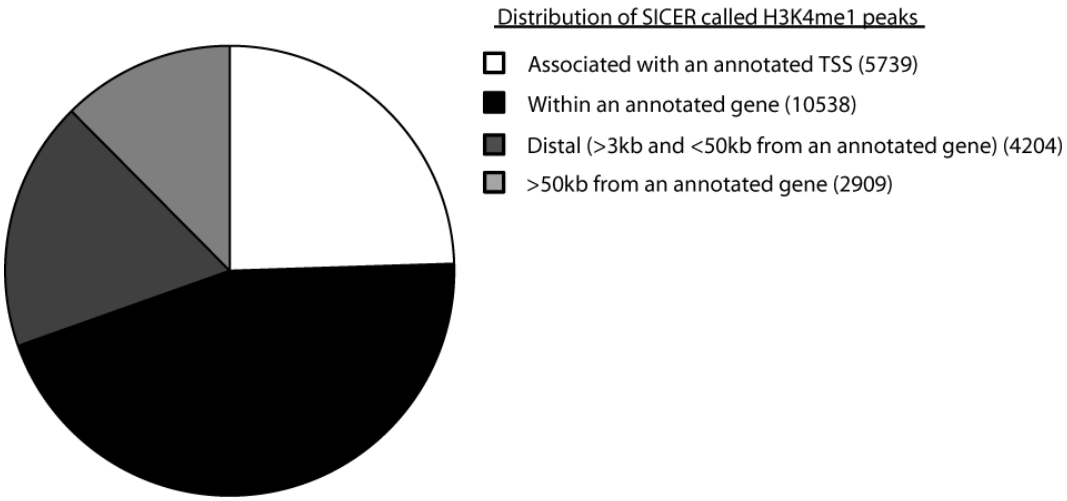

Figure 5.2.15 - Classifying the location of SICER called regions of H3K4me1 enrichment in relation to the closest gene – The 23,528 SICER called regions of H3K4me1 enrichment were classified based upon their linear distance from the closest annotated gene in the RefSeq database using the GenomicAnnotation Tool in ChIPSeeqer 2.0. Peaks were classified as those associated with annotated TSSs (white segment), those that were located within an annotated gene (black segment), those that were greater than 3kb but less than 50kb from an annotated gene (dark grey segment) and those that were located greater than 50kb from an annotated gene (light grey segment).

5.2.4.1 H3K4me1 regions of enrichment that overlap annotated TSSs

As for H3K4me3, the profile of H3K4me1 enrichments around annotated TSSs was compared to previously published datasets (Barski et al. 2007). CEAS analysis (Figure 5.2.16) demonstrated that when all genes were averaged, there was an enrichment of H3K4me1 around the TSS that did not extend further than 1kb into the gene body. This enrichment around an average TSS was similar in profile to that determined for H3K4me3 (Figure 5.2.7), however, the magnitude of the enrichment of reads was less for H3K4me1. This data differs from Barski *et al.*, who indicated that H3K4me1 was enriched both upstream and downstream of a region of H3K4me3 enrichment at an average TSS. There are, however, a number of examples of this profile of enrichment within the dataset generated from cultured ASMCs. Figure 5.2.17 demonstrates the profile of H3K4me1 and H3K4me3 enrichments over the *VEGFA* gene. It is clear that at the *VEGFA* gene there is an enrichment of

H3K4me3 over the annotated TSS that is flanked on either side by a region of H3K4me1 enrichment.

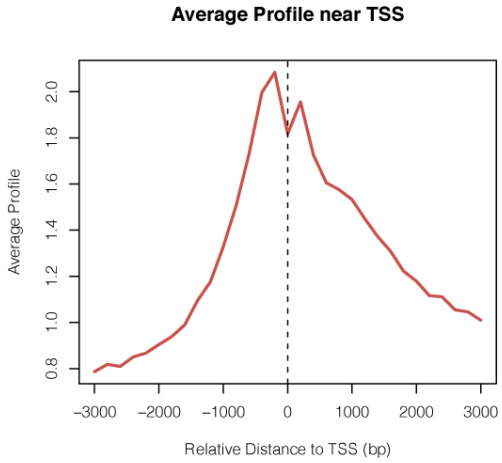

Figure 5.2.16 - CEAS report on the distribution of H3K4me1 over an average TSS – Aligned sequences from the H3K4me1 ChIP library analysed using the CEAS tool. The graphic is obtained from the CEAS output file and shows the average distribution of H3K4me1 sequences from 3kb downstream to 3kb upstream of an average TSS of annotated genes.

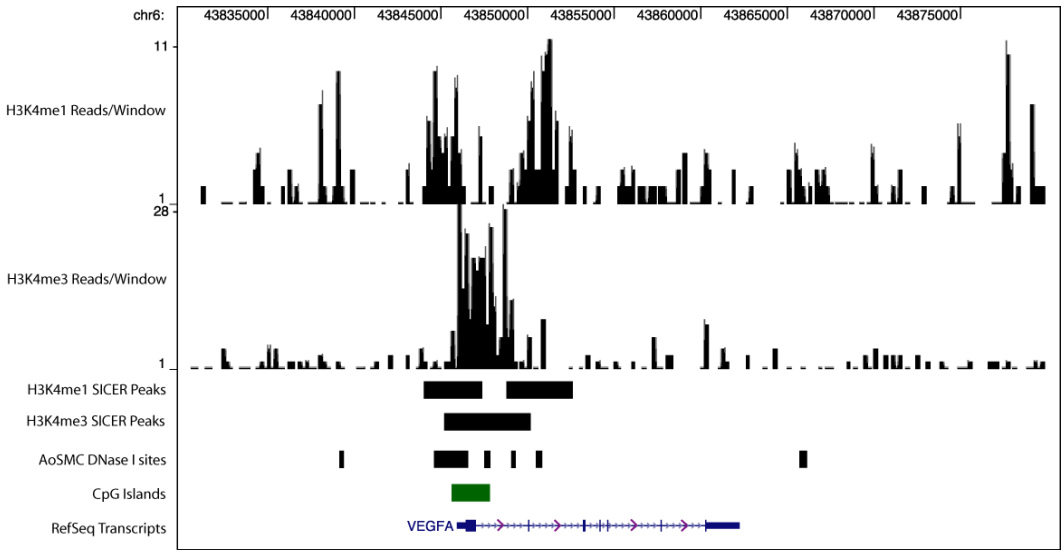

Figure 5.2.17 - Demonstrates regions of H3K4me1 enrichment flanking a TSS enriched with H3K4me3 at the *VEGFA* gene – Aligned H3K4me1 and H3K4me3 sequences are depicted as reads/200 base pair window in the UCSC genome browser. Regions called as enriched for either H3K4me1 or H3K4me3 by SICER were uploaded as .bed files and are displayed as UCSC tracks along with along with annotated CpG islands and regions of DNase I hypersensitivity in aortic smooth muscle cells. Genome co-ordinates and annotated RefSeq transcripts are shown at the top and bottom of the figure respectively.

5.2.4.2 H3K4me1 enrichment distal to annotated TSSs

A total of 7133 (30.3%) regions of H3K4me1 enrichment were found to be greater than 3kb from a RefSeq annotated TSS and were thus classified as distal. Of these 7133 regions of enrichment, 4204 were located less than 50kb from an annotated RefSeq transcript whilst 2909 were located greater than 50kb from an annotated RefSeq transcript (Figure 5.2.15).

The majority of evidence regarding H3K4me1 indicates that it is enriched at regulatory regions, particularly enhancers (see Chapter 5.1.3). This data implies that the genome-wide profile of regions of H3K4me1 enrichments produced in this project could facilitate the identification of distal regulatory regions involved in the regulation of gene expression of genes that may be important in ASM function and potentially deregulated in asthma. To increase confidence that regions of H3K4me1 enrichment represented regulatory regions, the overlap of H3K4me1 enrichments with AoSMC DNase I hypersensitivity sites was determined. This analysis indicated that 16,805 out of 23,528 (>70%) regions of H3K4me1 enrichment overlapped an AoSMC DNase I hypersensitivity site (Table xvi). Further confidence in these results was drawn from the fact that only 5,069 out of 22,510 sites (22%) of H3K4me1 enrichment identified in *in vitro* differentiated Th2 cells (data provided by Dr P Lavender) overlapped with a region of DNase I hypersensitivity in AoSMCs. The regions of H3K4me1 enrichment identified in ASMCs may therefore demarcate regulatory regions involved in the regulation of genes with roles in ASM biology. Figure 5.2.18 demonstrates the profile of H3K4me1 and H3K4me3 enrichments around the *VEGFA* gene. As shown in Figure 5.2.17 there is enrichment of both H3K4me1 and H3K4me3 around the TSS of *VEGFA*, however, in addition there are a number of regions enriched in H3K4me1 upstream of the *VEGFA* TSS. These regions demarcate previously identified enhancer regions involved in the regulation of *VEGFA* expression (Figure 5.2.18, Box I and II, -56kb and -46kb) and potential novel enhancer regions (Figure 5.2.18, Box III, -70kb). The potential relevance of this data is discussed in more detail in Chapter 5.3.1.2.

	Total number of H3K4me1 peaks	Overlap with DNase I (Number)	Overlap with DNase I (%)
Overall	23528	16805	71.4
TSS	5739	4798	83.6
Within Gene	10537	6995	66.4
>3kb and <50kb	4205	3008	71.6
>50kb	2909	1908	65.6

Table xvi – Greater than 70% of defined regions of H3K4me1 enrichment in cultured ASMCs overlap a DNase I hypersensitivity site from AoSMCs – Regions of H3K4me1 enrichment that overlapped with DNase I hypersensitivity sites in aortic smooth muscle were identified using the FindOverlappingPeaks tool in ChIPseeqer 2.0.

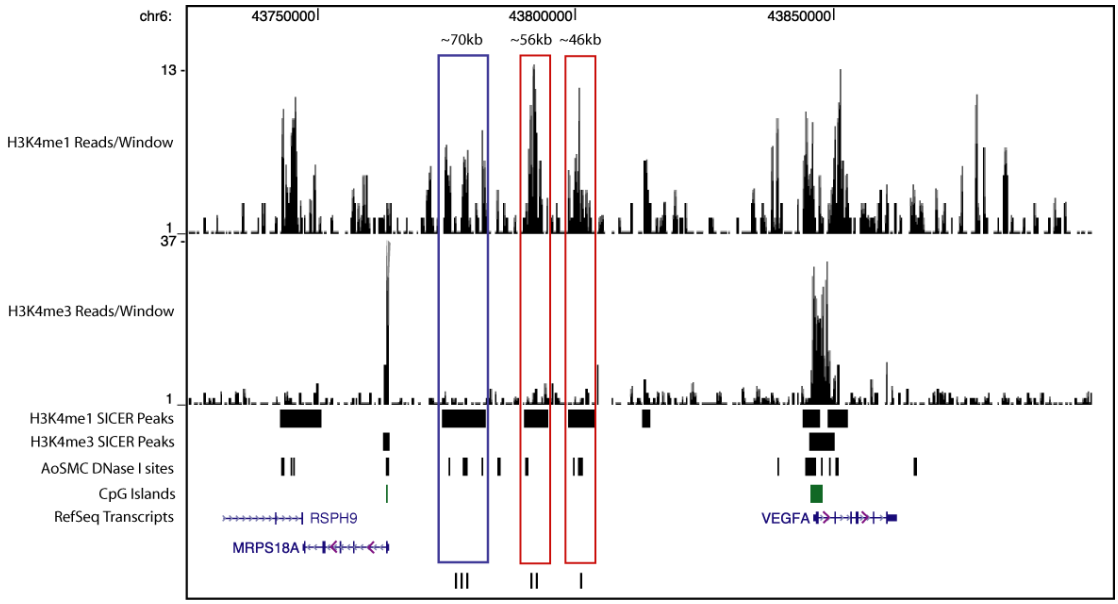

Figure 5.2.18 – H3K4me1 demarcates both known and possible novel enhancer elements upstream of the *VEGFA* gene – H3K4me1 and H3K4me3 reads/200 base pairs were uploaded to the UCSC genome browser as .bigwig files. SICER defined regions of H3K4me1 and H3K4me3 enrichment in cultured ASMCs were uploaded as .bed files. Annotated CpG islands, regions of DNase I hypersensitivity in AoSMCs and RefSeq transcripts are shown for comparison. Boxes I and II (red, ~46kb and ~56kb) demarcate regions that have been shown as regions that function as enhancer elements involved in regulating *VEGFA* expression. Box III (blue, ~70kb) demarcates a region containing elements marked with H3K4me1 that overlaps DNase I hypersensitivity sites in AoSMCs and may represent novel regulatory regions involved in regulating *VEGFA* expression.

Figure 5.2.19 demonstrates the profile of H3K4me1 and H3K4me3 around the *BIC* locus, which was expressed at diminished levels in cultured ASMCs isolated from moderate asthmatic compared to healthy individuals (Figure 4.2.1). This profile indicates a region of H3K4me3 enrichment at the annotated TSS of the locus, as would be expected of a gene that is known to be actively expressed in cultured ASMCs. In addition there is also enrichment of H3K4me1 throughout the gene body, including over the region of the 3rd exon where the miR-155 sequence is located, which may signify the presence of additional regulatory elements involved in controlling expression of the *BIC* locus. As the data presented in Figure 4.2.1 suggests a possible difference at the level of transcription of the *BIC* locus in cultured ASMCs isolated from healthy and moderate asthmatic volunteers, it is interesting to speculate whether the enrichment of H3K4me3 over the TSS or the H3K4me1 enrichment throughout the gene body may differ between the groups and whether differences in histone modifications may be involved in regulating the differential expression of BIC mRNA.

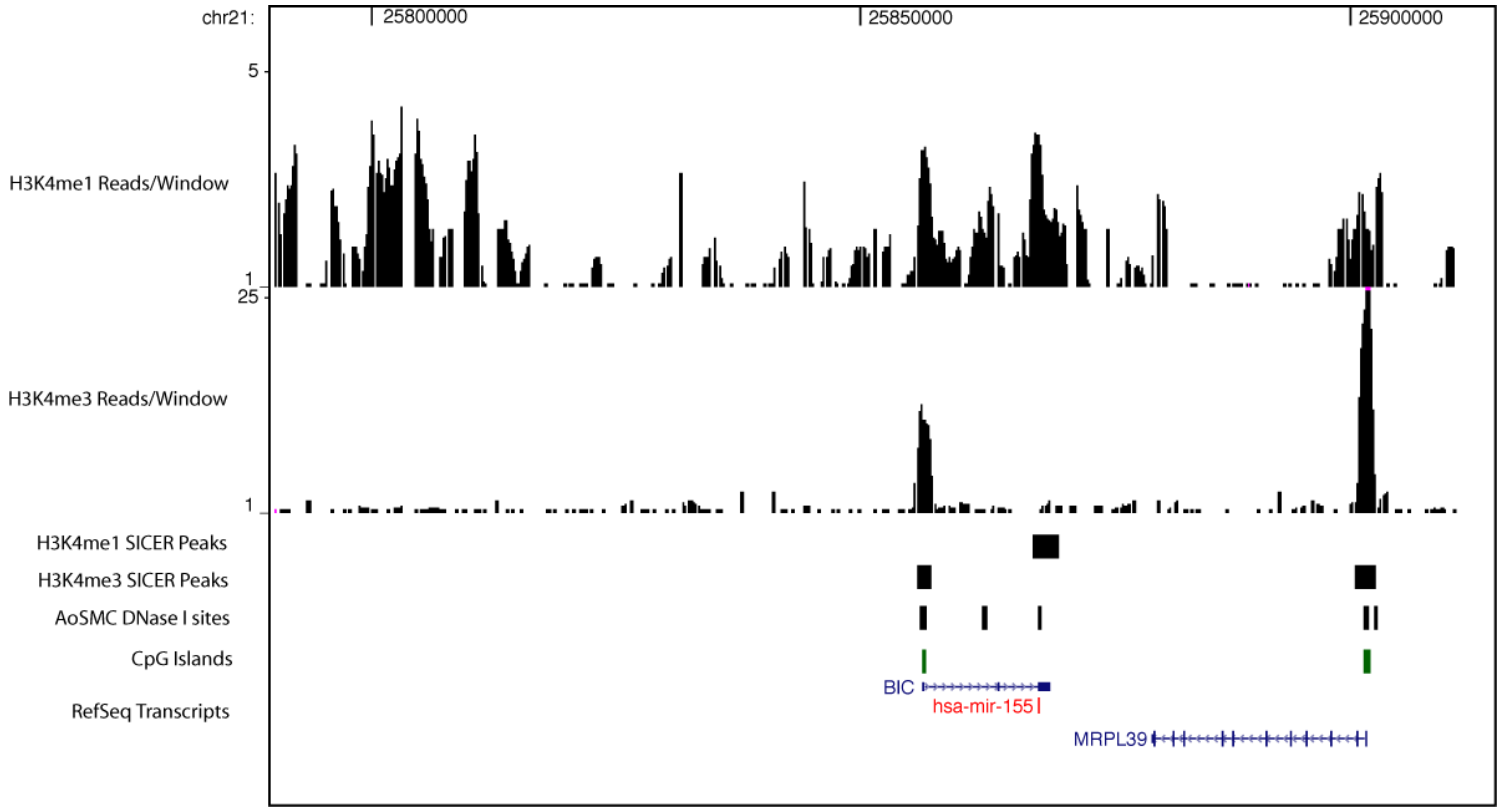

Figure 5.2.19 – Profile of H3K4me1 and H3K4me3 around the *BIC* locus – H3K4me1 and H3K4me3 reads/200 base pairs were uploaded to the UCSC genome browser as .bigwig files. SICER defined regions of H3K4me1 and H3K4me3 enrichment in cultured ASMCs were uploaded as .bed files. Annotated CpG islands, regions of DNase I hypersensitivity in AoSMCs and RefSeq transcripts are shown for comparison. The *BIC* locus is demarcated by a region of H£K4me3 enrichment at the annotated TSS and also contains a regions of H3K4me1 enrichment across the gene body, including over the 3rd exon where miR-155 is located.

Further confidence that the H3K4me1 data set generated in this chapter would be useful for identifying distal regulatory regions could be drawn from the identification of cell type specific profiles of enrichment. Unfortunately this requires in depth studies of specific loci that at the present time are not available for ASM. Increased confidence in the specificity of the H3K4me1 enrichments described in Figure 5.2.18, however, can be drawn from the fact that the analysis of H3K4me1 and H3K4me3 enrichments in *in vitro* cultured Th2 did not identify the regions upstream of *VEGFA* as being enriched for H3K4me1 (Figure 5.2.20). The analysis of the H3K4me1 and H3K4me3 enrichments in *in vitro* differentiated Th2 cells has, however, has enabled the identification of cell type specific patterns of histone modifications in the signature 5q locus of Th2 cells (Figure 5.2.21). The cytokines IL-4, IL-5 and IL-13 are regarded as the signature cytokines of Th2 cells and as such are highly expressed in this cell type. Figure 5.2.21 demonstrates that each of the signature Th2 cytokines is demarcated by an enrichment of H3K4me3 at the TSS in Th2 cells but not in cultured ASMCs, suggesting the genes are unlikely to rapidly upregulated and expressed in ASMCs. This data is supported by the Affymetrix U133.2 transcriptome microarrays performed in the Asthma, Allergy and Respiratory Science Department, which gave no indication of expression of IL-4, IL-5 or IL-13 in cultured ASMCs. There are numerous regions of H3K4me1 enrichment present across the loci in Th2 cells, whereas, there is very little evidence of H3K4me1 enrichment in the ASMCs. In addition, the regions of H3K4me1 enrichment present in Th2 cells coincide with previously identified regions of DNase I hypersensitivity in Th2 cells that are not present in AoSMCs (Sabo et al. 2006). This is further evidence that these H3K4me1 enrichments may be regulatory regions involved in the expression of *IL4*, *IL5* or *IL13* and that they are not utilised in ASMCs. Specific regions previously identified as enhancer regions are demarcated by H3K4me1 enrichment in Th2 cells. For example, this data demonstrates that regulatory regions located at the 3' end of the *RAD50* gene, which have previously been shown to be important in the regulation of *IL13* expression (Fields et al. 2004), are enriched with H3K4me1 in Th2 cells but not in ASMCs (Figure 5.2.22). This is in contrast to the enrichment of H3K4me3 that occurs at the TSSs of the housekeeping genes, *RAD50* and *KIF3A*, in both cell types. The cell-type specific enrichment of H3K4me1 in Th2 cells suggests the enrichments of H3K4me1 identified in ASMCs may be useful to facilitate the identification of distal regions involved in the regulation of gene expression in ASM.

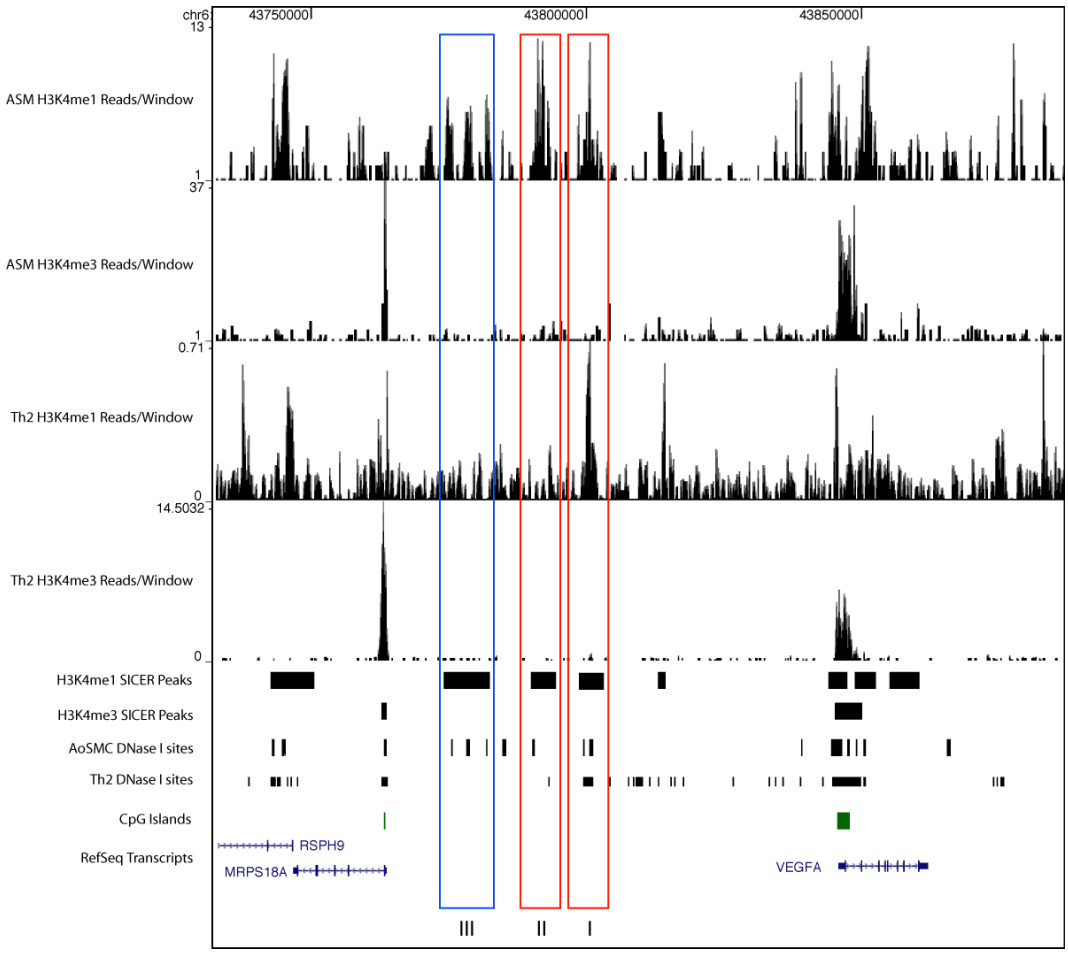

Figure 5.2.20 – H3K4me1 enrichments demarcate reported and potential novel enhancer regions upstream of the *VEGFA* gene in cultured ASMCs but not Th2 cells – Comparison of ChIP-seq interrogation of H3K4me1 and H3K4me3 enrichments in *in vitro* differentiated Th2 and cultured ASMCs. H3K4me1 and H3K4me3 SICER defined enrichments in ASMCs, AoSMC and Th2 sites of DNase I hypersensitivity and CpG islands are shown for reference and comparison. Boxes I and II (Red) indicate previously reported enhancer regions with the ability to regulate *VEGFA* expression whilst Box III (Blue) indicates potential novel regulatory regions.

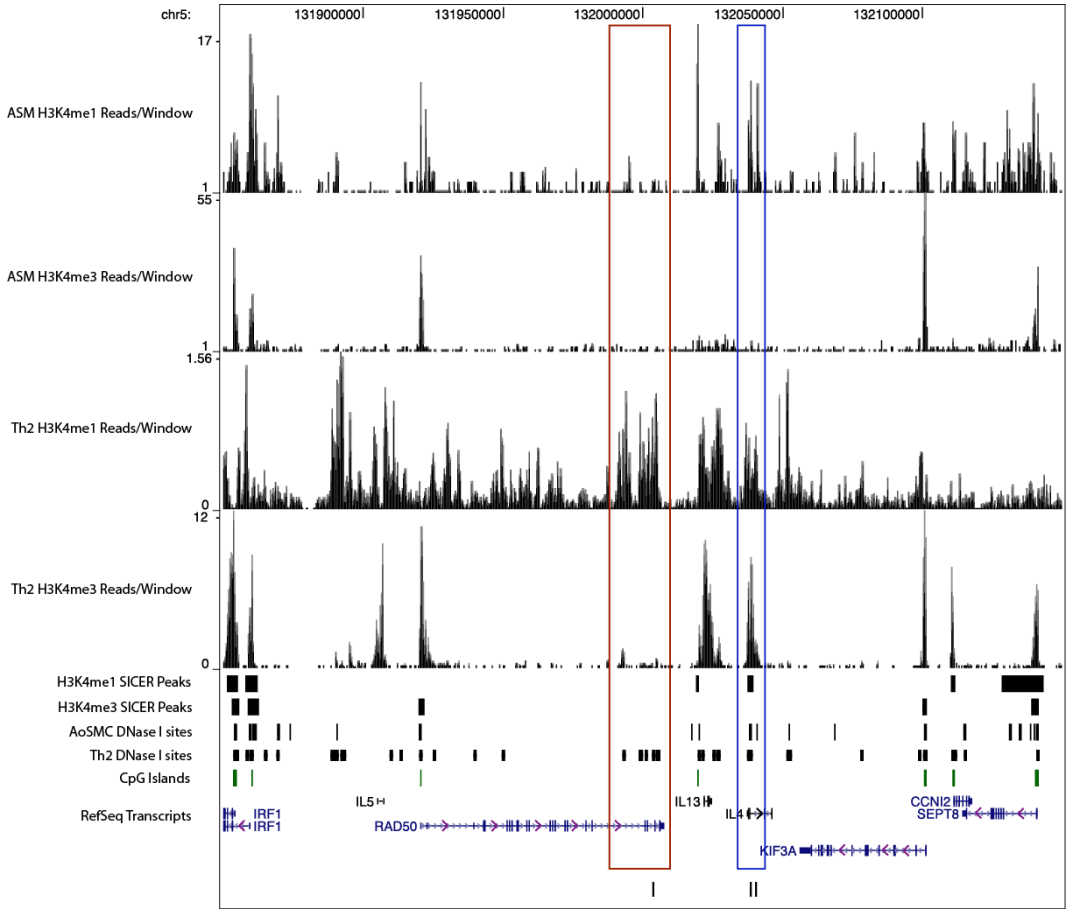

Figure 5.2.21 – H3K4me1 enrichments demarcate known enhancer regions in the 5q locus in Th2 but not ASMCs – Comparison of ChIP-seq interrogation of H3K4me1 enrichments in *in vitro* differentiated Th2 and cultured ASMCs. Box I (Red) shows a region known to be a locus control region involved in the regulation of IL-13 expression which is demarcated with H3K4me1 in Th2 but not ASMCs. Box II (Blue) shows a known regulatory region at the 5' end of the IL-4 gene that is demarcated with H3K4me1 in both Th2 and ASMCs.

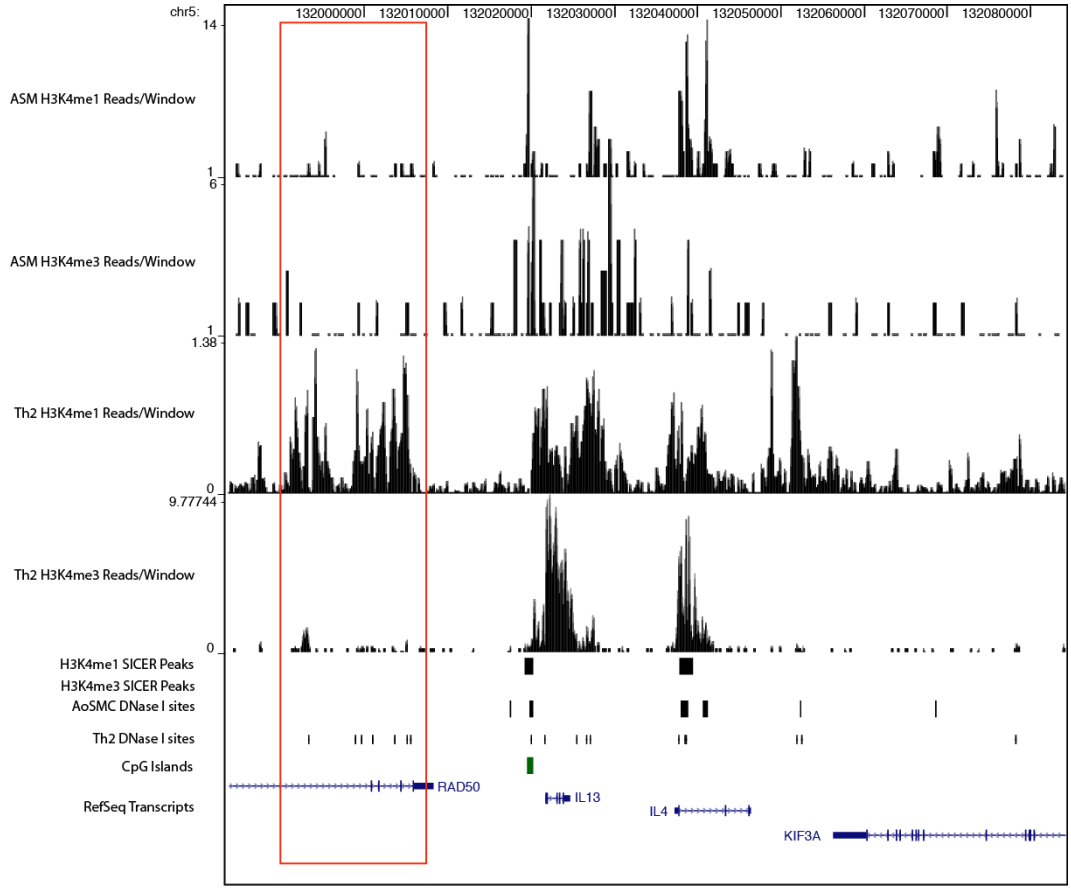

Figure 5.2.22 – Detailed view of the profile of H3K4me1 and H3K4me3 enrichments around the IL-13 and IL-4 genes in *in vitro* differentiated Th2 cells and cultured ASMCs – Comparison of ChIP-seq interrogation of H3K4me1 enrichments in *in vitro* differentiated Th2 and cultured ASMCs. The red box shows a region known to be a locus control region involved in the regulation of IL-13 expression, which is demarcated with H3K4me1 in Th2 but not ASMCs.

5.2.4.3 Identification of binding motifs over-represented in potential enhancer regions in cultured ASMCs

In an attempt to identify potential general functions for distal regions of SICER-defined H3K4me1 enrichment (>3kb and <50kb from a RefSeq annotated gene), novel motif finding analysis using Multiple Em for Motif Elicitation (MEME) motif discovery was undertaken in collaboration with Dr V Pullabhatla (Bailey et al. 1994). It was decided to search for common sequence motifs in sequences underlying sites of AoSMC DNase I hypersensitivity that fell within regions of H3K4me1 enrichment, as these were the regions most likely to represent potential regulatory regions. This resulted in an input list of ~5000 DNase I hypersensitive sites with a mean width of 440bp and therefore constituted approximately 2,200,000 bps that were searched for common motifs. MEME was performed following the user defined searching parameters of a minimum motif width of 8 bases and occurrence in zero or one of the input regions (ZOOPS method).

The most notable sequence identified from the MEME analysis was a motif that closely resembled the JASPAR consensus binding motif for CTCF (Kim et al. 2007) (Figure 5.2.23), which was identified as being present within 270 of the 5000 DNase I hypersensitive sites. These results may indicate a hitherto poorly reported potential interaction between CTCF and H3K4me1. Unfortunately, the novel motif searching in distal regions of H3K4me1 enrichment has proven to be more complex than was originally anticipated and, due to this fact, analysis is currently ongoing.

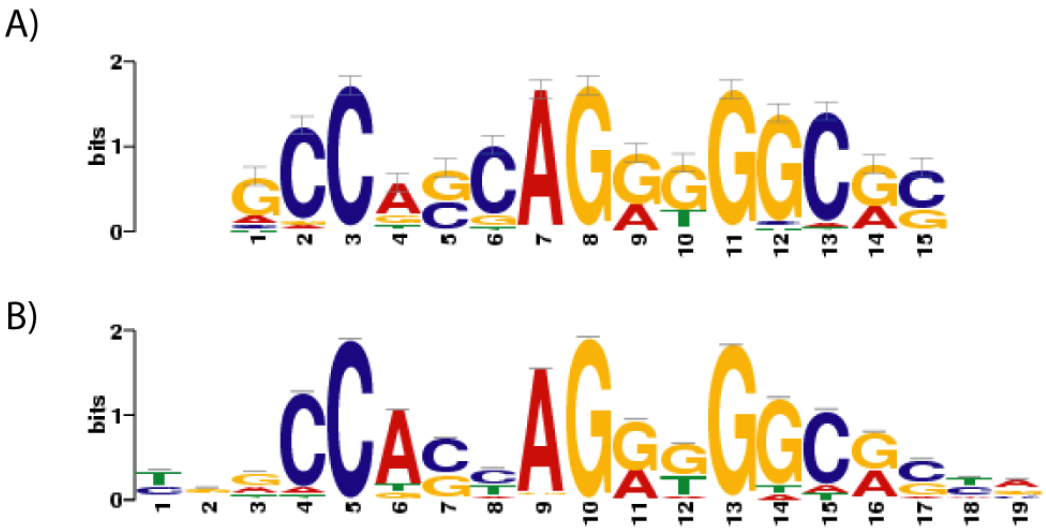

Figure 5.2.23 – CTCF binding motifs were enriched in AoSMC DNase I hypersensitive sites located within distal regions of H3K4me1 enrichment – Novel motif discovery was performed using MEME analysis to search for over-represented sequences present within 5000 AoSMC DNase I hypersensitivity sites that were located within distal regions of H3K4me1 enrichment. **A)** Shows the major motif identified by MEME motif discovery analysis. **B)** Shows the canonical binding motif for CTCF as defined by the JASPAR database.

5.2.5 ChIP-chip profiling of H3K4me1 and H3K4me3 enrichments in cultured ASMCs

It is noted that the ChIP-seq analysis of histone methylation modfications was performed on a single biological replicate. It was envisaged that the reproducibility of H3K4me1 and H3K4me3 enrichments identified in the ChIP-seq experiment would be demonstrated through ChIP-chip studies to profile the enrichment of these modifications at a number of loci in an increased number of biological replicates. These studies included ChIP material derived from cultured ASMCs isolated from both healthy and asthmatic individuals and it was predicted that the ChIP-chip results would not only increase confidence in the ChIP-seq data set but also allow a preliminary analysis of differential histone modifications in cultured ASMCs isolated from either healthy or asthmatic individuals. Unfortunately, due to technical issues the ChIP-chip studies did not produce data of the quality that was expected, primarily due to uneven signal generation across the array and high background meaning that enrichments of H3K4me1 or H3K4me3 were difficult to interpret at a number of loci analysed. Restrictions in terms of both time and resources meant that the studies could not be repeated and it was therefore not possible to perform any comparative analysis of the profile of H3K4me1 and H3K4me3 enrichments in cultured ASMCs isolated from healthy or asthmatic individuals.

It is important that the reproducibility of histone modification enrichments across a number of biological replicates is demonstrated, particularly for H3K4me1 enrichments, which are not as closely associated with TSSs as H3K4me3. Figure 5.2.24 demonstrates a region of H3K4me1 enrichment at the 3' end of the *CCDC97* gene that overlaps three sites of DNase I hypersensitivity in AoSMCs and may represent a novel regulatory region, possibly involved in the regulation of TGFβ expression. This region demonstrates an enrichment of H3K4me1 in two of the replicates analysed during the ChIP-chip investigations, increasing confidence that it may represent a *bone fide* region of H3K4me1 enrichment.

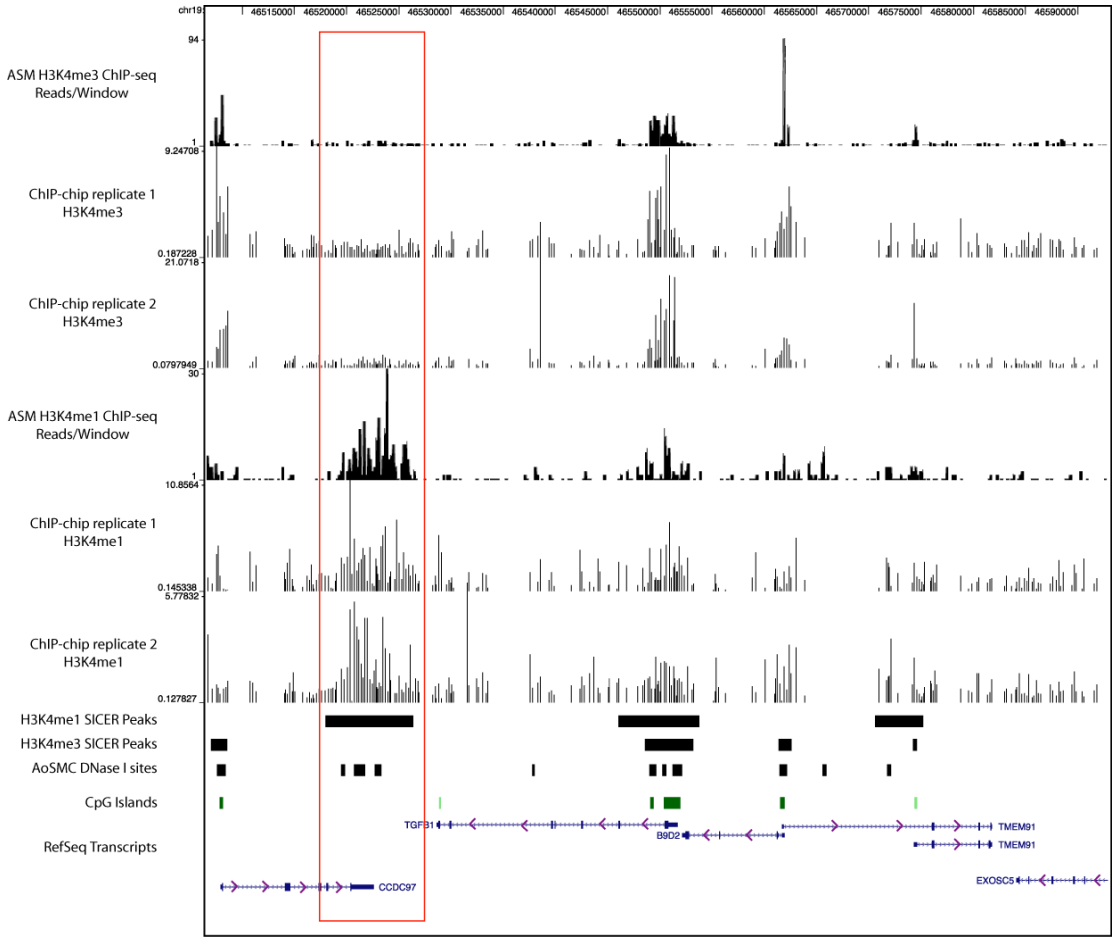

Figure 5.2.24 – Reproducibility of profiles of H3K4me1 and H3K4me3 enrichment across biological replicates – The number of reads / 200 base pair window generated from the H3K4me1 and H3K4me3 ChIP-seq experiment is depicted along with the normalised intensity of probes tiled across the same genomic region analysed during ChIP-chip experiments. The signal intensity of the ChIP-chip tracks represents the intensity enrichment over the corresponding Input sample. Regions defined as enriched for H3K4me1 or H3K4me3 by SICER analysis, sites of DNase I hypersensitivity in AoSMCs, CpG islands and annotated Refseq transcripts are also displayed. The red box signifies a region enriched for H3K4me1 in the ChIP-seq studies and in two biological replicates analysed in the ChIP-chip studies.

5.2.6 Profiling of H3K27me3 enrichments across the genome of a healthy ASMC culture

The profile of H3K27me3 enrichments was determined as it is a modification that has a strong association with regions of chromatin that are not permissive for transcription. Integrating the profiles of H3K4me1, H3K4me3 and H3K27me3 enrichments therefore provides a good overview of the regions of chromatin that are permissive or repressive of transcription in cultured ASMCs. Illumina GAIIx sequencing of a H3K27me3 ChIP library generated from a single healthy ASMC culture produced 30,705,370 sequences, of which 9,994,756 were aligned to a unique location within the reference genome (Figure 5.2.4). Peak calling was performed using SICER with a window size of 500 bases and a gap size of 2000 bases (performed by Dr. V Pullabhatla). These parameters are recommended for the identification of regions of H3K27me3 enrichment using SICER (Zang et al. 2009) as the modification is known to demarcate much broader regions than either H3K4me1 or H3K4me3 and an increased window size allows broader regions with a lower level of enrichment compared to the Input control to be identified (see Chapter 5.1.8). It is important to note, however, that the identification of broad regions of H3K27me3 enrichment remains a challenge for bioinformatics. The list of regions of H3K27me3 subsequently discussed are therefore intending to demonstrate the features of various types of H3K27me3 enrichment that were identified through both SICER analysis and manual inspection of enrichments in the UCSC genome browser. The determination of regions of H3K27me3 enrichment by SICER resulted in the identification of 15,434 regions. Due to the fact regions of H3K27me3 enrichments tend cover broad areas, it was difficult to perform a thresholding exercise as was performed for H3K4me1 and H3K4me3 (see Chapter 5.3.3 and 5.3.4). It should therefore be noted that there may be an increased frequency of false positive regions of H3K27me3 enrichment in comparison to the two previous modifications analysed.

5.2.6.1 Profiling the distribution of H3K27me3 enrichments relative to annotated genes

The profile of H3K27me3 enrichments relative to annotated genes in the RefSeq database was performed using the GenomicAnnotation script in ChIPseeqer-2.0. This analysis identified 448 (2.9%) regions of H3K27me3 enrichment being defined as promoter associated, 4172 (27.1%) as being located within an annotated gene, 3866 (37.8%) as distal to an annotated gene and 4969 (32.2%) as intergenic (Figure 5.2.25).

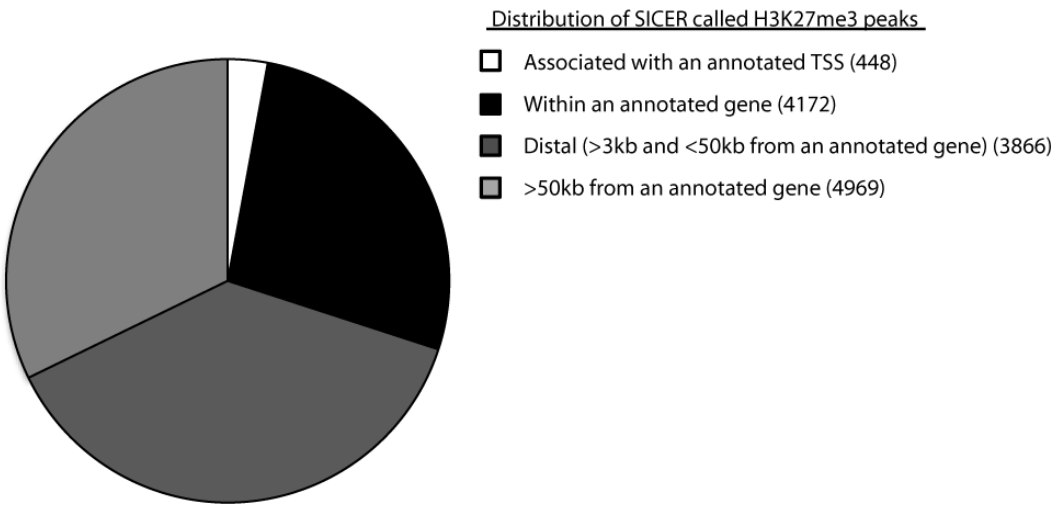

Figure 5.2.25 - Classifying the location of SICER called regions of H3K27me3 enrichment in relation to the closest gene – The 15,434 SICER defined regions of H3K27me3 enrichment were classified based upon their linear distance from the closest annotated gene in the RefSeq database using the GenomicAnnotation Tool in ChIPSeeqer 2.0. Peaks were classified as those that overlapped with annotated TSSs (white segment), those that were located within an annotated gene (black segment), those that were greater than 3kb but less than 50kb from an annotated gene (dark grey segment) and those that were located greater than 50kb from an annotated gene (light grey segment). The bracketed number indicates the number of H3K27me3 enrichments in each classification.

5.2.6.2 H3K27me3 enrichments associated with genes

As stated, H3K27me3 is generally associated with regions of the genome that are not permissive for transcription. The 4172 regions of H3K27me3 enrichment that were found to associate with an annotated RefSeq gene were therefore correlated to the level of expression of the corresponding transcript. The expression levels for individual transcripts were derived from Affymetrix U133.2 microarray studies as described in Chapter 5.2.3.1 and the correlation of H3K27me3 enrichments with transcript expression levels was performed as described for TSS-associated regions of H3K4me3 enrichments. Once regions of H3K27me3 enrichment were matched to

their corresponding locus, the transcripts were sorted based upon expression level and bins of 1000 genes collected at every 3000 data points. The percentage of genes in each bin associated with a region of H3K27me3 was then calculated (Figure 5.2.26). These results were encouraging, as it was shown that none of the top 1000 expressed genes in cultured ASMCs were associated with a region of H3K27me3, whilst ~25% of 1000 genes with the lowest level of expression were associated with a region of H3K27me3.

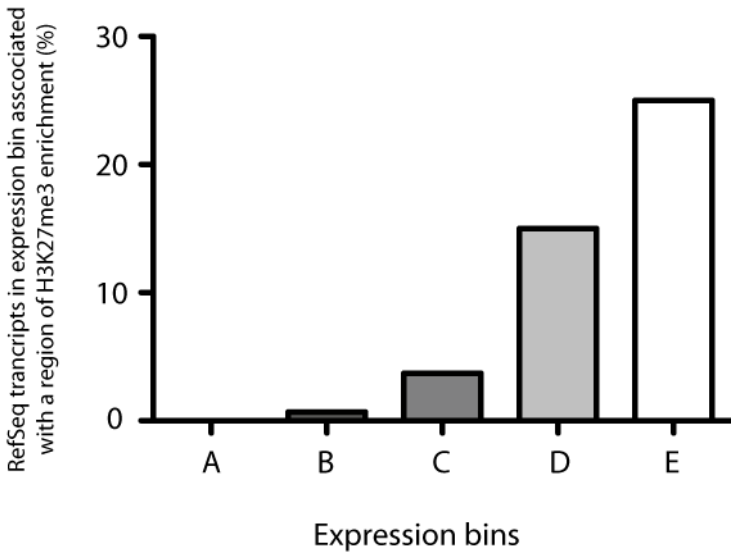

Figure 5.2.26 – Genes from which low levels of transcript are detected are more commonly associated with regions of H3K27me3 enrichment compared to genes from which high levels of transcript are detected – Loci that were associated with a SICER-defined region of H3K27me3 enrichment were determined using the GenomicAnnotation Tool in ChIPSeeqer. These loci were compared to Affymetrix microarray expression data to determine the relationship between the abundance of a transcript and the presence of a H3K27me3 enrichment within that gene. 5 bins of Refseq transcripts were defined based upon expression levels, with Bin A containing the 1000 transcripts with the highest level of detection and subsequent bins of 1000 transcripts were taken at 3000 data point intervals until Bin E, which contains the 1000 transcripts with the lowest level of detection. The percentage of transcripts in each bin that were associated with a region of H3K27me3 enrichment was then calculated.

Genes associated with a SICER defined region of H3K27me3 enrichment were analysed further by using GeneCodis 2.0 (Nogales-Cadenas et al. 2009), (Carmona-Saez et al. 2007) to determine if the genes that displayed features of being actively silenced in cultured ASMCs were involved in similar processes and functions. GeneCodis 2.0 is an online tool that determines if an input gene list contains an overrepresentation of genes involved in particular annotated Gene Ontology (GO) pathways and uses a hypergeometric distribution and Benjamini and Hochberg correction to determine the statistical significance of any

overrepresentation. Determination of GO Pathway enrichment demonstrated that genes actively silenced in cultured ASMCs were overrepresented in pathways involved in development and the regulation of signaling pathways. Figure 5.2.27 demonstrates part of the output generated from GeneCodis and indicates the top ten pathways associated with genes demarcated with H3K27me3 as defined by the number of genes from the complete GO Biological Pathway annotation identified. These top ten pathways included multicellular organismal development, signal transduction, regulation of transcription and cell differentiation (Figure 5.2.27 (A)). In addition, the statistical analysis of the overrepresentation of the top ten pathways is shown (Figure 5.2.27 (B)) and demonstrates a high level of confidence in the pathway enrichment.

A)

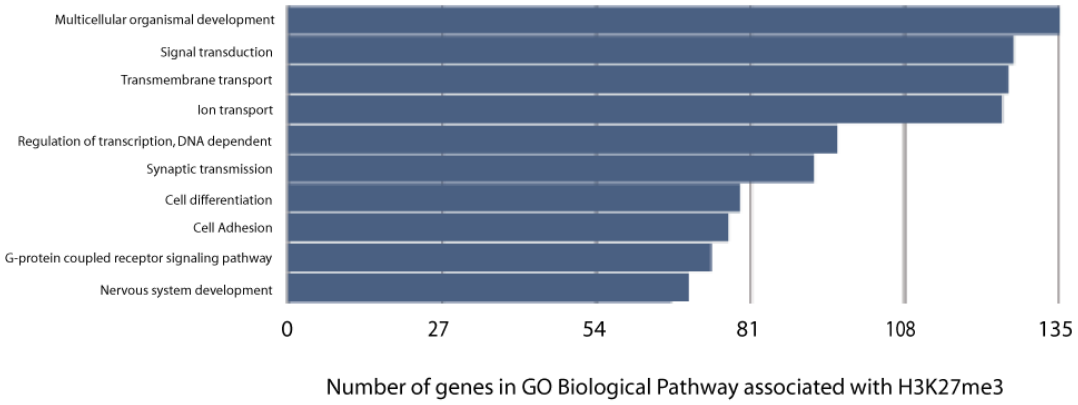

B)

GO ID	GO Biological Pathway	Corrected p-value
GO:0007275	Multicellular organismal development	1.73E-28
GO:0007165	Signal transduction	3.64E-16
GO:0055085	Transmembrane transport	7.87E-41
GO:0006811	Ion transport	2.04E-44
GO:0006355	Regulation of transcription, DNA-dependent	5.94E-11
GO:0007268	Synaptic transmission	7.70E-37
GO:0030154	Cell differentiation	1.02E-17
GO:0007155	Cell adhesion	7.80E-15
GO:0007186	G-protein coupled receptor protein signaling pathway	1.88E-20
GO:0007399	Nervous system development	2.72E-16

Figure 5.2.27 – GeneCodis 2.0 analysis indicates that loci demarcated with H3K27me3 in cultured ASMCs are primarily involved in development and the regulation of signaling pathways – The 1724 genes that were defined by SICER analysis as being associated with H3K27me3 across the body of the locus were used as an input list for GeneCodis 2.0. The resulting output identifies pathways in which genes included in the input list are overrepresented. **A)** Shows the top ten overrepresented pathways as determined by the number of genes in the input list present within each pathway. **B)** Shows the statistical significant of the top ten overrepresented pathways.

Regions demarcated by H3K27me3 are often flanked by genes that are actively transcribed and are therefore demarcated with signatures of active transcription, such as H3K4me3 and H3K4me1. An example of this is *WNT-inhibitory factor 1 (WIF1)*, which is involved in somitogenesis and is expressed in a highly regulated manner during both *C. elegans* and *D. rerio* development (Nathans et al. 1999). Figure 5.2.28 demonstrates that the *WIF1* locus, along with the *TBC1D20* and *FLJ41278* loci, is located in a chromatin environment that is repressive of transcription and does not appear to be expressed in healthy cultured ASMCs. It is flanked on either side, however, by *GNS* and *LEMD3*, each of which is marked by H3K4me3 and is detected at levels above that of background in Affymetrix U133.2 microarray studies performed in the Asthma, Allergy and Respiratory Science department prior to the initiation of this project (Figure 5.2.28 (A)). This is a clear indication as to the depth of information regarding the regulation of transcription at points throughout the genome that can be gained from the analysis of multiple histone modifications. It also demonstrates that the differential demarcation of histones with specific modifications allows local transcription states to be inferred.

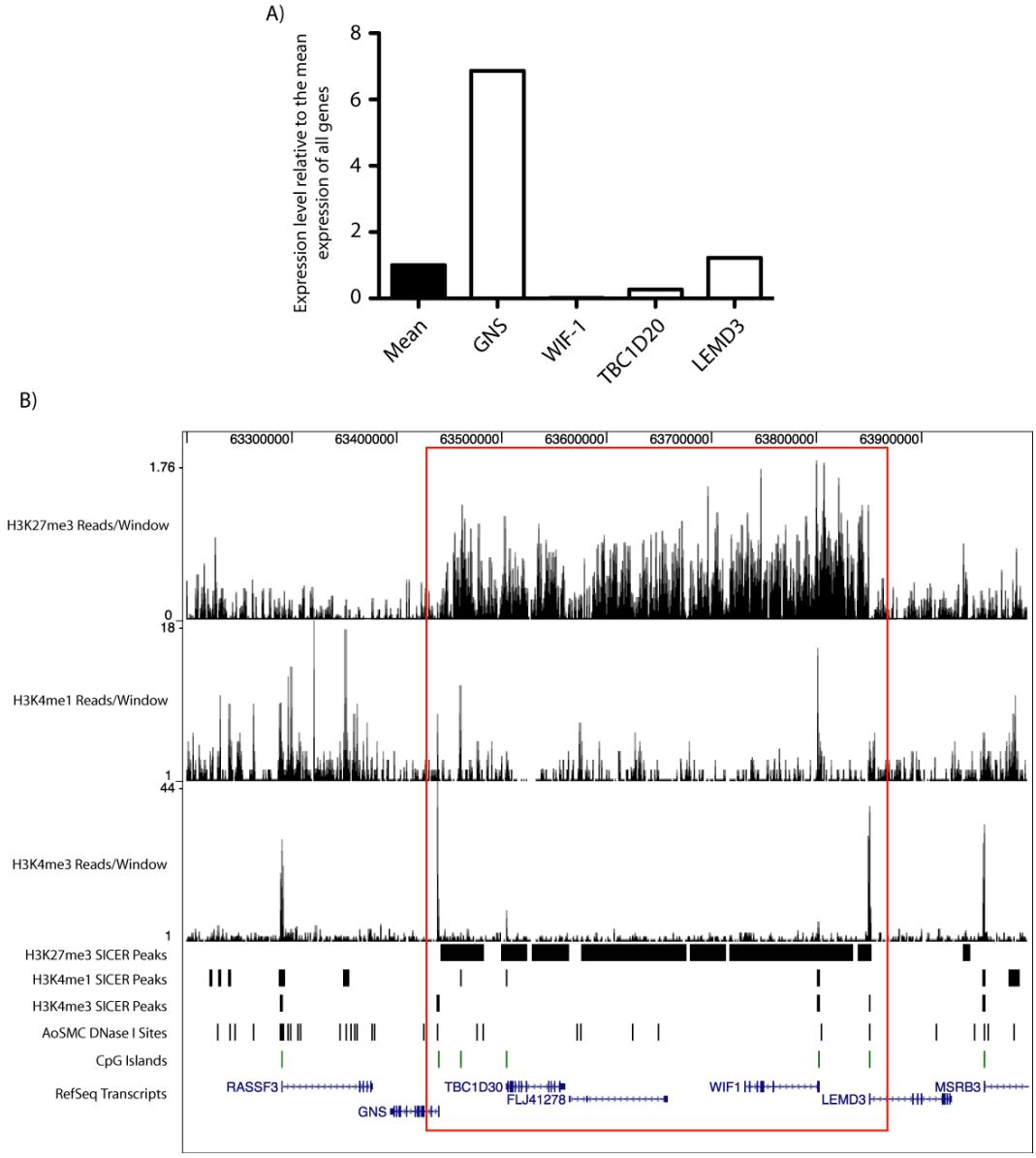

Figure 5.2.28 – H3K27me3 is enriched over the *WIF1* but not the *GNS* or *LEMD3* loci – A) The average level of detectable transcripts from all genes in cultured ASMCs was calculated from intensity values generated from Affymetrix U133.2 expression arrays. The chart shows the mean expression of all genes and the relative expression of GNS, WIF-1, TBC1D20 and LEMD3. FLJ41278 is not assayed on the Affymetrix U133.2 arrays. **B)** H3K4me1, H3K4me3 and H3K27me3 aligned reads were uploaded to the UCSC genome browser as .bigwig files whilst regions determined by SICER to be enriched for each modification were uploaded as .bed files. Annotated CpG islands, regions of DNase I hypersensitivity in aortic smooth muscle and RefSeq transcripts are shown for comparison.

5.2.6.3 Intergenic enrichments of H3K27me3

In addition to the regions of H3K27me3 enrichments that were identified as being associated with an annotated gene, there were a number of regions of enrichment that were located in intergenic regions, as defined by the RefSeq database. In total 10806 regions of H3K27me3 enrichment were defined as intergenic and these were further classified as focal or broad enrichments depending upon whether they spanned a distance of fewer or greater than 10kb. The differentiation of intergenic peaks based upon their width resulted in the identification of 3,733 focal and 7,073 broad regions of enrichment. Figure 5.3.29 demonstrates an example of a broad region of H3K27me3 enrichment between *RPP21* and *HLA-E*, whilst Figure 5.3.30 demonstrates an example of a focal region of H3K27me3 enrichment between *DLG1* and *BDH1.* In both of these examples it is important to note the presence of CpG islands within the region of H3K27me3 enrichment, indicating that unannotated loci may be present within these regions. A second possibility, however, is that these regions of intergenic H3K27me3 enrichment represent insulator-like elements that allow the transcription of individual loci to be independently regulated.

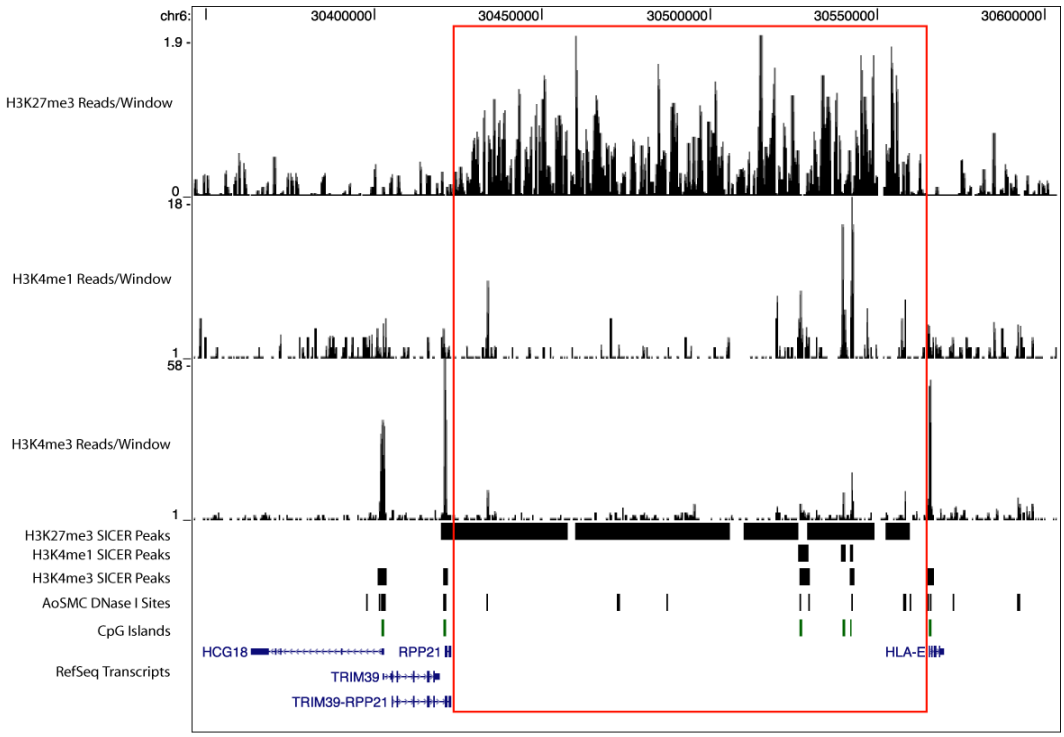

Figure 5.2.29 – An example of a broad region of intergenic H3K27me3 enrichment between the *RPP21* and *HLA-E* loci - H3K4me1, H3K4me3 and H3K27me3 aligned sequences were uploaded to the UCSC genome browser as .bigwig files whilst regions determined by SICER to be enriched for each modification were uploaded as .bed files. Annotated CpG islands, regions of DNase I hypersensitivity in aortic smooth muscle and RefSeq transcripts are shown for comparison. The red box indicates a broad region of intergenic H3K27me3 enrichment between regions of chromatin that are permissive for active transcription at the *RPP21* and *HLA-E* loci.

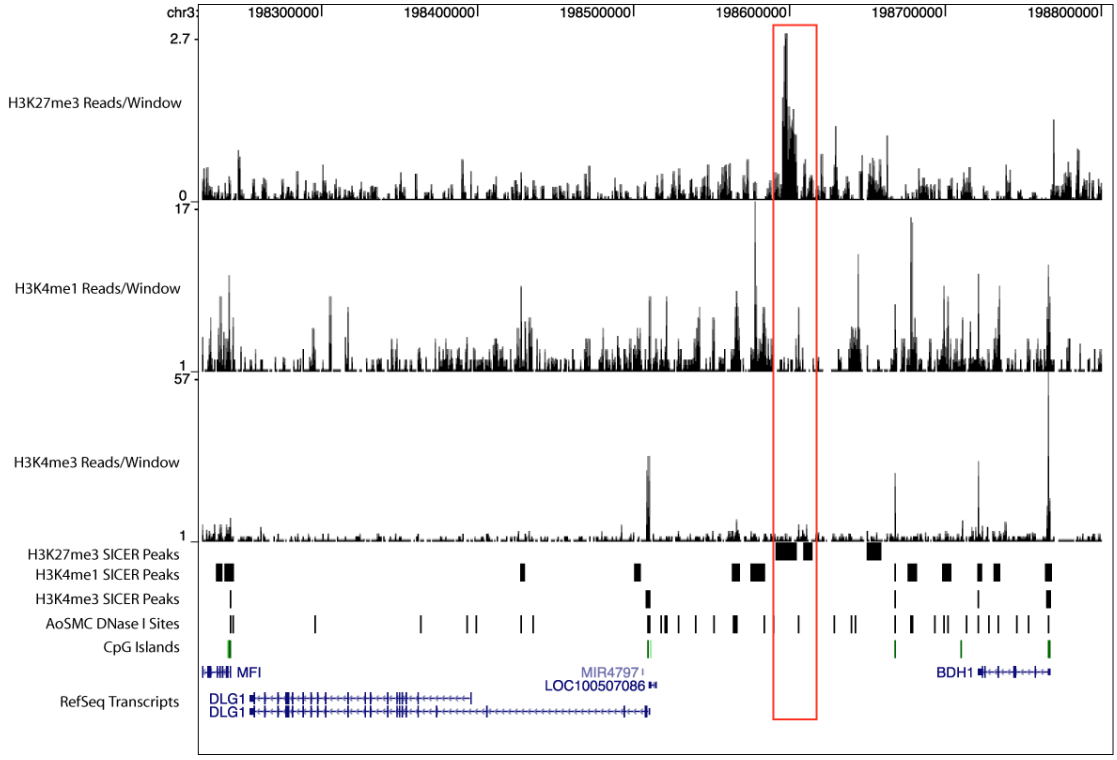

Figure 5.2.30 – An example of a focal intergenic enrichment of H3K27me3 between the *DLG1* and *BDH1* loci - H3K4me1, H3K4me3 and H3K27me3 aligned sequences were uploaded to the UCSC genome browser as .bigwig files whilst regions determined by SICER to be enriched for each modification were uploaded as .bed files. Annotated CpG islands, regions of DNase I hypersensitivity in aortic smooth muscle and RefSeq transcripts are shown for comparison. The red box indicates a focal region of intergenic H3K27me3 enrichment between regions of chromatin that are permissive for active transcription at the *DLG1* and *BDH1* loci.

5.3 Discussion

5.3.1 Summary and interpretation of results

The main aim of the experiments described in this chapter was to generate a profile of specific histone methylation modifications across the genome of a healthy ASMC culture using ChIP-seq technology. Specifically, regions enriched for H3K4me1, H3K4me3 or H3K27me3 were identified and the enrichment profile for each histone modification was compared to data sets generated from other cell types available in the literature. The rationale for investigating the profile of histone modifications in cultured ASMCs is that the data will allow researchers interested in the regulation of specific genes to identify regulatory regions of potential interest that would be unlikely to be identified by classical methods. In addition, the comparison of histone modifications around specific loci in ASMCs compared to other cell types may identify potential cell type specific regulation. It was hoped that studies would be performed to investigate potential differences in chromatin structure between healthy and asthmatic ASMCs. Due to technical difficulties, however, these experiments could not be completed.

At the time of writing, the dataset described in Chapter 5.2 represented the first genome-wide study of histone methylations in cultured ASMCs. Initially, a protocol was optimized to enable chromatin fragments to be isolated from cultured ASMCs. The main requirements of this protocol were that the chromatin was harvested in a cross-linked state, such that it could be archived, and that the chromatin fragments were predominantly of mononucleosomal size (Figure 5.2.1). The importance of recovering material of mononucleosomal size is borne from the fact that this allows greater resolution of the location of a DNA sequence associated with a modified histone. The majority of the results in Chapter 5.2 describe the genome-wide analysis, by ChIP-seq, of H3K4me1, H3K4me3 and H3K27me3 enrichments in a healthy ASMC culture. ChIP-seq involves the preparation of libraries from DNA isolated by specific ChIPs (Figure 5.2.3) followed by the sequencing of these libraries. The sequences generated were mapped to a reference genome (hg18) and regions that were overrepresented in each ChIP sample, and thus represented a region of chromatin demarcated with the histone modification of interest, were identified using the ChIP-seq peak-finding programme, SICER.

5.3.1.1 The genome-wide profile of H3K4me3 enrichments in a healthy ASMC culture

The analysis of sequences generated from an anti-H3K4me3 ChIP-seq experiment identified 16,935 regions that were enriched for H3K4me3 (Figure 5.2.5). Previous data has shown that H3K4me3 is generally associated with TSSs at which transcription is actively initiating (Barski et al. 2007). The data generated in Chapter 5.2.3 corroborate this profile in the context of ASMCs as defining each region of H3K4me3 enrichment based upon its distance from the closest annotated gene in the RefSeq database determined that over 70% of regions defined as enriched for H3K4me3 were associated with an annotated TSS (Figure 5.2.6). It was also shown that the profile of H3K4me3 over an average gene demonstrated enrichment around the TSS (Figure 5.2.7) and that genes with a high level of expression in cultured ASMCs were more likely to be demarcated by a TSS-associated region of H3K4me3 enrichment than those with low levels of expression (Figure 5.2.9). Although this trend was expected, one unanticipated aspect was that only 90% of the top 1000 genes, as defined by normalised expression levels generated during mRNA expression profiling studies, were associated with a region of H3K4me3 enrichment at the TSS. A manual appraisal of the top twenty and bottom twenty genes, in terms of expression level, that lacked a TSS-associated region of H3K4me3 enrichment gave some insight into this result. Seven of the top twenty expressed genes without a positive match between the expression data and TSS-associated H3K4me3 peak list were ribosomal genes that upon manual inspection did have a TSS-associated H3K4me3 enrichment. This suggests that in some circumstances there was a failure to match the expression level gene identifier to the peak location identifier. This was possibly caused by slight differences in the RefSeq release used by the software from which each list was generated. In addition, seven of the top twenty transcripts not matched to a TSS-associated H3K4me3 peak transcripts had a small enrichment of reads that was not called as a peak, a phenomenon likely to be caused by a lack of sequencing depth. In contrast to this 19 out 20 genes with the lowest levels of expression had no indication of a TSS-associated H3K4me3 enrichment.

There were a number of genes that produced levels of transcript that were undetectable above background levels as determined during the Affymetrix U133.2 transcriptome studies that were demarcated by a TSS-associated H3K4me3 enrichment (Figure 5.2.9). This class of genes has been noted in previous studies of

H3K4me3 enrichments (Araki 2009) and is likely to represent genes that are capable of being rapidly upregulated by specific stimuli. The normalised number of reads within a TSS-associated H3K4me3 enrichment was shown to positively correlate with the abundance of transcript derived from the associated gene (Figure 5.2.10), as has been shown previously in other cell types (Barski et al. 2007) (Araki 2009). This suggests that the level of H3K4me3 enrichment at a particular TSS is indicative of the level of transcript that is derived from the associated gene. It should be noted, however, that the data presented in Figure 5.2.10 is derived from the averages of 'gene bins' and it is not the case that the level of H3K4me3 at a TSS is absolutely predictive of transcript levels. It is also established that gene expression can be regulated at various levels other than the initiation of transcription and through mechanisms that do not involve histone modifications. Genes that were not detectable above background levels but were associated with TSS-proximal H3K4me3 enrichments may therefore represent genes that are rapidly upregulated following stimulation by exogenous stimuli or they may be loci where transcriptional initiation is occurring in the absence of productive elgongation. Interrogation of elongation associated histone modifications such as H3K36me3 or H3K79me3 (Barski et al 2007) (Morillon et al. 2005) or RNA polymerase levels across the gene may offer greater insight into this mechanism. Alternatively the transcripts may be subject to post-transcriptional regulation at the level of mRNA stability.

Increased confidence in the validity of a ChIP-seq dataset can be gained from the comparison of regions of enrichment with other architectural or regulatory features. A commonly used signature for identifying regions with a potential regulatory function is DNase I hypersensitivity. As stated in Chapter 5.2.3.1, a public, genome-wide dataset describing sites of DNase I hypersensitivity in ASM was not available at the time of writing. It was therefore decided that regions of H3K4me3 enrichment in cultured ASMCs would be compared to a genome-wide dataset describing sites of DNase I hypersensitivity in AoSMCs, as this was the most similar cell type for which data was available [GEO accession GSM816638]. This analysis indicated that over 80% of regions of H3K4me3 enrichment in cultured ASMCs overlapped with a site of DNase I hypersensitivity in AoSMCs (Table xv). When this analysis was restricted to TSS-associated regions of H3K4me3 enrichment, the percentage overlap was greater than 90% (Table xv). This high level of overlap between regions of H3K4me3 enrichment and sites of DNase I hypersensitivity, combined with the high

percentage of regions of H3K4me3 enrichment associated with annotated TSSs, indicates that the data is of high quality and useful for investigating the regulation of gene expression in ASM. This was encouraging as one purpose of analysing H3K4me3 enrichments in cultured ASMCs was to demonstrate that the well-defined profile of H3K4me3 enrichments would be recapitulated. This data set therefore served as a very useful training dataset for subsequent investigations. In addition to this, however, the integration of TSS-associated regions of H3K4me3 enrichment with mRNA expression data allows gene expression to be investigated and promoter usage in specific cell types to be determined. The *IL-16* locus is shown as an example of this (Figure 5.2.11). It is shown that cultured ASMCs utilise a different TSS at the IL-16 locus compared to Th2 cells and it is therefore likely that IL-16 is regulated by different factors and/or performs different functions in each cell type. IL-16 has been described as a chemoattractant for a variety of immune cells, including $CD4^+$ T cells (Berman et al. 1985), monocytes (Cruikshank et al. 1987), eosinophils (Rand et al. 1991) and dendritic cells (Kaser et al. 1999). It has been shown that polymorphisms in the promoter region of the TSS demarcated by H3K4me3 in Th2 cells are associated with asthma (Burkart et al. 2006). The major isoform of the gene, originally described in T cells and bronchial epithelial cells, is a 631 amino acid protein that requires cleavage by caspase-3 to generate the bioactive protein (Baier et al. 1997) (Baier et al. 1997) (Zhang 1998). The functional, chemoattractant domain has been determined to be located at the carboxyl-terminus (Nicoll et al. 1999). This original isoform is generated by transcription originating from the TSS demarcated with H3K4me3 in Th2 but not ASMCs (Figure 5.2.11). Subsequent studies have identified a larger isoform of IL-16 that was originally believed to be neuronal specific (NIL-16) (Kurschner & Yuzaki 1999). This isoform generates a 1322 amino acid protein, of which the C-terminal 624 amino acids are identical to those of the originally described IL-16 isoform, whilst the N-terminal region has been shown to contain four additional PDZ domains. Interestingly, Bannert *et al.* have used yeast-two hybrid screens to determine that the N-terminal region of NIL-16 interacts with members of the myosin phosphatase targeting (MYPT) family, particularly MYPT-1 (Bannert et al. 2003). MYPT-1 is a component of myosin light chain phosphatase (MLCP) that is involved in dephosphorylation of MLC and therefore the regulation of ASM contraction (Chiba & Misawa 2004). The fact the ASMCs express an isoform of IL-16 that is able to interact with MYTP-1 indicates a potential novel mechanism for the regulation of ASM contraction.

There were a number of SICER-defined regions of H3K4me3 enrichment that were not associated with annotated TSSs within the RefSeq database (Figure 5.2.6) and these enrichments may demarcate unannotated TSSs or potential distal regulatory regions (Pekowska et al. 2011). It is possible that the 1840 regions of H3K4me3 enrichment defined as distal in Figure 5.2.6 may be associated with TSSs not contained within the RefSeq database. Assessing the association of H3K4me3 enrichments with the UCSC gene list resulted in 1737 regions of enrichment that were defined as distal and 1410 regions that did not associate with a TSS annotated in either the RefSeq or UCSC databases. Of these 1410 distal regions of H3K4me3 enrichments, 40% were associated with CpG islands, suggesting that they may be sites of transcriptional initiation. The lack of association between distal H3K4me3 enrichments and TSSs annotated in either the UCSC or RefSeq databases does not prove that some of these regions do not signify TSSs and comparison to expressed sequence tag database should be performed for specific loci of interest. If specific regions of distal H3K4me3 enrichment do not appear to associate with expressed sequence tag data, it may be that they represent distal regulatory regions as a recent report has suggested that functional enhancer elements are demarcated with H3K4me3 rather than H3K4me1 (Pekowska et al. 2011).

5.3.1.2 The genome-wide profile of H3K4me1 enrichments in a healthy ASMC culture

The genome-wide profile of H3K4me1 enrichments was generated in the same manner as for H3K4me3, including the annotation of regions of enrichment based upon their distance from loci in the RefSeq database (Figure 5.2.15). This analysis indicated 45% of regions of H3K4me1 enrichment occurred within annotated genes, whilst 24.4% were located at TSSs, 17.9% between 3kb and 50kb from annotated genes and 12.4% greater than 50kb from an annotated gene. Previously published datasets describing the profile of histone modifications across gene bodies have indicated that H3K4me1 is enriched close to the TSS of a gene and that it generally flanks a region of H3K4me3 enrichment that is more focal in distribution (Barski et al. 2007). Data generated during this project did indicate an enrichment of H3K4me1 around the TSS of genes, however, it appeared to be restricted to a similar area both upstream and downstream of the TSS as H3K4me3 (Figure 5.2.16). Despite this, however, there were examples of individual genes where H3K4me1 enrichments were found to flank H3K4me3 enrichments at the TSS, for example at the *VEGFA* locus (Figure 5.2.17).

Enrichment of H3K4me1 is generally described at regulatory regions, particularly enhancers (Visel et al. 2009) (Heintzman et al. 2007). To increase confidence that regions demarcated with H3K4me1 in the dataset described in Chapter 5.2 represent regulatory regions, the percentage overlap with sites of DNase I hypersensitivity in AoSMCs was determined. This analysis indicated that over 70% of regions of H3K4me1 enrichment in cultured ASMCs overlapped with a DNase I hypersensitivity site in AoSMCs (Table xvi). Further confidence as to the specificity of this analysis was drawn from the fact that performing the same analysis with regions of H3K4me1 enrichment in *in vitro* polarized Th2 cells (data provided by Dr P Lavender), of which there were a similar total number to those identified in ASMCs, resulted in an overlap of only 22%. This dataset may therefore be useful for the identification of regions involved in the regulation of gene expression in ASMCs. As an example of this, regions of H3K4me1 enrichment upstream of the *VEGFA* locus are shown (Figure 5.3.18). Two of these regions (~46kb and ~56kb upstream of *VEGFA*) have been shown, by ChIP-seq studies, to bind the oestrogen receptor (Carroll et al. 2006) and have subsequently been shown to act as distal enhancer elements involved in the regulation of *VEGFA* expression in an oestrogen-dependent manner (Tang et al. 2011). In addition to these validated enhancer regions there are further regions of H3K4me1 enrichment that overlap AoSMC DNase I hypersensitivity sites ~70kb upstream of the *VEGFA* gene, implying that these may signify as yet undiscovered enhancers involved in the regulation of *VEGFA* expression. Unfortunately, it was not possible to determine the functionality of potential enhancer regions during the course of this project. The combination of the identification of previously annotated enhancers, both at genes expressed in ASM (Figure 5.2.18) and in well defined loci from other cell types (Figure 5.2.20), makes it very likely that a number of the identified regions of H3K4me1 enrichment represent *bone fide* regulatory regions. In terms of functional data, a number of identified potential regulatory regions, including those upstream of the *VEGFA* locus (Figure 5.2.18), are currently being analysed through *in vitro* luciferase assays to allow determination of enhancer activity.

It was envisaged that motif searching within distal regions of SICER-defined H3K4me1 enrichment using the MEME motif discovery tool would identify subgroups of potential regulatory regions containing binding motifs for varying combinations of transcription factors and co-factors. Unfortunately this was not the case, as relatively few obvious consensus binding motifs were identified. There are

a number of possible reasons for this result, however, a major factor is likely to be that MEME and other analogous algorithms were originally designed to identify common motifs within an input list of similar sequences. Specifically, MEME was designed to identify a common binding motif in DNA sequences identified from ChIP experiments targeted against discrete proteins. It may therefore be the case that the sequences within the DNase I hypersensitive/H3K4me1 enrichment overlaps are too varied for the algorithm to successfully interpret common motifs within subgroups of the total population. In addition, this style of analysis is generally performed on lower numbers of input sequences and it may be that the input list used in Chapter 5.2.4.3 was larger than optimal for novel motif discovery. It is, however, difficult to rationally justify how one would restrict the list further in order to aid the technical aspects of the analysis. Alternative approaches that could be followed to determine the functionality of potential distal regulatory regions include analysis of their ability to act as enhancer elements *in vitro* and this analysis is currently being undertaken. Additionally, it would be beneficial to perform conservation analysis of distal regions of H3K4me1 enrichment, as it would be expected that non-coding, distal regions of DNA that are involved in regulatory functions will be evolutionary conserved to a greater extent than general non-coding sequences.

One motif that was present within regions of overlap between DNase I hypersensitivity and distal H3K4me1 enrichment was a CTCF binding motif (Figure 5.2.24). CTCF was originally discovered in 1990 as a transcriptional repressor of the chicken lysozyme gene (Baniahmad et al. 1990) and chicken myc gene (Lobanenkov et al. 1990), however, it has subsequently been shown that CTCF can also function as a transcriptional activator (Vostrov et al 1997). The classically described function of CTCF is that of an enhancer blocker acting at insulator elements, most notably associated with the chicken *β-globin* and mammalian *H19/Igf2* loci (Bell et al 1999) (Felsenfeld & Bell 2000) (Tilghman et al. 2000), where it acts to prevent interactions between distal enhancer and core promoter regions. Most data concerning insulators, however, is derived from experiments utilising transgene constructs with insulator sequences inserted between an enhancer and core promoter region (Gaszner & Felsenfeld 2006). The *in vivo* function of CTCF at insulator elements therefore remains an open area of investigation. More recent data has shown that CTCF co-localizes with and targets the cohesin complex to sites within the genome (Parelho et al. 2008) (Wendt et al. 2008). Cohesin is a multi-protein complex

historically associated with sister chromatid alignment (Uhlmann 2004), however, it is now apparent that cohesin is involved in the establishment of many chromatin loop structures that are required for the regulation of transcription at specific genomic loci (Merkenschlager 2010). As a specific example, CTCF directed recruitment of cohesin is required for the establishment of chromatin loops around the *IFNG* gene in Th1 cells, facilitating expression of IFNγ in Th1 but not Th2 cells (Hadjur et al. 2009). In addition cohesin is required for the facilitation of active gene expression in murine embryonic stem cells, however, this appeared to be a role that was independent of CTCF (Kagey et al. 2010). A number of reports detailing the genome-wide distribution of CTCF and H3K4me1 within a cell population have reported an enrichment of H3K4me1 at average CTCF binding sites (Barski et al. 2007) or a co-localisation of H3K4me1 and CTCF at a subgroup of CTCF binding sites (Ernst et al. 2011) (Heintzman et al. 2009). Sites defined as functional enhancers by p300 enrichment, however, have been shown to be depleted of CTCF (Heintzman 2009). This suggests that there may be a subgroup of CTCF binding sites at which H3K4me1 enrichment is also present and the potential function of such sites has not as yet been investigated. It is noted that the analysis described in Chapter 5.2.4.3 is based upon DNA sequence motif searching and it is not shown that CTCF is recruited to regions where its consensus binding site has been identified. The biological relevance of the presence of CTCF binding sites within regions of H3K4me1 therefore requires further investigation and further experiments should include ChIP investigations to determine if CTCF binding occurs at sites where a CTCF binding motif has been identified within regions of H3K4me1 enrichment. CTCF recruitment has been shown to be prevented by the demethylation of CpG dinucleotides (Vostrov 2002). It may therefore be interesting to investigate the ability of CTCF to bind to DNA within the context of modified histones using a technique such as the recent described SILAC nulceosome affinity purification (Bartke 2010) (Nikolov 2011).

5.3.1.3 The genome-wide profile of H3K27me3 enrichments in a healthy ASMC culture

As stated, the enrichment of H3K27me3 is generally associated with regions of the genome that are not actively transcribed (Martens 2005) (Barski et al. 2007). In studies focusing on the enrichment of H3K27me3 over annotated genes it has been reported that the enrichments are often focal in nature and centre around the annotated TSS (Boyer et al. 2006), however, when more unbiased approaches have

been utilised it has been shown that H3K27me3 enrichments can span over tens of megabases (Chadwick 2004). The data generated in Chapter 5.2.5 indicated four main locations of H3K27me3 enrichment, with 2.9% associated with an annotated TSS, 27.1% located within an annotated gene, 37.8% between 3kb and 50kb of an annotated gene and 32.2% greater than 50kb from an annotated gene (Figure 5.2.25).

The profile of H3K27me3 enrichments has been studied in most depth in embryonic stem cells (ESCs). It has been shown that genes encoding regulators of differentiation are enriched for H3K27me3 in ESCs, indicating that they are actively silenced (Boyer et al. 2006) (Zhao et al. 2007) (Pan et al. 2007). As differentiation to a specific cell type proceeds, a combination of these regulator genes lose their H3K27me3 enrichments (Bracken 2006) (Lee et al. 2007a) whilst genes involved in early development become marked with H3K27me3 (Ringrose et al. 2004). These data appear to be corroborated by the data generated in Chapter 5.2.5, as it was shown that genes associated H3K27me3 enrichments were overrepresented in pathways involved in early stages of development (Figure 5.2.27). The quality of the data generated in Chapter 5.2 is strengthened when combinations of histone methylation marks are analysed. An example of this is demonstrated in Figure 5.2.28 where it is shown that the *WIF1* locus, along with the *TBC1D20* and *FLJ41278* loci, are located in a chromatin environment that is enriched for H3K27me3 and therefore repressive of transcription. These genes are flanked by *GNS* and *LEMD3*, each of which is marked by H3K4me3 and is detected at levels above that of background in Affymetrix U133.2 microarray studies performed in the Asthma, Allergy and Respiratory Science department prior to the initiation of this project. This data therefore demonstrates the correlation of histone modifications with the regulation of gene transcription at distinct loci within the genome.

In addition to the previously described enrichments of H3K27me3 over annotated genes, the data generated in Chapter 5.2.5 also indicated a number of H3K27me3 enrichments in intergenic regions (Figures 5.2.29 and 5.2.30). There are previous reports of H3K27me3 enrichments in intergenic regions in the mouse (Pauler 2009) and it was proposed that these regions may be involved in demarcating and specifying regions of chromatin that are regulated independently at the level of transcription. Although it was not possible during this timescale to perform in depth analysis of these intergenic regions of H3K27me3 enrichment, it is

interestingly to speculate that they may be involved in an 'insulator-like' function to prevent the cross-regulation of adjacent loci. To investigate this hypothesis further it would be useful to investigate the binding of CTCF to determine if this correlated with intergenic regions of H3K27me3 enrichment.

5.3.2 Caveats and limitations

The data generated in any ChIP-based assay is absolutely reliant on the quality and specificity of the antibody (Carey et al. 2009). If the antibody used does not specifically immunoprecipitate the desired protein then any downstream analysis is extremely limited. In terms of this study, a high level of confidence can be held regarding the quality of the antibodies for a number of reasons. Foremost, each of the histone modifications analysed has a well-defined profile of enrichment determined across a variety of cell types and each of these profiles was recapitulated within ASMCs (Figure 5.2.6, 5.2.15 and 5.3.25). In addition, the corroboration of enrichments for each histone modification with distinct architectural features increases confidence in the integrity of the regions of enrichment for the histone modifications. It has been shown, for example, that H3K4me3 is localised to focal regions, most commonly located at annotated TSSs (Figure 5.2.6). Further, a large percentage of both H3K4me3 and H3K4me1 enrichments overlap with sites of DNase I hypersensitivity in AoSMCs (Table xv). The anti-H3K4me1 antibody used during these studies has previously been used in the Lavender Laboratory to identified regions of H3K4me1 enrichment that overlap annotated enhancer regions in Th2 cells (Figure 5.2.20) and during experiments conducted in this project immunoprecipitated regions of DNA previously identified as enhancer regions in ASMCs (Figure 5.2.18). H3K27me3 has been shown during these studies to typically display broader profiles of enrichment, as has previously been noted (Pauler 2009). In addition, the fact that a number of genes that were found to be actively silenced in ASMCs are involved in development and differentiation, and are not expressed in ASMCs, increases confidence in this dataset (Figure 5.2.27).

There are a number of technical aspects to consider when performing ChIP-seq experiments and the novel nature of the technology means that many of these issues remain subject to debate within the field. The determination of regions of enrichment for a particular histone modification is based upon an overrepresentation of DNA sequences within a defined window of the reference

genome in the ChIP sample compared to the Input control (see Chapter 5.1.8). There are a number of algorithms currently available for the identification of enriched regions within ChIP samples. SICER was used to identify enriched regions during this project as it was specifically designed for the identification of enrichments of histone modifications (Zang et al. 2009) and has been shown to perform favourably in this type of analysis when compared to other algorithms (Micsinai et al. 2012). When regions of enrichment are determined based upon an over-representation of sequences in the ChIP sample compared to the Input it is important to consider the depth of sequence coverage in the Input sample. This issue is particularly important when considering regions that are called as enriched in the ChIP sample but have no reads in the Input, as the lack of coverage in the Input sample may lead to a number of false positive determinations of regions of enrichment. To account for this issue during the analysis of ChIP-seq experiments described in Chapter 5.2, regions of enrichment for H3K4me1 and H3K4me3 were discounted if they did not contain greater than 30 reads within the ChIP sample (see Chapter 5.2.3). This restriction could not be performed for H3K27me3, as the regions of enrichment are generally broader and of a lesser magnitude. It may therefore be the case that the H3K27me3 dataset contains an increased proportion of false positive peaks.

The determination of false positive results from enriched region lists generated by peak-calling algorithms, such as SICER, is challenging (Wilbanks & Facciotti 2010). It is generally accepted that lists of enrichment must be combined with previous biological knowledge, as was performed in Chapter 5.2, in order to increase confidence in the results gained. It is also accepted that there is a region in all enrichment lists generated at which the data becomes unreliable and that a greater number of high confidence peaks can be gained if the depth of sequencing is greater. Confirmation of peak integrity is often achieved through qPCR studies of a range of potential regions of enrichment that were identified with diminishing statistical confidence. A subjective decision is made that the regions of enrichment that were assessed a particular statistical confidence are of poor quality and regions with lower levels of statistical confidence than this are discounted from subsequent analyses. It is clear that not every called region of enrichment can be tested and there will therefore be a number of ambiguous regions of enrichment. During this project it was not possible to performed qPCR validation due to a lack of ASMCs and time restraints. It is because of this that stringent thresholds of $p<10x10^{-10}$ and

greater than 30 reads in the ChIP sample were imparted for the analysis of H3K4me1 and H3K4me3.

It was hoped that the ChIP-chip investigations performed to analyse the profile of H3K4me1 and H3K4me3 enrichments in ASMCs isolated from healthy and asthmatic individuals would allow the validation of regions of enrichment identified during the ChIP-seq studies across an increased number of biological replicates. In addition it was envisaged that this data set would enable the preliminary comparison of histone methylation modifications in ASMCs isolated from either healthy or moderate asthmatic individuals. As previously stated (see Chapter 5.2.4.3), the data generated from these experiments was not of the quality that was expected as technical problems resulted in uneven data quality across the microarrays. This resulted in specific regions of enrichment for specific histone modifications being difficult to identify when compared to control signals generated from the Input channel at a number of loci. Figure 5.2.24 demonstrates that it was possible to identify reproducible enrichments of histone modifications at certain loci and suggests that the regions of H3K4me1 enrichment at the 3' end of the *CCDC97* gene may demarcate regulatory regions. Reproducibility demonstrated through ChIP-chip studies would be expected to be of greater quality than that demonstrated by qPCR, as each probe set on the ChIP-chip tiling arrays represents approximately 250 base pairs of DNA. A broad region of enrichment, such as that depicted in Figure 5.2.22, therefore represents the equivalent of a qPCR assay using multiple adjacent primers to define a region of enrichment.

The bioinformatics analysis described throughout Chapter 5.2 is intended to enable to identification of trends, for example that distribution of specific histone modifications, and allow their comparison to data sets generated in other cell types. It is clear that there will be numerous examples where specific events do not fit the general trends of the average data, for example the small proportion of CTCF binding sites that have been reported to overlap H3K4me1 enrichments (Ernst et al. 2011). It is therefore intended that manual appraisal of chromatin architecture proximal to specific genes should be performed to identify potential factors involved in their regulation.

5.3.3 Relevance and context of results

As stated, the data presented in this chapter describe the first unbiased, genome-wide analysis of histone methylation modifications in ASMCs. Previous work investigating the role of histone modifications in ASMCs has focused upon the regulation of specific genes following a stimulus, for example the exposure to a pro-inflammatory cytokine, and the affect that this has on the acetylation of promoter-proximal histones. At the time of writing, no reports discussing histone methylation in ASMCs could be identified. It has been shown that the bradykinin or IL-1β mediated induction of cyclooxygenase-2 (COX-2) expression in ASMCs involves the recruitment of cAMP responsive binding protein-1 (CREB1) and NFκB and an increase in the acetylation of H4 at the COX-2 promoter region (Nie 2003). The upregulation of CXCL10 or CCL11 expression in ASMCs has also been shown to require an increase in the level of H4 acetylation at their respective promoters (Clarke et al. 2008) (Clarke et al. 2010). The regulation of histone modifications is implicated in the mechanism of action of asthma therapies. Nie *et al.* have demonstrated that the repression of TNFα-induced expression of eotaxin in ASMCs by fluticasone, salbutamol or β_2-agonists involves a decrease in the level of H4 acetylation at the eotaxin promoter element (Nie et al. 2005) (Nie et al. 2004).

There is contradictory evidence as to the potential for targeting the regulation of histone modifications in asthma therapies through the use HDAC inhibitors. Banerjee *et al.* have recently reported that the use of Trichostatin A, a HDAC1 and HDAC2 inhibitor, reduced the level of methacholine-induced hyperresponsiveness in both naïve and *A.fumigatus* sensitised mice. Trichostatin A was also shown to reduce the level of intracellular calcium release in ASMCs following histamine treatment (Banerjee et al. 2011). An earlier report had previously suggested that Trichostatin A treatment abrogated inflammation and airway hyperresponsiveness in a different murine model (Choi et al. 2005), however, these findings were not recapitulated by Banerjee *et al..* These differences may be caused by the different Trichostatin A dosing strategies used or differences in genetic background and the sensitisation procedures of the models. These data suggesting HDAC inhibitors as potential asthma therapies contradict data gathered from molecular biology-based approaches. These include data that indicated lower levels of HDAC1 and HDAC2 expression in bronchial biopsies isolated from asthmatic patients compared to healthy control subjects. Further, steroid treated asthmatic patients had increased HDAC expression compared to untreated patients and it was postulated that lower

levels of HDAC activity in asthmatic patients may lead to increased acetylation and expression of proinflammatory genes (Ito et al. 2002). HDAC2 is able to deacetylate the glucocorticoid receptor, which enables it to bind NFκB and hence prevent the induction of proinflammatory gene (Ito et al. 2006). This may offer a potential mechanism for the involvement of HDAC2 in mediated the glucocorticoid action.

Although reports concerning the targeting of histone modifying enzymes for potential asthma therapies are directed towards broad classes of enzymes, such as HDACs, exciting data is beginning to emerge from other fields regarding the potential manipulation of histone modifying enzymes in a specific manner. Nicodeme *et al.* reported that a small molecule inhibitor of the 'Bromodomain and extra-terminal (BET) proteins (BRD2, BRD3 and BRD4), which function histone acetylation readers and govern the assembly of histone acetylation-dependent chromatin complexes that regulate inflammatory gene expression, was able to diminish the pro-inflammatory transcriptional response following *in vitro* LPS-induced stimulation of bone marrow derived macrophages (Nicodeme et al. 2010). This effect was shown to correlate with a decrease in the amount of promoter-associated BET and H3 and H4 acetylation at pro-inflammatory genes. More recently it has been shown that the small molecule inhibitor of BET is able to induce early cell cycle arrest and apoptosis in human and murine leukaemic cell lines by inhibiting the expression of oncogenes such as Bcl-2, c-Myc and CDK6 (Dawson et al. 2011). These reports serve as exciting proof-of-principle studies for potential targeted 'epigenetic-based' therapeutic approaches. An interesting report by Marazzi *et al.* has demonstrated that Influenza A H3N2 possesses a 'histone-like' sequence (non-structural protein (NS)-1) that is used by the virus to target the human PAF1 transcription elgonation complex (hPAF1c) (Marazzi et al. 2012). The binding of hPAF1c by NS-1 inhibits essential hPAF1c mediated transcription and contributes to diminishing the host anti-viral response. This interaction between NS-1 and hPAF1c offers a potential strategy for the use of histone mimics as a novel therapeutic approach to target transcriptional regulation.

There are a number of reports investigating the molecular regulation of gene expression in a variety of cell types that are known to be involved in the establishment and maintenance of the asthmatic phenotype, including ASMCs (Clifford et al. 2008) (Clarke et al. 2009) (Ammit et al. 2009). It is extremely noticeable, however, that the majority of such reports focus on the recruitment of

transcription factors, the modification of histones and the structure of chromatin at promoter-proximal cis-acting elements. Increasing evidence from a number of high impact reports has indicated that distal enhancers are integral for the regulation of transcription at specific loci. As discussed previously, the specific modification of histones, particularly the presence of H3K4me1, can be used to identify potential enhancer regions (Heintzman et al. 2009) and the differential modification of histones at enhancers has been shown to be predictive of enhancer activity (Visel et al. 2009). Enhancer activity is required for the regulation of mammalian development (Kranz et al. 2011) and for the modification of transcriptional profiles in response to extracellular stimuli (Wang et al. 2011), indicating that enhancers are required for the rapid regulation of transcription at individual genes. Degner *et al.* have recently generated very interesting data regarding expression quantitative trait loci (eQTL) (Degner et al. 2012). eQTLs are sites of genetic variation that correlate with differences in gene expression and have been shown to have important influences on phenotypes (Cheung et al. 2005) (Nicolae et al. 2010), (Nica et al. 2010), possibly through single nucleotide polymorphisms (SNPs) that cause the differential recruitment of transcription factors and thus influence transcription rates of specific genes (Kasowski et al. 2010) (McDaniell et al. 2010). Degner *et al.* performed DNase I sequencing to identify sites of DNase I hypersensitivity in 70 Yoruba lymphoblastoid cell lines and integrated that data with genome-wide genotypes and transcriptome data to identify DNase I hypersensitivity sites that overlapped with eQLTs. This data indicated that over 55% of eQTLs occurred in regions of DNase I hypersensitivity and that an eQTL could be located tens of kilobases from the gene with which it was associated. This data suggests that variation in DNA sequences at distal regulatory regions is important in the regulation of gene transcription, possibly through impacting the recruitment of transcription factors to enhancer regions.

As the combination of H3K4me1 enrichment and a site of DNase I hypersensitivity is recognised to be a reliable signature of potential enhancer regions, it is envisaged that the genome-wide dataset describing regions of H3K4me1 and DNase I hypersensitivity overlaps will be utilised by researchers interested in the regulation of gene expression, particularly in ASMCs. As stated, there are examples whereby this dataset has identified previously annotated enhancer regions and it is expected that large proportion of the remaining regions of H3K4me1 and DNase I hypersensitivity overlaps represent novel, unannotated enhancer regions. In view

of this, experiments are currently being undertaken to determine the functionality of a number of these potential enhancer regions in luciferase transfection systems. It is hoped that these studies will act as a proof-of-principle that the data generated in Chapter 5.2 regarding H3K4me1 will be of use to researchers wishing to identify novel, regulatory regions influencing the expression of particular genes. If particular enhancers are shown to be functional in luciferase assay systems the identification of factors recruited to these regions may offer insight into the potential physiological regulation of specific genes and how this regulation may be affected in asthma.

Chapter 6 - General Discussion

The rationale of the work described in this thesis was to utilise molecular techniques to investigate the regulation of gene expression in ASM using a model system of *ex vivo* cultured ASMCs isolated from bronchial biopsies.

Asthma is characterised by reversible and reoccurring symptoms that include airflow obstruction, bronchial hyperresponsiveness and underlying inflammation (Wills-Karp 1999). ASM is central to the pathophysiology of asthma, as demonstrated by the efficacy of ASM targeted therapies such as β2-agonists and bronchial thermoplasty. There are now a large number of reports detailing an altered phenotype of ASM in asthmatic patients compared to healthy individuals and these differences have been shown to be caused by intrinsic differences in the ASMCs themselves or through responses to the inflammatory milieu present in the asthmatic lung. Examples of altered ASM phenotypes in asthma include cellular hypertrophy and hyperplasia, increased rates of proliferation, increased cellular migration, hypercontractility and the altered secretion of immunomodulatory molecules. Preliminary transcriptome analysis performed in the Asthma, Allergy and Respiratory Science Department prior to the initiation of this project indicated that there were a number of differences in gene expression between cultured ASMCs isolated from healthy or asthmatic volunteers that appeared to be retained throughout a period of ex *vivo* culture. The primary aim of this project was therefore to add to this data by investigating potential mechanisms involved in the regulation of gene expression in cultured ASMCs, with the ultimate aim of identifying differences between ASMCs isolated from healthy or asthmatic individuals. In addition to performing comparative experiments, the data generated is also intended to act as a resource for investigators interested in the regulation of specific genes, particularly in ASMCs.

The experimental work described in this thesis has therefore focused on two major facets;

i) the profiling of miRNA expression in cultured ASMCs and the comparison of miRNA expression in ASMCs isolated from either healthy or moderate asthmatic individuals,
ii) the generation of genome-wide profiles of histone methylations in cultured ASMCs.

Chapters 3 and 4 describe investigations focused on assessing miRNA functions in cultured ASMCs. In Chapter 3 miRNA expression profiling was performed to enable a general profile of miRNA expression in cultured ASMCs to be generated and to compare the expression of miRNAs in ASMCs isolated from either healthy or moderate asthmatic individuals. Although the general profile of miRNA expression was found to be very similar between healthy and asthmatic ASMCs, a number of miRNAs with potential differential expression were identified. It was shown that both miR-155 and its housing transcript, BIC, were expressed at lower levels in cultured ASMCs isolated from asthmatic compared to healthy individuals. Due to previous evidence indicating that a mouse knock-out of miR-155 demonstrated spontaneous airway remodeling similar to that which occurs in asthma (Rodriguez et al. 2007) it was decided to investigate the potential mRNA targets for miR-155 in cultured human ASMCs. Chapter 4 describes experiments performed to identify endogenous mRNA targets of miR-155 in cultured ASMCs. Unfortunately, despite attempting various experimental strategies, the work undertaken was unable to generate strong evidence identifying a *bone fide* target for miR-155 in cultured ASMCs. It is hoped that future investigations will identify targets and functions of miR-155 expression in ASMCs and that this may lead to the understanding of novel pathways of post-transcriptional gene expression regulation.

Future work following from the data generated during the miRNA investigations described in Chapters 3 and 4 could proceed in a variety of directions. It would be very important to determine if potential differences in miRNA expression were reproducible across an increased number of replicates, included differing severities of asthmatic individuals. It was hoped that this would be achieved in part during this project through the analysis of miRNA expression in laser capture microdissections of ASM bundles. Unfortunately, however, this was ultimately not possible during the timeframe of this project due to various difficulties regarding the accumulation of biopsies. It would be interesting to investigate potential unbiased approaches for the identification of miRNA targets in cultured ASMCs. These experiments could include the PAR-CLIP technique described by Hafner *et al* (Hafner et al. 2010), which would provide a complete picture of mRNAs that are incorporated into the RISC complex in cultured ASMCs through immunoprecipitation and DNA sequencing. Alternatively it may be possible to identify endogenous targets of specific miRNAs, for example miR-155, in cultured human ASMCs through a more comprehensive transcriptome analysis following the

modulation of levels of particular miRNAs. It would be interesting to give greater focus to the functional impact of differential miR-155 expression in cultured ASMCs isolated from asthmatic individuals through the investigation of functional features of ASM, such as proliferation, the secretion of immunomodulatory molecules and contraction following the specific modulation of miR-155 expression levels. Whether miR-155 alters intrinsic properties of cultured ASMCs or specific responses to pro-asthmatic cytokines could also be investigated.

Chapter 5 describes the generation of genome-wide profiles of the histone methylation modifications H3K4me1, H3K4me3 and H3K27me3 in cultured ASMCs through the use of ChIP-seq technology. At the time of writing there were no published reports of genome-wide histone modification profiles in cultured ASMCs. These histone methylation profiles are intended as a resource for investigators interested in the regulation of expression of specific genes, especially in ASMCs. In particular, due to the increasing number of investigations assessing the molecular regulation of gene expression in ASMCs (Clifford et al. 2008) (Clarke et al. 2009), it is hoped that the identification of regions of H3K4me1 enrichment that coincide with sites of DNase I hypersensitivity will enable researchers to identify distal elements involved in regulating the expression of their genes of interest. The histone methylation profiles generated will also be incorporated into larger projects aimed at generating genome-wide histone modification profiles across a variety of immune and structural cells, including T cells, dendritic cells, monocytes and epithelial cells, involved in the asthmatic response. It is envisaged that the cumulative data produced from epigenetic and transcriptome studies will provide insights into the regulation of gene expression in the cell types involved in the asthmatic response and will give a greater understanding as to the cell-type specific regulation of gene expression.

Initial future work following from the histone modification profiles should focus on demonstrating the general reproducibility of enrichments in an increased number of biological replicates. It was envisaged that this would be achieved during the course of this project through the ChIP-chip studies described in Chapter 5.2.5, however, as detailed this was not possible due to the poor performance of the tiling arrays used in the experiment. The use of a ChIP-chip platform remains well-suited to these validation studies, as it would serve both to validate regions of enrichment identified in the ChIP-seq experiment and, through the use of ChIP material isolated

from both healthy and asthmatic ASMCs, allow preliminary determinations of differential histone modification enrichments between cultured ASMCs isolated from healthy and asthmatic individuals. In addition to determining the reproducibility of regions of enrichments, it would also be important to demonstrate functions for potential regulatory regions. This is currently being undertaken for a subset of regions of H3K4me1 enrichment that overlap DNase I hypersensitivity sites to determine if these are able to function as putative enhancers elements during *in vitro* assays. It would also be interesting to continue bioinformatics analysis of potential regulatory regions to determine common features that may define distinct classes of elements, for example through the continuation of motif finding, transcription factor binding analysis and pathways analysis. Previous reports describing chromatin architecture in specific cell types have performed a wide-range of ChIP-seq experiments for a variety of histone modifications and transcription factors, as this allows greater confidence to be gained in the function of specifically modified regions (Barski et al. 2007) (Visel et al. 2009) (Heintzman et al. 2007) (Birney et al. 2007). Clearly this would be a beneficial undertaking in order to increase the information available regarding chromatin architecture in cultured ASMCs, however, a great deal of resources are required to perform experiments on this scale. It may be particular pertinent to determine the genome-wide distribution of H3K27Ac and p300 binding as these features, in addition to H3K4me1 enrichment, would increase confidence in the identification of potential distal enhancer regions.

As an alternative experimental approach, the DNA methylation profile in cultured ASMCs could be investigated as a complementary dataset to the histone modification profiles. DNA methylation at gene promoters is associated with the transcriptional repression of the locus and it has been shown the differential DNA methylation patterns correlate with gene expression in various disease settings, including asthma (Ho 2010). It may therefore be of interest to investigate the general DNA methylation profile of cultured ASMCs and integrate this with profiles of histone modifications and to compare DNA methylation in ASMCs isolated from healthy or asthmatic individuals.

In summary the data generated during this thesis will be combined with a growing body of literature investigating the regulation of gene expression in ASMCs. It is

hoped that both the miRNA expression profiling and generation of histone methylation maps will provide the basis for future investigations.

References

Abbott, D.W., 2001. Characterization of the Stability and Folding of H2A.Z Chromatin Particles. IMPLICATIONS FOR TRANSCRIPTIONAL ACTIVATION. *Journal of Biological Chemistry*, 276(45), pp.41945–41949.

Acosta-Rodriguez, E. Napolitani, G. Lanzavecchia, A. & Sallusto, F. 2007. Interleukins 1beta and 6 but not transforming growth factor-beta are essential for the differentiation of interleukin 17-producing human T helper cells. *Nature Immunology*, 8(9), pp.942–949.

Bracken AP. et al. 2006. Genome-wide mapping of Polycomb target genes unravels their roles in cell fate transitions. *Genes & Development*, 20(9), p.1123.

Ahmad, K. & Henikoff, S., 2002. The histone variant H3.3 marks active chromatin by replication-independent nucleosome assembly. *Molecular Cell*, 9(6), pp.1191–1200.

Allan, J. et al., 1980. The structure of histone H1 and its location in chromatin. *Nature*, 288(5792), pp.675–679.

Allfrey, V.G., Faulkner, R. & Mirsky, A.E. 1964. Acetylation and methylation of histones and their possible role in the regulation of RNA synthesis. *Proceedings of the National Academy of Sciences of the United States of America*, 51, pp.786–794.

Allis, C.D. et al., 1980. Histone variants specific to the transcriptionally active, amitotically dividing macronucleus of the unicellular eucaryote, Tetrahymena thermophila. *Cell*, 20(3), pp.609–617.

Allis, C.D. et al., 2007. New nomenclature for chromatin-modifying enzymes. *Cell*, 131(4), pp.633–636.

Ammit, A.J. et al., 2009. The effect of asthma therapeutics on signalling and transcriptional regulation of airway smooth muscle function. *Pulmonary Pharmacology & Therapeutics*, 22(5), pp.446–454.

Ammit, A.J., Armour, C.L. & Black, J.L., 2000. Smooth-muscle myosin light-chain kinase content is increased in human sensitized airways. *American Journal of Respiratory and Critical Care Medicine*, 161(1), pp.257–263.

Amrani, Y. & Bronner, C., 1993. Tumor necrosis factor alpha potentiates the increase in cytosolic free calcium induced by bradykinin in guinea-pig tracheal smooth muscle cells. *Comptes rendus de l'Académie des sciences. Série III, Sciences de la vie*, 316(12), pp.1489–1494.

Amrani, Y. et al., 1996. Activation of the TNF alpha-p55 receptor induces myocyte proliferation and modulates agonist-evoked calcium transients in cultured human tracheal smooth muscle cells. *American Journal of Respiratory Cell and Molecular Biology*, 15(1), pp.55–63.

Araki, Y. et al., 2009. Genome-wide analysis of histone methylation reveals chromatin state-based complex regulation of differential gene transcription and function of CD8 memory T cells. *Immunity*, 30(6), p.912.

Asthma, U., 2011. Where do we stand now?, pp.1–16.

Auphan, N. et al., 1995. Immunosuppression by glucocorticoids: inhibition of NF-kappa B activity through induction of I kappa B synthesis. *Science*, 270(5234), pp.286–290.

Bagga, S. et al., 2005. Regulation by let-7 and lin-4 miRNAs results in target mRNA degradation. *Cell*, 122(4), pp.553–563.

Bai, T.R., 1990. Abnormalities in airway smooth muscle in fatal asthma. *The American review of respiratory disease*, 141(3), pp.552–557.

Baier, M. et al., 1997. Molecular cloning, sequence, expression, and processing of the interleukin 16 precursor. *Proceedings of the National Academy of Sciences of the United States of America*, 94(10), pp.5273–5277.

Bailey, T.L et al., 1994. Fitting a mixture model by expectation maximization to discover motifs in bioploymers. *Proceedings of the Second International Conference on Intelligent Systems for Molecular Biology,* pp28-36

Banerjee, A. et al., Trichostatin a abrogates airway co... [Am J Respir Cell Mol Biol. 2012] - PubMed - NCBI. *American Journal of Respiratory Cell and Molecular Biology*, 46(2), pp.132–138.

Baniahmad, A. et al., 1990. Modular structure of a chicken lysozyme silencer: Involvement of an unusual thyroid hormone receptor binding site. *Cell*, 61(3), pp.505–514.

Bannert, N., Vollhardt, K. & Kurth, R., 2003. PDZ Domain-mediated Interaction of Interleukin-

16 Precursor Proteins with Myosin Phosphatase Targeting Subunits. *Journal of Biological Chemistry*, 278(43), pp.42190–42199.
Bannister, A.J. et al., 2001. Selective recognition of methylated lysine 9 on histone H3 by the HP1 chromo domain. *Nature*, 410(6824), pp.120–124.
Barski, A. et al., 2007. High-Resolution Profiling of Histone Methylations in the Human Genome. *Cell*, 129(4), pp.823–837.
Bartel, D.P., 2009. MicroRNAs: target recognition and regulatory functions. *Cell*, 136(2), pp.215–233.
Bartke, T. et al., 2010. Nucleosome-Interacting Proteins Regulated by DNA and Histone Methylation. *Cell*, 143(3), pp.470–484.
Begley, C.G. et al., 1986. Purified colony-stimulating factors enhance the survival of human neutrophils and eosinophils in vitro: a rapid and sensitive microassay for colony-stimulating factors. *Blood*, 68(1), pp.162–166.
Begueret, H. et al., 2007. Inflammation of bronchial smooth muscle in allergic asthma. *Thorax*, 62(1), pp.8–15.
Bell, A.C., West, A.G. & Felsenfeld, G., 1999. The Protein CTCF Is Required for the Enhancer Blocking Activity of Vertebrate Insulators. *Cell*, 98(3), pp.387–396.
Belmont, A.S., 2006. Mitotic chromosome structure and condensation. *Current Opinion in Cell Biology*, 18(6), pp.632–638.
Benayoun, L. et al., 2003. Airway structural alterations selectively associated with severe asthma. *American Journal of Respiratory and Critical Care Medicine*, 167(10), pp.1360–1368.
Berger, P. et al., 2003. Tryptase-stimulated human airway smooth muscle cells induce cytokine synthesis and mast cell chemotaxis. *The FASEB journal : official publication of the Federation of American Societies for Experimental Biology*, 17(14), pp.2139–2141.
Berkman, N. et al., 1996. Expression of RANTES mRNA and protein in airways of patients with mild asthma. *American Journal of Respiratory and Critical Care Medicine*, 154(6 Pt 1), pp.1804–1811.
Berman, J., Cruikshank, W. & Beer, D., Chemoattractant lymphokines specific for the helper/inducer T-lymphocyte subset. *Cellular immunology*, 1, pp.105–112.
Bernstein, B.E., Meissner, A. & Lander, E.S., 2007. The mammalian epigenome. *Cell*, 128(4), pp.669–681.
Bernstein, E. et al., 2003. Dicer is essential for mouse development. *Nature Genetics*, 35(3), pp.215–217.
Berry, M. et al., 2007. Pathological features and inhaled corticosteroid response of eosinophilic and non-eosinophilic asthma. *Thorax*, 62(12), pp.1043–1049.
Bhattacharyya, S. et al., 2011. Elevated miR-155 Promotes Inflammation in Cystic Fibrosis by Driving Hyperexpression of Interleukin-8. *Journal of Biological Chemistry*, 286(13), pp.11604–11615.
Birney, E. et al., 2007. Identification and analysis of functional elements in 1% of the human genome by the ENCODE pilot project. *Nature*, 447(7146), pp.799–816.
Black, P.N., Young, P.G. & Skinner, S.J., 1996. Response of airway smooth muscle cells to TGF-beta 1: effects on growth and synthesis of glycosaminoglycans. *The American journal of physiology*, 271(6 Pt 1), pp.L910–7.
Boettger, T. et al., 2009. Acquisition of the contractile phenotype by murine arterial smooth muscle cells depends on the Mir143/145 gene cluster. *The Journal of clinical investigation*, 119(9), pp.2634–2647.
Bolisetty, M.T. et al., 2009. Reticuloendotheliosis virus strain T induces miR-155, which targets JARID2 and promotes cell survival. *Journal of virology*, 83(23), pp.12009–12017.
Borchert, G.M., Lanier, W. & Davidson, B.L., 2006. RNA polymerase III transcribes human microRNAs. *Nature Publishing Group*, 13(12), pp.1097–1101.
Botuyan, M.V. et al., 2006. Structural basis for the methylation state-specific recognition of histone H4-K20 by 53BP1 and Crb2 in DNA repair. *Cell*, 127(7), pp.1361–1373.
Bousquet, J. et al., 1990. Eosinophilic inflammation in asthma. *The New England journal of medicine*, 323(15), pp.1033–1039.
Boyer, L.A. et al., 2006. Polycomb complexes repress developmental regulators in murine embryonic stem cells. *Nature Cell Biology*, 441(7091), pp.349–353.
Bramley, A.M. et al., 1994. Hypothesis: excessive bronchoconstriction in asthma is due to decreased airway elastance. *The European respiratory journal : official journal of the*

European Society for Clinical Respiratory Physiology, 7(2), pp.337–341.
Braunschweig, U. et al., 2009. Histone H1 binding is inhibited by histone variant H3.3. *The EMBO journal*, 28(23), pp.3635–3645.
Bremerich, D.H. et al., 1997. Role of protein kinase C in calcium sensitization during muscarinic stimulation in airway smooth muscle. *The American journal of physiology*, 273(4 Pt 1), pp.L775–81.
Brennecke, J. et al., 2005. Principles of microRNA-target recognition. *PLoS biology*, 3(3), p.e85.
Chadwick, B.P. et al., 2004. Multiple spatially distinct types of facultative heterochromatin on the human inactive X chromosome. *Proceedings of the National Academy of Sciences of the United States of America*, 101(50), p.17450.
Brightling, C.E. et al., 2002. Mast-cell infiltration of airway smooth muscle in asthma. *The New England journal of medicine*, 346(22), pp.1699–1705.
Brightling, C.E. et al., 2005. The CXCL10/CXCR3 axis mediates human lung mast cell migration to asthmatic airway smooth muscle. *American Journal of Respiratory and Critical Care Medicine*, 171(10), pp.1103–1108.
British Thoracic Society Scottish Intercollegiate Guidelines Network, 2008. British Guideline on the Management of Asthma. *Thorax*, 63 Suppl 4, pp.iv1–121.
Burkart, K. et al., 2006. Association of asthma with a functional promoter polymorphism in the IL16 gene. *Journal of Allergy and Clinical Immunology*, 117(1), pp.86–91.
Busse, W., 2001. Omalizumab, anti-IgE recombinant humanized monoclonal antibody, for the treatment of severe allergic asthma. *Journal of Allergy and Clinical Immunology*, 108(2), pp.184–190.
Bamberger, C.M., et al., 1995. Glucocorticoid receptor beta, a potential endogenous inhibitor of glucocorticoid action in humans. *Journal of Clinical Investigation*, 95(6), p.2435.
Campbell, H.D. et al., 1988. Isolation, structure and expression of cDNA and genomic clones for murine eosinophil differentiation factor. Comparison with other eosinophilopoietic lymphokines and identity with interleukin-5. *European journal of biochemistry / FEBS*, 174(2), pp.345–352.
Cardoso, A.L. et al., 2011. miR-155 modulates microglia-mediated immune response by down-regulating SOCS-1 and promoting cytokine and nitric oxide production. *Immunology*, 135(1), pp.73–88.
Carey, M.F., Peterson, C.L. & Smale, S.T., 2009. Chromatin immunoprecipitation (ChIP). *Cold Spring Harbor protocols*, 2009(9), p.pdb.prot5279.
Carmona-Saez, P. et al., 2007. GENECODIS: a web-based tool for finding significant concurrent annotations in gene lists. *Genome Biology*, 8(1), p.R3.
Carroll, J.S. et al., 2006. Genome-wide analysis of estrogen receptor binding sites. *Nature Genetics*, 38(11), pp.1289–1297.
Castro, M. et al., 2010. Effectiveness and safety of bronchial thermoplasty in the treatment of severe asthma: a multicenter, randomized, double-blind, sham-controlled clinical trial. *American Journal of Respiratory and Critical Care Medicine*, 181(2), pp.116–124.
Cerutti, L., Mian, N. & Bateman, A., 2000. Domains in gene silencing and cell differentiation proteins: the novel PAZ domain and redefinition of the Piwi domain. *Trends in biochemical sciences*, 25(10), pp.481–482.
Chakir, J. et al., 2003. Airway remodeling-associated mediators in moderate to severe asthma: effect of steroids on TGF-beta, IL-11, IL-17, and type I and type III collagen expression. *The Journal of allergy and clinical immunology*, 111(6), pp.1293–1298.
Chan, V., 2006. Extracellular Matrix Regulates Enhanced Eotaxin Expression in Asthmatic Airway Smooth Muscle Cells. *American Journal of Respiratory and Critical Care Medicine*, 174(4), pp.379–385.
Chen, F.H. et al., 2004. Airway remodeling: a comparison between fatal and nonfatal asthma. *The Journal of asthma : official journal of the Association for the Care of Asthma*, 41(6), pp.631–638.
Chen, X. et al., 2011. Identification of ten serum microRNAs from a genome-wide serum microRNA expression profile as novel noninvasive biomarkers for nonsmall cell lung cancer diagnosis. *International journal of cancer. Journal international du cancer*, 130(7), pp.1620–1628.
Chen, Z. et al., 2007. Distinct regulation of interleukin-17 in human T helper lymphocytes. *Arthritis and rheumatism*, 56(9), pp.2936–2946.

Su, C. et al., 2011. Ectopic expression of microRNA-155 enhances innate antiviral immunity against HBV infection in human hepatoma cells. *Virology Journal*, 8, p.354.
Cheung, P. et al., 2000. Synergistic coupling of histone H3 phosphorylation and acetylation in response to epidermal growth factor stimulation. *Molecular Cell*, 5(6), pp.905–915.
Cheung, V.G. et al., 2005. Mapping determinants of human gene expression by regional and genome-wide association. *Nature Cell Biology*, 437(7063), pp.1365–1369.
Chhabra, J. et al., 2007. Histamine and tryptase modulate asthmatic airway smooth muscle GM-CSF and RANTES release. *The European respiratory journal : official journal of the European Society for Clinical Respiratory Physiology*, 29(5), pp.861–870.
Chiba, Y. & Misawa, M., 2004. The role of RhoA-mediated Ca2+ sensitization of bronchial smooth muscle contraction in airway hyperresponsiveness. *Journal of Smooth Muscle Research*, 40(4/5), pp.155–167.
Chiba, Y. et al., 1999. Augmented acetylcholine-induced, Rho-mediated Ca2+ sensitization of bronchial smooth muscle contraction in antigen-induced airway hyperresponsive rats. *British Journal of Pharmacology*, 127(3), pp.597–600.
Chiba, Y., Tanabe, M., et al., 2009a. Down-Regulation of miR-133a Contributes to Up-Regulation of RhoA in Bronchial Smooth Muscle Cells. *American Journal of Respiratory and Critical Care Medicine*, 180(8), pp.713–719.
Chiba, Y., Nakazawa, S., et al., 2009b. Interleukin-13 augments bronchial smooth muscle contractility with an up-regulation of RhoA protein. *American Journal of Respiratory Cell and Molecular Biology*, 40(2), pp.159–167.
Cho, S.H. et al., 2003. Regulation of activin A expression in mast cells and asthma: its effect on the proliferation of human airway smooth muscle cells. *Journal of immunology (Baltimore, Md : 1950)*, 170(8), pp.4045–4052.
Choi, J.H. et al., 2005. Trichostatin A attenuates airway inflammation in mouse asthma model. *Clinical and experimental allergy : journal of the British Society for Allergy and Clinical Immunology*, 35(1), pp.89–96.
Chu, H.W. et al., 1998. Collagen deposition in large airways may not differentiate severe asthma from milder forms of the disease. *American Journal of Respiratory and Critical Care Medicine*, 158(6), pp.1936–1944.
Clarke, D. et al., 2009. Transcriptional regulation of cytokine function in airway smooth muscle cells. *Pulmonary Pharmacology & Therapeutics*, pp.1–10.
Clarke, D.L. et al., 2008. PKCbetaII augments NF-kappaB-dependent transcription at the CCL11 promoter via p300/CBP-associated factor recruitment and histone H4 acetylation. *The Journal of Immunology*, 181(5), pp.3503–3514.
Clarke, D.L. et al., 2010. TNF and IFN Synergistically Enhance Transcriptional Activation of CXCL10 in Human Airway Smooth Muscle Cells via STAT-1, NF- B, and the Transcriptional Coactivator CREB-binding Protein. *Journal of Biological Chemistry*, 285(38), pp.29101–29110.
Clifford, R. et al., Transcriptional Regulation of Inflammatory Genes Associated with Severe Asthma. *Current Pharmaceutical Design*, 17(7), pp.653–666. Available at: http://www.benthamdirect.org/pages/content.php?CPD/2011/00000017/00000007/0001B.SGM [Accessed February 27, 2012].
Clurman, B.E. & Hayward, W.S., 1989. Multiple proto-oncogene activations in avian leukosis virus-induced lymphomas: evidence for stage-specific events. *Molecular and Cellular Biology*, 9(6), pp.2657–2664.
Cochrane Collaboration., 2011. Anti-IgE for chronic asthma in adults and children. pp.1–60.
Collison, A., Herbert, C., et al., 2011a. Altered expression of microRNA in the airway wall in chronic asthma: miR-126 as a potential therapeutic target. *BMC Pulmonary Medicine*, 11(1), p.29.
Collison, A., Mattes, J., et al., 2011b. Inhibition of house dust mite-induced allergic airways disease by antagonism of microRNA-145 is comparable to glucocorticoid treatment. *The Journal of allergy and clinical immunology*, 128(1), pp.160–167.e4.
Cordes, K.R. et al., 2009. miR-145 and miR-143 regulate smooth muscle cell fate and plasticity. *Nature*, pp.1–7.
Corren, J. et al., 2010. A Randomized, Controlled, Phase 2 Study of AMG 317, an IL-4R Antagonist, in Patients with Asthma. *American Journal of Respiratory and Critical Care Medicine*, 181(8), pp.788–796.
Corren, J. et al., 2011. Lebrikizumab Treatment in Adults with Asthma — NEJM. *The New*

England journal of medicine, 365(12), pp.1088–1098.
Costinean, S. et al., 2009. Src homology 2 domain-containing inositol-5-phosphatase and CCAAT enhancer-binding protein are targeted by miR-155 in B cells of E -MiR-155 transgenic mice. *Blood*, 114(7), pp.1374–1382.
Cousins, D.J., Lee, T.H. & Staynov, D.Z., 2002. Cytokine coexpression during human Th1/Th2 cell differentiation: direct evidence for coordinated expression of Th2 cytokines. *Journal of immunology (Baltimore, Md : 1950)*, 169(5), pp.2498–2506.
Coutts, A. et al., 2001. Release of biologically active TGF-beta from airway smooth muscle cells induces autocrine synthesis of collagen. *American journal of physiology Lung cellular and molecular physiology*, 280(5), pp.L999–1008.
Cox, G. et al., 2007. Asthma control during the year after bronchial thermoplasty. *The New England journal of medicine*, 356(13), pp.1327–1337.
Cruikshank, W.W. et al., 1987. Lymphokine activation of T4+ T lymphocytes and monocytes. *Journal of immunology (Baltimore, Md : 1950)*, 138(11), pp.3817–3823.
Cruikshank, W.W., Kornfeld, H. & Center, D.M., 2000. Interleukin-16. *Journal of leukocyte biology*, 67(6), pp.757–766.
Cundall, M. et al., 2003. Neutrophil-derived matrix metalloproteinase-9 is increased in severe asthma and poorly inhibited by glucocorticoids. *The Journal of allergy and clinical immunology*, 112(6), pp.1064–1071.
Czech, B. et al., 2009. Hierarchical rules for Argonaute loading in Drosophila. *Molecular Cell*, 36(3), pp.445–456.
Davies, D.E., 2009. The Role of the Epithelium in Airway Remodeling in Asthma. *Proceedings of the American Thoracic Society*, 6(8), pp.678–682.
Davis, B.N. et al., 2008. SMAD proteins control DROSHA-mediated microRNA maturation. *Nature*, 454(7200), pp.56–61.
Davis, E. et al., 2005. RNAi-mediated allelic trans-interaction at the imprinted Rtl1/Peg11 locus. *Current biology : CB*, 15(8), pp.743–749.
Dawson, M.A. et al., 2011. Inhibition of BET recruitment to chromatin as an effective treatment for MLL-fusion leukaemia. *Nature*, 478(7370), pp.529–533.
Degner, J.F. et al., 2012. DNase I sensitivity QTLs are a major determinant of human expression variation. *Nature*.
Denslow, S.A. & Wade, P.A., 2007. The human Mi-2/NuRD complex and gene regulation. *Oncogene*, 26(37), pp.5433–5438.
Deshpande, A. et al., 2009. 3'UTR mediated regulation of the cyclin D1 proto-oncogene. *Cell cycle (Georgetown, Tex.)*, 8(21), pp.3584–3592.
Deshpande, D.A. et al., 2003. CD38/cyclic ADP-ribose-mediated Ca2+ signaling contributes to airway smooth muscle hyper-responsiveness. *The FASEB journal : official publication of the Federation of American Societies for Experimental Biology*, 17(3), pp.452–454.
Deshpande, D.A. et al., 2004. Modulation of calcium signaling by interleukin-13 in human airway smooth muscle: role of CD38/cyclic adenosine diphosphate ribose pathway. *American Journal of Respiratory Cell and Molecular Biology*, 31(1), pp.36–42.
Dhalluin, C. et al., 1999. Structure and ligand of a histone acetyltransferase bromodomain. *Nature*, 399(6735), pp.491–496.
Didiano, D. & Hobert, O., 2008. Molecular architecture of a miRNA-regulated 3' UTR. *RNA*, 14(7), pp.1297–1317.
Didiano, D. & Hobert, O., 2006. Perfect seed pairing is not a generally reliable predictor for miRNA-target interactions. *Nature Publishing Group*, 13(9), pp.849–851.
Djuranovic, S. et al., 2010. Allosteric regulation of Argonaute proteins by miRNAs. *Nature Structural & Molecular Biology*, 17(2), pp.144–150.
Djuranovic, S., Nahvi, A. & Green, R., 2011. A Parsimonious Model for Gene Regulation by miRNAs. *Science*, 331(6017), pp.550–553.
Djuranovic, S., Nahvi, A. & Green, R., 2012. miRNA-Mediated Gene Silencing by Translational Repression Followed by mRNA Deadenylation and Decay. *Science*, 336(6078), pp.237–240.
Doench, J.G. & Sharp, P.A., 2004. Specificity of microRNA target selection in translational repression. *Genes & Development*, 18(5), pp.504–511.
Dorigo, B. et al., 2004. Nucleosome arrays reveal the two-start organization of the chromatin fiber. *Science*, 306(5701), pp.1571–1573.
Dorsett, Y. et al., 2008. MicroRNA-155 Suppresses Activation-Induced Cytidine Deaminase-

Mediated Myc-Igh Translocation. *Immunity*, 28(5), pp.630–638.
Druilhe, A. et al., 1998. Apoptosis, proliferation, and expression of Bcl-2, Fas, and Fas ligand in bronchial biopsies from asthmatics. *American Journal of Respiratory Cell and Molecular Biology*, 19(5), pp.747–757.
Dunnill, M.S., Massarella, G.R. & Anderson, J.A., 1969. A comparison of the quantitative anatomy of the bronchi in normal subjects, in status asthmaticus, in chronic bronchitis, and in emphysema. *Thorax*, 24(2), pp.176–179.
Durham, A., Adcock, I. & Tliba, O., 2011. Steroid resistance in severe asthma: current mechanisms and future treatment. A. Durham, I. Adcock, & O. Tliba, eds. *Curr Pharm Des*, 17(7), pp.674–684.
Ebina, M. et al., 1993. Cellular hypertrophy and hyperplasia of airway smooth muscles underlying bronchial asthma. A 3-D morphometric study. *The American review of respiratory disease*, 148(3), pp.720–726.
Edmunds, J.W., Mahadevan, L.C. & Clayton, A.L., 2008. Dynamic histone H3 methylation during gene induction: HYPB/Setd2 mediates all H3K36 trimethylation. *The EMBO journal*, 27(2), pp.406–420.
Enright, A.J. et al., 2003. MicroRNA targets in Drosophila. *Genome Biology*, 5(1), p.R1.
Ernst, J. et al., 2011. Mapping and analysis of chromatin state dynamics in nine human cell types. *Nature*, 473(7345), pp.43–49.
Esau, C. et al., 2006. miR-122 regulation of lipid metabolism revealed by in vivo antisense targeting. *Cell metabolism*, 3(2), pp.87–98.
Espinosa, K. et al., 2003. CysLT1 receptor upregulation by TGF-beta and IL-13 is associated with bronchial smooth muscle cell proliferation in response to LTD4. *The Journal of allergy and clinical immunology*, 111(5), pp.1032–1040.
Faffe, D.S. et al., 2003. IL-13 and IL-4 promote TARC release in human airway smooth muscle cells: role of IL-4 receptor genotype. *American journal of physiology Lung cellular and molecular physiology*, 285(4), pp.L907–14.
Fahy, J.V., 2009. Eosinophilic and Neutrophilic Inflammation in Asthma: Insights from Clinical Studies. *Proceedings of the American Thoracic Society*, 6(3), pp.256–259.
Faller, M. et al., 2010. DGCR8 recognizes primary transcripts of microRNAs through highly cooperative binding and formation of higher-order structures. *RNA*, 16(8), pp.1570–1583.
Faraoni, I. et al., 2009. miR-155 gene: A typical multifunctional microRNA. *Biochimica et Biophysica Acta (BBA) - Molecular Basis of Disease*, 1792(6), pp.497–505.
Fedorov, I.A. et al., 2005. Epithelial stress and structural remodelling in childhood asthma. *Thorax*, 60(5), pp.389–394.
Felsenfeld, G. & Bell, A.C., 2000. Methylation of a CTCF-dependent boundary controls imprinted expression of the Igf2 gene. *Nature*, 405(6785), pp.482–485.
Fields, P.E. et al., 2004. Th2-specific chromatin remodeling and enhancer activity in the Th2 cytokine locus control region. *Immunity*, 21(6), pp.865–876.
Finkelman, F.D. et al., 1988. IL-4 is required to generate and sustain in vivo IgE responses. *Journal of immunology (Baltimore, Md : 1950)*, 141(7), pp.2335–2341.
Fischle, W. et al., 2003. Molecular basis for the discrimination of repressive methyl-lysine marks in histone H3 by Polycomb and HP1 chromodomains. *Genes & Development*, 17(15), pp.1870–1881.
Fischle, W. et al., 2005. Regulation of HP1-chromatin binding by histone H3 methylation and phosphorylation. *Nature*, 438(7071), pp.1116–1122.
Flanagan, J.F. et al., 2005. Double chromodomains cooperate to recognize the methylated histone H3 tail. *Nature*, 438(7071), pp.1181–1185.
Flaus, A. et al., 2004. Sin mutations alter inherent nucleosome mobility. *The EMBO journal*, 23(2), pp.343–353.
Flavahan, N.A. et al., 1988. Human eosinophil major basic protein causes hyperreactivity of respiratory smooth muscle. Role of the epithelium. *The American review of respiratory disease*, 138(3), pp.685–688.
Flood-Page, P. et al., 2007. A Study to Evaluate Safety and Efficacy of Mepolizumab in Patients with Moderate Persistent Asthma. *American Journal of Respiratory and Critical Care Medicine*, 176(11), pp.1062–1071.
Pauler, F.M. et al., 2009. H3K27me3 forms BLOCs over silent genes and intergenic regions and specifies a histone banding pattern on a mouse autosomal chromosome. *Genome*

research, 19(2), p.221.
Foley, S.C. & Hamid, Q., 2007. Images in allergy and immunology: neutrophils in asthma. *The Journal of allergy and clinical immunology*, 119(5), pp.1282–1286.
Fossiez, F. et al., 1996. T cell interleukin-17 induces stromal cells to produce proinflammatory and hematopoietic cytokines. *The Journal of experimental medicine*, 183(6), pp.2593–2603.
Fukuda, T. et al., 2007. DEAD-box RNA helicase subunits of the Drosha complex are required for processing of rRNA and a subset of microRNAs. *Nature Cell Biology*, 9(5), pp.604–611.
Gaszner, M. & Felsenfeld, G., 2006. Insulators: exploiting transcriptional and epigenetic mechanisms. *Nature Reviews Genetics*, 7(9), pp.703–713.
Ghaffar, O. et al., 1999. Constitutive and cytokine-stimulated expression of eotaxin by human airway smooth muscle cells. *American Journal of Respiratory and Critical Care Medicine*, 159(6), pp.1933–1942.
Ghildiyal, M. et al., 2010. Sorting of Drosophila small silencing RNAs partitions microRNA* strands into the RNA interference pathway. *RNA*, 16(1), pp.43–56.
Giannopoulou, E.G. & Elemento, O., 2011. An integrated ChIP-seq analysis platform with customizable workflows. *BMC bioinformatics*, 12, p.277.
Gironella, M. et al., 2007. Tumor protein 53-induced nuclear protein 1 expression is repressed by miR-155, and its restoration inhibits pancreatic tumor development. *Proceedings of the National Academy of Sciences of the United States of America*, 104(41), pp.16170–16175.
Goncharova, E.A. et al., 2003. Cyclic AMP-mobilizing agents and glucocorticoids modulate human smooth muscle cell migration. *American Journal of Respiratory Cell and Molecular Biology*, 29(1), pp.19–27.
Gould, H.J. et al., 2003. T HE BIOLOGY OF IGE AND THE BASIS OF ALLERGIC DISEASE. *Annual review of immunology*, 21(1), pp.579–628.
Grant, P.A. et al., 1997. Yeast Gcn5 functions in two multisubunit complexes to acetylate nucleosomal histones: characterization of an Ada complex and the SAGA (Spt/Ada) complex. *Genes & Development*, 11(13), pp.1640–1650.
Gregory, R.I. et al., 2004. The Microprocessor complex mediates the genesis of microRNAs. *Nature*, 432(7014), pp.235–240.
Grimson, A. et al., 2007. MicroRNA targeting specificity in mammals: determinants beyond seed pairing. *Molecular Cell*, 27(1), pp.91–105.
Gu, S. et al., 2009. Biological basis for restriction of microRNA targets to the 3′ untranslated region in mammalian mRNAs. *Nature Structural & Molecular Biology*, 16(2), pp.144–150.
Gu, W. & Roeder, R.G., 1997. Activation of p53 sequence-specific DNA binding by acetylation of the p53 C-terminal domain. *Cell*, 90(4), pp.595–606.
Guccione, E. et al., 2007. Methylation of histone H3R2 by PRMT6 and H3K4 by an MLL complex are mutually exclusive. *Nature*, 449(7164), pp.933–937.
Guedes, A.G.P. et al., 2006. CD38-deficient mice have reduced airway hyperresponsiveness following IL-13 challenge. *AJP: Lung Cellular and Molecular Physiology*, 291(6), pp.L1286–L1293.
Guelen, L. et al., 2008. Domain organization of human chromosomes revealed by mapping of nuclear lamina interactions. *Nature*, 453(7197), pp.948–951.
Gundel, R.H., Letts, L.G. & Gleich, G.J., 1991. Human eosinophil major basic protein induces airway constriction and airway hyperresponsiveness in primates. *The Journal of clinical investigation*, 87(4), pp.1470–1473.
Guo, H. et al., 2010. Mammalian microRNAs predominantly act to decrease target mRNA levels. *Nature*, 466(7308), pp.835–840.
Ha, I., Wightman, B. & Ruvkun, G., 1996. A bulged lin-4/lin-14 RNA duplex is sufficient for Caenorhabditis elegans lin-14 temporal gradient formation. *Genes & Development*, 10(23), pp.3041–3050.
Haasch, D. et al., 2002. T cell activation induces a noncoding RNA transcript sensitive to inhibition by immunosuppressant drugs and encoded by the proto-oncogene, BIC. *Cellular immunology*, 217(1-2), pp.78–86.
Hadjur, S. et al., 2009. Cohesins form chromosomal cis-interactions at the developmentally regulated IFNG locus. *Nature*, 460(7253), pp.410–413.
Hafner, M. et al., 2010. Transcriptome-wide Identification of RNA-Binding Protein and

MicroRNA Target Sites by PAR-CLIP. *Cell*, 141(1), pp.129–141.
Hakonarson, H. et al., 1999. Regulation of TH1- and TH2-type cytokine expression and action in atopic asthmatic sensitized airway smooth muscle. *The Journal of clinical investigation*, 103(7), pp.1077–1087.
Halayko, A.J. et al., 1996. Markers of airway smooth muscle cell phenotype. *The American journal of physiology*, 270(6 Pt 1), pp.L1040–51.
Haldar, P. et al., 2009. Mepolizumab and exacerbations of refractory eosinophilic asthma. *The New England journal of medicine*, 360(10), pp.973–984.
Hamann, K.J. et al., 2000. Fas cross-linking induces apoptosis in human airway smooth muscle cells. *American journal of physiology Lung cellular and molecular physiology*, 278(3), pp.L618–24.
Han, J. et al., 2006. Molecular basis for the recognition of primary microRNAs by the Drosha-DGCR8 complex. *Cell*, 125(5), pp.887–901.
Larner-Svensson, H.M. et al., 2010. Pharmacological studies of the mechanism and function of interleukin-1β-induced miRNA-146a expression in primary human airway smooth muscle. *Respiratory Research*, 11(1), p.68.
Harris, N. & Gause, W.C., 2011. To B or not to B: B cells and the Th2-type immune response to helminths. *Trends in immunology*, 32(2), pp.80–88.
Hastie, A.T. et al., 1987. The effect of purified human eosinophil major basic protein on mammalian ciliary activity. *The American review of respiratory disease*, 135(4), pp.848–853.
He, W.Q. et al., 2008. Myosin Light Chain Kinase Is Central to Smooth Muscle Contraction and Required for Gastrointestinal Motility in Mice. *Gastroenterology*, 135(2), pp.610–620.e2.
Hedges, J.C. et al., 1999. A role for p38(MAPK)/HSP27 pathway in smooth muscle cell migration. *The Journal of biological chemistry*, 274(34), pp.24211–24219.
Heintzman, N.D. et al., 2007. Distinct and predictive chromatin signatures of transcriptional promoters and enhancers in the human genome. *Nature Genetics*, 39(3), pp.311–318.
Heintzman, N.D. et al., 2009. Histone modifications at human enhancers reflect global cell-type-specific gene expression. *Nature*, 459(7243), pp.108–112.
Hirata, H. et al., 2012. MicroRNA-1826 targets VEGFC, beta-catenin (CTNNB1) and MEK1 (MAP2K1) in human bladder cancer. *Carcinogenesis*, 33(1), pp.41–48.
Hirst, S.J., Barnes, P.J. & Twort, C.H., 1996. PDGF isoform-induced proliferation and receptor expression in human cultured airway smooth muscle cells. *The American journal of physiology*, 270(3 Pt 1), pp.L415–28.
Hirst, S.J., Twort, C.H. & Lee, T.H., 2000. Differential effects of extracellular matrix proteins on human airway smooth muscle cell proliferation and phenotype. *American Journal of Respiratory Cell and Molecular Biology*, 23(3), pp.335–344.
Hisamatsu, K. et al., 1990. Cytotoxicity of human eosinophil granule major basic protein to human nasal sinus mucosa in vitro. *The Journal of allergy and clinical immunology*, 86(1), pp.52–63.
Ho, S.-M., 2010. Environmental epigenetics of asthma: An update. *Journal of Allergy and Clinical Immunology*, 126(3), pp.453–465.
Huang, F. et al., 2007. Requirement for both JAK-mediated PI3K signaling and ACT1/TRAF6/TAK1-dependent NF-kappaB activation by IL-17A in enhancing cytokine expression in human airway epithelial cells. *Journal of immunology (Baltimore, Md : 1950)*, 179(10), pp.6504–6513.
Huang, Y. et al., 2006. Recognition of histone H3 lysine-4 methylation by the double tudor domain of JMJD2A. *Science*, 312(5774), pp.748–751.
Huber, H., 1922. *The pathology of bronchial asthma*, Studies from the Otho SA Sprague Memorial Institute: ….
Hughes, R.M. et al., 2007. Recognition of trimethyllysine by a chromodomain is not driven by the hydrophobic effect. *Proceedings of the National Academy of Sciences of the United States of America*, 104(27), pp.11184–11188.
Hulme, E.C., Birdsall, N.J. & Buckley, N.J., 1990. Muscarinic receptor subtypes. *Annual review of pharmacology and toxicology*, 30, pp.633–673.
Humbert, M. et al., 1996. IL-4 and IL-5 mRNA and protein in bronchial biopsies from patients with atopic and nonatopic asthma: evidence against "intrinsic" asthma being a distinct immunopathologic entity. *American Journal of Respiratory and Critical Care Medicine*, 154(5), pp.1497–1504.

Hutvágner, G. et al., 2001. A cellular function for the RNA-interference enzyme Dicer in the maturation of the let-7 small temporal RNA. *Science*, 293(5531), pp.834–838.
Irizarry, R.A. et al., 2003. Exploration, normalization, and summaries of high density oligonucleotide array probe level data. *Biostatistics (Oxford, England)*, 4(2), pp.249–264.
Ito, K. et al., 2002. Expression and Activity of Histone Deacetylases in Human Asthmatic Airways. *American Journal of Respiratory and Critical Care Medicine*, 166(3), pp.392–396.
Ito, K. et al., 2006. Histone deacetylase 2-mediated deacetylation of the glucocorticoid receptor enables NF- B suppression. *The Journal of experimental medicine*, 203(1), pp.7–13.
Ito, K., Barnes, P.J. & Adcock, I.M., 2000. Glucocorticoid receptor recruitment of histone deacetylase 2 inhibits interleukin-1beta-induced histone H4 acetylation on lysines 8 and 12. *Molecular and Cellular Biology*, 20(18), pp.6891–6903.
Ruby, J.G. et al., 2007. Intronic microRNA precursors that bypass Drosha processing. *Nature*, 448(7149), p.83.
Jacobs, S.A. & Khorasanizadeh, S., 2002. Structure of HP1 chromodomain bound to a lysine 9-methylated histone H3 tail. *Science*, 295(5562), pp.2080–2083.
Jacobson, R.H. et al., 2000. Structure and function of a human TAFII250 double bromodomain module. *Science*, 288(5470), pp.1422–1425.
Jarai, G. et al., 2004. Effects of interleukin-1beta, interleukin-13 and transforming growth factor-beta on gene expression in human airway smooth muscle using gene microarrays. *European journal of pharmacology*, 497(3), pp.255–265.
Jeffery, P.K. et al., 1989. Bronchial biopsies in asthma. An ultrastructural, quantitative study and correlation with hyperreactivity. *The American review of respiratory disease*, 140(6), pp.1745–1753.
Vinther, J. et al., 2006. Identification of miRNA targets with stable isotope labeling by amino acids in cell culture. *Nucleic Acids Research*, 34(16), p.e107.
Jin, C. et al., 2009. H3.3/H2A.Z double variant–containing nucleosomes mark "nucleosome-free regions" of active promoters and other regulatory regions. *Nature Genetics*, 41(8), pp.941–945.
John, M. et al., 1997. Human airway smooth muscle cells express and release RANTES in response to T helper 1 cytokines: regulation by T helper 2 cytokines and corticosteroids. *Journal of immunology (Baltimore, Md : 1950)*, 158(4), pp.1841–1847.
John, M. et al., 1998. Inhaled corticosteroids increase interleukin-10 but reduce macrophage inflammatory protein-1alpha, granulocyte-macrophage colony-stimulating factor, and interferon-gamma release from alveolar macrophages in asthma. *American Journal of Respiratory and Critical Care Medicine*, 157(1), pp.256–262.
Johnson, P.R. et al., 2001. Airway smooth muscle cell proliferation is increased in asthma. *American Journal of Respiratory and Critical Care Medicine*, 164(3), pp.474–477.
Johnson, P.R. et al., 2000. The production of extracellular matrix proteins by human passively sensitized airway smooth-muscle cells in culture: the effect of beclomethasone. *American Journal of Respiratory and Critical Care Medicine*, 162(6), pp.2145–2151.
Jonat, C. et al., 1990. Antitumor promotion and antiinflammation: down-modulation of AP-1 (Fos/Jun) activity by glucocorticoid hormone. *Cell*, 62(6), pp.1189–1204.
Joos, G.F. et al., 2003. Indirect airway challenges. *The European respiratory journal : official journal of the European Society for Clinical Respiratory Physiology*, 21(6), pp.1050–1068.
Martens, J.H. et al., 2005. The profile of repeat-associated histone lysine methylation states in the mouse epigenome. *The EMBO journal*, 24(4), p.800.
Joubert, P. et al., 2005. CCR3 expression and function in asthmatic airway smooth muscle cells. *Journal of immunology (Baltimore, Md : 1950)*, 175(4), pp.2702–2708.
Juan, L.J. et al., 1994. Differential repression of transcription factor binding by histone H1 is regulated by the core histone amino termini. *The EMBO journal*, 13(24), pp.6031–6040.
Kagey, M.H. et al., 2010. Mediator and cohesin connect gene expression and chromatin architecture. *Nature*, 467(7314), pp.430–435.
Kaser, A. et al., 1999. A role for IL-16 in the cross-talk between dendritic cells and T cells. *Journal of immunology (Baltimore, Md : 1950)*, 163(6), pp.3232–3238.
Kasowski, M. et al., 2010. Variation in Transcription Factor Binding Among Humans. *Science*, 328(5975), pp.232–235.
Kaur, D. et al., 2010. Airway smooth muscle proliferation and survival is not modulated by

mast cells. *Clinical & Experimental Allergy*, 40(2), pp.279–288.
Kertesz, M. et al., 2007. The role of site accessibility in microRNA target recognition. *Nature Genetics*, 39(10), pp.1278–1284.
Khvorova, A., Reynolds, A. & Jayasena, S.D., 2003. Functional siRNAs and miRNAs exhibit strand bias. *Cell*, 115(2), pp.209–216.
Kim, J.I. et al., 1999. The transcription factor c-Maf controls the production of interleukin-4 but not other Th2 cytokines. *Immunity*, 10(6), pp.745–751.
Kim, T.H et al., 2007. Analysis of the Vertebrate Insulator Protein CTCF-Binding sites in the Human Genome. *Cell* 128(6), pp1231-1245
Kim, S. et al., 2011. Pre-mRNA splicing is a determinant of histone H3K36 methylation. *Proceedings of the National Academy of Sciences of the United States of America*.
Kirmizis, A. et al., 2007. Arginine methylation at histone H3R2 controls deposition of H3K4 trimethylation. *Nature*, 449(7164), pp.928–932.
Kluiver, J. et al., 2006. Regulation of pri-microRNA BIC transcription and processing in Burkitt lymphoma. *Oncogene*, 26(26), pp.3769–3776.
Kohlhaas, S. et al., 2009. Cutting edge: the Foxp3 target miR-155 contributes to the development of regulatory T cells. *The Journal of Immunology*, 182(5), pp.2578–2582.
Kolasinska-Zwierz, P. et al., 2009. Differential chromatin marking of introns and expressed exons by H3K36me3. *Nature Genetics*, 41(3), pp.376–381.
Kong, W. et al., 2008. MicroRNA-155 Is Regulated by the Transforming Growth Factor /Smad Pathway and Contributes to Epithelial Cell Plasticity by Targeting RhoA. *Molecular and Cellular Biology*, 28(22), pp.6773–6784.
Kouzarides, T., 2007. Chromatin modifications and their function. *Cell*, 128(4), pp.693–705.
Kranz, A.L., Eils, R. & Konig, R., 2011. Enhancers regulate progression of development in mammalian cells. *Nucleic Acids Research*, 39(20), pp.8689–8702.
Krimmer, D.I. et al., 2009. CD40 and OX40 ligand are differentially regulated on asthmatic airway smooth muscle. *Allergy*, 64(7), pp.1074–1082.
Krymskaya, V.P. et al., 1999. EGF activates ErbB-2 and stimulates phosphatidylinositol 3-kinase in human airway smooth muscle cells. *The American journal of physiology*, 276(2 Pt 1), pp.L246–55.
Kuhn, AR. et al., 2010. MicroRNA Expression in Human Airway Smooth Muscle Cells: Role of miR-25 in Regulation of Airway Smooth Muscle Phenotype. *American Journal of Respiratory Cell and Molecular Biology*, 42(4), p.506.
Kumar, R., 2006. ZNF652, A Novel Zinc Finger Protein, Interacts with the Putative Breast Tumor Suppressor CBFA2T3 to Repress Transcription. *Molecular Cancer Research*, 4(9), pp.655–665.
Kumar, R. et al., 2008. CBFA2T3-ZNF652 corepressor complex regulates transcription of the E-box gene HEB. *The Journal of biological chemistry*, 283(27), pp.19026–19038.
Kumar, R. et al., 2011. Genome-wide mapping of ZNF652 promoter binding sites in breast cancer cells. *Journal of Cellular Biochemistry*, pp.n/a–n/a.
Kurdistani, S.K., Tavazoie, S. & Grunstein, M., 2004. Mapping global histone acetylation patterns to gene expression. *Cell*, 117(6), pp.721–733.
Kurschner, C. & Yuzaki, M., 1999. Neuronal interleukin-16 (NIL-16): a dual function PDZ domain protein. *The Journal of neuroscience : the official journal of the Society for Neuroscience*, 19(18), pp.7770–7780.
Kuwano, K. et al., 1993. Small airways dimensions in asthma and in chronic obstructive pulmonary disease. *The American review of respiratory disease*, 148(5), pp.1220–1225.
Laan, M. et al., 1999. Neutrophil recruitment by human IL-17 via C-X-C chemokine release in the airways. *Journal of immunology (Baltimore, Md : 1950)*, 162(4), pp.2347–2352.
Lachner, M. et al., 2001. Methylation of histone H3 lysine 9 creates a binding site for HP1 proteins. *Nature*, 410(6824), pp.116–120.
Lackie, P.M. et al., 1997. Expression of CD44 isoforms is increased in the airway epithelium of asthmatic subjects. *American Journal of Respiratory Cell and Molecular Biology*, 16(1), pp.14–22.
Lagos-Quintana, M. et al., 2001. Identification of novel genes coding for small expressed RNAs. *Science*, 294(5543), pp.853–858.
Lagos-Quintana, M. et al., 2002. Identification of tissue-specific microRNAs from mouse. *Current biology : CB*, 12(9), pp.735–739.
Laitinen, L.A. et al., 1985. Damage of the airway epithelium and bronchial reactivity in

patients with asthma. *The American review of respiratory disease*, 131(4), pp.599–606.
Lambert, R.K. et al., 1993. Functional significance of increased airway smooth muscle in asthma and COPD. *Journal of applied physiology (Bethesda, Md. : 1985)*, 74(6), pp.2771–2781.
Lanford, R.E. et al., 2010. Therapeutic Silencing of MicroRNA-122 in Primates with Chronic Hepatitis C Virus Infection. *Science*, 327(5962), pp.198–201.
Lange, P. et al., 1990. Relation of ventilatory impairment and of chronic mucus hypersecretion to mortality from obstructive lung disease and from all causes. *Thorax*, 45(8), pp.579–585.
Lau, N.C. et al., 2001. An abundant class of tiny RNAs with probable regulatory roles in Caenorhabditis elegans. *Science*, 294(5543), pp.858–862.
Lawrie, C.H. et al., 2007. MicroRNA expression distinguishes between germinal center B cell-like and activated B cell-like subtypes of diffuse large B cell lymphoma. *International journal of cancer. Journal international du cancer*, 121(5), pp.1156–1161.
Lazaar, A.L. et al., 1998. CD40-mediated signal transduction in human airway smooth muscle. *Journal of immunology (Baltimore, Md : 1950)*, 161(6), pp.3120–3127.
Lazaar, A.L. et al., 2002. Mast cell chymase modifies cell-matrix interactions and inhibits mitogen-induced proliferation of human airway smooth muscle cells. *Journal of immunology (Baltimore, Md : 1950)*, 169(2), pp.1014–1020.
Lazaar, A.L. et al., 1994. T lymphocytes adhere to airway smooth muscle cells via integrins and CD44 and induce smooth muscle cell DNA synthesis. *The Journal of experimental medicine*, 180(3), pp.807–816.
Leckie, M.J. et al., 2000. Effects of an interleukin-5 blocking monoclonal antibody on eosinophils, airway hyper-responsiveness, and the late asthmatic response. *Lancet*, 356(9248), pp.2144–2148.
Lee, D.Y. et al., 1993a. A positive role for histone acetylation in transcription factor access to nucleosomal DNA. *Cell*, 72(1), pp.73–84.
Lee, E.R., Murdoch, F.E. & Fritsch, M.K., 2007a. High Histone Acetylation and Decreased Polycomb Repressive Complex 2 Member Levels Regulate Gene Specific Transcriptional Changes During Early Embryonic Stem Cell Differentiation Induced by Retinoic Acid. *Stem Cells*, 25(9), pp.2191–2199.
Lee, J.-S. et al., 2007b. Histone crosstalk between H2B monoubiquitination and H3 methylation mediated by COMPASS. *Cell*, 131(6), pp.1084–1096.
Lee, R.C. & Ambros, V., 2001. An extensive class of small RNAs in Caenorhabditis elegans. *Science*, 294(5543), pp.862–864.
Lee, R.C., Feinbaum, R.L. & Ambros, V., 1993b. The C. elegans heterochronic gene lin-4 encodes small RNAs with antisense complementarity to lin-14. *Cell*, 75(5), pp.843–854.
Lee, T.I. et al., 2006. Control of developmental regulators by Polycomb in human embryonic stem cells. *Cell*, 125(2), pp.301–313.
Lee, Y. et al., 2004. MicroRNA genes are transcribed by RNA polymerase II. *The EMBO journal*, 23(20), pp.4051–4060.
Lee, Y. et al., 2003. The nuclear RNase III Drosha initiates microRNA processing. *Nature*, 425(6956), pp.415–419.
Elia, E. et al., 2009. The knockout of miR-143 and -145 alters smooth muscle cell maintenance and vascular homeostasis in mice: correlates with human disease. *Cell death and differentiation*, 16(12), p.1590.
Lewis, B.P. et al., 2003. Prediction of mammalian microRNA targets. *Cell*, 115(7), pp.787–798.
Lewis, B.P., Burge, C.B. & Bartel, D.P., 2005. Conserved seed pairing, often flanked by adenosines, indicates that thousands of human genes are microRNA targets. *Cell*, 120(1), pp.15–20.
Li, B. et al., 2007. Combined action of PHD and chromo domains directs the Rpd3S HDAC to transcribed chromatin. *Science*, 316(5827), pp.1050–1054.
Li, H. et al., 2006. Molecular basis for site-specific read-out of histone H3K4me3 by the BPTF PHD finger of NURF. *Nature*, 442(7098), pp.91–95.
Lim, L.P. et al., 2005. Microarray analysis shows that some microRNAs downregulate large numbers of target mRNAs. *Nature*, 433(7027), pp.769–773.
Lindroth, A.M. et al., 2004. Dual histone H3 methylation marks at lysines 9 and 27 required for interaction with CHROMOMETHYLASE3. *The EMBO journal*, 23(21), pp.4286–4296.
Lingel, A. et al., 2004. Nucleic acid 3′-end recognition by the Argonaute2 PAZ domain. *Nature*

Structural & Molecular Biology, 11(6), pp.576–577.
Liu, J. et al., 2004. Argonaute2 is the catalytic engine of mammalian RNAi. *Science*, 305(5689), pp.1437–1441.
Lobanenkov, V.V. et al., 1990. A novel sequence-specific DNA binding protein which interacts with three regularly spaced direct repeats of the CCCTC-motif in the 5'-flanking sequence of the chicken c-myc gene. *Oncogene*, 12, pp.1743–1753.
Lodish, H. et al., Molecular Cell Biology.
Louis, R. et al., 2002. Sputum eosinophil count in a large population of patients with mild to moderate steroid-naive asthma: distribution and relationship with methacholine bronchial hyperresponsiveness. *Allergy*, 57(10), pp.907–912.
Louise Laurent, E.W. et al., 2010. Dynamic changes in the human methylome during differentiation. *Genome research*, 20(3), p.320.
Lößner, C. et al., 2011. Quantitative Proteomics Identify Novel miR-155 Target Proteins. *PLoS ONE*, 6(7), p.e22146.
Lötvall, J. et al., 2011. Asthma endotypes: A new approach to classification of disease entities within the asthma syndrome. *Journal of Allergy and Clinical Immunology*, 127(2), pp.355–360.
Lu, N.Z. & Cidlowski, J.A., 2004. The origin and functions of multiple human glucocorticoid receptor isoforms. *Annals of the New York Academy of Sciences*, 1024, pp.102–123.
Lu, N.Z. & Cidlowski, J.A., 2005. Translational regulatory mechanisms generate N-terminal glucocorticoid receptor isoforms with unique transcriptional target genes. *Molecular Cell*, 18(3), pp.331–342.
Lu, T.X. et al., 2011. MicroRNA-21 limits in vivo immune response-mediated activation of the IL-12/IFN-gamma pathway, Th1 polarization, and the severity of delayed-type hypersensitivity. *The Journal of Immunology*, 187(6), pp.3362–3373.
Lu, T.X., Munitz, A. & Rothenberg, M.E., 2009. MicroRNA-21 Is Up-Regulated in Allergic Airway Inflammation and Regulates IL-12p35 Expression. *The Journal of Immunology*, 182(8), pp.4994–5002.
Luger, K. et al., 1997. Crystal structure of the nucleosome core particle at 2.8 A resolution. *Nature*, 389(6648), pp.251–260.
Lund, E. & Dahlberg, J.E., 2006. Substrate selectivity of exportin 5 and Dicer in the biogenesis of microRNAs. *Cold Spring Harbor symposia on quantitative biology*, 71, pp.59–66.
Lund, E. et al., 2004. Nuclear export of microRNA precursors. *Science*, 303(5654), pp.95–98.
Lusser, A., Urwin, D.L. & Kadonaga, J.T., 2005. Distinct activities of CHD1 and ACF in ATP-dependent chromatin assembly. *Nature Publishing Group*, 12(2), pp.160–166.
Lutter, L.C., Judis, L. & Paretti, R.F., 1992. Effects of histone acetylation on chromatin topology in vivo. *Molecular and Cellular Biology*, 12(11), pp.5004–5014.
Ma, F. et al., 2010. MicroRNA-466l upregulates IL-10 expression in TLR-triggered macrophages by antagonizing RNA-binding protein tristetraprolin-mediated IL-10 mRNA degradation. *The Journal of Immunology*, 184(11), pp.6053–6059.
Ma, J.-B., Ye, K. & Patel, D.J., 2004. Structural basis for overhang-specific small interfering RNA recognition by the PAZ domain. *Nature Cell Biology*, 429(6989), pp.318–322.
Ma, X. et al., 2002. Changes in biophysical and biochemical properties of single bronchial smooth muscle cells from asthmatic subjects. *American journal of physiology Lung cellular and molecular physiology*, 283(6), pp.L1181–9.
Madden, K.B. et al., 1991. Antibodies to IL-3 and IL-4 suppress helminth-induced intestinal mastocytosis. *Journal of immunology (Baltimore, Md : 1950)*, 147(4), pp.1387–1391.
Marazzi, I. et al., 2012. Suppression of the antiviral response by an influenza histone mimic. *Nature*, 483(7390), pp.428–433.
Marmorstein, R. & Trievel, R.C., 2009. Histone modifying enzymes: Structures, mechanisms, and specificities. *Biochimica et Biophysica Acta (BBA) - Gene Regulatory Mechanisms*, 1789(1), pp.58–68.
Martin, D.G.E. et al., 2006a. Methylation of histone H3 mediates the association of the NuA3 histone acetyltransferase with chromatin. *Molecular and Cellular Biology*, 26(8), pp.3018–3028.
Martin, J.G. & Ramos-Barbón, D., 2003. Airway smooth muscle growth from the perspective of animal models. *Respiratory physiology & neurobiology*, 137(2-3), pp.251–261.
Martin, M.M. et al., 2006. MicroRNA-155 regulates human angiotensin II type 1 receptor expression in fibroblasts. *The Journal of biological chemistry*, 281(27), pp.18277–18284.

Martin, M.M. et al., 2007. The human angiotensin II type 1 receptor +1166 A/C polymorphism attenuates microrna-155 binding. *The Journal of biological chemistry*, 282(33), pp.24262–24269.
Martinez, J. & Tuschl, T., 2004. RISC is a 5' phosphomonoester-producing RNA endonuclease. *Genes & Development*, 18(9), pp.975–980.
Martinez-Nunez, R.T. et al., 2009. MicroRNA-155 modulates the pathogen binding ability of dendritic cells (DCs) by down-regulation of DC-specific intercellular adhesion molecule-3 grabbing non-integrin (DC-SIGN). *The Journal of biological chemistry*, 284(24), pp.16334–16342.
Mateescu, B. et al., 2008. Regulation of an inducible promoter by an HP1beta-HP1gamma switch. *EMBO reports*, 9(3), pp.267–272.
Mathonnet, G. et al., 2007. MicroRNA Inhibition of Translation Initiation in Vitro by Targeting the Cap-Binding Complex eIF4F. *Science*, 317(5845), pp.1764–1767.
Mattes, J. et al., 2009. Antagonism of microRNA-126 suppresses the effector function of TH2 cells and the development of allergic airways disease. *Proceedings of the National Academy of Sciences of the United States of America*, 106(44), pp.18704–18709.
McCoy, C.E. et al., 2010. IL-10 Inhibits miR-155 Induction by Toll-like Receptors. *Journal of Biological Chemistry*, 285(27), pp.20492–20498.
McDaniell, R. et al., 2010. Heritable Individual-Specific and Allele-Specific Chromatin Signatures in Humans. *Science*, 328(5975), pp.235–239.
McWhinnie, R. et al., 2007. Endothelin-1 induces hypertrophy and inhibits apoptosis in human airway smooth muscle cells. *American journal of physiology Lung cellular and molecular physiology*, 292(1), pp.L278–86.
Mehr, S. et al., 2009. Treatment of a Case of Pediatric Hypereosinophilic Syndrome with Anti-Interleukin-5. *The Journal of Pediatrics*, 155(2), pp.289–291.
Nie, M. et al., 2003. Transcriptional Regulation of Cyclooxygenase 2 by Bradykinin and Interleukin-1β in Human Airway Smooth Muscle Cells: Involvement of Different Promoter Elements, Transcription Factors, and Histone H4 Acetylation. *Molecular and Cellular Biology*, 23(24), p.9233.
Meister, G. et al., 2004. Human Argonaute2 Mediates RNA Cleavage Targeted by miRNAs and siRNAs. *Molecular Cell*, 15(2), pp.185–197.
Meneghini, M.D., Wu, M. & Madhani, H.D., 2003. Conserved Histone Variant H2A.Z Protects Euchromatin from the Ectopic Spread of Silent Heterochromatin. *Cell*, 112(5), pp.725–736.
Merkenschlager, M., 2010. Cohesin: a global player in chromosome biology with local ties to gene regulation. *Current Opinion in Genetics & Development*, 20(5), pp.555–561.
Metcalf, D. et al., 1987. Quantitative responsiveness of murine hemopoietic populations in vitro and in vivo to recombinant multi-CSF (IL-3). *Exp Hematol*, 15(3), pp.288–295.
Micsinai, M. et al., 2012. Picking ChIP-seq peak detectors for analyzing chromatin modification experiments. *Nucleic Acids Research*.
Mignery, G.A. & Südhof, T.C., 1990. The ligand binding site and transduction mechanism in the inositol-1,4,5-triphosphate receptor. *The EMBO journal*, 9(12), pp.3893–3898.
Milgrom, H. et al., 2001. Treatment of childhood asthma with anti-immunoglobulin E antibody (omalizumab). *Pediatrics*, 108(2), p.E36.
Min, J., Zhang, Y. & Xu, R.-M., 2003. Structural basis for specific binding of Polycomb chromodomain to histone H3 methylated at Lys 27. *Genes & Development*, 17(15), pp.1823–1828.
Miska, E.A. et al., 2007. Most Caenorhabditis elegans microRNAs Are Individually Not Essential for Development or Viability. *PLoS Genetics*, 3(12), p.e215.
Mitzner, W., 2004. Airway smooth muscle: the appendix of the lung. *American Journal of Respiratory and Critical Care Medicine*, 169(7), pp.787–790.
Mohamed, J.S., Lopez, M.A. & Boriek, A.M., 2010. Mechanical Stretch Up-regulates MicroRNA-26a and Induces Human Airway Smooth Muscle Hypertrophy by Suppressing Glycogen Synthase Kinase-3. *Journal of Biological Chemistry*, 285(38), pp.29336–29347.
Molet, S. et al., 2001. IL-17 is increased in asthmatic airways and induces human bronchial fibroblasts to produce cytokines. *The Journal of allergy and clinical immunology*, 108(3), pp.430–438.
Morillon, A. et al., 2005. Dynamic lysine methylation on histone H3 defines the regulatory phase of gene transcription. *Molecular Cell*, 18(6), pp.723–734.

Mosmann, T.R. et al., 1986. *Two types of murine helper T cell clone. I. Definition according to profiles of lymphokine activities and secreted proteins*,
Moss, E.G., Lee, R.C. & Ambros, V., 1997. The cold shock domain protein LIN-28 controls developmental timing in C. elegans and is regulated by the lin-4 RNA. *Cell*, 88(5), pp.637–646.
Murray, R.K. & Kotlikoff, M.I., 1991. Receptor-activated calcium influx in human airway smooth muscle cells. *The Journal of physiology*, 435, pp.123–144.
Murugaiyan, G. et al., 2011. Silencing MicroRNA-155 Ameliorates Experimental Autoimmune Encephalomyelitis. *The Journal of Immunology*, 187(5), pp.2213–2221.
Nakamura, K.T. & McCray, P.B., 2000. Fetal airway smooth-muscle contractility and lung development. A player in the band or just someone in the audience? *American Journal of Respiratory Cell and Molecular Biology*, 23(1), pp.3–6.
Nakanishi, S. et al., 2008. A comprehensive library of histone mutants identifies nucleosomal residues required for H3K4 methylation. *Nature Structural & Molecular Biology*, 15(8), pp.881–888.
Nathans, J. et al., 1999. A new secreted protein that binds to Wnt proteins and inhibits their activites. *Nature*, 398(6726), pp.431–436.
Naureckas, E.T. et al., 1999. Bronchoalveolar lavage fluid from asthmatic subjects is mitogenic for human airway smooth muscle. *American Journal of Respiratory and Critical Care Medicine*, 160(6), pp.2062–2066.
Blackledge, N.P. et al., 2010. CpG Islands Recruit a Histone H3 Lysine 36 Demethylase. *Molecular Cell*, 38(2-2), p.179.
Neumann, H. et al., 2009. A method for genetically installing site-specific acetylation in recombinant histones defines the effects of H3 K56 acetylation. *Molecular Cell*, 36(1), pp.153–163.
Newman, M.A., Thomson, J.M. & Hammond, S.M., 2008. Lin-28 interaction with the Let-7 precursor loop mediates regulated microRNA processing. *RNA*, 14(8), pp.1539–1549.
Newton-Cheh, C. et al., 2009. Genome-wide association study identifies eight loci associated with blood pressure. *Nature Genetics*, 41(6), pp.666–676.
Nica, A.C. et al., 2010. Candidate Causal Regulatory Effects by Integration of Expression QTLs with Complex Trait Genetic Associations. *PLoS Genetics*, 6(4), p.e1000895.
Nicodeme, E. et al., 2010. Suppression of inflammation by a synthetic histone mimic. *Nature*, 468(7327), pp.1119–1123.
Nicolae, D.L. et al., 2010. Trait-Associated SNPs Are More Likely to Be eQTLs: Annotation to Enhance Discovery from GWAS. *PLoS Genetics*, 6(4), p.e1000888.
Nicolas, E. et al., 2007. Distinct roles of HDAC complexes in promoter silencing, antisense suppression and DNA damage protection. *Nature Publishing Group*, 14(5), pp.372–380.
Nicoll, J. et al., 1999. Identification of domains in IL-16 critical for biological activity. *Journal of immunology (Baltimore, Md : 1950)*, 163(4), pp.1827–1832.
Nie, M. et al., 2004. Differential Regulation of Chemokine Expression by Peroxisome Proliferator-activated Receptor Agonists: INTERACTIONS WITH GLUCOCORTICOIDS AND 2-AGONISTS. *Journal of Biological Chemistry*, 280(4), pp.2550–2561.
Nie, M., Knox, A.J. & Pang, L., 2005. beta2-Adrenoceptor agonists, like glucocorticoids, repress eotaxin gene transcription by selective inhibition of histone H4 acetylation. *Journal of immunology (Baltimore, Md : 1950)*, 175(1), pp.478–486.
Nielsen, P.R. et al., 2002. Structure of the HP1 chromodomain bound to histone H3 methylated at lysine 9. *Nature*, 416(6876), pp.103–107.
Nikolov, M. et al., 2011. Chromatin Affinity Purification and Quantitative Mass Spectrometry Defining the Interactome of Histone Modification Patterns. *Molecular & Cellular Proteomics*, 10(11), pp.M110.005371–M110.005371.
Nissen, R.M. & Yamamoto, K.R., 2000. The glucocorticoid receptor inhibits NFkappaB by interfering with serine-2 phosphorylation of the RNA polymerase II carboxy-terminal domain. *Genes & Development*, 14(18), pp.2314–2329.
Nogales-Cadenas, R. et al., 2009. GeneCodis: interpreting gene lists through enrichment analysis and integration of diverse biological information. *Nucleic Acids Research*, 37(Web Server), pp.W317–W322.
Noll, M. & Kornberg, R.D., 1977. Action of micrococcal nuclease on chromatin and the location of histone H1. *Journal of molecular biology*, 109(3), pp.393–404.
O'Connell, R.M. et al., 2009. Inositol phosphatase SHIP1 is a primary target of miR-155.

Proceedings of the National Academy of Sciences of the United States of America, 106(17), pp.7113–7118.
O'Connell, R.M. et al., 2007. MicroRNA-155 is induced during the macrophage inflammatory response. *Proceedings of the National Academy of Sciences of the United States of America*, 104(5), pp.1604–1609.
O'Connell, R.M. et al., 2010. MicroRNA-155 promotes autoimmune inflammation by enhancing inflammatory T cell development. *Immunity*, 33(4), pp.607–619.
O'Connell, R.M. et al., 2008. Sustained expression of microRNA-155 in hematopoietic stem cells causes a myeloproliferative disorder. *The Journal of experimental medicine*, 205(3), pp.585–594.
Oakley, R., Sar, M. & Cidlowski, J.A., 1996. The Human Glucocorticoid Receptor beta Isoform. *Journal of Biological Chemistry*, 271(16), pp.9550–9559.
Okamura, K. et al., 2008. The regulatory activity of microRNA* species has substantial influence on microRNA and 3' UTR evolution. *Nature Structural & Molecular Biology*, 15(4), pp.354–363.
Olsen, P.H. & Ambros, V., 1999. The lin-4 regulatory RNA controls developmental timing in Caenorhabditis elegans by blocking LIN-14 protein synthesis after the initiation of translation. *Developmental biology*, 216(2), pp.671–680.
Oltmanns, U. et al., 2005. Induction of human airway smooth muscle apoptosis by neutrophils and neutrophil elastase. *American Journal of Respiratory Cell and Molecular Biology*, 32(4), pp.334–341.
Oltmanns, U. et al., 2003. Role of c-jun N-terminal kinase in the induced release of GM-CSF, RANTES and IL-8 from human airway smooth muscle cells. *British Journal of Pharmacology*, 139(6), pp.1228–1234.
Ono, S., 2000. Molecular genetics of allergic diseases. *Annual review of immunology*.
Ordoñez, C.L. et al., 2000. Increased neutrophil numbers and IL-8 levels in airway secretions in acute severe asthma: Clinical and biologic significance. *American Journal of Respiratory and Critical Care Medicine*, 161(4 Pt 1), pp.1185–1190.
Ordoñez, C.L. et al., 2001. Mild and moderate asthma is associated with airway goblet cell hyperplasia and abnormalities in mucin gene expression. *American Journal of Respiratory and Critical Care Medicine*, 163(2), pp.517–523.
Ouyang, W. et al., 2000. Stat6-independent GATA-3 autoactivation directs IL-4-independent Th2 development and commitment. *Immunity*, 12(1), pp.27–37.
Pagdin, T. & Lavender, P., 2011. MicroRNAs in lung diseases. *Thorax*.
Pan, G. et al., 2007. Whole-genome analysis of histone H3 lysine 4 and lysine 27 methylation in human embryonic stem cells. *Cell Stem Cell*, 1(3), pp.299–312.
Panettieri, R.A. et al., 1998. Effects of LTD4 on human airway smooth muscle cell proliferation, matrix expression, and contraction In vitro: differential sensitivity to cysteinyl leukotriene receptor antagonists. *American Journal of Respiratory Cell and Molecular Biology*, 19(3), pp.453–461.
Pang, L. & Knox, A.J., 1998. Bradykinin stimulates IL-8 production in cultured human airway smooth muscle cells: role of cyclooxygenase products. *Journal of immunology (Baltimore, Md : 1950)*, 161(5), pp.2509–2515.
Pang, L. & Knox, A.J., 2001. Regulation of TNF-alpha-induced eotaxin release from cultured human airway smooth muscle cells by beta2-agonists and corticosteroids. *The FASEB journal : official publication of the Federation of American Societies for Experimental Biology*, 15(1), pp.261–269.
Parelho, V. et al., 2008. Cohesins Functionally Associate with CTCF on Mammalian Chromosome Arms. *Cell*, 132(3), pp.422–433.
Park, Y.J. et al., 2004. A New Fluorescence Resonance Energy Transfer Approach Demonstrates That the Histone Variant H2AZ Stabilizes the Histone Octamer within the Nucleosome. *Journal of Biological Chemistry*, 279(23), pp.24274–24282.
Parker, J.S., Roe, S.M. & Barford, D., 2005. Structural insights into mRNA recognition from a PIWI domain|[ndash]|siRNA guide complex. *Nature*, 434(7033), pp.663–666.
Paro, R. & Hogness, D.S., 1991. The Polycomb protein shares a homologous domain with a heterochromatin-associated protein of Drosophila. *Proceedings of the National Academy of Sciences of the United States of America*, 88(1), pp.263–267.
Parthun, M.R., 2007. Hat1: the emerging cellular roles of a type B histone acetyltransferase. *Oncogene*, 26(37), pp.5319–5328.

Pavord, I.D. et al., 2007. Safety and efficacy of bronchial thermoplasty in symptomatic, severe asthma. *American Journal of Respiratory and Critical Care Medicine*, 176(12), pp.1185–1191.
Pedersen, I.M. et al., 2009. Onco-miR-155 targets SHIP1 to promote TNFα-dependent growth of B cell lymphomas. *EMBO Molecular Medicine*, 1(5), pp.288–295.
Pekowska, A. et al., 2011. H3K4 tri-methylation provides an epigenetic signature of active enhancers. *The EMBO journal*.
Pelaia, G. et al., 2008. Molecular mechanisms underlying airway smooth muscle contraction and proliferation: implications for asthma. *Respiratory medicine*, 102(8), pp.1173–1181.
Peng, Q. et al., 2005. Multiple beta 1 integrins mediate enhancement of human airway smooth muscle cytokine secretion by fibronectin and type I collagen. *Journal of immunology (Baltimore, Md : 1950)*, 174(4), pp.2258–2264.
Pepe, C. et al., 2005. Differences in airway remodeling between subjects with severe and moderate asthma. *The Journal of allergy and clinical immunology*, 116(3), pp.544–549.
Kharchenko, P.V. et al., 2008. Design and analysis of ChIP-seq experiments for DNA-binding proteins. *Nature biotechnology*, 26(12), p.1351.
Pillai, R.S. et al., 2005. Inhibition of translational initiation by Let-7 MicroRNA in human cells. *Science*, 309(5740), pp.1573–1576.
Placek, B.J. et al., 2009. The histone variant H3.3 regulates gene expression during lytic infection with herpes simplex virus type 1. *Journal of virology*, 83(3), pp.1416–1421.
Pottier, N. et al., 2009. Identification of Keratinocyte Growth Factor as a Target of microRNA-155 in Lung Fibroblasts: Implication in Epithelial-Mesenchymal Interactions. *PLoS ONE*, 4(8), p.e6718.
Powell, D.W. et al., 1999. Myofibroblasts. I. Paracrine cells important in health and disease. *The American journal of physiology*, 277(1 Pt 1), pp.C1–9.
Prunell, A. & Kornberg, R.D., 1982. Variable center to center distance of nucleosomes in chromatin. *Journal of molecular biology*, 154(3), pp.515–523.
Ptashne, M., 2007. On the use of the word 'epigenetic'. *Current biology : CB*, 17(7), pp.R233–6.
Puddicombe, S.M. et al., 2000. Involvement of the epidermal growth factor receptor in epithelial repair in asthma. *The FASEB journal : official publication of the Federation of American Societies for Experimental Biology*, 14(10), pp.1362–1374.
Puig, O.M. et al., 1998. Interaction between N-terminal domain of H4 and DNA is regulated by the acetylation degree. *Biochimica et biophysica acta*, 1397(1), pp.79–90.
Punnonen, J. et al., 1993. Interleukin 13 induces interleukin 4-independent IgG4 and IgE synthesis and CD23 expression by human B cells. *Proceedings of the National Academy of Sciences of the United States of America*, 90(8), pp.3730–3734.
Yin, Q. et al., 2008. MicroRNA-155 Is an Epstein-Barr Virus-Induced Gene That Modulates Epstein-Barr Virus-Regulated Gene Expression Pathways. *Journal of virology*, 82(11), p.5295.
Raisner, R.M. et al., 2005. Histone variant H2A.Z marks the 5' ends of both active and inactive genes in euchromatin. *Cell*, 123(2), pp.233–248.
Rand, T. et al., 1991. CD4-mediated stimulation of human eosinophils: lymphocyte chemoattractant factor and other CD4-binding ligands elicit eosinophil migration. *The Journal of experimental medicine*, 173(6), p.1521.
Rani, A. et al., 2011. IL-2 regulates expression of C-MAF in human CD4 T cells. *The Journal of Immunology*, 187(7), pp.3721–3729.
Ray, A. & Prefontaine, K.E., 1994. Physical association and functional antagonism between the p65 subunit of transcription factor NF-kappa B and the glucocorticoid receptor. *Proceedings of the National Academy of Sciences of the United States of America*, 91(2), pp.752–756.
Rea, S. et al., 2000. Regulation of chromatin structure by site-specific histone H3 methyltransferases. *Nature*, 406(6796), pp.593–599.
Skalsky, R.L. et al., 2007. Kaposi's Sarcoma-Associated Herpesvirus Encodes an Ortholog of miR-155. *Journal of virology*, 81(23), p.12836.
Ringrose, L., Ehret, H. & Paro, R., 2004. Distinct Contributions of Histone H3 Lysine 9 and 27 Methylation to Locus-Specific Stability of Polycomb Complexes. *Molecular Cell*, 16(4), pp.641–653.
Ritchie, W., Flamant, S. & Rasko, J.E.J., 2009. Predicting microRNA targets and functions: traps for the unwary. *Nature Methods*, 6(6), pp.397–398.

Ro, S. et al., 2007. Tissue-dependent paired expression of miRNAs. *Nucleic Acids Research*, 35(17), pp.5944–5953.
Roberts, J.A., Rodger, I.W. & Thomson, N.C., 1987. In vivo and in vitro human airway responsiveness to leukotriene D4 in patients without asthma. *The Journal of allergy and clinical immunology*, 80(5), pp.688–694.
Robins, H., Li, Y. & Padgett, R.W., 2005. Incorporating structure to predict microRNA targets. *Proceedings of the National Academy of Sciences of the United States of America*, 102(11), pp.4006–4009.
Robinson, D.S. et al., 1992. Predominant TH2-like bronchoalveolar T-lymphocyte population in atopic asthma. *The New England journal of medicine*, 326(5), pp.298–304.
Robinson, P.J.J. et al., 2006. EM measurements define the dimensions of the "30-nm" chromatin fiber: evidence for a compact, interdigitated structure. *Proceedings of the National Academy of Sciences of the United States of America*, 103(17), pp.6506–6511.
Roche, W.R., 1998. Inflammatory and structural changes in the small airways in bronchial asthma. *American Journal of Respiratory and Critical Care Medicine*, 157(5 Pt 2), pp.S191–4.
Rodriguez, A. et al., 2007. Requirement of bic/microRNA-155 for Normal Immune Function. *Science*, 316(5824), pp.608–611.
Roffel, A.F., Elzinga, C.R. & Zaagsma, J., 1990. Muscarinic M3 receptors mediate contraction of human central and peripheral airway smooth muscle. *Pulmonary pharmacology*, 3(1), pp.47–51.
Ruddy, M.J. et al., 2004. Interleukin-17 regulates expression of the CXC chemokine LIX/CXCL5 in osteoblasts: implications for inflammation and neutrophil recruitment. *Journal of leukocyte biology*, 76(1), pp.135–144.
Ruthenburg, A.J. et al., 2011. Recognition of a mononucleosomal histone modification pattern by BPTF via multivalent interactions. *Cell*, 145(5), pp.692–706.
Sabo, P.J. et al., 2006. Genome-scale mapping of DNase I sensitivity in vivo using tiling DNA microarrays. *Nature Methods*, 3(7), pp.511–518.
Saetta, M. et al., 1991. Quantitative structural analysis of peripheral airways and arteries in sudden fatal asthma. *The American review of respiratory disease*, 143(1), pp.138–143.
Sanders, S.L. et al., 2004. Methylation of histone H4 lysine 20 controls recruitment of Crb2 to sites of DNA damage. *Cell*, 119(5), pp.603–614.
Santaguida, S. & Musacchio, A., 2009. The life and miracles of kinetochores. *The EMBO journal*, 28(17), pp.2511–2531.
Santangelo, S. et al., 2009. Chromatin structure and DNA methylation of the IL-4 gene in human T(H)2 cells. *Chromosome research : an international journal on the molecular, supramolecular and evolutionary aspects of chromosome biology*, 17(4), pp.485–496.
Sapienza, S. et al., 1991. Structural changes in the airways of sensitized brown Norway rats after antigen challenge. *The American review of respiratory disease*, 144(2), pp.423–427.
Sasaki, T. et al., 2003. Identification of eight members of the Argonaute family in the human genome small star, filled. *Genomics*, 82(3), pp.323–330.
Sato, T. et al., 2011. IL-4 induces differentiation of human embryonic stem cells into fibrogenic fibroblast-like cells. *Journal of Allergy and Clinical Immunology*, 127(6), pp.1595–1603.e9.
Schalch, T. et al., 2005. X-ray structure of a tetranucleosome and its implications for the chromatin fibre. *Nature*, 436(7047), pp.138–141.
Schleimer, R.P. et al., 1992. IL-4 induces adherence of human eosinophils and basophils but not neutrophils to endothelium. Association with expression of VCAM-1. *Journal of immunology (Baltimore, Md : 1950)*, 148(4), pp.1086–1092.
Schmeier, S. et al., 2009. Deciphering the transcriptional circuitry of microRNA genes expressed during human monocytic differentiation. *BMC genomics*, 10, p.595.
Schmidt, M. et al., 2003. Identification of circulating fibrocytes as precursors of bronchial myofibroblasts in asthma. *Journal of immunology (Baltimore, Md : 1950)*, 171(1), pp.380–389.
Schones, D.E. et al., 2008. Dynamic Regulation of Nucleosome Positioning in the Human Genome. *Cell*, 132(5), pp.887–898.
Schroeder, A. et al., 2006. The RIN: an RNA integrity number for assigning integrity values to RNA measurements. *BMC molecular biology*, 7, p.3.
Schuger, L. et al., 1997. Laminin alpha1 chain synthesis in the mouse developing lung:

requirement for epithelial-mesenchymal contact and possible role in bronchial smooth muscle development. *The Journal of cell biology*, 139(2), pp.553–562.
Schwartz, B.E. & Ahmad, K., 2005. Transcriptional activation triggers deposition and removal of the histone variant H3.3. *Genes & Development*, 19(7), pp.804–814.
Schwartz, S., Meshorer, E. & Ast, G., 2009. Chromatin organization marks exon-intron structure. *Nature Structural & Molecular Biology*, 16(9), pp.990–995.
Schwarz, D.S. et al., 2003. Asymmetry in the assembly of the RNAi enzyme complex. *Cell*, 115(2), pp.199–208.
Seggerson, K., Tang, L. & Moss, E.G., 2002. Two genetic circuits repress the Caenorhabditis elegans heterochronic gene lin-28 after translation initiation. *Developmental biology*, 243(2), pp.215–225.
Selbach, M. et al., 2008. Widespread changes in protein synthesis induced by microRNAs. *Nature*, 455(7209), pp.58–63.
Sethupathy, P. et al., 2007. Human microRNA-155 on chromosome 21 differentially interacts with its polymorphic target in the AGTR1 3' untranslated region: a mechanism for functional single-nucleotide polymorphisms related to phenotypes. *American journal of human genetics*, 81(2), pp.405–413.
Shahana, S. et al., 2005. Ultrastructure of bronchial biopsies from patients with allergic and non-allergic asthma. *Respiratory medicine*, 99(4), pp.429–443.
Shebani, E. et al., 2005. Attachment of columnar airway epithelial cells in asthma. *Tissue & cell*, 37(2), pp.145–152.
Shi, X. et al., 2006. ING2 PHD domain links histone H3 lysine 4 methylation to active gene repression. *Nature*, 442(7098), pp.96–99.
Shi, Y. et al., 2004. Histone demethylation mediated by the nuclear amine oxidase homolog LSD1. *Cell*, 119(7), pp.941–953.
Shi, Y. et al., 1991. Transcriptional repression by YY1, a human GLI-Krüippel-related protein, and relief of repression by adenovirus E1A protein. *Cell*, 67(2), pp.377–388.
Shiba, K. et al., 2002. Structural changes of the airway wall impair respiratory function, even in mild asthma. *Chest*, 122(5), pp.1622–1626.
Shin, C. et al., 2010. Expanding the microRNA targeting code: functional sites with centered pairing. *Molecular Cell*, 38(6), pp.789–802.
Shogren-Knaak, M. et al., 2006. Histone H4-K16 acetylation controls chromatin structure and protein interactions. *Science*, 311(5762), pp.844–847.
Shoji, S. et al., 1989. Lung fibroblasts produce chemotactic factors for bronchial epithelial cells. *The American journal of physiology*, 257(2 Pt 1), pp.L71–9.
Sohn, S.Y. et al., 2007. Crystal structure of human DGCR8 core. *Nature Publishing Group*, 14(9), pp.847–853.
Song, J.-J. et al., 2004. Crystal structure of Argonaute and its implications for RISC slicer activity. *Science*, 305(5689), pp.1434–1437.
Sousa, A.R. et al., 2000. Glucocorticoid resistance in asthma is associated with elevated in vivo expression of the glucocorticoid receptor beta-isoform. *The Journal of allergy and clinical immunology*, 105(5), pp.943–950.
Sparrow, M.P., Warwick, S.P. & Everett, A.W., 1995. Innervation and function of the distal airways in the developing bronchial tree of fetal pig lung. *American Journal of Respiratory Cell and Molecular Biology*, 13(5), pp.518–525.
Srinivasan, G., Patel, N.T. & Thompson, E.B., 1994. Heat shock protein is tightly associated with the recombinant human glucocorticoid receptor:glucocorticoid response element complex. *Molecular endocrinology (Baltimore, Md.)*, 8(2), pp.189–196.
Stanczyk, J. et al., 2008. Altered expression of MicroRNA in synovial fibroblasts and synovial tissue in rheumatoid arthritis. *Arthritis and rheumatism*, 58(4), pp.1001–1009.
Stone, K.D., Prussin, C. & Metcalfe, D.D., 2010. IgE, mast cells, basophils, and eosinophils. *Journal of Allergy and Clinical Immunology*, 125(2), pp.S73–S80.
Su, W.-L., Kleinhanz, R.R. & Schadt, E.E., 2011. Characterizing the role of miRNAs within gene regulatory networks using integrative genomics techniques. *Molecular Systems Biology*, 7(1), pp.–.
Tahiliani, M. et al., 2007. The histone H3K4 demethylase SMCX links REST target genes to X-linked mental retardation. *Nature*, 447(7144), pp.601–605.
Talbert, P.B. & Henikoff, S., 2010. Histone variants — ancient wrap artists of the epigenome. *Nature Reviews Molecular Cell Biology*, 11(4), pp.264–275.

Tam, W., 2001. Identification and characterization of human BIC, a gene on chromosome 21 that encodes a noncoding RNA. *Gene*, 274(1-2), pp.157–167.
Tam, W., Ben-Yehuda, D. & Hayward, W.S., 1997. bic, a novel gene activated by proviral insertions in avian leukosis virus-induced lymphomas, is likely to function through its noncoding RNA. *Molecular and Cellular Biology*, 17(3), pp.1490–1502.
Tamura, T. et al., 2009. Inducible Deposition of the Histone Variant H3.3 in Interferon-stimulated Genes. *Journal of Biological Chemistry*, 284(18), pp.12217–12225.
Tang, B. et al., 2010. Identification of MyD88 as a novel target of miR-155, involved in negative regulation of Helicobacter pylori-induced inflammation. *FEBS letters*, 584(8), pp.1481–1486.
Tang, M. et al., 2011. Restraint of angiogenesis by zinc finger transcription factor CTCF-dependent chromatin insulation. *Proceedings of the National Academy of Sciences of the United States of America*, 108(37), pp.15231–15236.
Taverna, S.D. et al., 2007. How chromatin-binding modules interpret histone modifications: lessons from professional pocket pickers. *Nature Structural & Molecular Biology*, 14(11), pp.1025–1040.
Taverna, S.D. et al., 2006. Yng1 PHD finger binding to H3 trimethylated at K4 promotes NuA3 HAT activity at K14 of H3 and transcription at a subset of targeted ORFs. *Molecular Cell*, 24(5), pp.785–796.
Thai, T.-H. et al., 2007. Regulation of the germinal center response by microRNA-155. *Science*, 316(5824), pp.604–608.
Thakar, A. et al., 2009. H2A.Z and H3.3 Histone Variants Affect Nucleosome Structure: Biochemical and Biophysical Studies. *Biochemistry*, 48(46), pp.10852–10857.
Thoma, F., Koller, T. & Klug, A., 1979. Involvement of histone H1 in the organization of the nucleosome and of the salt-dependent superstructures of chromatin. *The Journal of cell biology*, 83(2 Pt 1), pp.403–427.
Thomson, J.M. et al., 2006. Extensive post-transcriptional regulation of microRNAs and its implications for cancer. *Genes & Development*, 20(16), pp.2202–2207.
Thomson, R.J., Bramley, A.M. & Schellenberg, R.R., 1996. Airway muscle stereology: implications for increased shortening in asthma. *American Journal of Respiratory and Critical Care Medicine*, 154(3 Pt 1), pp.749–757.
Tilghman, S.M. et al., 2000. CTCF mediates methylation-sensitive enhancer-blocking activity at the
H19/Igf2 locus. *Nature*, 405(6785), pp.486–489.
Tliba, O. et al., 2003. IL-13 enhances agonist-evoked calcium signals and contractile responses in airway smooth muscle. *British Journal of Pharmacology*, 140(7), pp.1159–1162.
Tollet, J., Everett, A.W. & Sparrow, M.P., 2001. Spatial and temporal distribution of nerves, ganglia, and smooth muscle during the early pseudoglandular stage of fetal mouse lung development. *Developmental dynamics : an official publication of the American Association of Anatomists*, 221(1), pp.48–60.
Tsukada, Y.-I. et al., 2006. Histone demethylation by a family of JmjC domain-containing proteins. *Nature*, 439(7078), pp.811–816.
Tsukiyama, T. & Wu, C., 1995. Purification and properties of an ATP-dependent nucleosome remodeling factor. *Cell*, 83(6), pp.1011–1020.
Tunon-de-Lara, J.-M., Berger, P. & Bégueret, H., 2002. Mast cells in airway smooth muscle. *The New England journal of medicine*, 347(13), pp.1040–1; author reply 1040–1.
Uhlmann, F., 2004. The mechanism of sister chromatid cohesion. *Experimental Cell Research*, 296(1), pp.80–85.
Upadhyay, A.K. & Cheng, X., 2011. Dynamics of histone lysine methylation: structures of methyl writers and erasers. *Progress in drug research. Fortschritte der Arzneimittelforschung. Progrès des recherches pharmaceutiques*, 67, pp.107–124.
van den Berg, A. et al., 2003. High expression of B-cell receptor inducible geneBIC in all subtypes of Hodgkin lymphoma. *Genes, Chromosomes and Cancer*, 37(1), pp.20–28.
van Leeuwen, F., Gafken, P.R. & Gottschling, D.E., 2002. Dot1p modulates silencing in yeast by methylation of the nucleosome core. *Cell*, 109(6), pp.745–756.
van Rooij, E. et al., 2006. A signature pattern of stress-responsive microRNAs that can evoke cardiac hypertrophy and heart failure. *Proceedings of the National Academy of Sciences of the United States of America*, 103(48), pp.18255–18260.

Vasudevan, S., Tong, Y. & Steitz, J.A., 2007. Switching from Repression to Activation: MicroRNAs Can Up-Regulate Translation. *Science*, 318(5858), pp.1931–1934.
Vella, M.C. et al., 2004. The C. elegans microRNA let-7 binds to imperfect let-7 complementary sites from the lin-41 3'UTR. *Genes & Development*, 18(2), pp.132–137.
Vermeulen, M. et al., 2007. Selective anchoring of TFIID to nucleosomes by trimethylation of histone H3 lysine 4. *Cell*, 131(1), pp.58–69.
Vignola, A.M. et al., 1998. Sputum metalloproteinase-9/tissue inhibitor of metalloproteinase-1 ratio correlates with airflow obstruction in asthma and chronic bronchitis. *American Journal of Respiratory and Critical Care Medicine*, 158(6), pp.1945–1950.
Vigorito, E. et al., 2007. microRNA-155 regulates the generation of immunoglobulin class-switched plasma cells. *Immunity*, 27(6), pp.847–859.
Visel, A. et al., 2009. ChIP-seq accurately predicts tissue-specific activity of enhancers. *Nature*, 457(7231), pp.854–858.
Viswanathan, S.R., Daley, G.Q. & Gregory, R.I., 2008. Selective blockade of microRNA processing by Lin28. *Science*, 320(5872), pp.97–100.
Vostrov, A.A. & Quitschke, W.W., 1997. The Zinc Finger Protein CTCF Binds to the APBbeta Domain of the Amyloid beta -Protein Precursor Promoter. EVIDENCE FOR A ROLE IN TRANSCRIPTIONAL ACTIVATION. *Journal of Biological Chemistry*, 272(52), pp.33353–33359.
Wang, D. et al., 2011. Reprogramming transcription by distinct classes of enhancers functionally defined by eRNA. *Nature*, 474(7351), pp.390–394.
Wang, P. et al., 2010a. Inducible microRNA-155 feedback promotes type I IFN signaling in antiviral innate immunity by targeting suppressor of cytokine signaling 1. *The Journal of Immunology*, 185(10), pp.6226–6233.
Wang, X., Hu, G. & Zhou, J., 2010b. Repression of Versican Expression by MicroRNA-143. *Journal of Biological Chemistry*, 285(30), pp.23241–23250.
Wang, Z. et al., 2008. Combinatorial patterns of histone acetylations and methylations in the human genome. *Nature Genetics*, 40(7), pp.897–903.
Ward, J.E. et al., 2008. Proliferation is not increased in airway myofibroblasts isolated from asthmatics. *European Respiratory Journal*, 32(2), pp.362–371.
Wardlaw, A.J. et al., 1988. Eosinophils and mast cells in bronchoalveolar lavage in subjects with mild asthma. Relationship to bronchial hyperreactivity. *The American review of respiratory disease*, 137(1), pp.62–69.
Watson, M.L. et al., 1998. Interleukin 8 and monocyte chemoattractant protein 1 production by cultured human airway smooth muscle cells. *Cytokine*, 10(5), pp.346–352.
Weller, P.F. et al., 1996. Role of the eosinophil in allergic reactions. *The European respiratory journal. Supplement*, 22, pp.109s–115s.
Wendt, K.S. et al., 2008. Cohesin mediates transcriptional insulation by CCCTC-binding factor. *Nature*, 451(7180), pp.796–801.
Wenzel, S. et al., 2007. Effect of an interleukin-4 variant on late phase asthmatic response to allergen challenge in asthmatic patients: results of two phase 2a studies. *The Lancet*, 370(9596), pp.1422–1431.
Wenzel, S.E., 2006. Myofibroblast or Smooth Muscle: Do In Vitro Systems Adequately Replicate Tissue Smooth Muscle? *American Journal of Respiratory and Critical Care Medicine*, 174(4), pp.364–365.
Wenzel, S.E. et al., 1997. Bronchoscopic evaluation of severe asthma. Persistent inflammation associated with high dose glucocorticoids. *American Journal of Respiratory and Critical Care Medicine*, 156(3 Pt 1), pp.737–743.
Wicks, J. et al., 2006. Enhanced upregulation of smooth muscle related transcripts by TGF beta2 in asthmatic (myo) fibroblasts. *Thorax*, 61(4), pp.313–319.
Widdicombe, J.G., 1963. Regulation of tracheobronchial smooth muscle. *Physiological reviews*, 43, pp.1–37.
Widom, J. & Klug, A., 1985. Structure of the 300A chromatin filament: X-ray diffraction from oriented samples. *Cell*, 43(1), pp.207–213.
Wilbanks, E.G. & Facciotti, M.T., 2010. Evaluation of Algorithm Performance in ChIP-Seq Peak Detection. *PLoS ONE*, 5(7), p.e11471.
Williams, A.E. et al., 2009. MicroRNA Expression Profiling in Mild Asthmatic Human Airways and Effect of Corticosteroid Therapy. *PLoS ONE*, 4(6), p.e5889.
Williams, S.P. et al., 1986. Chromatin fibers are left-handed double helices with diameter and

mass per unit length that depend on linker length. *Biophysical journal*, 49(1), pp.233–248.
Willis, B.C., duBois, R.M. & Borok, Z., 2006. Epithelial origin of myofibroblasts during fibrosis in the lung. *Proceedings of the American Thoracic Society*, 3(4), pp.377–382.
Wills-Karp, M., 1999. Immunologic basis of antigen-induced airway hyperresponsiveness. *Annual review of immunology*, 17, pp.255–281.
Wilson, J.W. & Li, X., 1997. The measurement of reticular basement membrane and submucosal collagen in the asthmatic airway. *Clinical and experimental allergy : journal of the British Society for Allergy and Clinical Immunology*, 27(4), pp.363–371.
Wilson, N.J. et al., 2007. Development, cytokine profile and function of human interleukin 17-producing helper T cells. *Nature Immunology*, 8(9), pp.950–957.
Woltmann, G. et al., 1999. Objective quantitative analysis of eosinophils and bronchial epithelial cells in induced sputum by laser scanning cytometry. *Thorax*, 54(2), pp.124–130.
Wong, L.H. et al., 2008. Histone H3.3 incorporation provides a unique and functionally essential telomeric chromatin in embryonic stem cells. *Genome research*, 19(3), pp.404–414.
Woodruff, P.G. et al., 2004. Hyperplasia of smooth muscle in mild to moderate asthma without changes in cell size or gene expression. *American Journal of Respiratory and Critical Care Medicine*, 169(9), pp.1001–1006.
Woodruff, P.G. et al., 2001. Relationship between airway inflammation, hyperresponsiveness, and obstruction in asthma. *The Journal of allergy and clinical immunology*, 108(5), pp.753–758.
Wysocka, J. et al., 2006. A PHD finger of NURF couples histone H3 lysine 4 trimethylation with chromatin remodelling. *Nature*, 442(7098), pp.86–90.
Xin, M. et al., 2009. MicroRNAs miR-143 and miR-145 modulate cytoskeletal dynamics and responsiveness of smooth muscle cells to injury. *Genes & Development*, 23(18), pp.2166–2178.
Yanaihara, N. et al., 2006. Unique microRNA molecular profiles in lung cancer diagnosis and prognosis. *Cancer cell*, 9(3), pp.189–198.
Yang, Y. et al., 1999. Embryonic mesenchymal cells share the potential for smooth muscle differentiation: myogenesis is controlled by the cell's shape. *Development (Cambridge, England)*, 126(13), pp.3027–3033.
Yang, Y. et al., 2000. Stretch-induced alternative splicing of serum response factor promotes bronchial myogenesis and is defective in lung hypoplasia. *The Journal of clinical investigation*, 106(11), pp.1321–1330.
Yekta, S., Shih, I.-H. & Bartel, D.P., 2004. MicroRNA-directed cleavage of HOXB8 mRNA. *Science*, 304(5670), pp.594–596.
Yi, R. et al., 2003. Exportin-5 mediates the nuclear export of pre-microRNAs and short hairpin RNAs. *Genes & Development*, 17(24), pp.3011–3016.
Yoshii, A. et al., 1999. Relaxation of contracted rabbit tracheal and human bronchial smooth muscle by Y-27632 through inhibition of Ca2+ sensitization. *American Journal of Respiratory Cell and Molecular Biology*, 20(6), pp.1190–1200.
Yu, S.-L. et al., 2008. MicroRNA Signature Predicts Survival and Relapse in Lung Cancer. *Cancer cell*, 13(1), pp.48–57.
Yuan, Y.-R. et al., 2005. Crystal Structure of A. aeolicus Argonaute, a Site-Specific DNA-Guided Endoribonuclease, Provides Insights into RISC-Mediated mRNA Cleavage. *Molecular Cell*, 19(3), pp.405–419.
Zang, C. et al., 2009. A clustering approach for identification of enriched domains from histone modification ChIP-Seq data. *Bioinformatics*, 25(15), pp.1952–1958.
Zeng, Y. & Cullen, B.R., 2005. Efficient processing of primary microRNA hairpins by Drosha requires flanking nonstructured RNA sequences. *The Journal of biological chemistry*, 280(30), pp.27595–27603.
Zeng, Y. & Cullen, B.R., 2004. Structural requirements for pre-microRNA binding and nuclear export by Exportin 5. *Nucleic Acids Research*, 32(16), pp.4776–4785.
Zeng, Y., Yi, R. & Cullen, B.R., 2005. Recognition and cleavage of primary microRNA precursors by the nuclear processing enzyme Drosha. *The EMBO journal*, 24(1), pp.138–148.
Zhang, H. et al., 2002. Human Dicer preferentially cleaves dsRNAs at their termini without a

requirement for ATP. *The EMBO journal*, 21(21), pp.5875–5885.
Zhang, H., Roberts, D.N. & Cairns, B.R., 2005. Genome-wide dynamics of Htz1, a histone H2A variant that poises repressed/basal promoters for activation through histone loss. *Cell*, 123(2), pp.219–231.
Zhang, S. et al., 1999. Growth factors secreted by bronchial epithelial cells control myofibroblast proliferation: an in vitro co-culture model of airway remodeling in asthma. *Laboratory investigation; a journal of technical methods and pathology*, 79(4), pp.395–405.
Zhang, W. et al., 1998. Essential and redundant functions of histone acetylation revealed by mutation of target lysines and loss of the Gcn5p acetyltransferase. *The EMBO journal*, 17(11), pp.3155–3167.
Zhang, Y., 1998. Processing and Activation of Pro-Interleukin-16 by Caspase-3. *Journal of Biological Chemistry*, 273(2), pp.1144–1149.
Zhang, Y. et al., 2008. Model-based Analysis of ChIP-Seq (MACS). *Genome Biology*, 9(9), p.R137.
Zhao, X.D. et al., 2007. Whole-Genome Mapping of Histone H3 Lys4 and 27 Trimethylations Reveals Distinct Genomic Compartments in Human Embryonic Stem Cells. *Cell Stem Cell*, 1(3), pp.286–298.
Zheng, Y. et al., 2012. Glucocorticoids inhibit lipopolysaccharide-mediated inflammatory response by downregulating microRNA-155: a novel anti-inflammation mechanism. *Free radical biology & medicine*, 52(8), pp.1307–1317.
Zippo, A. et al., 2009. Histone crosstalk between H3S10ph and H4K16ac generates a histone code that mediates transcription elongation. *Cell*, 138(6), pp.1122–1136.
Ørom, U.A., Nielsen, F.C. & Lund, A.H., 2008. MicroRNA-10a binds the 5'UTR of ribosomal protein mRNAs and enhances their translation. *Molecular Cell*, 30(4), pp.460–471.

Appendices

Appendix I – Average expression of miRNAs in cultured human ASMCS

ProbeSet Name	H1	H2	H3	A1	A2	A3	Average
hsa-miR-1826_st	13.19	12.98	13.66	13.71	13.42	13.71	13.44
hsa-let-7b_st	13.45	13.54	13.36	13.55	13.23	13.29	13.40
hsa-miR-638_st	12.88	12.34	13.12	12.63	13.55	13.56	13.01
hsa-miR-923_st	12.80	12.68	13.00	12.92	12.40	12.71	12.75
hsa-miR-125b_st	12.41	12.61	12.72	12.64	12.62	12.81	12.64
hsa-let-7c_st	12.42	12.86	12.51	12.82	12.41	12.41	12.57
hsa-miR-24_st	12.62	12.20	12.16	12.21	12.19	12.53	12.32
hsa-miR-222_st	12.30	12.55	12.30	12.40	12.38	11.96	12.31
hsa-miR-221_st	12.34	12.43	12.35	12.49	11.94	12.16	12.29
hsa-miR-1228-star_st	12.03	11.96	12.42	12.02	12.94	12.31	12.28
hsa-let-7a_st	12.05	12.38	11.98	12.35	12.12	12.29	12.20
hsa-miR-23a_st	12.26	11.98	12.24	11.81	11.75	12.11	12.03
hsa-miR-26a_st	11.87	11.86	11.85	12.03	11.56	11.70	11.81
hsa-miR-663_st	11.00	11.11	11.52	11.49	12.16	11.66	11.49
hsa-miR-149-star_st	11.02	11.15	11.56	11.16	12.47	11.57	11.49
hsa-miR-145_st	11.27	11.68	11.37	11.79	11.17	11.54	11.47
hsa-miR-23b_st	11.39	11.26	11.66	11.06	11.09	11.86	11.39
hsa-miR-100_st	11.50	11.47	11.38	11.33	11.17	11.23	11.35
hsa-miR-31_st	11.35	11.67	11.01	11.52	11.62	10.43	11.27
hsa-miR-22_st	11.00	10.58	10.95	11.12	10.40	11.42	10.91
hsa-miR-103_st	10.71	10.84	10.51	10.69	10.43	10.49	10.61
hsa-miR-29a_st	10.86	10.64	10.54	10.39	10.26	10.85	10.59
hsa-let-7e_st	10.56	10.96	10.64	10.45	10.25	10.58	10.57
hsa-miR-107_st	10.51	10.55	10.29	10.43	10.48	10.25	10.42
hsa-miR-16_st	10.26	10.37	10.35	10.31	10.40	10.20	10.32
hsa-let-7d_st	10.27	10.57	10.25	10.48	9.82	10.28	10.28
hsa-miR-199a-5p_st	10.38	10.34	10.11	10.25	9.99	10.01	10.18
hsa-miR-1308_st	10.20	11.05	9.47	11.50	9.35	9.44	10.17
hsa-miR-191_st	10.16	10.36	10.09	10.09	10.05	9.91	10.11
hsa-miR-199b-3p_st	10.21	10.09	10.30	10.23	9.37	10.40	10.10
hsa-miR-199a-3p_st	10.23	10.15	10.36	10.18	9.17	10.39	10.08
hsa-miR-27a_st	10.53	10.08	9.83	9.61	9.58	10.61	10.04
hsa-miR-125a-5p_st	10.08	10.42	9.97	9.83	9.94	9.83	10.01
hsa-miR-494_st	9.40	9.84	10.12	10.96	9.69	9.76	9.96
hsa-miR-320a_st	9.98	10.23	10.10	9.97	10.15	9.30	9.95
hsa-miR-127-3p_st	9.54	10.23	9.77	10.76	9.68	9.67	9.94
hsa-miR-320b_st	9.98	10.33	10.11	9.76	10.19	9.28	9.94
hsa-let-7i_st	9.74	9.94	9.60	9.83	9.69	10.27	9.84
hsa-miR-320c_st	9.75	10.01	9.87	9.78	9.79	9.25	9.74
hsa-miR-143_st	9.56	9.52	9.37	9.84	9.08	10.47	9.64
hsa-miR-193b_st	9.50	10.05	9.51	10.08	9.28	9.06	9.58
hsa-miR-151-5p_st	9.57	9.68	9.49	9.57	9.58	9.32	9.54
hsa-miR-99a_st	9.19	9.39	9.53	9.26	9.49	9.50	9.39
hsa-miR-214_st	9.28	9.69	9.33	9.07	9.60	8.87	9.31

hsa-miR-34a_st	9.69	9.06	9.02	9.40	8.81	9.46	9.24
hsa-miR-574-3p_st	8.90	9.73	9.27	9.42	8.92	8.83	9.18
hsa-miR-99b_st	9.22	9.13	9.11	9.34	8.92	8.84	9.09
hsa-miR-768-5p_st	8.62	8.87	8.77	9.58	8.37	8.84	8.84
hsa-miR-92a_st	9.25	9.12	8.56	8.63	9.14	8.25	8.82
hsa-miR-181a_st	9.05	9.15	8.21	8.96	8.56	8.95	8.81
hsa-miR-361-5p_st	9.26	8.85	9.03	8.51	8.48	8.57	8.78
hsa-miR-138_st	9.55	9.74	7.54	8.73	8.04	8.37	8.66
hsa-miR-93_st	9.10	9.19	8.42	8.35	8.29	7.98	8.56
hsa-miR-768-3p_st	7.94	7.85	8.82	9.02	8.36	9.24	8.54
hsa-miR-27b_st	8.45	8.57	8.63	8.46	7.60	9.41	8.52
hsa-miR-320d_st	8.44	8.69	8.73	8.51	8.34	8.32	8.51
hsa-miR-155_st	9.29	9.48	8.47	8.07	8.06	7.23	8.43
hsa-miR-409-3p_st	8.64	8.54	8.15	8.74	8.26	8.05	8.40
hsa-miR-1268_st	7.74	8.19	8.77	7.94	8.67	8.81	8.35
hsa-miR-30c_st	8.03	8.44	8.59	8.11	8.14	8.57	8.31
hsa-miR-342-3p_st	7.89	8.60	8.04	8.61	8.07	8.09	8.22
hsa-miR-423-3p_st	8.25	8.46	8.00	8.21	8.41	7.91	8.21
hsa-miR-1207-5p_st	7.65	8.48	8.49	8.05	8.37	8.17	8.20
hsa-miR-92b-star_st	7.83	7.91	8.64	7.82	8.16	8.34	8.12
hsa-miR-15b_st	7.69	8.44	8.22	8.40	8.34	7.40	8.08
hsa-miR-17_st	8.91	8.11	8.15	7.27	8.18	7.53	8.02
hsa-miR-1231_st	7.77	7.65	8.73	7.67	8.37	7.83	8.00
hsa-miR-185_st	8.35	7.91	7.64	8.04	7.72	8.33	8.00
hsa-miR-455-3p_st	8.30	8.49	8.27	7.87	7.24	7.81	8.00
hsa-miR-152_st	8.18	7.83	7.84	8.13	7.18	8.52	7.95
hsa-let-7f_st	7.61	8.07	7.80	8.20	7.34	8.42	7.91
hsa-miR-106a_st	8.65	8.05	8.02	7.15	7.88	7.34	7.85
hsa-miR-487b_st	7.89	7.82	7.48	8.36	7.46	7.94	7.82
hsa-miR-708_st	7.50	8.16	7.79	7.70	7.94	7.85	7.82
hsa-miR-134_st	7.83	8.26	7.71	8.57	7.28	7.04	7.78
hsa-miR-193a-5p_st	7.96	7.94	7.76	7.44	8.04	7.09	7.70
hsa-miR-130a_st	7.80	7.27	7.86	7.45	7.52	8.04	7.66
hsa-miR-30a_st	7.78	7.43	7.32	7.27	7.33	8.51	7.61
hsa-miR-181b_st	7.94	7.81	7.30	7.34	7.33	7.53	7.54
hsa-miR-432_st	7.57	7.87	7.57	8.22	6.72	7.30	7.54
hsa-miR-379_st	7.71	7.94	6.87	8.33	7.11	7.12	7.51
hsa-miR-1307_st	7.49	7.31	7.91	7.37	7.33	7.54	7.49
hsa-miR-10a_st	7.26	7.35	7.65	7.80	6.79	7.65	7.41
hsa-miR-20a_st	8.58	7.51	7.37	6.57	7.40	6.91	7.39
hsa-miR-106b_st	8.10	7.07	7.45	6.95	7.08	7.49	7.36
hsa-miR-140-3p_st	7.67	7.17	7.91	6.78	7.45	7.09	7.34
hsa-miR-744_st	7.10	7.17	7.47	6.97	7.90	7.00	7.27
hsa-miR-503_st	8.08	7.49	7.17	6.45	7.10	7.32	7.27
hsa-miR-19b_st	7.92	6.51	7.47	7.20	6.97	7.50	7.26
hsa-miR-21_st	7.42	7.08	6.82	7.41	6.48	8.20	7.24
hsa-miR-1280_st	6.99	7.35	6.51	6.93	8.09	7.32	7.20
hsa-miR-130b_st	7.51	7.44	7.08	7.25	7.09	6.45	7.14
hsa-miR-720_st	6.78	7.00	6.73	7.16	7.83	7.30	7.13
hsa-miR-382_st	6.95	7.38	6.88	8.07	6.53	6.96	7.13
hsa-miR-138-1-star_st	7.34	8.01	6.61	7.54	6.49	6.38	7.06

hsa-miR-425_st	7.17	7.33	7.06	7.08	6.65	7.05	7.06
hsa-miR-151-3p_st	7.12	7.24	6.92	7.28	6.85	6.93	7.05
hsa-miR-197_st	6.96	8.03	6.76	7.40	6.72	6.41	7.05
hsa-miR-210_st	6.75	7.58	6.71	6.62	7.08	7.51	7.04
hsa-miR-30d_st	6.99	7.04	6.75	7.16	6.73	7.53	7.03
hsa-miR-346_st	6.67	6.54	7.16	6.90	7.51	7.12	6.98
hsa-let-7g_st	6.98	7.18	6.77	7.36	6.23	7.21	6.96
hsa-miR-1225-5p_st	6.65	7.01	6.68	6.39	8.19	6.71	6.94
hsa-miR-30b_st	6.51	6.84	7.07	6.99	7.12	7.08	6.94
hsa-miR-886-5p_st	7.15	7.19	6.81	6.20	7.19	6.88	6.90
hsa-miR-28-5p_st	7.04	7.19	7.00	7.18	5.95	7.05	6.90
hsa-miR-25_st	6.85	7.13	6.84	7.03	6.47	6.80	6.85
hsa-miR-149_st	6.77	7.22	7.05	7.37	6.37	6.31	6.85
hsa-miR-324-3p_st	6.47	6.91	6.43	7.39	6.46	6.49	6.69
hsa-miR-132_st	6.61	7.04	6.74	6.60	6.15	6.64	6.63
hsa-miR-195_st	6.48	6.39	7.05	6.19	6.55	7.12	6.63
hsa-miR-424-star_st	6.98	7.34	6.53	6.25	6.70	5.94	6.62
hsa-miR-324-5p_st	6.87	6.86	5.85	6.99	6.51	6.57	6.61
hsa-miR-612_st	7.14	6.72	6.23	7.54	6.20	5.42	6.54
hsa-miR-1246_st	6.74	6.18	6.74	5.65	6.72	7.16	6.53
hsa-miR-502-3p_st	6.65	7.22	6.25	7.08	5.85	6.14	6.53
hsa-miR-574-5p_st	6.37	7.04	6.49	6.43	6.37	6.42	6.52
hsa-miR-423-5p_st	6.83	6.78	6.30	6.26	6.41	6.28	6.48
hsa-miR-654-3p_st	6.32	6.95	6.46	7.24	5.44	6.43	6.47
hsa-miR-885-3p_st	6.26	6.37	6.37	5.95	6.85	6.87	6.45
hsa-miR-125b-1-star_st	6.50	7.04	6.71	6.13	6.05	5.93	6.39
hsa-miR-409-5p_st	6.85	6.64	6.27	7.09	5.12	6.37	6.39
hsa-miR-337-5p_st	6.24	5.98	6.46	6.59	6.05	6.69	6.34
hsa-miR-92b_st	6.22	6.49	6.37	6.29	6.47	6.09	6.32
hsa-miR-874_st	5.99	6.04	6.29	6.38	6.52	6.70	6.32
hsa-miR-500-star_st	6.06	6.69	6.13	7.10	5.61	6.06	6.27
hsa-miR-943_st	6.04	6.00	6.46	6.18	6.42	6.21	6.22
hsa-miR-378_st	6.63	6.51	5.40	6.90	6.05	5.79	6.21
hsa-miR-493_st	6.31	6.75	5.81	6.55	5.59	6.17	6.20
hsa-miR-532-3p_st	6.20	6.61	5.80	6.48	5.74	6.25	6.18
hsa-miR-30a-star_st	6.52	6.19	6.33	6.58	5.15	6.30	6.18
hsa-miR-532-5p_st	6.48	5.80	6.14	6.58	5.90	5.98	6.15
hsa-miR-370_st	6.36	6.23	5.75	7.16	5.91	5.36	6.13
hsa-miR-28-3p_st	5.94	6.69	6.31	6.00	5.25	6.56	6.13
hsa-miR-885-5p_st	5.36	5.90	6.23	6.17	6.60	6.40	6.11
hsa-miR-1275_st	6.11	6.03	6.21	6.23	6.02	5.86	6.08
hsa-miR-1271_st	5.42	6.45	6.17	6.48	5.91	5.90	6.06
hsa-miR-362-5p_st	6.22	6.70	6.24	6.33	5.34	5.50	6.05
hsa-miR-125b-2-star_st	5.70	6.41	6.13	6.55	5.69	5.66	6.02
hsa-miR-146b-5p_st	6.04	6.38	6.69	6.10	4.93	5.88	6.00
hsa-miR-1281_st	5.85	5.84	6.04	6.11	5.36	6.77	5.99
hsa-miR-345_st	6.07	6.61	5.65	5.77	6.06	5.62	5.97
hsa-miR-339-5p_st	6.57	6.31	5.94	5.18	6.15	5.63	5.96
hsa-miR-411_st	5.89	6.10	5.71	6.61	5.17	6.12	5.94
hsa-miR-425-	5.86	5.81	6.30	5.63	5.75	6.25	5.94

star_st							
hsa-miR-335_st	5.26	5.24	5.34	6.20	7.55	6.00	5.94
hsa-miR-671-5p_st	5.99	6.33	5.86	5.61	6.10	5.69	5.93
hsa-miR-132-star_st	5.61	5.80	5.76	5.73	6.96	5.70	5.93
hsa-miR-939_st	5.25	5.35	6.61	5.88	6.09	6.32	5.92
hsa-miR-299-5p_st	5.95	6.04	6.12	6.49	5.11	5.40	5.85
hsa-miR-328_st	5.92	5.71	5.65	5.68	6.08	5.88	5.82
hsa-miR-500_st	6.42	5.98	5.77	6.02	5.07	5.59	5.81
hsa-miR-675_st	5.48	6.68	6.04	6.09	6.03	4.52	5.81
hsa-miR-376c_st	5.54	5.96	5.75	6.34	5.17	5.97	5.79
hsa-miR-181a-star_st	5.31	4.48	5.91	5.86	7.13	5.93	5.77
hsa-miR-181c-star_st	5.49	5.64	4.28	6.06	6.70	6.40	5.76
hsa-miR-191-star_st	5.76	5.51	5.81	5.83	5.72	5.91	5.76
hsa-miR-625_st	5.58	6.23	6.01	5.40	5.57	5.73	5.75
hsa-miR-1237_st	5.87	5.57	5.82	5.55	5.83	5.65	5.71
hsa-miR-18a_st	7.22	4.73	5.48	5.47	5.96	5.39	5.71
hsa-miR-15a_st	6.53	5.01	5.65	5.48	5.40	6.06	5.69
hsa-miR-501-3p_st	4.88	6.27	5.14	6.22	5.78	5.80	5.68
hsa-miR-1260_st	5.56	5.71	5.45	5.85	5.91	5.60	5.68
hsa-miR-886-3p_st	5.97	5.34	5.79	4.42	5.95	6.43	5.65
hsa-miR-665_st	5.38	5.61	5.59	6.03	5.71	5.56	5.65
hsa-miR-24-2-star_st	6.50	5.52	5.68	5.82	4.34	5.93	5.63
hsa-miR-1274b_st	4.46	5.78	5.20	5.86	6.19	6.00	5.58
hsa-miR-491-5p_st	6.13	5.38	5.35	5.50	5.81	5.31	5.58
hsa-miR-484_st	5.86	5.83	5.09	5.59	5.29	5.46	5.52
hsa-miR-596_st	5.18	4.86	5.86	5.75	5.28	6.05	5.49
hsa-miR-602_st	4.75	5.15	6.03	5.24	5.91	5.79	5.48
hsa-miR-1228_st	5.44	5.50	5.47	5.61	5.51	5.32	5.48
hsa-miR-299-3p_st	5.58	5.33	4.83	6.03	5.66	5.38	5.47
hsa-miR-296-5p_st	5.30	5.84	5.47	5.29	5.89	4.98	5.46
hsa-miR-29b-1-star_st	5.96	5.58	5.66	5.81	4.21	5.42	5.44
hsa-miR-154_st	4.53	5.36	5.60	6.52	5.01	5.61	5.44
hsa-miR-99b-star_st	5.83	5.67	5.49	5.38	5.15	5.08	5.43
hsa-miR-505-star_st	5.81	5.66	5.21	5.44	5.20	5.11	5.41
hsa-miR-146a_st	5.42	6.00	6.62	5.58	4.79	4.02	5.40
hsa-miR-490-5p_st	5.84	5.15	5.54	6.14	4.18	5.54	5.40
hsa-miR-93-star_st	5.60	5.65	5.32	5.23	5.35	5.05	5.37
hsa-miR-431_st	5.61	5.01	5.10	5.79	5.14	5.51	5.36
hsa-miR-615-5p_st	5.09	5.26	5.64	5.47	5.02	5.61	5.35
hsa-miR-572_st	4.96	4.16	6.01	5.23	5.43	6.24	5.34
hsa-miR-331-3p_st	5.27	5.66	5.29	5.11	5.21	5.43	5.33
hsa-miR-497_st	5.06	5.48	5.91	5.12	5.13	5.27	5.33
hsa-miR-199b-5p_st	5.43	5.22	5.56	5.60	4.74	5.41	5.33
hsa-miR-34c-5p_st	5.83	5.33	5.40	5.45	4.67	5.21	5.31
hsa-miR-150-star_st	5.61	5.36	5.65	5.17	4.86	5.11	5.29
hsa-miR-485-3p_st	5.07	5.45	5.34	5.68	4.78	5.33	5.28
hsa-miR-495_st	4.92	4.87	5.37	5.73	5.22	5.45	5.26
hsa-miR-485-5p_st	5.58	5.26	5.39	5.69	4.77	4.84	5.25

hsa-miR-181a-2-star_st	4.66	5.99	4.79	5.41	5.39	5.27	5.25
hsa-miR-187-star_st	5.13	4.84	5.39	5.23	5.51	5.35	5.24
hsa-miR-625-star_st	5.14	5.41	5.48	5.08	5.21	5.11	5.24
hsa-miR-933_st	4.75	4.91	5.53	5.71	5.18	5.31	5.23
hsa-miR-636_st	4.90	5.03	5.15	5.59	5.54	5.16	5.23
hsa-miR-1249_st	5.52	5.68	5.17	5.03	5.21	4.74	5.22
hsa-miR-940_st	5.72	4.97	4.65	5.24	5.64	5.10	5.22
hsa-miR-877_st	5.23	5.53	5.35	5.15	5.00	5.04	5.22
hsa-miR-1238_st	4.82	5.30	5.45	5.36	4.93	5.34	5.20
hsa-miR-543_st	5.22	5.16	5.13	5.51	4.43	5.76	5.20
hsa-miR-193a-3p_st	4.96	5.12	5.20	5.46	4.94	5.24	5.15
hsa-miR-106b-star_st	4.89	5.44	4.97	5.05	5.13	5.31	5.13
hsa-miR-22-star_st	5.28	4.77	5.25	4.95	4.69	5.71	5.11
hsa-miR-652_st	4.43	5.77	5.32	5.41	5.17	4.53	5.11
hsa-miR-1244_st	4.62	5.25	4.78	5.99	5.16	4.80	5.10
hsa-miR-1202_st	4.55	4.72	5.61	5.66	4.42	5.58	5.09
hsa-miR-654-5p_st	5.20	5.26	4.67	5.34	4.98	4.94	5.07
hsa-miR-127-5p_st	5.18	4.81	4.37	5.52	5.32	5.18	5.06
hsa-miR-129-star_st	4.24	4.53	5.02	4.85	5.72	5.97	5.06
hsa-miR-487a_st	5.22	5.36	4.32	5.19	4.76	5.42	5.04
hsa-miR-498_st	4.87	5.09	4.75	5.12	5.50	4.93	5.04
hsa-miR-329_st	4.38	4.76	5.26	6.04	4.55	5.25	5.04
hsa-miR-125a-3p_st	5.43	5.16	4.62	5.27	4.86	4.89	5.04
hsa-miR-542-5p_st	5.28	5.17	4.86	4.90	5.00	4.96	5.03
hsa-miR-576-3p_st	3.85	4.40	4.22	4.65	7.01	6.02	5.02
hsa-miR-129-3p_st	5.09	4.73	4.77	4.26	5.87	5.38	5.02
hsa-miR-34c-3p_st	5.11	5.65	4.96	4.78	4.64	4.89	5.00
hsa-miR-20b_st	5.49	5.01	5.17	4.78	4.46	5.06	5.00
hsa-miR-483-5p_st	4.78	4.91	5.14	4.73	5.01	5.39	4.99
hsa-miR-25-star_st	4.43	5.73	4.77	5.28	4.94	4.77	4.99
hsa-miR-769-5p_st	4.79	4.54	4.89	5.39	5.10	5.17	4.98
hsa-miR-1234_st	5.30	4.70	5.04	5.35	4.72	4.72	4.97
hsa-miR-381_st	5.16	4.15	4.91	5.37	4.69	5.51	4.96
hsa-miR-214-star_st	4.64	4.69	5.41	5.17	4.77	4.96	4.94
hsa-miR-935_st	4.65	4.42	5.43	5.16	4.51	5.36	4.92
hsa-miR-1227_st	4.85	5.42	4.96	5.07	4.67	4.54	4.92
hsa-miR-490-3p_st	5.07	4.64	5.11	5.42	3.85	5.39	4.91
hsa-miR-361-3p_st	5.01	4.81	4.91	5.09	4.74	4.89	4.91
hsa-miR-181d_st	4.99	4.83	4.95	4.51	4.48	5.66	4.90
hsa-miR-330-3p_st	4.50	4.79	5.17	4.94	5.00	5.02	4.90
hsa-miR-31-star_st	6.05	5.28	4.90	3.98	4.38	4.76	4.89
hsa-miR-193b-star_st	4.85	4.46	4.91	5.05	5.10	4.95	4.89
hsa-let-7d-star_st	4.49	4.62	5.03	5.24	4.99	4.84	4.87
hsa-miR-29b-2-star_st	4.96	4.62	4.94	5.38	4.13	5.08	4.85
hsa-miR-1825_st	4.67	5.00	4.63	4.96	4.82	5.00	4.85
hsa-miR-198_st	4.73	4.45	5.29	4.81	4.56	5.24	4.85
hsa-miR-377-star_st	4.48	5.01	5.04	5.69	3.98	4.86	4.84
hsa-miR-1225-	5.16	5.10	4.59	4.51	5.17	4.49	4.84

3p_st							
hsa-miR-606_st	4.19	4.45	4.38	4.46	6.00	5.31	4.80
hsa-miR-433_st	4.38	4.57	4.62	5.43	4.71	5.03	4.79
hsa-miR-373-star_st	3.95	5.27	5.64	4.86	4.15	4.88	4.79
hsa-miR-128_st	4.46	4.07	5.25	4.80	4.96	5.17	4.78
hsa-miR-637_st	4.74	4.32	4.54	5.11	4.56	5.42	4.78
hsa-miR-339-3p_st	4.85	5.32	4.69	4.35	4.20	5.23	4.77
hsa-let-7b-star_st	4.59	4.01	4.83	4.83	5.23	5.09	4.76
hsa-miR-29c_st	5.30	3.85	4.59	4.47	4.52	5.75	4.75
hsa-miR-1180_st	4.96	5.05	4.95	4.64	4.35	4.46	4.73
hsa-miR-411-star_st	4.89	4.77	4.47	4.59	4.40	5.20	4.72
hsa-miR-30e_st	4.28	3.78	4.52	4.55	5.40	5.74	4.71
hsa-miR-1301_st	5.33	4.27	4.70	4.45	4.62	4.89	4.71
hsa-miR-374a-star_st	4.02	4.57	4.08	4.64	5.94	4.98	4.70
hsa-miR-1184_st	4.28	5.17	4.68	4.80	4.75	4.51	4.70
hsa-miR-421_st	5.12	4.59	4.52	4.94	4.03	4.96	4.69
hsa-miR-376a_st	4.77	4.18	4.70	5.05	4.76	4.63	4.68
hsa-miR-1267_st	4.77	4.72	4.26	4.81	4.70	4.79	4.67
hsa-miR-181c_st	4.68	4.25	4.53	4.45	4.99	5.14	4.67
hsa-miR-34a-star_st	4.24	4.15	4.91	5.05	4.46	5.14	4.66
hsa-miR-1224-3p_st	5.03	4.43	4.48	4.61	4.95	4.44	4.66
hsa-miR-221-star_st	4.46	4.88	4.83	4.68	4.04	5.02	4.65
hsa-miR-483-3p_st	5.07	3.94	4.94	4.76	4.85	4.29	4.64
hsa-miR-1287_st	5.13	4.73	4.42	4.89	4.07	4.51	4.63
hsa-miR-877-star_st	4.72	5.00	4.42	4.73	4.41	4.42	4.62
hsa-miR-21-star_st	5.46	4.26	4.41	4.58	4.42	4.56	4.62
hsa-miR-1296_st	4.55	4.39	4.95	4.06	5.02	4.71	4.61
hsa-miR-634_st	4.49	4.37	4.37	5.00	4.88	4.54	4.61
hsa-miR-493-star_st	3.79	4.70	4.29	5.33	4.37	5.12	4.60
hsa-miR-1224-5p_st	4.79	4.45	4.17	4.49	4.55	5.06	4.59
hsa-miR-135a-star_st	4.14	4.45	4.56	4.62	4.87	4.88	4.59
hsa-miR-212_st	4.78	5.03	4.17	4.71	4.20	4.62	4.58
hsa-miR-365_st	4.25	4.09	4.49	3.98	5.44	5.24	4.58
hsa-miR-1236_st	4.75	4.75	4.41	4.55	5.01	4.02	4.58
hsa-miR-7-2-star_st	4.36	4.56	4.52	4.52	4.76	4.74	4.58
hsa-miR-194_st	4.65	4.92	4.64	4.01	4.05	5.19	4.58
hsa-miR-660_st	4.72	4.26	5.30	4.52	3.91	4.75	4.58
hsa-miR-559_st	4.40	4.40	4.14	3.99	5.44	5.08	4.58
hsa-miR-584_st	4.73	4.78	5.32	4.24	3.92	4.44	4.57
hsa-miR-664_st	4.97	4.80	4.62	4.34	4.51	4.19	4.57
hsa-miR-921_st	4.14	4.68	4.77	4.36	4.79	4.67	4.57
hsa-miR-371-5p_st	4.22	4.34	4.42	4.35	5.02	5.00	4.56
hsa-miR-27b-star_st	4.35	4.70	5.07	4.21	4.26	4.72	4.55
hsa-miR-30c-2-star_st	4.46	4.20	4.95	5.18	3.73	4.77	4.55
hsa-miR-1233_st	4.37	4.69	4.39	4.46	4.89	4.48	4.55
hsa-miR-29b_st	5.92	3.95	4.46	4.22	4.29	4.41	4.54
hsa-miR-140-5p_st	5.07	3.99	4.64	4.46	4.49	4.60	4.54

hsa-miR-659_st	4.51	4.60	4.61	4.71	4.03	4.78	4.54
hsa-miR-34b_st	4.39	3.82	4.36	5.06	4.89	4.69	4.53
hsa-miR-98_st	3.90	4.74	4.63	4.55	4.50	4.88	4.53
hsa-miR-668_st	4.85	3.91	4.73	4.54	4.40	4.73	4.52
hsa-miR-505_st	4.45	5.52	4.39	4.12	4.27	4.40	4.52
hsa-miR-1229_st	4.94	5.34	4.59	3.50	4.34	4.39	4.52
hsa-miR-501-5p_st	4.79	4.16	4.27	4.85	4.32	4.69	4.52
hsa-miR-589-star_st	4.55	4.61	4.34	5.00	4.46	4.13	4.51
hsa-miR-1300_st	4.00	4.97	4.47	4.26	4.81	4.57	4.51
hsa-miR-422a_st	4.04	5.02	4.06	5.03	4.06	4.82	4.50
hsa-miR-1288_st	4.06	4.91	4.15	4.12	4.78	4.89	4.49
hsa-miR-1181_st	3.93	4.82	4.47	4.72	4.69	4.27	4.49
hsa-miR-504_st	4.49	4.58	4.70	4.47	4.37	4.15	4.46
hsa-miR-223_st	4.62	4.54	4.47	4.34	4.46	4.33	4.46
hsa-miR-454-star_st	3.95	4.45	3.72	4.33	5.75	4.54	4.46
hsa-miR-548e_st	3.78	4.11	3.86	3.95	5.80	5.19	4.45
hsa-miR-664-star_st	3.78	4.36	4.76	4.33	4.30	5.17	4.45
hsa-miR-338-5p_st	4.54	4.73	4.28	4.33	4.48	4.26	4.44
hsa-miR-129-5p_st	4.37	5.01	4.13	3.93	4.45	4.64	4.42
hsa-miR-296-3p_st	4.44	4.44	4.62	4.29	4.25	4.45	4.42
hsa-miR-148b_st	4.41	4.17	4.44	4.43	4.16	4.88	4.42
hsa-miR-539_st	4.82	4.18	4.14	4.56	4.46	4.31	4.41
hsa-miR-595_st	4.02	4.66	4.15	4.31	4.73	4.60	4.41
hsa-miR-17-star_st	4.80	4.71	4.49	4.21	4.10	4.14	4.41
hsa-miR-548f_st	3.89	4.27	4.08	4.00	5.24	4.90	4.40
hsa-miR-1274a_st	3.70	4.51	3.99	4.61	4.54	4.99	4.39
hsa-miR-758_st	4.77	4.51	4.39	4.46	3.59	4.62	4.39
hsa-miR-766_st	4.56	4.61	3.86	4.26	4.67	4.38	4.39
hsa-miR-133a_st	4.93	4.15	4.25	4.25	4.55	4.20	4.39
hsa-miR-1247_st	4.74	4.41	4.59	4.88	3.84	3.82	4.38
hsa-miR-424_st	4.21	4.36	4.36	4.31	4.40	4.63	4.38
hsa-miR-802_st	4.49	4.27	4.29	4.33	4.84	4.03	4.38
hsa-miR-887_st	4.83	4.64	4.30	4.01	4.09	4.37	4.37
hsa-let-7f-1-star_st	4.07	4.26	4.74	4.76	3.96	4.42	4.37
hsa-miR-629_st	4.80	3.89	3.87	4.64	4.63	4.38	4.37
hsa-miR-513a-5p_st	4.76	4.16	4.11	4.29	4.49	4.36	4.36
hsa-miR-492_st	4.34	4.31	4.28	4.52	4.44	4.28	4.36
hsa-miR-769-3p_st	4.58	5.27	3.75	4.27	4.01	4.29	4.36
hsa-miR-133b_st	4.03	4.69	4.55	4.48	4.35	4.07	4.36
hsa-miR-342-5p_st	4.18	4.58	4.35	4.43	3.90	4.72	4.36
hsa-miR-563_st	4.25	5.09	4.42	3.93	4.15	4.30	4.36
hsa-miR-18b-star_st	4.17	4.49	4.43	4.29	4.69	4.03	4.35
hsa-miR-564_st	4.38	4.29	4.59	4.69	4.10	4.04	4.35
hsa-miR-1254_st	4.47	4.58	4.76	3.76	4.44	4.07	4.35
hsa-miR-486-5p_st	3.95	4.70	4.66	4.29	4.10	4.38	4.35
hsa-let-7e-star_st	4.25	4.25	4.18	4.37	4.64	4.28	4.33
hsa-miR-208a_st	3.92	3.99	4.00	4.00	5.40	4.65	4.32
hsa-miR-548c-3p_st	4.10	4.10	4.08	4.19	4.59	4.85	4.32
hsa-miR-629-star_st	4.13	4.34	4.22	4.17	4.26	4.78	4.32
hsa-miR-615-3p_st	4.40	4.04	4.39	4.80	4.31	3.92	4.31

hsa-miR-208b_st	4.22	4.13	4.30	4.07	4.56	4.58	4.31
hsa-miR-30c-1-star_st	4.16	4.11	4.17	4.43	4.29	4.63	4.30
hsa-miR-551b-star_st	4.37	4.14	4.30	4.58	4.25	4.10	4.29
hsa-miR-623_st	3.97	4.20	4.36	4.61	4.21	4.35	4.28
hsa-miR-744-star_st	4.30	4.63	4.14	4.38	4.12	4.10	4.28
hsa-miR-1183_st	4.49	4.40	4.19	4.58	3.92	4.09	4.28
hsa-miR-627_st	4.11	3.86	4.18	4.08	4.92	4.52	4.28
hsa-miR-517-star_st	4.57	4.21	4.14	3.95	4.61	4.15	4.27
hsa-miR-628-3p_st	4.05	4.08	4.58	4.17	4.02	4.73	4.27
hsa-miR-1273_st	4.59	4.36	4.09	4.27	4.14	4.16	4.27
hsa-miR-126_st	4.48	4.08	4.30	4.36	3.69	4.68	4.27
hsa-miR-888_st	3.73	4.31	3.67	3.77	5.18	4.90	4.26
hsa-miR-557_st	3.55	3.77	4.54	4.69	4.73	4.28	4.26
hsa-miR-550-star_st	4.26	4.34	4.28	4.32	3.98	4.38	4.26
hsa-miR-326_st	4.02	4.22	4.54	4.28	4.06	4.43	4.26
hsa-miR-1285_st	4.02	4.37	4.43	4.34	3.75	4.62	4.26
hsa-miR-518b_st	4.45	4.50	4.09	4.49	3.90	4.11	4.26
hsa-miR-27a-star_st	4.29	4.17	4.56	4.66	4.08	3.75	4.25
hsa-miR-938_st	4.22	4.74	4.11	4.16	4.22	4.05	4.25
hsa-miR-26b_st	4.32	4.40	4.19	4.61	3.68	4.23	4.24
hsa-miR-374b_st	3.95	4.32	4.36	4.33	4.21	4.26	4.24
hsa-miR-1293_st	4.33	3.79	4.31	4.06	4.55	4.40	4.24
hsa-miR-143-star_st	3.50	4.95	3.98	4.79	3.51	4.67	4.23
hsa-miR-641_st	4.28	4.49	4.15	4.35	4.03	4.10	4.23
hsa-miR-1303_st	3.82	4.26	3.75	4.38	4.80	4.38	4.23
hsa-miR-633_st	4.38	4.18	4.11	4.07	4.66	3.97	4.23
hsa-miR-30e-star_st	3.89	3.81	4.02	4.99	3.90	4.74	4.22
hsa-miR-23b-star_st	4.48	4.14	4.09	3.93	3.96	4.76	4.22
hsa-miR-10b_st	4.15	3.88	4.48	4.25	4.19	4.40	4.22
hsa-miR-188-5p_st	4.31	4.30	3.90	4.34	4.24	4.24	4.22
hsa-miR-323-3p_st	3.83	4.63	3.61	4.47	4.37	4.37	4.21
hsa-miR-605_st	4.42	4.10	4.00	4.58	4.22	3.92	4.21
hsa-miR-1255a_st	3.95	3.94	4.06	4.06	4.94	4.27	4.20
hsa-miR-548p_st	4.22	3.91	4.28	4.22	4.57	4.03	4.20
hsa-miR-10a-star_st	4.05	3.93	4.23	4.60	3.89	4.50	4.20
hsa-miR-220a_st	4.31	4.26	3.91	4.03	4.44	4.22	4.20
hsa-miR-1272_st	4.15	4.26	4.28	4.25	4.16	4.07	4.19
hsa-miR-582-3p_st	4.32	4.15	4.29	4.25	4.07	4.08	4.19
hsa-miR-1290_st	3.85	4.14	4.13	3.95	4.13	4.95	4.19
hsa-miR-337-3p_st	3.86	4.66	4.16	4.24	3.95	4.29	4.19
hsa-miR-148a_st	4.19	4.07	4.07	3.68	4.66	4.46	4.19
hsa-miR-130b-star_st	4.41	3.92	4.35	3.95	4.26	4.23	4.19
hsa-miR-513b_st	4.05	3.78	4.79	4.30	4.10	4.09	4.19
hsa-miR-378-star_st	4.68	4.17	3.97	4.24	3.86	4.20	4.19
hsa-miR-219-1-3p_st	4.16	4.68	3.92	4.19	3.75	4.42	4.19
hsa-miR-195-star_st	4.04	4.30	4.30	4.19	4.32	3.94	4.18

hsa-miR-1323_st	4.12	4.63	3.95	4.11	4.11	4.16	4.18
hsa-miR-489_st	4.31	4.28	4.06	4.41	4.09	3.92	4.18
hsa-miR-541-star_st	3.65	3.82	4.67	4.42	4.03	4.47	4.18
hsa-miR-29c-star_st	4.13	4.45	4.44	4.11	3.88	4.01	4.17
hsa-miR-583_st	4.57	3.93	3.97	4.31	4.15	4.09	4.17
hsa-miR-1262_st	4.13	4.08	4.16	4.14	4.34	4.13	4.16
hsa-miR-1258_st	3.95	4.18	4.11	4.43	4.11	4.20	4.16
hsa-miR-454_st	4.35	3.96	3.94	4.01	4.26	4.46	4.16
hsa-miR-626_st	4.15	4.52	4.08	3.99	4.06	4.17	4.16
hsa-miR-1208_st	3.76	4.38	4.15	4.18	4.63	3.87	4.16
hsa-miR-196a-star_st	4.48	4.02	3.73	4.18	4.22	4.31	4.16
hsa-miR-635_st	4.66	4.08	4.14	4.36	3.78	3.91	4.16
hsa-miR-765_st	4.21	3.94	4.57	3.98	4.05	4.18	4.15
hsa-miR-224_st	4.30	4.21	4.05	4.06	4.21	4.08	4.15
hsa-miR-137_st	4.37	3.93	3.83	4.16	4.24	4.35	4.15
hsa-miR-222-star_st	3.90	4.29	4.20	4.11	4.00	4.38	4.15
hsa-miR-506_st	4.23	4.04	4.40	3.60	4.11	4.48	4.14
hsa-miR-335-star_st	4.13	3.85	4.25	4.34	4.04	4.23	4.14
hsa-miR-920_st	3.83	4.13	4.51	3.92	4.26	4.19	4.14
hsa-miR-671-3p_st	4.60	4.38	3.83	3.95	4.35	3.71	4.14
hsa-miR-204_st	4.02	4.13	4.18	4.11	4.24	4.13	4.13
hsa-miR-520b_st	4.20	4.49	4.32	4.49	3.38	3.93	4.13
hsa-miR-508-3p_st	3.93	4.29	4.26	4.00	4.29	4.02	4.13
hsa-miR-452-star_st	3.98	4.00	4.14	4.01	4.55	4.06	4.12
hsa-miR-889_st	3.54	3.90	4.07	4.11	4.63	4.49	4.12
hsa-miR-1204_st	3.89	3.84	4.14	4.31	4.15	4.40	4.12
hsa-miR-620_st	3.90	4.07	4.25	4.03	4.28	4.19	4.12
hsa-miR-371-3p_st	3.94	3.95	4.07	4.26	4.81	3.68	4.12
hsa-miR-455-5p_st	4.79	3.54	4.30	3.97	4.10	4.01	4.12
hsa-miR-567_st	4.17	4.21	4.01	4.54	3.92	3.85	4.12
hsa-miR-19a_st	4.17	4.06	4.18	4.01	4.12	4.16	4.12
hsa-miR-122-star_st	4.14	4.05	4.11	4.10	4.16	4.14	4.12
hsa-miR-154-star_st	4.13	3.95	4.07	4.03	3.78	4.72	4.11
hsa-miR-183-star_st	4.05	4.00	4.11	4.31	4.12	4.09	4.11
hsa-miR-622_st	3.54	3.72	4.02	4.36	4.72	4.30	4.11
hsa-miR-1291_st	3.90	3.64	4.35	4.20	4.94	3.63	4.11
hsa-miR-656_st	4.10	3.98	4.01	4.17	4.33	4.07	4.11
hsa-miR-1257_st	4.60	4.28	3.81	3.96	4.03	3.99	4.11
hsa-miR-92a-2-star_st	4.03	3.92	4.09	3.99	4.14	4.46	4.11
hsa-miR-558_st	3.64	4.47	3.94	4.03	4.32	4.23	4.11
hsa-miR-7-1-star_st	4.25	3.97	4.15	3.97	4.13	4.15	4.10
hsa-miR-363_st	3.88	4.07	3.78	3.87	4.62	4.40	4.10
hsa-miR-452_st	4.36	4.08	4.29	4.10	3.87	3.89	4.10
hsa-miR-1252_st	4.38	4.15	4.22	4.00	3.87	3.97	4.10
hsa-miR-598_st	4.35	4.12	4.01	4.27	3.72	4.12	4.10
hsa-miR-561_st	4.01	4.40	4.27	4.16	3.65	4.09	4.10
hsa-miR-1226_st	3.81	4.31	3.91	4.20	4.36	3.97	4.09
hsa-miR-519d_st	4.08	4.57	4.09	4.21	3.91	3.70	4.09

hsa-miR-760_st	3.91	4.21	3.90	4.28	4.06	4.18	4.09
hsa-miR-650_st	3.91	3.63	4.50	4.03	4.43	4.02	4.09
hsa-miR-9-star_st	3.87	4.26	4.06	4.06	4.12	4.14	4.09
hsa-miR-200c_st	4.23	4.17	3.89	4.15	4.05	4.01	4.08
hsa-miR-34b-star_st	4.15	3.91	4.01	4.09	3.91	4.43	4.08
hsa-miR-205_st	4.28	3.86	3.94	4.08	4.65	3.67	4.08
hsa-miR-552_st	4.35	3.90	4.15	4.20	4.15	3.71	4.08
hsa-miR-369-5p_st	3.95	4.10	4.20	4.47	3.46	4.29	4.08
hsa-miR-624-star_st	4.04	3.97	3.98	4.05	4.51	3.90	4.08
hsa-miR-379-star_st	3.90	3.84	4.24	4.06	4.28	4.13	4.07
hsa-miR-1298_st	4.36	3.79	4.03	4.27	3.90	4.09	4.07
hsa-miR-192_st	4.05	4.15	3.82	3.98	4.43	3.99	4.07
hsa-miR-1263_st	3.72	4.09	4.46	3.89	4.13	4.12	4.07
hsa-miR-575_st	3.74	4.19	4.19	3.83	3.97	4.46	4.07
hsa-miR-18b_st	4.36	3.89	3.57	4.35	4.02	4.21	4.07
hsa-miR-767-3p_st	4.10	4.18	3.98	4.01	3.93	4.18	4.06
hsa-miR-593_st	3.89	4.21	3.86	4.19	3.99	4.23	4.06
hsa-miR-410_st	3.72	3.82	4.31	4.30	3.95	4.27	4.06
hsa-miR-33a-star_st	4.66	4.10	3.94	4.26	3.52	3.89	4.06
hsa-miR-618_st	3.91	3.92	4.21	4.32	4.15	3.85	4.06
hsa-miR-362-3p_st	3.78	3.82	3.96	4.21	4.28	4.30	4.06
hsa-let-7c-star_st	4.16	4.10	3.88	3.93	4.28	3.98	4.05
hsa-miR-550_st	4.35	3.65	3.97	3.66	4.21	4.46	4.05
hsa-miR-325_st	3.91	3.94	4.01	4.36	3.92	4.15	4.05
hsa-miR-99a-star_st	3.87	3.89	3.99	4.66	3.80	4.08	4.05
hsa-miR-32-star_st	4.30	4.18	3.84	4.09	3.63	4.21	4.04
hsa-miR-520d-3p_st	3.80	4.74	3.88	3.88	3.85	4.10	4.04
hsa-miR-218-1-star_st	4.53	3.87	4.07	4.03	3.76	4.00	4.04
hsa-miR-1255b_st	4.19	3.89	3.45	3.93	4.66	4.12	4.04
hsa-miR-591_st	3.96	3.97	4.19	3.90	4.23	3.97	4.04
hsa-miR-941_st	4.20	4.48	4.12	4.05	4.05	3.32	4.03
hsa-miR-377_st	3.82	3.92	4.28	4.05	4.09	4.06	4.03
hsa-miR-219-2-3p_st	4.07	4.12	4.15	3.86	4.06	3.92	4.03
hsa-miR-1_st	4.10	4.47	3.94	3.95	3.65	4.08	4.03
hsa-miR-203_st	3.89	4.08	3.85	4.15	4.32	3.91	4.03
hsa-miR-211_st	4.10	3.82	4.49	3.84	4.12	3.81	4.03
hsa-miR-657_st	3.88	4.31	4.08	4.14	3.83	3.93	4.03
hsa-miR-1284_st	3.99	3.78	3.75	4.24	4.18	4.22	4.03
hsa-miR-548b-3p_st	4.13	4.06	4.08	4.01	4.06	3.84	4.03
hsa-miR-101_st	3.91	4.38	4.09	3.68	4.14	3.94	4.02
hsa-miR-330-5p_st	3.81	4.70	4.21	3.86	3.46	4.08	4.02
hsa-miR-491-3p_st	4.11	3.82	4.08	3.83	4.18	4.08	4.02
hsa-miR-520h_st	3.95	4.18	3.80	4.21	3.92	4.07	4.02
hsa-miR-215_st	3.96	3.77	3.82	3.83	4.44	4.29	4.02
hsa-miR-631_st	3.92	3.76	4.38	3.63	4.45	3.96	4.02
hsa-miR-577_st	3.73	3.93	4.36	4.03	4.04	3.99	4.02
hsa-miR-194-star_st	3.85	3.72	4.24	4.06	4.36	3.84	4.01
hsa-miR-548d-3p_st	3.65	3.73	3.92	4.36	4.32	4.07	4.01

hsa-miR-1245_st	3.71	3.93	4.12	4.35	3.91	4.03	4.01
hsa-miR-944_st	4.45	4.13	3.85	4.19	3.82	3.61	4.01
hsa-miR-579_st	4.30	3.67	3.96	3.89	4.28	3.93	4.01
hsa-miR-542-3p_st	4.16	3.68	4.27	3.93	3.88	4.11	4.01
hsa-miR-497-star_st	4.02	3.68	3.84	3.94	4.50	4.05	4.01
hsa-miR-628-5p_st	4.15	3.90	4.06	4.11	3.67	4.11	4.00
hsa-miR-298_st	3.85	4.47	4.32	3.55	3.89	3.91	4.00
hsa-miR-182_st	4.21	3.99	3.76	3.96	3.96	4.12	4.00
hsa-miR-300_st	3.89	4.27	4.12	3.81	4.00	3.91	4.00
hsa-miR-200c-star_st	3.58	4.50	4.00	4.34	3.95	3.62	4.00
hsa-miR-616-star_st	3.53	4.08	4.06	4.07	4.55	3.69	4.00
hsa-miR-1226-star_st	4.04	4.14	4.80	3.01	3.83	4.16	4.00
hsa-miR-621_st	3.95	3.88	3.83	3.93	4.17	4.23	4.00
hsa-miR-135b-star_st	4.05	4.29	3.80	4.03	3.87	3.94	4.00
hsa-miR-553_st	4.01	3.82	4.03	3.68	4.25	4.14	3.99
hsa-miR-1827_st	3.73	3.73	4.14	3.88	4.45	4.00	3.99
hsa-miR-155-star_st	3.88	3.98	3.97	4.18	4.13	3.78	3.99
hsa-miR-380-star_st	4.12	3.89	4.11	4.04	3.75	4.00	3.99
hsa-miR-643_st	4.21	4.10	4.35	3.98	3.56	3.72	3.99
hsa-miR-1324_st	4.29	3.98	3.74	4.06	3.80	4.05	3.99
hsa-miR-508-5p_st	3.77	3.90	4.26	4.05	4.09	3.84	3.99
hsa-miR-142-3p_st	3.89	4.04	3.82	4.21	4.06	3.89	3.99
hsa-miR-432-star_st	3.85	4.03	3.63	3.90	4.23	4.26	3.98
hsa-miR-1305_st	3.89	4.22	3.63	4.16	4.07	3.94	3.98
hsa-miR-124_st	3.99	4.31	3.93	3.81	3.98	3.88	3.98
hsa-miR-548j_st	3.84	3.94	4.24	3.95	3.93	4.00	3.98
hsa-miR-607_st	3.94	4.36	3.66	4.03	4.02	3.89	3.98
hsa-miR-548i_st	4.23	4.13	3.85	3.72	4.10	3.85	3.98
hsa-miR-630_st	3.99	3.99	4.06	3.86	4.07	3.91	3.98
hsa-miR-340_st	3.92	4.10	3.84	4.18	3.83	4.01	3.98
hsa-miR-206_st	4.10	4.08	3.96	4.03	3.90	3.81	3.98
hsa-miR-600_st	3.97	3.84	4.09	3.86	4.36	3.76	3.98
hsa-miR-891b_st	4.05	4.04	3.97	3.92	3.94	3.95	3.98
hsa-miR-186-star_st	4.01	4.09	3.92	4.03	3.90	3.91	3.98
hsa-let-7i-star_st	3.59	4.49	3.97	3.92	3.68	4.22	3.98
hsa-miR-15a-star_st	3.50	3.89	3.94	4.17	4.10	4.25	3.98
hsa-miR-135a_st	3.92	3.86	4.24	3.92	3.79	4.11	3.98
hsa-miR-891a_st	3.72	3.69	4.05	4.59	4.00	3.80	3.97
hsa-miR-548a-5p_st	3.84	4.03	3.81	4.29	3.87	4.00	3.97
hsa-miR-1253_st	4.34	3.88	3.72	4.10	3.84	3.96	3.97
hsa-miR-518f-star_st	4.21	3.96	4.06	3.75	3.90	3.95	3.97
hsa-miR-412_st	3.76	3.78	4.35	3.99	3.86	4.10	3.97
hsa-miR-651_st	3.82	4.20	3.76	4.06	3.88	4.10	3.97
hsa-miR-569_st	3.89	4.08	3.83	4.13	3.80	4.10	3.97
hsa-miR-589_st	4.05	4.36	3.69	3.92	3.99	3.81	3.97
hsa-miR-30b-star_st	4.04	3.73	3.89	3.86	4.17	4.09	3.96
hsa-miR-26a-2-	3.71	4.56	3.72	4.03	3.86	3.90	3.96

star_st							
hsa-miR-548g_st	3.93	3.73	4.02	4.06	4.01	4.02	3.96
hsa-miR-590-3p_st	3.97	3.92	3.90	3.92	4.11	3.94	3.96
hsa-miR-186_st	4.06	4.05	3.94	3.87	3.95	3.87	3.96
hsa-miR-302b-star_st	3.78	4.13	3.93	4.11	3.74	4.06	3.96
hsa-miR-302f_st	3.98	4.02	3.68	4.46	3.68	3.92	3.96
hsa-miR-16-2-star_st	3.87	3.81	4.34	3.83	3.93	3.95	3.96
hsa-miR-551a_st	3.74	3.84	3.74	4.14	4.38	3.88	3.96
hsa-miR-545-star_st	3.85	4.16	4.38	3.80	3.62	3.92	3.95
hsa-miR-549_st	4.03	4.00	4.15	4.06	3.61	3.85	3.95
hsa-miR-1182_st	4.05	4.08	4.42	3.69	3.59	3.88	3.95
hsa-miR-548n_st	3.98	4.27	4.02	3.82	3.80	3.81	3.95
hsa-miR-372_st	4.15	3.89	4.00	3.98	3.78	3.90	3.95
hsa-miR-1299_st	3.96	4.00	3.83	3.82	3.95	4.13	3.95
hsa-miR-202_st	3.72	3.76	4.04	4.30	3.78	4.10	3.95
hsa-miR-376a-star_st	4.07	4.01	3.99	4.05	3.67	3.90	3.95
hsa-miR-188-3p_st	3.99	3.95	4.23	4.17	3.58	3.77	3.95
hsa-miR-519b-3p_st	3.94	3.78	4.00	4.27	3.80	3.90	3.95
hsa-miR-376b_st	3.58	3.99	3.75	3.98	4.15	4.23	3.95
hsa-miR-520a-3p_st	3.90	4.13	4.07	4.00	3.84	3.74	3.95
hsa-miR-541_st	3.67	3.73	4.14	4.35	4.06	3.74	3.95
hsa-miR-936_st	3.69	4.01	4.18	3.95	4.25	3.59	3.95
hsa-miR-1201_st	3.91	3.90	3.94	3.72	4.10	4.10	3.94
hsa-miR-429_st	4.21	3.93	3.97	3.96	3.85	3.75	3.94
hsa-miR-524-5p_st	3.98	3.94	3.91	3.72	3.98	4.13	3.94
hsa-miR-515-5p_st	3.90	4.34	3.61	3.76	4.45	3.60	3.94
hsa-miR-640_st	3.70	3.64	4.14	4.17	3.78	4.23	3.94
hsa-miR-521_st	3.89	3.90	4.26	3.77	3.91	3.92	3.94
hsa-miR-1264_st	4.27	4.12	4.18	3.82	3.71	3.55	3.94
hsa-miR-509-3-5p_st	4.18	4.07	4.35	3.58	3.88	3.59	3.94
hsa-miR-617_st	3.89	3.88	4.06	3.80	3.93	4.09	3.94
hsa-miR-597_st	4.08	4.03	3.93	3.78	4.03	3.80	3.94
hsa-miR-518e_st	4.20	3.83	3.89	3.97	3.90	3.85	3.94
hsa-miR-301a_st	4.06	3.94	3.67	4.26	3.90	3.80	3.94
hsa-miR-20b-star_st	3.91	4.04	3.82	3.89	3.61	4.36	3.94
hsa-miR-200b_st	3.86	4.09	3.72	3.95	4.25	3.75	3.93
hsa-miR-182-star_st	4.09	4.03	3.77	4.18	3.86	3.66	3.93
hsa-miR-548l_st	4.14	3.91	3.91	3.89	4.06	3.68	3.93
hsa-miR-548c-5p_st	3.99	3.93	3.99	4.12	3.92	3.65	3.93
hsa-miR-568_st	4.08	3.91	4.04	4.05	3.65	3.85	3.93
hsa-miR-374a_st	3.92	3.85	4.06	3.75	3.66	4.34	3.93
hsa-miR-555_st	3.84	3.87	3.72	4.15	3.90	4.09	3.93
hsa-miR-653_st	4.24	3.82	3.72	3.78	4.09	3.94	3.93
hsa-miR-453_st	3.88	4.29	3.93	3.84	3.56	4.07	3.93
hsa-miR-144_st	3.71	3.87	4.09	3.97	4.00	3.94	3.93
hsa-miR-384_st	3.78	3.89	3.92	4.11	3.98	3.88	3.93
hsa-miR-586_st	3.99	3.83	3.77	4.20	3.88	3.89	3.93
hsa-miR-520g_st	4.03	3.86	4.00	4.14	3.67	3.84	3.92

hsa-miR-185-star_st	3.79	3.48	4.24	4.63	3.71	3.69	3.92
hsa-miR-578_st	3.73	4.44	3.85	3.73	3.79	4.01	3.92
hsa-miR-624_st	3.66	4.06	4.09	3.93	4.05	3.74	3.92
hsa-miR-380_st	3.86	4.12	3.85	3.88	3.84	3.97	3.92
hsa-miR-1270_st	3.79	3.88	4.03	3.96	3.99	3.85	3.92
hsa-miR-1259_st	3.80	3.83	4.04	4.08	3.83	3.93	3.92
hsa-miR-527_st	4.27	3.85	3.94	3.89	3.86	3.70	3.92
hsa-miR-1278_st	3.69	3.88	3.81	3.99	3.98	4.14	3.92
hsa-miR-1294_st	4.43	3.94	3.68	3.76	4.03	3.64	3.91
hsa-miR-488-star_st	4.10	4.15	3.72	3.71	3.89	3.92	3.91
hsa-miR-708-star_st	3.88	4.04	3.85	3.70	3.96	4.04	3.91
hsa-miR-450b-5p_st	3.97	4.12	3.88	3.90	3.75	3.84	3.91
hsa-miR-369-3p_st	3.91	3.80	4.06	4.08	3.85	3.76	3.91
hsa-miR-92a-1-star_st	3.65	4.26	3.92	3.78	4.04	3.82	3.91
hsa-miR-875-5p_st	4.00	3.73	3.85	4.07	3.87	3.94	3.91
hsa-miR-183_st	3.92	4.11	4.03	4.06	3.79	3.56	3.91
hsa-miR-1286_st	3.77	4.31	3.94	3.85	4.11	3.48	3.91
hsa-miR-220c_st	3.82	3.94	3.91	4.27	3.64	3.87	3.91
hsa-miR-1277_st	3.94	3.78	4.02	3.96	3.77	3.98	3.91
hsa-miR-23a-star_st	3.99	3.79	3.35	4.16	4.08	4.08	3.91
hsa-miR-513a-3p_st	3.96	3.88	4.02	3.82	3.89	3.87	3.91
hsa-miR-145-star_st	3.97	4.08	3.91	3.65	4.02	3.82	3.91
hsa-miR-142-5p_st	3.80	4.10	3.80	3.89	3.85	3.99	3.91
hsa-miR-1250_st	4.00	3.94	3.73	3.80	3.90	4.06	3.91
hsa-miR-934_st	3.97	4.00	3.90	3.80	4.02	3.73	3.90
hsa-miR-16-1-star_st	4.65	3.79	3.56	3.64	3.79	3.98	3.90
hsa-miR-302d-star_st	4.18	3.59	3.73	4.00	4.15	3.78	3.90
hsa-miR-517a_st	4.10	3.90	3.89	3.83	3.77	3.92	3.90
hsa-miR-518d-5p_st	3.89	4.09	4.12	3.64	3.92	3.75	3.90
hsa-miR-519e_st	3.81	4.01	4.13	3.78	3.81	3.87	3.90
hsa-miR-1266_st	3.83	3.92	3.99	4.32	3.82	3.52	3.90
hsa-miR-374b-star_st	4.03	4.02	3.68	3.72	3.74	4.20	3.90
hsa-miR-548h_st	3.78	4.03	3.79	3.87	4.33	3.59	3.90
hsa-miR-192-star_st	3.64	4.15	3.60	3.77	4.17	4.07	3.90
hsa-miR-520c-5p_st	3.90	4.24	4.06	4.04	3.59	3.56	3.90
hsa-miR-509-5p_st	3.79	3.88	3.98	3.77	3.89	4.07	3.90
hsa-miR-518a-5p_st	3.84	3.99	3.97	3.79	4.05	3.72	3.90
hsa-miR-184_st	3.95	3.80	3.88	3.83	3.82	4.10	3.90
hsa-miR-587_st	4.09	4.08	3.91	3.86	3.80	3.62	3.90
hsa-miR-141_st	3.74	3.98	3.87	3.87	3.98	3.93	3.89
hsa-miR-302a-star_st	3.78	3.92	4.10	4.03	3.75	3.78	3.89
hsa-miR-7_st	3.82	3.77	3.84	4.00	4.07	3.84	3.89
hsa-miR-1292_st	3.53	4.85	3.08	2.99	3.85	5.06	3.89
hsa-miR-1251_st	3.82	3.77	3.91	4.21	3.68	3.95	3.89
hsa-miR-216b_st	3.84	4.10	3.78	3.91	3.41	4.30	3.89

hsa-miR-19b-2-star_st	4.03	3.85	3.68	3.99	4.02	3.75	3.89
hsa-miR-18a-star_st	3.22	4.58	3.90	3.90	3.72	4.01	3.89
hsa-miR-590-5p_st	3.72	3.92	4.24	3.82	3.95	3.67	3.89
hsa-miR-431-star_st	4.14	3.62	4.10	4.30	3.61	3.54	3.88
hsa-miR-570_st	3.81	4.09	3.76	4.05	3.78	3.83	3.88
hsa-miR-585_st	3.91	3.88	3.79	3.84	4.11	3.77	3.88
hsa-miR-499-3p_st	3.97	3.79	3.82	4.10	3.72	3.89	3.88
hsa-miR-105-star_st	4.42	3.70	3.79	3.50	3.85	4.01	3.88
hsa-miR-218-2-star_st	4.06	4.24	3.81	3.57	3.72	3.88	3.88
hsa-miR-616_st	3.69	3.90	3.99	3.83	3.93	3.93	3.88
hsa-miR-580_st	3.78	3.99	3.97	3.88	3.77	3.87	3.88
hsa-miR-502-5p_st	3.66	3.74	4.14	3.82	3.75	4.15	3.88
hsa-miR-514_st	3.86	4.17	3.68	4.04	3.98	3.53	3.88
hsa-miR-218_st	4.05	3.73	3.77	3.66	4.07	3.98	3.88
hsa-miR-301b_st	3.90	3.91	4.18	3.49	4.09	3.68	3.87
hsa-miR-516a-5p_st	3.97	4.37	3.51	3.67	3.92	3.81	3.87
hsa-miR-95_st	3.89	3.64	3.88	3.91	4.27	3.64	3.87
hsa-miR-331-5p_st	3.76	3.93	3.76	3.86	3.95	3.97	3.87
hsa-miR-1302_st	3.67	4.10	3.58	4.02	3.74	4.12	3.87
hsa-miR-144-star_st	3.83	3.69	3.99	3.83	3.94	3.95	3.87
hsa-miR-613_st	3.75	3.95	3.95	3.80	4.00	3.77	3.87
hsa-miR-1276_st	3.81	3.87	3.92	3.80	3.90	3.93	3.87
hsa-miR-876-5p_st	3.95	3.87	4.15	3.97	3.74	3.53	3.87
hsa-miR-19b-1-star_st	3.90	3.74	3.93	3.83	3.85	3.96	3.87
hsa-miR-20a-star_st	3.88	3.73	3.82	3.94	3.98	3.85	3.87
hsa-miR-302c-star_st	3.62	4.02	3.93	3.83	3.98	3.82	3.87
hsa-miR-105_st	3.89	4.00	3.97	3.93	3.60	3.81	3.87
hsa-miR-1185_st	3.81	3.97	3.80	4.04	3.78	3.81	3.87
hsa-miR-1261_st	3.70	3.92	3.70	3.92	3.84	4.12	3.87
hsa-miR-1265_st	4.23	3.60	3.84	3.75	3.86	3.92	3.87
hsa-miR-609_st	3.63	3.72	3.92	4.06	4.24	3.62	3.87
hsa-miR-576-5p_st	3.84	4.08	3.92	3.76	3.80	3.79	3.86
hsa-miR-554_st	3.99	3.86	3.69	3.90	3.90	3.86	3.86
hsa-miR-522_st	3.78	3.84	3.84	3.94	3.96	3.82	3.86
hsa-miR-29a-star_st	3.87	3.85	3.96	3.93	3.85	3.72	3.86
hsa-miR-367-star_st	3.81	4.00	3.89	4.00	3.65	3.83	3.86
hsa-miR-126-star_st	3.79	4.08	3.76	3.98	3.90	3.66	3.86
hsa-miR-1248_st	3.78	3.95	4.19	3.70	3.78	3.77	3.86
hsa-miR-1297_st	3.78	3.84	3.93	3.78	3.76	4.09	3.86
hsa-miR-1279_st	3.97	3.51	4.09	4.08	3.79	3.73	3.86
hsa-miR-582-5p_st	4.10	3.79	3.93	3.87	3.76	3.72	3.86
hsa-miR-770-5p_st	3.63	3.36	3.90	4.43	3.94	3.91	3.86
hsa-miR-153_st	3.86	4.04	3.54	3.71	3.84	4.16	3.86
hsa-miR-383_st	3.83	3.79	4.09	3.93	3.90	3.61	3.86
hsa-miR-648_st	3.90	3.90	3.58	3.72	4.10	3.95	3.86
hsa-miR-1206_st	3.82	3.91	3.77	3.75	4.07	3.83	3.86
hsa-miR-518c-	3.61	3.73	4.28	3.66	3.99	3.86	3.85

star_st							
hsa-miR-1283_st	3.87	3.94	4.04	3.97	3.75	3.56	3.85
hsa-miR-556-5p_st	3.71	3.70	3.94	3.99	4.05	3.74	3.85
hsa-miR-135b_st	3.91	3.85	3.77	3.66	3.90	4.02	3.85
hsa-miR-1197_st	4.35	3.58	3.87	3.92	3.82	3.57	3.85
hsa-miR-610_st	3.97	3.91	3.74	3.94	3.95	3.60	3.85
hsa-let-7a-star_st	3.93	3.87	3.86	3.91	3.65	3.90	3.85
hsa-miR-512-5p_st	3.79	3.98	3.74	3.60	4.06	3.93	3.85
hsa-miR-525-3p_st	3.69	3.87	4.06	3.94	3.60	3.96	3.85
hsa-miR-876-3p_st	3.63	3.91	3.77	4.03	3.87	3.88	3.85
hsa-miR-513c_st	3.78	3.84	4.16	3.75	3.94	3.61	3.85
hsa-miR-190b_st	3.95	3.68	3.94	3.66	3.97	3.88	3.85
hsa-miR-200a-star_st	3.60	4.55	3.82	3.87	3.59	3.66	3.85
hsa-miR-655_st	3.87	3.87	3.78	3.83	4.01	3.72	3.85
hsa-miR-190_st	4.10	3.82	3.67	3.90	3.86	3.74	3.85
hsa-miR-875-3p_st	3.77	3.62	3.98	4.08	3.80	3.82	3.85
hsa-miR-122_st	3.89	3.71	3.82	3.88	3.94	3.81	3.84
hsa-miR-1306_st	3.76	4.16	3.70	3.96	3.53	3.95	3.84
hsa-miR-146a-star_st	3.82	3.98	3.76	3.70	3.73	4.07	3.84
hsa-miR-486-3p_st	3.69	3.62	4.10	3.72	4.14	3.78	3.84
hsa-miR-922_st	3.94	4.02	3.91	3.77	3.61	3.81	3.84
hsa-miR-1321_st	3.68	4.20	3.60	3.80	3.92	3.84	3.84
hsa-miR-649_st	3.84	3.81	3.97	3.79	3.75	3.86	3.84
hsa-miR-511_st	3.93	3.69	3.88	3.87	3.98	3.67	3.84
hsa-miR-26b-star_st	3.63	3.99	3.90	4.11	3.66	3.73	3.84
hsa-miR-220b_st	3.53	3.75	4.01	4.27	3.57	3.88	3.84
hsa-miR-518a-3p_st	3.98	4.02	3.79	3.79	3.72	3.71	3.84
hsa-let-7g-star_st	3.92	3.81	3.97	3.59	3.59	4.13	3.83
hsa-miR-297_st	3.85	3.88	3.94	3.77	3.70	3.86	3.83
hsa-miR-517b_st	3.67	4.04	3.73	3.80	3.94	3.80	3.83
hsa-miR-488_st	3.99	3.57	3.64	3.82	4.21	3.76	3.83
hsa-miR-647_st	4.10	3.84	3.85	3.76	3.47	3.98	3.83
hsa-miR-520e_st	4.03	3.72	3.82	4.05	3.65	3.72	3.83
hsa-miR-496_st	4.03	3.78	3.79	3.80	3.65	3.93	3.83
hsa-miR-138-2-star_st	3.81	4.03	3.54	3.86	4.04	3.71	3.83
hsa-miR-373_st	3.72	3.87	3.74	3.90	3.84	3.91	3.83
hsa-miR-302a_st	4.26	3.55	3.94	3.84	3.92	3.46	3.83
hsa-miR-139-5p_st	3.75	4.09	3.92	3.88	3.88	3.44	3.83
hsa-miR-632_st	4.12	3.80	3.86	3.58	3.84	3.76	3.83
hsa-miR-767-5p_st	3.79	3.79	4.06	3.89	3.72	3.71	3.83
hsa-miR-1207-3p_st	3.74	3.74	3.55	4.01	4.04	3.89	3.83
hsa-miR-556-3p_st	3.90	3.89	3.67	3.78	3.75	3.97	3.83
hsa-miR-32_st	4.07	3.79	3.68	3.74	3.92	3.75	3.82
hsa-miR-1282_st	3.65	4.07	3.77	3.88	3.81	3.76	3.82
hsa-miR-451_st	3.92	3.92	3.68	4.00	3.88	3.54	3.82
hsa-miR-545_st	3.45	4.10	3.86	3.90	3.87	3.76	3.82
hsa-miR-139-3p_st	3.47	3.89	3.72	3.83	4.33	3.68	3.82
hsa-miR-96_st	4.01	3.79	3.88	3.77	3.71	3.75	3.82
hsa-miR-520c-3p_st	4.05	3.86	3.94	3.63	3.61	3.83	3.82
hsa-miR-136-	3.80	3.84	3.72	4.02	3.91	3.61	3.82

star_st							
hsa-miR-544_st	3.71	3.86	3.75	3.80	3.90	3.88	3.82
hsa-miR-150_st	3.76	3.78	3.82	3.93	3.80	3.81	3.82
hsa-miR-619_st	3.72	3.68	3.97	3.97	3.43	4.12	3.82
hsa-miR-601_st	3.58	4.05	3.83	3.83	3.64	3.97	3.82
hsa-miR-510_st	3.73	3.76	3.52	3.85	3.84	4.18	3.81
hsa-miR-548b-5p_st	3.90	3.85	3.69	3.98	3.64	3.81	3.81
hsa-miR-518c_st	3.85	3.89	3.85	3.52	4.02	3.75	3.81
hsa-miR-106a-star_st	3.99	3.75	4.13	3.79	3.70	3.51	3.81
hsa-miR-302b_st	3.92	3.68	3.88	3.87	3.73	3.79	3.81
hsa-miR-548k_st	3.84	3.89	3.97	3.80	3.67	3.69	3.81
hsa-miR-196a_st	3.61	4.18	3.77	3.72	3.97	3.60	3.81
hsa-miR-548d-5p_st	3.93	3.84	3.68	3.71	3.83	3.86	3.81
hsa-miR-1256_st	4.06	3.66	3.55	3.71	3.83	4.03	3.81
hsa-miR-196b_st	4.18	3.73	3.65	3.76	3.80	3.72	3.81
hsa-miR-520d-5p_st	3.85	3.48	3.96	3.74	4.14	3.65	3.80
hsa-miR-646_st	3.45	4.06	3.68	4.10	3.64	3.89	3.80
hsa-miR-450a_st	4.21	3.92	3.54	3.66	3.61	3.87	3.80
hsa-miR-1243_st	3.65	3.85	3.84	3.79	3.77	3.90	3.80
hsa-miR-141-star_st	3.85	3.64	3.75	3.62	3.90	4.04	3.80
hsa-miR-148b-star_st	3.80	3.88	3.84	3.98	3.69	3.61	3.80
hsa-miR-148a-star_st	3.90	3.50	4.08	3.79	3.83	3.69	3.80
hsa-miR-518d-3p_st	3.97	3.97	3.34	3.97	4.03	3.51	3.80
hsa-miR-890_st	3.74	3.95	3.94	3.47	3.91	3.78	3.80
hsa-miR-588_st	3.76	3.60	3.95	3.51	4.17	3.78	3.80
hsa-miR-507_st	3.65	3.51	3.71	4.10	4.05	3.76	3.80
hsa-miR-566_st	3.94	3.47	3.69	3.86	3.88	3.94	3.79
hsa-miR-200b-star_st	4.01	3.57	3.93	3.91	3.71	3.62	3.79
hsa-miR-448_st	3.80	3.76	3.80	3.90	3.78	3.72	3.79
hsa-miR-450b-3p_st	4.01	3.70	3.60	3.78	3.85	3.81	3.79
hsa-miR-662_st	3.95	3.50	3.48	4.03	3.84	3.94	3.79
hsa-miR-136_st	3.68	3.62	3.83	3.72	3.86	4.04	3.79
hsa-miR-30d-star_st	4.08	3.72	3.83	3.77	3.65	3.71	3.79
hsa-miR-515-3p_st	3.51	3.80	3.91	3.93	3.84	3.73	3.79
hsa-miR-562_st	3.67	4.13	3.71	3.62	4.04	3.56	3.79
hsa-miR-509-3p_st	3.64	3.43	4.19	4.02	3.79	3.66	3.79
hsa-miR-216a_st	4.01	3.63	3.62	3.78	3.80	3.87	3.79
hsa-miR-526b_st	3.82	3.66	3.89	3.83	3.78	3.73	3.79
hsa-miR-523_st	3.68	3.96	3.97	3.71	3.70	3.69	3.78
hsa-miR-519e-star_st	4.10	4.00	3.35	3.68	3.73	3.83	3.78
hsa-miR-551b_st	3.79	3.99	3.71	3.66	3.65	3.90	3.78
hsa-miR-1179_st	3.67	3.96	3.59	3.84	3.82	3.81	3.78
hsa-miR-130a-star_st	3.78	3.96	3.70	3.76	3.85	3.64	3.78
hsa-miR-924_st	3.97	3.70	3.76	3.92	3.69	3.63	3.78
hsa-miR-100-star_st	3.84	3.88	3.79	3.62	3.75	3.81	3.78
hsa-miR-548m_st	3.72	3.83	3.85	3.60	3.73	3.93	3.78

hsa-miR-340-star_st	3.85	3.70	3.73	3.96	3.85	3.56	3.78
hsa-miR-517c_st	4.01	3.58	3.74	3.78	3.73	3.81	3.78
hsa-miR-1289_st	3.76	3.60	3.73	3.89	3.90	3.77	3.77
hsa-miR-519a_st	3.63	3.68	3.79	4.16	3.65	3.72	3.77
hsa-miR-519c-3p_st	3.72	3.98	3.56	3.66	3.80	3.91	3.77
hsa-miR-147_st	4.04	3.93	3.70	3.88	3.47	3.61	3.77
hsa-miR-524-3p_st	3.65	3.73	3.68	4.06	3.73	3.79	3.77
hsa-miR-599_st	3.85	3.62	3.79	3.71	3.66	4.00	3.77
hsa-miR-1322_st	4.23	3.46	3.65	3.46	4.13	3.70	3.77
hsa-miR-592_st	3.59	3.94	3.81	3.83	3.74	3.73	3.77
hsa-miR-302e_st	3.81	3.85	3.63	3.81	3.72	3.82	3.77
hsa-miR-603_st	3.70	3.84	4.02	3.61	3.78	3.68	3.77
hsa-miR-1178_st	3.82	3.66	3.46	4.03	3.79	3.87	3.77
hsa-miR-573_st	4.05	3.50	4.11	3.30	3.75	3.90	3.77
hsa-miR-644_st	3.58	3.89	4.02	3.78	3.59	3.73	3.77
hsa-miR-363-star_st	3.53	3.61	4.09	3.91	3.69	3.76	3.76
hsa-miR-15b-star_st	3.92	3.78	3.86	3.71	3.78	3.53	3.76
hsa-miR-19a-star_st	3.45	3.75	3.84	3.93	3.84	3.76	3.76
hsa-miR-1200_st	3.92	3.53	4.22	3.70	3.45	3.76	3.76
hsa-miR-548a-3p_st	3.67	3.76	3.87	3.80	3.75	3.71	3.76
hsa-miR-526b-star_st	4.06	3.64	3.66	3.87	3.68	3.66	3.76
hsa-miR-937_st	3.49	3.65	3.70	3.60	4.14	3.97	3.76
hsa-miR-200a_st	3.66	3.57	3.93	3.71	3.66	4.02	3.76
hsa-miR-10b-star_st	3.72	3.84	3.83	4.01	3.54	3.62	3.76
hsa-miR-526a_st	3.94	3.88	3.81	3.61	3.75	3.56	3.76
hsa-miR-548o_st	3.65	3.58	4.32	3.62	3.59	3.78	3.76
hsa-miR-217_st	4.31	3.31	3.58	3.76	3.94	3.63	3.76
hsa-miR-642_st	3.55	3.94	3.71	3.74	3.90	3.68	3.76
hsa-miR-367_st	3.58	3.86	3.72	3.69	3.96	3.72	3.75
hsa-miR-101-star_st	3.57	3.44	4.15	3.78	3.75	3.83	3.75
hsa-miR-873_st	3.71	3.69	3.81	3.75	3.68	3.83	3.75
hsa-miR-302c_st	4.04	3.60	3.73	3.46	3.67	3.96	3.74
hsa-miR-219-5p_st	3.87	3.68	3.79	3.83	3.60	3.65	3.74
hsa-miR-604_st	4.04	3.78	3.37	3.68	3.99	3.53	3.73
hsa-miR-9_st	3.64	3.84	3.75	3.91	3.48	3.76	3.73
hsa-miR-96-star_st	3.88	3.58	3.79	3.62	3.65	3.86	3.73
hsa-miR-520f_st	3.95	3.94	3.75	3.61	3.70	3.42	3.73
hsa-miR-888-star_st	3.86	3.59	3.77	3.81	3.80	3.53	3.73
hsa-miR-581_st	4.13	3.49	3.48	3.74	3.84	3.67	3.73
hsa-miR-518f_st	3.92	3.66	3.53	3.69	3.80	3.76	3.73
hsa-miR-645_st	4.00	3.58	3.71	3.54	3.62	3.90	3.72
hsa-miR-338-3p_st	3.84	3.93	3.75	3.77	3.43	3.61	3.72
hsa-miR-499-5p_st	3.65	3.68	3.80	3.81	3.81	3.57	3.72
hsa-miR-147b_st	3.65	3.82	3.79	3.67	3.84	3.55	3.72
hsa-miR-449a_st	3.74	3.81	3.72	3.74	3.43	3.88	3.72
hsa-miR-1304_st	3.60	3.90	3.98	3.61	3.76	3.46	3.72
hsa-miR-512-3p_st	3.49	3.61	3.88	3.97	3.43	3.89	3.71
hsa-miR-1295_st	3.81	3.54	3.57	3.72	3.85	3.78	3.71

hsa-miR-375_st	3.75	3.58	3.58	3.60	3.83	3.89	3.71
hsa-miR-892b_st	3.83	4.22	3.54	3.60	3.38	3.66	3.71
hsa-miR-26a-1-star_st	3.85	3.63	3.72	3.82	3.51	3.67	3.70
hsa-miR-202-star_st	3.59	3.94	3.55	3.43	3.91	3.77	3.70
hsa-miR-223-star_st	3.60	3.87	3.80	3.72	3.51	3.70	3.70
hsa-miR-520a-5p_st	3.80	4.00	3.46	3.76	3.53	3.63	3.70
hsa-miR-892a_st	3.89	3.96	3.51	3.84	3.41	3.58	3.70
hsa-let-7f-2-star_st	3.69	3.75	3.83	3.87	3.38	3.66	3.70
hsa-miR-302d_st	3.78	3.78	3.72	3.58	3.69	3.61	3.69
hsa-miR-516b_st	3.84	3.96	3.89	3.67	3.36	3.45	3.69
hsa-miR-146b-3p_st	3.62	4.03	3.51	3.71	3.64	3.62	3.69
hsa-miR-33a_st	3.71	3.50	4.06	3.77	3.41	3.60	3.68
hsa-miR-522-star_st	3.72	3.72	3.70	3.62	3.74	3.53	3.67
hsa-miR-33b_st	3.80	3.65	3.58	3.71	3.65	3.62	3.67
hsa-miR-519c-5p_st	3.61	3.77	3.63	3.88	3.40	3.69	3.67
hsa-miR-1269_st	3.39	4.05	3.49	3.64	3.79	3.62	3.66
hsa-miR-1205_st	3.84	3.53	3.61	3.83	3.59	3.56	3.66
hsa-miR-571_st	3.68	3.80	3.64	3.85	3.34	3.64	3.66
hsa-miR-449b_st	3.66	3.66	3.60	3.73	3.62	3.65	3.65
hsa-miR-525-5p_st	3.51	4.00	3.60	3.54	3.35	3.88	3.65
hsa-miR-24-1-star_st	3.70	3.39	3.73	3.62	3.48	3.91	3.64
hsa-miR-519a-star_st	4.10	3.75	3.45	3.77	3.30	3.45	3.64
hsa-miR-1203_st	3.28	3.96	3.63	3.94	3.92	3.09	3.64
hsa-miR-516b-star_st	3.89	3.45	3.75	3.46	3.86	3.39	3.63
hsa-miR-516a-3p_st	3.53	3.60	3.82	3.69	3.58	3.44	3.61
hsa-miR-187_st	3.52	3.42	3.65	3.44	3.74	3.88	3.61
hsa-miR-639_st	3.22	3.63	3.99	3.87	3.18	3.72	3.60
hsa-miR-519b-5p_st	3.63	3.88	3.28	3.56	3.55	3.63	3.59
hsa-miR-942_st	3.68	3.43	3.50	3.39	3.47	4.03	3.58
hsa-miR-124-star_st	3.70	3.81	3.60	3.65	3.38	3.34	3.58
hsa-miR-663b_st	1.99	4.53	3.57	3.64	4.13	3.61	3.58
hsa-miR-523-star_st	3.43	3.55	3.58	3.69	3.68	3.51	3.57
hsa-miR-518e-star_st	3.64	3.86	3.27	3.45	3.71	3.41	3.55
hsa-miR-658_st	3.22	4.19	3.64	3.51	3.59	3.02	3.53
hsa-miR-614_st	3.50	3.13	3.49	3.77	3.03	3.63	3.43
hsa-miR-323-5p_st	3.02	4.22	3.01	3.04	1.68	2.44	2.90
hsa-miR-608_st	3.42	2.20	1.05	1.97	2.81	1.86	2.22
hsa-miR-33b-star_st	2.57	2.21	1.91	1.44	2.74	2.08	2.16
hsa-miR-661_st	4.09	2.54	1.19	1.49	3.45	-0.61	2.02
hsa-miR-611_st	3.94	-19.25	3.88	3.51	3.43	3.54	-0.16
hsa-miR-593-star_st	3.45	-11.55	2.72	3.59	-11.64	1.72	-1.95

Appendix III – Publications

Downloaded from thorax.bmj.com on August 15, 2011 - Published by group.bmj.com
Thorax Online First, published on August 11, 2011 as 10.1136/thoraxjnl-2011-200532

BASIC SCIENCE FOR THE CHEST PHYSICIAN

MicroRNAs in lung diseases

Tom Pagdin, Paul Lavender

Department of Asthma, Allergy and Respiratory Science, MRC/Asthma UK Centre in Allergic Mechanisms of Asthma, King's College London, Guy's Hospital, London, UK

Correspondence to
Dr Paul Lavender, Department of Asthma, Allergy & Respiratory Science, MRC/Asthma UK Centre in Allergic Mechanisms of Asthma, King's College London, 5th Floor Tower Wing, Guy's Hospital, London SE1 9RT, UK; paul.lavender@kcl.ac.uk

Received 26 May 2011
Accepted 14 July 2011

ABSTRACT

The advent of RNA sequencing technology has stimulated rapid advances in our understanding of the transcriptome, including discovery of the vast RNA complement generated by transcript splice variation and the expansion of our knowledge of non-coding RNAs. One non-coding RNA subtype, microRNAs (miRNAs), are particularly well studied, primarily because of their important roles as post-transcriptional gene regulators. The first miRNA was identified in the early 1990s and there are now thought to be around 1000 distinct miRNAs in man, with each cell type expressing a distinct repertoire. Increasing evidence has implicated miRNAs as having causative roles in a variety of lung diseases and has driven investigations into their potential as therapeutic targets.

DERIVATION AND FUNCTION

miRNAs are generally derived from precursor transcripts termed pri-miRNAs. These pri-miRNAs can either contain a single short miRNA hairpin of only about 100 nucleotides (nt) in length, or they can contain multiple miRNA hairpins. A number of miRNAs, known as miRtrons, are excised from the introns of protein-coding genes by the cellular splicing machinery.

The product of miRNA processing is a 19–25 nt RNA molecule that can be incorporated into a cytoplasmic protein complex called RISC, the RNA-Induced Silencing Complex. Once in the context of RISC, miRNAs target specific mRNAs through Watson–Crick base pairing which predominately involves only bases 2–8 of the miRNA, known as the 'seed'. A single miRNA may bind to a number of target transcripts and a single transcript may contain multiple interaction motifs for a single miRNA or for different miRNAs. The interaction of a miRNA and target message culminates in degradation of the target mRNA, translational repression, or a combination of both (figure 1). It is thought that around 60% of all mRNAs within the cell are targeted by miRNAs, but should just one of those RNAs encode a critical component of a signal transduction pathway, then profound downstream influences may be triggered by its diminished expression.

TARGET IDENTIFICATION

Despite progress in our understanding of miRNA biology, the list of validated miRNA–mRNA interactions is not comprehensive. Target identification is a major hurdle in miRNA research and is complicated by the fact that the interaction of miRNAs with target mRNAs is tolerant of some degree of mismatch. Where are the regions of mRNAs that miRNAs target?

Recent unbiased approaches suggest that miRNA interaction sites may be located throughout the mRNA transcript. However, historic studies have shown that interaction motifs tend to be enriched in the 3′ untranslated region (3′UTR) of the target mRNA, a region often involved in the regulation of mRNA stability. Algorithms commonly used to predict miRNA targets exploit this bias towards the 3′ UTR, possibly leading to the under-investigation of other regions.

A growing body of literature suggests that there is disrupted expression of specific miRNAs either in lung pathologies themselves or experimental models thereof. Examples of this are cited for lung cancer, asthma, fibrosis and chronic obstructive pulmonary disease (COPD).

Lung cancer

The let-7 miRNA family and the miR-17-92 cluster, a single transcript which can give rise to seven distinct miRNAs, have well-defined roles in lung cancer as tumour suppressors and oncogenes, respectively. The let-7 family is frequently deleted in lung cancer and has been shown to regulate RNA stability of transcripts encoding multiple oncogenes including Ras[1] and cycle regulators such as cyclinD2. By contrast, miRNAs from the miR-17-92 cluster are overexpressed in small cell lung cancer and this overexpression is associated with inactivation of function of the retinoblastoma tumour suppressor.[2]

Asthma

Mouse models and in vitro studies of human cells have implicated miRNAs as having causative roles in asthma. Rodriguez *et al* have demonstrated that a total knockout of miR-155 causes the spontaneous development of an asthma-like phenotype, including inflammatory infiltration into the lung and airway remodelling.[3] TLR4-induced Th2 inflammation induces increased expression of miR-126 and administration of cholesterol-linked single-stranded inhibitors of miR-126 decreases the levels of TLR4-induced inflammatory infiltrate and airway hyper-responsiveness.[4] In addition, treatment of human bronchial smooth muscle cells with interleukin 13 causes a decrease in the expression of miR-133a. Artificial inhibition of miR-133a function in smooth muscle cells through the use of antagomirs was shown to increase the expression of RhoA, a known procontractile protein.[5]

Fibrosis

Liu *et al* have described increased miR-21 expression in both a murine bleomycin-induced fibrosis model and the lungs of patients with idiopathic pulmonary fibrosis. The authors speculate that miR-21

Copyright Article author (or their employer) 2011. Produced by BMJ Publishing Group Ltd (& BTS) under licence.

Downloaded from thorax.bmj.com on August 15, 2011 - Published by group.bmj.com

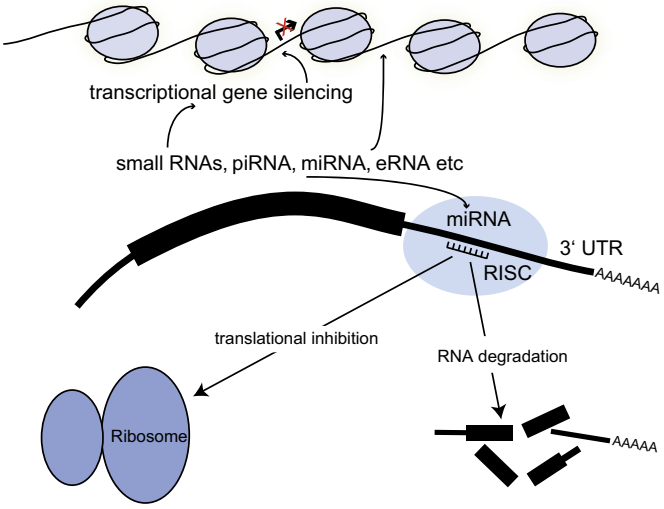

Figure 1 Advances in identification of RNA species through deep sequencing have revealed a number of novel RNA species such as eRNAs and identified more members of known families such as miRNAs. miRNAs have been the subject of intensive study and these have now been shown to anneal to target mRNAs through complementary base pairing. In most cases this interaction leads to cleavage of the target mRNA thereby preventing translation. A second mechanism of action involves blockade of mRNA translation.

may have a role in fibrosis through regulation of an inhibitory Smad, Smad7.[6] miRNA expression profiling of human fibrotic lung biopsies revealed differential expression of 46 miRNAs compared with cells from controls, including downregulation of miR-126 and let-7d. Reduction of let-7d expression resulted in increased collagen deposition and alveolar septal thickening in vivo and epithelial-mesenchymal transition in vitro.[7]

COPD

It is well established that smoking is a major risk factor for the development of COPD. A comparison of the miRNA expression profile of bronchial epithelial cells from smokers and never-smokers identified 28 miRNAs with differential expression and suggested that miR-218 in particular may play an important role in modulating epithelial gene expression following exposure to cigarette smoke.[8]

CLINICAL RELEVANCE

The increasing evidence for disrupted miRNA expression and function in disease processes makes them interesting targets for therapeutic intervention. Applications of miRNA-based therapy for lung disease are less advanced than for some other diseases.[9] However, promising data are emerging from model systems. In a recent report it has been shown that the systemic administration of miRNA mimics to the known tumour suppressor miRNAs miR-34a and let-7 decreases the in vivo tumour burden in a mouse model of non-small cell lung cancer (NSCLC).[10]

Perhaps a more immediate way of exploiting miRNAs in the pathogenesis of pulmonary disease is through molecular diagnostics, particularly risk stratification and outcome prediction. miR-155 and miR-let7a-2 expression correlate with poor overall survival in patients with lung adenocarcinoma,[11] while a five-miRNA signature (miR-137, mir-372, miR-182*, miR-221 and let-7a) has been shown to correlate with disease-free survival in patients with NSCLC.[12] A further feature of miRNAs is that they are stable and detectable in blood plasma and serum by qPCR or array hybridisation. Indeed, Chen *et al* have recently shown that the expression profile of serum miRNAs can serve as an NSCLC fingerprint.[13]

We are now reaching an exciting juncture in the miRNA field as continuing research into the mechanistic role of miRNAs in a wide range of diseases is occurring alongside demonstrations that miRNA are viable targets for both diagnostic screens and therapeutic intervention.

Competing interests None.

Contributors TP and PL wrote this document.

Provenance and peer review Commissioned; internally peer reviewed.

REFERENCES

1. **Johnson SM,** Grosshans H, Shingara J, *et al*. RAS is regulated by the let-7 microRNA family. *Cell* 2005;**120**:635–47.
2. **Hayashita Y,** Osada H, Tatematsu Y, *et al*. A polycistronic microRNA cluster, miR-17-92, is overexpressed in human lung cancers and enhances cell proliferation. *Cancer Res* 2005;**65**:9628–32.
3. **Rodriguez A,** Vigorito E, Clare S, *et al*. Requirement of bic/microRNA-155 for normal immune function. *Science* 2007;**316**:608–11.
4. **Mattes J,** Collison A, Plank M, *et al*. Antagonism of microRNA-126 suppresses the effector function of TH2 cells and the development of allergic airways disease. *Proc Natl Acad Sci U S A* 2009;**106**:18704–9.
5. **Chiba Y,** Tanabe M, Goto K, *et al*. Down-regulation of miR-133a contributes to up-regulation of Rhoa in bronchial smooth muscle cells. *Am J Respir Crit Care Med* 2009;**180**:713–19.
6. **Liu G,** Friggeri A, Yang Y, *et al*. miR-21 mediates fibrogenic activation of pulmonary fibroblasts and lung fibrosis. *J Exp Med* 2010;**207**:1589–97.
7. **Pandit KV,** Corcoran D, Yousef H, *et al*. Inhibition and role of let-7d in idiopathic pulmonary fibrosis. *Am J Respir Crit Care Med* 2010;**182**:220–9.
8. **Schembri F,** Sridhar S, Perdomo C, *et al*. MicroRNAs as modulators of smoking-induced gene expression changes in human airway epithelium. *Proc Natl Acad Sci U S A* 2009;**106**:2319–24.
9. **Haussecker D,** Kay MA. miR-122 continues to blaze the trail for microRNA therapeutics. *Mol Ther* 2010;**18**:240–2.
10. **Trang P,** Wiggins JF, Daige CL, *et al*. Systemic delivery of tumor suppressor microRNA mimics using a neutral lipid emulsion inhibits lung tumors in mice. *Mol Ther* 2011;**19**:1116–22.
11. **Yanaihara N,** Caplen N, Bowman E, *et al*. Unique microRNA molecular profiles in lung cancer diagnosis and prognosis. *Cancer Cell* 2006;**9**:189–98.
12. **Yu SL,** Chen HY, Chang GC, *et al*. MicroRNA signature predicts survival and relapse in lung cancer. *Cancer Cell* 2008;**13**:48–57.
13. **Chen X,** Hu Z, Wang W, *et al*. Identification of ten serum microRNAs from a genome-wide serum microRNA expression profile as novel non-invasive biomarkers for non-small cell lung cancer diagnosis. *Int J Cancer*. Published Online First: 9 May 2011. doi: 10.1002/ijc.26177.

Downloaded from thorax.bmj.com on August 15, 2011 - Published by group.bmj.com

MicroRNAs in lung diseases

Tom Pagdin and Paul Lavender

Thorax published online August 11, 2011
doi: 10.1136/thoraxjnl-2011-200532

Updated information and services can be found at:
http://thorax.bmj.com/content/early/2011/08/11/thoraxjnl-2011-200532.full.html

These include:

References This article cites 12 articles, 7 of which can be accessed free at:
http://thorax.bmj.com/content/early/2011/08/11/thoraxjnl-2011-200532.full.html#ref-list-1

P<P Published online August 11, 2011 in advance of the print journal.

Email alerting service Receive free email alerts when new articles cite this article. Sign up in the box at the top right corner of the online article.

Topic Collections Articles on similar topics can be found in the following collections

Lung neoplasms (280 articles)
Lung cancer (oncology) (1785 articles)
Asthma (5284 articles)
Lung cancer (respiratory medicine) (1745 articles)

Notes

Advance online articles have been peer reviewed and accepted for publication but have not yet appeared in the paper journal (edited, typeset versions may be posted when available prior to final publication). Advance online articles are citable and establish publication priority; they are indexed by PubMed from initial publication. Citations to Advance online articles must include the digital object identifier (DOIs) and date of initial publication.

To request permissions go to:
http://group.bmj.com/group/rights-licensing/permissions

To order reprints go to:
http://journals.bmj.com/cgi/reprintform

To subscribe to BMJ go to:
http://group.bmj.com/subscribe/